NOx formation and reduction by a coal, a lignite, an anthracite and a petroleum coke in conditions of cement plant calciner

Julien Cances

N° d'ordre : 2383 2006

Thèse présentée

en vue de l'obtention du grade de

Docteur de

L'INSTITUT NATIONAL POLYTECHNIQUE DE TOULOUSE

École Doctorale : Transfert, Dynamique des Fluides, Énergétique, Procédés

Spécialité : Énergétique et Transferts

par

Julien CANCES

Formation et réduction de NO_x par un charbon, un lignite, un anthracite et un coke de pétrole dans les conditions d'un précalcinateur de cimenterie

---

Soutenance le 26 octobre 2006, devant le jury composé de :

Philippe DAGAUT	Rapporteur
Anker JENSEN	Rapporteur
Karl LAMPE	Examinateur
Sylvain SALVADOR	Examinateur (Directeur de thèse)
Jean-Michel COMMANDRÉ	Examinateur (Encadrant de thèse)
Franck DELACROIX	Invité

Thèse préparée au centre de Recherche d'Albi en génie des Procédés des SOlides Divisés, de l'Énergie et de l'Environnement (RAPSODEE) de l'École des Mines d'Albi-Carmaux

Formation et réduction de NO_x
par un charbon, un lignite, un anthracite et un coke de pétrole
dans les conditions d'un précalcinateur de cimenterie

NO_x formation and reduction
by a coal, a lignite, an anthracite and a petroleum coke
in conditions of cement plant calciner

Remerciements – Acknowledgements

Ce travail a été réalisé en étroite collaboration entre le centre de Recherche d'Albi en génie des Procédés des SOlides Divisés, de l'Énergie et de l'Environnement (RAPSODEE) de l'École des Mines d'Albi-Carmaux, l'Agence de l'Environnement et de la Maîtrise de l'Énergie (ADEME) et la société Polysius.

Je tiens à remercier en premier lieu Messieurs Lecomte, David et Fages, successivement à la direction du centre, pour m'ont fait confiance et m'ont accueilli au sein du laboratoire.

Je tiens à remercier Messieurs Dagaut et Jensen pour m'avoir fait l'honneur d'accepter d'être les rapporteurs de ma thèse. Merci pour vos remarques constructives.

—

I would like to thank Mr Dagaut *and Mr* Jensen *to accept to review my Thesis. Thank you for your constructive remarks.*

—

Merci aussi, Philippe, pour m'avoir montré la voie... ...réactionnelle, biensûr !

—

Thank you, Karl, for your help, your kindness and patience all along the last three years. I would like to thank also the whole staff of Polysius – in Germany and in France – for their always cordial reception and their disponibility. It was very pleasant to work with you.

—

Merci à tous mes collègues avec qui j'ai eu le plaisir de travailler ces trois années durant, et en particulier à Bernard, sans qui le four à chute ne serait certainement pas ce qu'il est actuellement.

Sylvain, merci de m'avoir fait confiance et de m'avoir encadré tout au long de cette thèse. J'aurai beaucoup appris à ton contact et j'espère que ton indéniable sens de la Physique aura diffusé jusqu'à moi. Merci aussi pour la qualité de tes corrections qui améliorent à chaque fois la clarté et la précision des documents.

À Jean-Michel, je voudrais ici te signifier toute ma gratitude pour tous les efforts que tu as fait pour m'aider. Je te dois énormément, merci donc pour ton aide constante, ta patience, ta gentillesse... Je te souhaite de tout cœur d'obtenir ce que tu souhaites si fort, tu le mérites tellement !

Cédric et Thomas, mes deux colocataires... nous aurons partagé de drôles de moments tous les trois. Ça a toujours été un plaisir de vivre en votre compagnie pendant ces deux dernières années. Vous faites maintenant partie du clan très fermé de mes amis chers.

À mes parents, à ma sœur Mathilde, à mon frère Clément, à Clémence, à mon grand-père, à mes oncles et tantes, à mes amis Victor, Olivier et Nounours, à Jean-Jacques et Denise, je vous dois vos encouragements quand ça allait bien et surtout votre soutien quand ça allait moins bien. Vous êtes ce refuge, de havre de paix où je retrouve mes forces, mon courage et mon équilibre.

Delphine, je sais que cette thèse, tu l'as presque écrite et soutenue avec moi. Que d'épreuves avons-nous dû surmonter pour en arriver là ! Merci d'avoir eu la patience nécessaire

quand il le fallait, merci pour ton soutien indéfectible, merci de m'avoir fait voyager à travers toute la France et même au-delà, merci d'être restée à mes côtés. Maintenant, construisons la suite à deux.

Contents

Remerciements – Acknowledgements **v**

Contents **vii**

Introductions **3**

Introduction Générale **3**

General introduction **6**

I Bibliography **11**

Résumé de la partie I **13**

1 The cement production **17**

1.1 Introduction to the cement industry 17

1.2 The Portland cement production process 19

1.2.1 General overview 19

1.2.2 The modern cement plant : the dry process 20

1.2.3 Chemical reactions 20

2 Solid combustion **25**

2.1 The pulverized solid fuels 25

2.1.1 Natural fossil fuel description 25

2.1.2 Petcoke description 29

2.2 The carbonaceous particles combustion 29

2.2.1 The inert heating of the particle 30

2.2.2 The devolatilisation 30

2.2.3 The gas phase reactions : homogeneous oxidation and pollutant chemistry 35
2.2.4 The char oxidation . . . 37

3 The pollutants formation/reduction : the NO_x chemistry 41
3.1 Nitrogen oxides description . . . 41
3.1.1 Health impact . . . 42
3.1.2 Environmental effect . . . 42
3.2 NO_x formation . . . 42
3.2.1 Thermal-NO, or Zeldovich-NO . . . 43
3.2.2 Prompt-NO . . . 43
3.2.3 Fuel NO . . . 43
3.3 NO_x reduction . . . 45
3.3.1 NO_x reduction technologies . . . 45
3.3.2 Gas phase mechanisms . . . 48
3.3.3 Heterogeneous reactions . . . 51

II Experimental device, fuels and model description 53

Résumé de la partie II 55

4 Presentation of the experimental device 59
4.1 The Entrained Flow Reactor (EFR) . . . 59
4.1.1 General description of the EFR . . . 59
4.1.2 The solid fuel feeding . . . 61
4.1.3 The gas flow preheating . . . 61
4.1.4 The reactor furnace . . . 62
4.2 The gas sampling, filtration and analyzing device . . . 63
4.2.1 The sampling . . . 63
4.2.2 The filtration system . . . 66
4.2.3 The gas analysis device . . . 66
4.3 Determination of the residence time . . . 67

5 Preparation and characterization of the fuels and chars 71
5.1 Introduction . . . 71
5.2 Physico-chemical analysis methods . . . 72

5.2.1 The proximate analysis . . . 72
5.2.2 The ultimate analysis . . . 73
5.2.3 The physical properties . . . 73
5.3 Preparation and characterization of fuels . . . 73
5.3.1 Particle size calibration . . . 73
5.3.2 Physico-chemical analysis of the fuels . . . 73
5.4 Preparation and characterization of the chars . . . 75
5.4.1 "Flash" chars production . . . 75
5.4.2 "Flash" chars physico-chemical analysis . . . 76
5.4.3 Reference fixed bed chars characterization . . . 77
5.5 Discussion . . . 77
5.5.1 Fuels properties . . . 77
5.5.2 Chars properties . . . 78

6 The Entrained Flow Reactor model 83
6.1 Introduction . . . 83
6.2 Model description . . . 83
6.2.1 Main assumptions . . . 84
6.2.2 Particle properties . . . 85
6.2.3 Devolatilisation . . . 85
6.2.4 Char heterogeneous reactions . . . 89
6.2.5 Gas phase reactions . . . 92
6.2.6 Heat transfers . . . 94
6.3 Numerical integration . . . 95

III Characterization of the elementary heterogeneous reactions and detailed analysis of the reburning by solid fuels 97

Résumé de la partie III 99

Introduction 101

7 Characterization of the elementary heterogeneous reactions 103
7.1 Devolatilisation . . . 103
7.1.1 Experimental and modeling protocol . . . 103

7.1.2 Results . . . 106
7.2 Char oxidation . . . 115
7.2.1 Experimental and modeling protocol . . . 115
7.2.2 Results . . . 115
7.3 NO Reduction by char . . . 122
7.3.1 Experimental and modeling protocol . . . 122
7.3.2 Results . . . 122
7.4 Concluding synthesis . . . 124

8 Detailed analysis of the reburning conditions 127
8.1 Experiments and modelings of reburning with solid fuels . . . 128
8.1.1 Experimental and modeling protocol . . . 128
8.1.2 Results . . . 128
8.1.3 Synthesis . . . 136
8.2 Detailed analysis of the gas phase reactions . . . 140
8.2.1 Introduction . . . 140
8.2.2 Choice of the dates . . . 140
8.2.3 Identification of the pathways in gas phase reactions . . . 147
8.2.4 Results and discussion . . . 147
8.2.5 Discussion . . . 170
8.2.6 Synthesis . . . 172

Conclusions 177

Conclusion générale 177

General conclusions 179

Nomenclature **187**

References **195**

Appendix **205**

A Temperature measurements and corrections **205**

B Determination of the ratio $\beta = v_{gas}/\bar{U}$ **207**

C The gas analyzers **211**

C.1 The hydrocarbons analyzer 211

C.1.1 Principle of the measurement 211

C.1.2 Calibration 211

C.2 The O_2, CO, CO_2, SO_2 and NO analyzers 212

C.2.1 Principle of the measurement 212

C.2.2 Calibration 212

C.3 The quantification of various species with a FTIR 212

C.3.1 Principle of the measurement 212

C.3.2 Calibration 213

C.4 The H_2 analyzer 218

C.4.1 Principle of the measurement 218

C.4.2 Calibration 218

D Detailed chemical mechanism **219**

Introductions

Introduction générale

L'énergie est, sans conteste, le moteur du développement économique, comme le montre la très forte corrélation entre l'évolution du produit intérieur brut et la consommation d'énergie primaire sur le 30 dernières années en France [1] et en Europe [2]. Ainsi, d'ici 2030 la consommation mondiale d'énergie est supposée augmenter de 60 % [3]. Cette perspective, associée à l'épuisement annoncé des ressources pétrolières, ne fait que tendre encore plus le marché mondial de l'énergie (le prix du brut a quadruplé entre janvier 98 et août 2006 [4]) et compliquer la géopolitique mondiale. Dans ce contexte, le charbon fait figure de combustible d'avenir. En effet, ses réserves sont réparties plus uniformément à la surface terrestre que tout autre source d'énergie fossile [5] et devraient suffire pour encore plus de 250 ans au niveau actuel d'utilisation [6]. Toutefois, outre le CO_2 inhérent à l'oxydation de molécules carbonées, la combustion de solides pulvérisés entraîne la formation d'espèces polluantes, au premier rang desquels se trouvent les oxydes d'azote, ou NO_x.

C'est dans ces conditions que se développe l'industrie cimentière mondiale, elle-même grosse consommatrice de combustibles solides. En effet, une cimenterie consomme entre 2900 à 5900 kJ/kg de clinker produit (composant principal du ciment), soit entre 10 et 20 kg de charbon[1] pour 100 kg de clinker [7]. Le développement de ce secteur est lui aussi un très bon indicateur de la croissance mondiale. Ainsi, c'est dans les marchés en pleine expansion que la production et la consommation de ciment sont les plus importantes, la Chine et l'Inde occupant les deux premiers rangs mondiaux [8]. Au niveau français, l'industrie cimentière produit 1,5 % des émissions totales de NO_x et 14 % des émissions industrielles fixes [9].

Les réactions chimiques conduisant à la formation du clinker se déroulent à très haute température dans un four rotatif : le solide à environ 1500°C et le gaz à plus de 2000°C. A ce niveau de température apparaissent les NO_x thermiques résultant de l'oxydation de l'azote par l'oxygène tous deux présents dans l'air. Dans l'objectif d'améliorer les rendements énergétiques, une cimenterie moderne possède par ailleurs une tour de préchauffage accolée au four rotatif. Celle-ci est composée d'une cascade de cyclones et d'un précalcinateur doté d'une chambre de combustion supplémentaire où jusqu'à 60 % du combustible total est injecté. La température au sein du précalcinateur, maintenue à des valeurs plus basses comprises entre 800 et 1100°C, associée à la faible concentration d'oxygène impliquent de longs temps de séjour pour permettre l'oxydation complète du combustible solide, nécessaire tant d'un point de vue économique que pour la qualité du ciment. Du fait de ces faibles températures, les NO_x formés à cet endroit proviennent quasi exclusivement de l'oxydation de l'azote du combustible, pouvant atteindre

[1] Pouvoir calorifique du charbon pris à 30 MJ/kg

jusqu'à 2 % de sa masse.

Les deux flux chargés de NO_x provenant du four rotatif d'une part et de la chambre de combustion d'autre part sont classiquement rassemblés avant de traverser une zone réductrice. Dans celle-ci, l'ajout de combustible solide crée une zone riche en hydrocarbures, CO et carbone imbrûlés permettant la diminution de la concentration de NO_x ce qui s'apparente à du "reburning" au charbon.

La connaissance du comportement des combustibles les plus couramment utilisés dans les conditions d'un précalcinateur de cimenterie est donc un enjeu capital pour pouvoir concevoir des précalcinateurs plus performants en terme de rejets. L'objectif de ces travaux est de modéliser le reburning pour les quatre combustibles principalement utilisés dans l'industrie cimentière : un lignite, un charbon, un anthracite et un coke de pétrole. Ceci permettra d'aboutir à une bonne compréhension des mécanismes de formation et de réduction de ces polluants.

Les NO_x interagissent avec des combustibles solides suivant plusieurs mécanismes. Ainsi, les NO_x peuvent être réduits par les gaz dégagés lors de la pyrolyse ou bien à la surface du solide carboné résiduel. Une attention particulière va être portée à la quantification des contributions relatives des phénomènes se déroulant en phase gazeuse (réactions homogènes) ou à la surface du solide (réactions hétérogènes). En effet, lorsqu'un combustible solide est injecté dans un four industriel, tous les mécanismes décrits sur la Figure 1 sont mis en jeux simultanément.

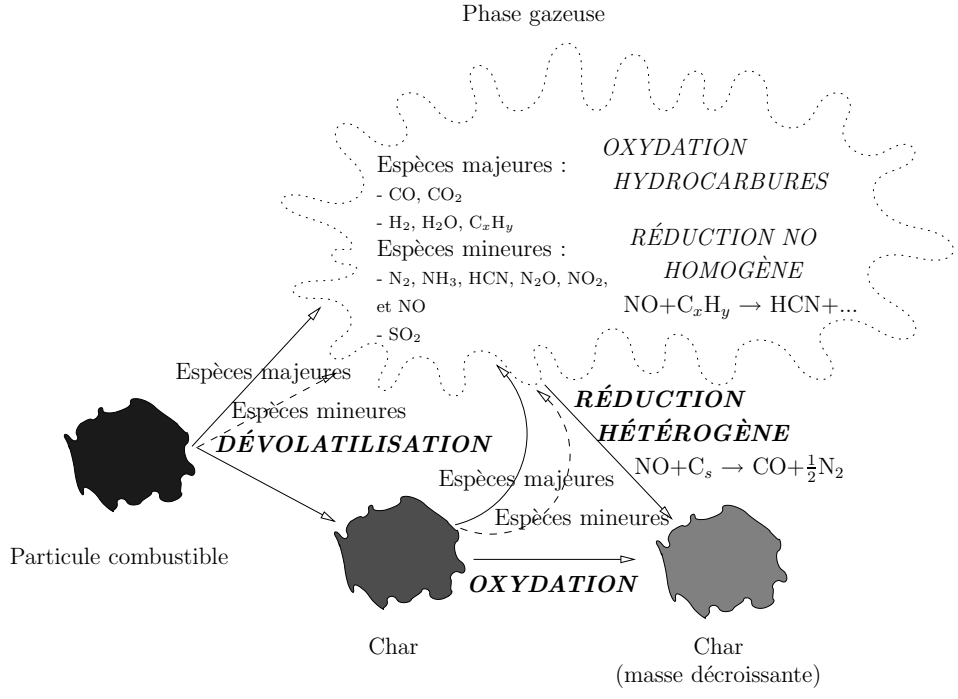

Figure 1: Représentation générale des mécanismes formant et réduisant le NO.

Ainsi, les travaux menés au cours de cette thèse permettent d'aboutir à une description quantitative des phénomènes qui conduisent à la formation et à la réduction du NO dans les conditions d'un précalcinateur de cimenterie. Ces travaux ont été menés sur deux plans : l'expérimentation et la modélisation.

L'organisation de ce mémoire s'articule en trois parties:

- La partie I consiste en une synthèse bibliographique, présentant dans un premier temps le procédé cimentier. Les principales perspectives économiques de ce secteur industriel ainsi que les aspects physico-chimiques de la production de ciment y sont décrits.

  La description des mécanismes dominant lors de la combustion des solides carbonés est ensuite abordée. Elle débute par une présentation des principaux combustibles utilisés dans la production de ciment, puis les différentes étapes gouvernant la combustion sont décrites individuellement.

  Enfin, la chimie des oxydes d'azote est détaillée. Les aspects toxicologiques et environnementaux relatifs aux NO_x sont décrits, suivis des différents mécanismes de formation et de réduction homogènes et hétérogènes.

- La partie II traite de la présentation des outils expérimentaux et des combustibles utilisés lors de cette étude.

  Le dispositif expérimental, présenté dans cette partie, est un Réacteur à Flux Entraîné (RFE). Les dispositifs périphériques sont également décrits un à un.

  La préparation et les analyses des quatre combustibles – un lignite, un charbon, un anthracite et un coke de pétrole – ainsi que celles de leurs résidus carbonés après pyrolyse sont présentées. La caractérisation des propriétés physiques et chimiques des solides pulvérisés utilisés est ensuite détaillée dans cette partie.

  Enfin, le modèle thermochimique utilisé dans ces travaux est décrit. Il considère une particule isolée et son environnement gazeux dont les compositions initiales sont données. Les principales réactions hétérogènes intervenant dans la chimie des NO_x – dévolatilisation, oxydation du char et réduction du NO sur le char – sont décrits avec des lois d'Arrhenius. La chimie en phase gazeuse est, quant à elle, prise en compte par des subroutines du programme CHEMKIN II.

- Dans la partie III, les résultats des expériences et des modélisations sont présentés et interprétés.

  Dans un premier temps, les trois mécanismes hétérogènes représentés en gras dans la Figure 1 (et listés ci-dessous) ont été caractérisés d'une part en terme de cinétiques de réaction et d'autre part en terme de quantités d'espèces formées/réduites. Il s'agit de :

  – la dévolatilisation,

  – l'oxydation du char

  – et la réduction du NO sur le char.

  Pour ce faire, trois séries d'expériences spécifiques ont été réalisées pour caractériser ces réactions solide/gaz à trois températures différentes : 800, 900 et 1000°C. La modélisation de chaque expérience à chaque température, a été entreprise par la suite pour caler les différents paramètres du modèle pour chaque combustible.

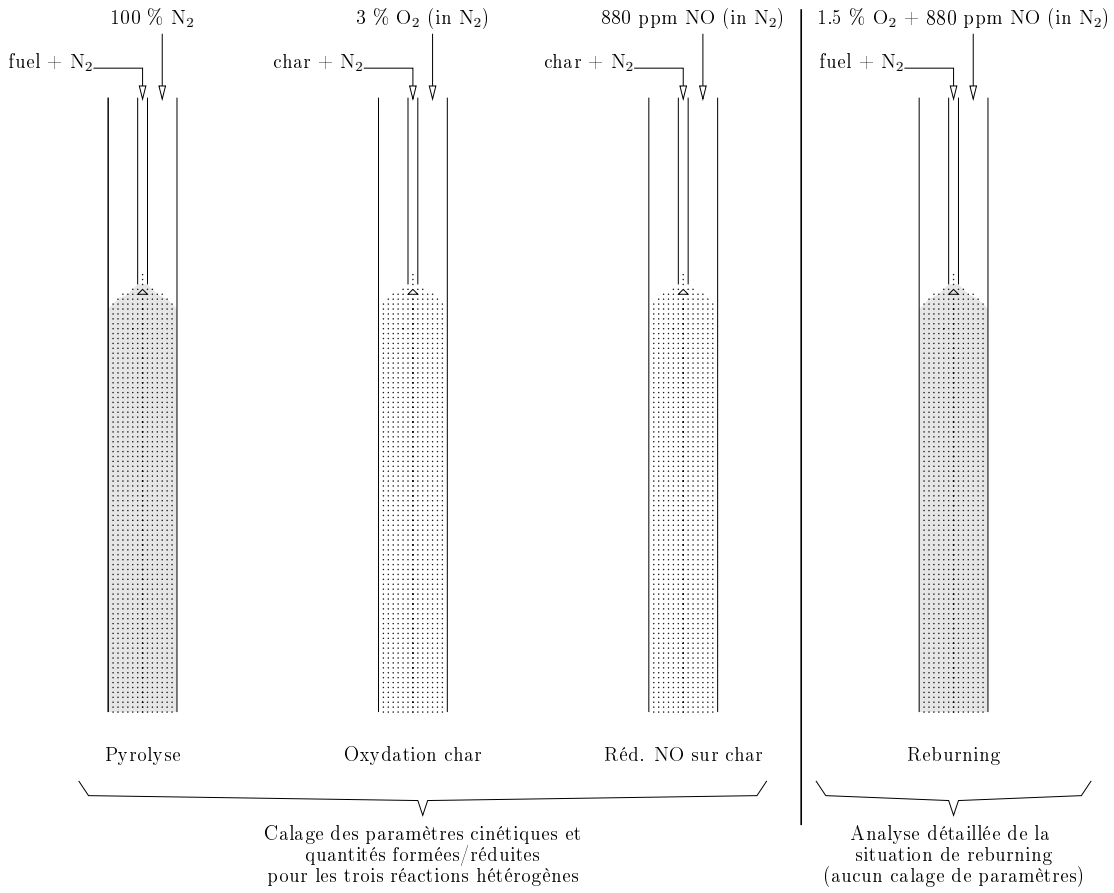

Figure 2: Représentation schématique des quatre types d'expériences.

Enfin, la situation de reburning – représentative de celle qui se déroule dans les précalcinateurs de cimenterie faisant l'objet de la thèse – a été reproduite expérimentalement et modélisée. Plus aucun paramètre n'est ajusté lors de cette étape. Les quatre types d'expériences sont schématisés dans la Figure 2. Ce travail permet une analyse détaillée des contributions des différents mécanismes.

General introduction

Energy is the main driving force behind economic development, as shown by the strong correlation between the evolution of gross domestic product and of primary energy consumption in France [1] and in Europe [2]. Thus, the world energy consumption is projected to grow almost 60 % by 2030 [3]. This perspective, associated to the depletion of mineral oil reserves, participate to strain the world energy market (crude oil prices quadrupled between January 98 and august 2006 [4]) and to complicate the geopolitics. In this context, coal is a fuel with good prospects. Indeed, its reserves are much more widely and evenly dispersed on earth than any other fossil energy source [5] and should be enough for more than 250 years at the actual consumption level [6]. However, in addition to CO_2 inherent in the carbonaceous molecules oxidation, combustion of solid fuels involve the formation of pollutants, the first of which are the nitrogen oxides, or NO_x.

These are conditions for the world cement industry development, which is itself a high solid fuels consumer. Indeed, a cement plant consumes between 2900 to 5900 kJ/kg of produced clinker (main component of cement), i.e. between 10 to 20 kg of coal[2] for 100 kg of clinker [7]. The development of this sector is also a very good indicator of the world growth. Thus, the production and consumption of cement are the most important in countries in full expansion, China and India are at the top ranks in the world [8]. At the french level, the cement industry produces 1.5 % of the total NO_x emissions and 14 % of the fixed industrial sources [9].

The chemical reactions leading to the clinker formation occur at very high temperature in a rotary kiln: the solid at approximately 1500°C and the gas at more than 2000°C. At this temperature level thermal NO_x appear. They result from the nitrogen oxidation by oxygen, both present in air. In aim to increase the energy efficiency, a preheating tower is added to the rotary kiln in modern cement plants. It is composed of a cyclone cascade and a calciner with a supplementary combustion chamber where up to 60 % of the total fuel income is injected. The temperature in calciner, maintained at lower values between 800°C and 1100°C, associated with the low oxygen concentration imply long residence times to allow the complete oxidation of the solid fuel. This is necessary both for an evident economic point of view and for the cement quality. Due to the low temperatures, almost exclusively NO_x from the fuel nitrogen oxidation are formed at this place.

The two flows loaded with NO_x coming for one part from the rotary kiln and for the other part from the combustion chamber are joined before crossing a reducing zone. Solid fuel injection in this zone create a fuel-rich zone with unburnt hydrocarbons, CO and solid carbon

[2]Calorific value of coal taken at 30 MJ/kg

that reduce the NO_x concentration. This is similar to the coal "reburning" process.

The knowledge of the behavior of the most commonly used fuels in the conditions of cement plant calciners is a capital stake for the design of future calciners more efficient in terms of emissions. The purpose of this work is to model the reburning for the four mostly used fuels in the cement industry: a lignite, a coal, an anthracite and a petroleum coke. This will lead to a better understanding of the formation and reduction mechanisms of these pollutants.

The interaction between NO_x and solid fuels follows several mechanisms. Thus, NO_x may be reduced by the gases released during pyrolysis or at the residual solid surface. A particular attention will be paid to quantify the relative contributions of the phenomena occurring in the gas phase (homogeneous reactions) or at the char surface (heterogeneous reactions). Indeed, when a solid fuel is injected in an industrial furnace, all the mechanisms depicted in the Figure 3 occur simultaneously.

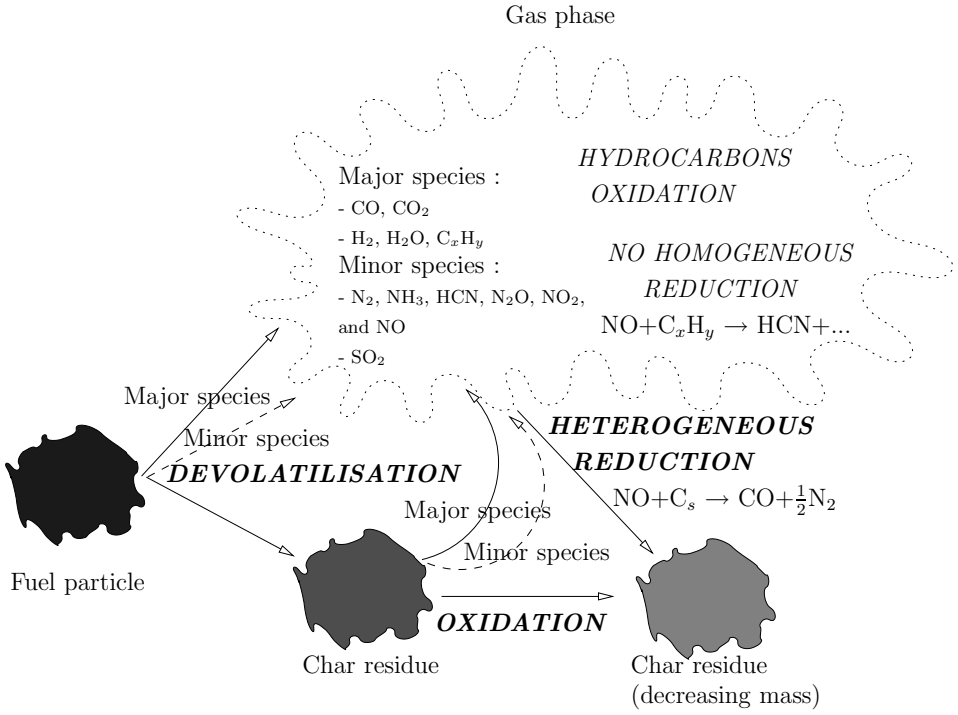

Figure 3: General representation of the mechanisms forming and reducing NO.

Thus, the work undertaken during this thesis makes it possible to describe quantitatively the phenomena that yield to the formation and reduction of NO in cement plant calciner conditions. Both modelings and experiments were realized during for the present work.

The organization of this thesis is articulated in three parts:

- The part I consists in a bibliographic synthesis, presenting first the cement production process. The principal economic outlooks for this industrial sector as well as the physico-chemical aspects of the production of cement are described there.

  The description of the mechanisms dominating the combustion of the carbonaceous solids is then presented. It begins with a description of the principal fuels used in the cement

production, then the various stages controlling combustion are described individually.

Finally, the chemistry of nitrogen oxides is detailed. The toxicological and environmental aspects relating to NO_x are described. Then the different homogeneous and heterogeneous formation and reduction mechanisms are detailed.

- The part II deals with the presentation of experimental and modeling tools and of the fuels used during this study.

  The experimental device, described in this part, is an Entrained Flow Reactor (EFR). The peripheral devices are also described one by one.

  The preparation and the analyzes of the four fuels – a lignite, a coal, an anthracite and a petroleum coke – as those of their carbonaceous residues after pyrolysis are presented. The characterization of the physico-chemical properties of the pulverized solids is detailed in this part.

  Finally, the thermo-chemical model used in this work is described. It considers a single particle and its gas environment whose initial compositions are given. The principal heterogeneous reactions involved in the NO_x chemistry – devolatilisation, char oxidation, and NO reduction by char – are described with Arrhenius laws. The gas phase chemistry is computed by subroutines from the CHEMKIN II package.

- In the part III, the results of the experiments and modelings are presented and interpreted.

  First, the three heterogeneous mechanisms represented in bold characters in Figure 3 (and listed below) were characterized on the one hand in term of reaction kinetics and on the other hand in term of formed/reduced quantities of species. The mechanisms are:

  – the devolatilisation,

  – the char oxidation

  – and the NO reduction by char.

  To achieve this, three series of specific experiments were carried out to characterize these solid/gas reactions at three different temperatures: 800, 900, and 1000°C. The modeling of each experiment at each temperature was then performed to adjust the different parameters of the model for each fuel.

  Finally, the reburning situation – representative of that which occur in cement plant calciners – was reproduced in experiments and modeled. At this stage, no more parameters were adjusted. The four experiments types are depicted in Figure 4.

  This work enables a detailed analysis of different mechanisms contributions.

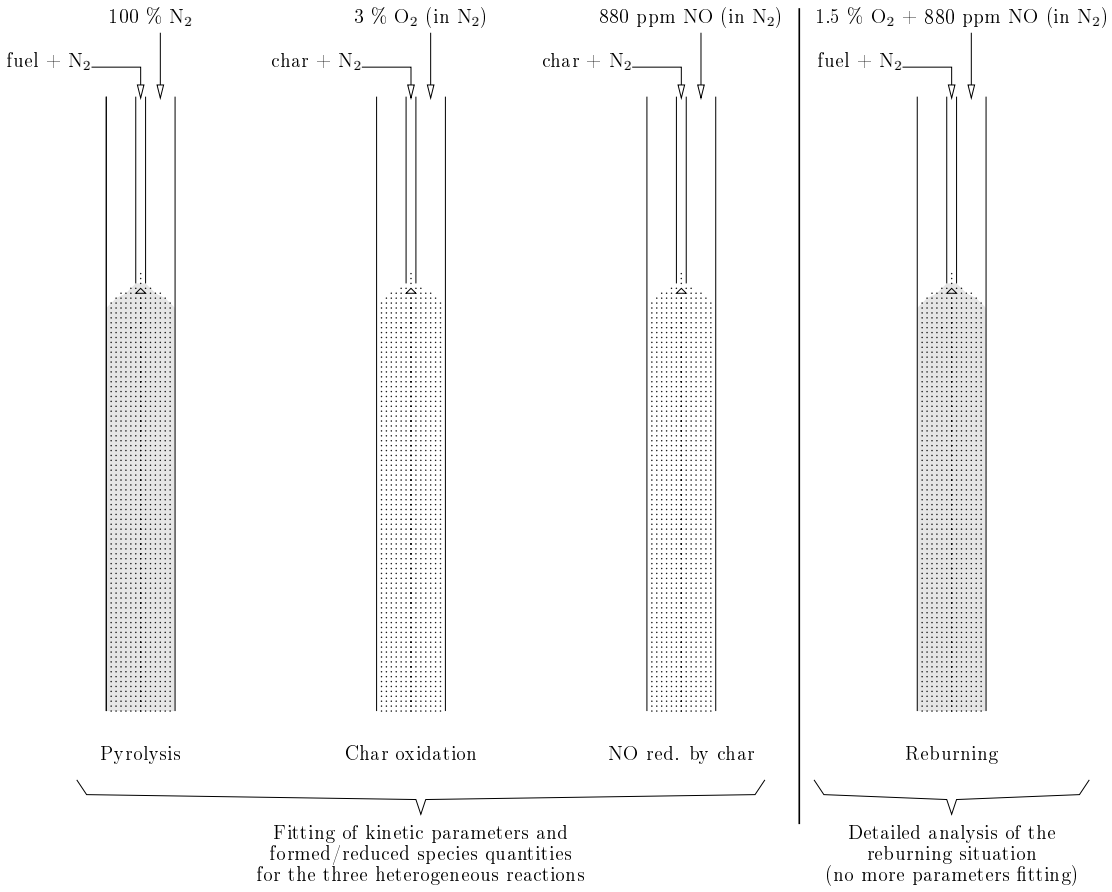

Figure 4: Schematic representation of the four types of experiments.

Part I

Bibliography

Résumé de la partie I

Le ciment

Le ciment est une fine poudre, inorganique et non-métallique, qui durcit lorsqu'elle est mélangée avec de l'eau. La production de l'industrie cimentière mondiale est totalement corrélée avec le marché de la construction et du génie civil, et donc de l'économie en général. La production et la consommation mondiale sont dominées par l'Asie et en particulier la Chine, qui représentent respectivement 67,6 % et 43,9 % de la production mondiale.

L'industrie cimentière est très consommatrice d'énergie qui représente 30 à 40 % des coûts de production. En effet le bilan énergétique d'une cimenterie est très fortement dominé dans un premier temps par l'énergie nécessaire à la décarbonatation du calcaire ($CaCO_3$) lors de sa transformation en chaux (CaO). Ensuite, lors de la clinkérisation, la chaux réagit à haute température avec divers oxydes métalliques pour former le clinker qui, une fois mélangé avec du gypse ($CaSO_4$,2(H_2O)), donnera du ciment. Cette énergie est principalement fournie en deux points par la combustion de solides carbonés pulvérisés (charbon, anthracite, lignite, petcokes, etc.).

La combustion de solides carbonés

Les combustibles fossiles naturels sont des résidus de la dégradation de déchets végétaux. On caractérise leur état de maturation par la notion de "rang". Plus celui-ci augmente, plus la teneur en carbone du combustible augmente, alors que les teneurs en oxygène, en hydrogène , et en matière volatiles diminuent.

Lors de la combustion d'un solide carboné, plusieurs étapes successives se produisent:

- la chauffe inerte,
- le séchage,
- la dévolatilisation,
- l'oxydation des matières volatiles au sein de la phase gazeuse et
- l'oxydation du char.

Si un charbon est représenté sous la forme d'une macromolécule (cf. Figure 2.2), alors la dévolatilisation – ou pyrolyse – consiste en la rupture des liaisons chimiques les plus faibles par l'apport d'énergie thermique lors de la chauffe de la particule. Lors de cette première étape très rapide, des hydrocarbures très lourds condensables à température ambiante sont relâchés : il s'agit des goudrons. D'autres gaz plus légers et incondensables sont aussi dégagés. Durant la seconde phase de cette décomposition thermique, le résidu carboné ainsi que les goudrons se craquent à nouveau pour libérer d'autres hydrocarbures légers (cf. Figure 2.4).

Ces gaz s'oxydent lorsqu'ils se mélangent à de l'O_2 à des températures élevées. Les réactions conduisant à CO_2 et à H_2O peuvent s'écrire soit de manière globale (Eq. 2.8), soit sous forme d'un ensemble de réactions élémentaires plus ou moins nombreuses. Ces mécanismes réactionnels permettent de décrire plus précisément la formation/réduction des espèces intermédiaires, telles que les radicaux, qui interviennent considérablement dans la chimie des espèces polluantes.

Lorsque l'oxygène atteint la surface de la particule de résidu carboné – ou char –, il réagit avec le solide. Cependant les particules de combustibles solides ont une porosité très développée, à fortiori après le sévère traitement thermique que représente la pyrolyse. Ainsi, faut-il prendre en compte les limitations par le transfert de masse à l'extérieur – diffusion à travers la couche limite de la particule – et à l'intérieur – diffusion au sein du milieu poreux – de la particule lors du calcul de la réactivité d'un solide.

La chimie des NO_x

Que ce soit lors de la pyrolyse, lors de l'oxydation des matières volatiles ou lors de l'oxydation du char, des polluants de type oxydes d'azote – ou NO_x – et oxydes de soufre – ou SO_x – sont dégagés. Les NO_x qui sont le principal sujet de cette étude sont toxiques pour l'homme et extrêmement nocifs pour l'environnement à différents niveaux : brouillards oxydants, pluies acides, effets de serre et dégradation de la couche d'ozone.

Les principaux mécanismes de formations sont de trois formes :

- Les NO_x dits "thermiques" qui sont dus à l'oxydation à haute température de l'azote par l'oxygène, tous deux présents dans l'air. Leur apparition commence à des températures supérieures à 1500°C.

- Les NO_x dit "précoces" sont, quant à eux, produits par la décomposition de N_2 en HCN (puis oxydation en NO) par les radicaux CH présents au voisinage d'un front de flamme. Ils apparaissent à des températures plus faibles que les NO_x thermiques (800°C).

- Les NO_x "combustibles" qui sont formés lors de l'oxydation de l'azote constitutif du combustible (matières volatiles ou char). Ce type de NO_x apparaît même à basse température.

Les mesures visant à réduire les émissions de NO_x peuvent être réunies en deux types distincts :

- Les mesures dites “primaires”, qui consistent à modifier les conditions de combustion à l'intérieur du foyer pour réduire la production globale de NO_x du procédé industriel. On compte parmi elles les mesures d'étagement d'air ou de combustible qui visent à créer une zone riche en combustible qui réduira les NO_x par le biais de réactions avec les radicaux hydrocarbonés (CH, CH_2, CH_3, HCCO). Dans le cas de solides carbonés, le NO est aussi réduit en N_2 par réaction avec surface de la particule solide. C'est à ce type de technique que nous nous intéressons.

- Les mesures “secondaires” visent à “nettoyer” les fumées à posteriori. Il s'agit principalement des technologies SCR (Selective Catalytic Reduction) et SNCR (Selective Non Catalytic Reduction). Ces deux techniques utilisent la faculté du radical NH_2 de réduire NO en N_2. Ces techniques nécessitent l'ajout d'ammoniac (NH_3), d'acide cyanurique ($(HOCN)_3$) ou d'urée ($(NH_2)_2C{=}O$), ce qui implique un coût de fonctionnement supplémentaire.

Chapter 1

The cement production

Contents

1.1 Introduction to the cement industry 17

1.2 The Portland cement production process 19

1.2.1 General overview 19

1.2.2 The modern cement plant : the dry process 20

1.2.3 Chemical reactions 20

Cement is a finely ground, non-metallic, inorganic powder. When mixed with water it forms a paste that sets and hardens. This hydraulic hardening is due to the formation of calcium silicate hydrates as a result of the reaction between water and the cement constituents.

Cement is a basic material for building and civil engineering construction. In Europe the use of cement and concrete (a mixture of cement, aggregates, sand and water) in large civil works can be traced back to antiquity. Portland cement, the most widely used cement in concrete construction, was patented in 1824 [10].

1.1 Introduction to the cement industry

Output from the cement industry is directly related to the state of the construction business in general and therefore tracks the overall economic situation closely [11]. The world production has grown continuously the last past years from 1.42 to 2.11 billion tons between 1995 and 2004. In 2004, the world production increased of 7 %, after an 8 % increase in 2003.

Asia represents two thirds of this market (Figure 1.1). In particular, China's production grew between 1995 and 2004 from 30 % to of 15 % on 44 % of the world production [8, 11].

In 2004, Europe in general produced almost 14 % and the actual 25 members of the EU represented 11 % of the world production, meaning 233 million tons.

There is generally little import and export of cement, mainly as a result of the high cost of road transport. World foreign trade in cement still account for 6–7 %, most of wich is transported by sea. Road deliveries of cement generally do not exceed distances of 150 km.

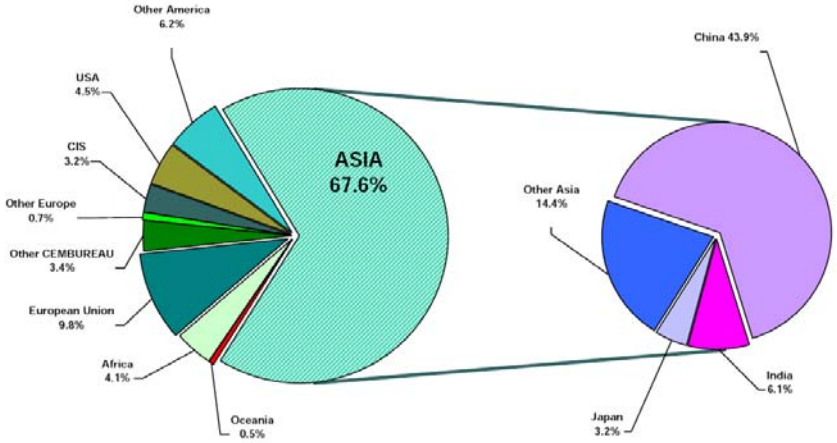

Figure 1.1: World cement production by region in 2004. (Total in the World = 2.11 billion tons) [8].

Producers in the European Union have increased cement output per man/year from 1700 tons in 1970 to 3500 in 1991. This increase in productivity is a result of the introduction of larger scale production units. The number of people employed in the cement industry in the European Union is now less than 60 000, whereas it was more than 90 000 in 1975.

The cost of a new cement plant is equivalent to around 3 years turnover, which ranks the cement industry among the most capital intensive industries. The profitability of the cement industry is around 10 % as a proportion of turnover (on the basis of pre-tax profits before interest repayments) [11].

The cement industry is an energy intensive industry with energy typically accounting for 30–40 % of production costs (i.e. excluding capital costs). Traditionally, the primary fuel used is coal. A wide range of other fuels are also used, including petroleum cokes (called "petcokes" in the following section of this document), natural gas and oil. In addition to these fuel types, the cement industry has been using various types of waste as fuel for more than 10 years [11].

Fuel type	[%]
Petcoke	39
Coal	36
Fuel oil	7
Lignite	6
Gas	2
Different types of waste	10

Table 1.1: Fuel consumption by the European cement industry in 1995 [11].

The emissions from cement plants which cause greatest concern are nitrogen oxides (NO_x), sulfur dioxide (SO_2) and dust. Other emissions to be considered are carbon oxides (CO, CO_2),

volatile organic compounds (VOCs), polychlorinated dibenzodioxins (PCDDs) and dibenzofurans (PCDFs), metals, and noise [11].

1.2 The Portland cement production process

1.2.1 General overview

The Portland cement results of the mixing and grinding of clinker with about 5 w.% gypsum ($CaSO_4$). Clinker normal composition is given in Table 1.2. The Alite, or C_3S, is the most important mineral in the clinker composition because it is responsible for its initial strength [12].

Species Name	Species formula	Species Abbreviation	[w.%]
Alite	$3CaO.SiO_2$	C_3S	45–65 %
Belite	$2CaO.SiO_2$	C_2S	10–30 %
Aluminate	$3CaO.Al_2O_3$	C_3A	5–25 %
Aluminoferrite	$2CaO.pAl_2O_3.(1-p)Fe_2O_3$	$C_2A_pF_{1-p}$	5–15 %

Table 1.2: Normal composition of clinker for a Portland cement [12].

Clinker is produced by sintering at high temperature (1450 °C) a mix of limestone (80 %) and diverse metal oxides (20 %), called "raw-meal" (see Table 1.3). The chemical changes in the primary matter are only due to a thermal treatment. The clinker production is a highly endothermic process with typical energy consumption in the range 2900 to 5900 $kJ/kg_{clinker}$, hanging on the production technology. The necessary heat is mostly provided by the combustion of carbonaceous particles, i.e. coals or petcokes.

Species name	[w.%]
$CaCO_3$	75–80 %
SiO_2	10–15 %
Al_2O_3	2–5 %
$MgCO_3$	0–6 %
Fe_2O_3	0.1–3 %
Na_2O+K_2O	0.1–1.5 %
SO_3	0–0.2 %

Table 1.3: Basic composition of raw-meal [7]

The majority of clinker is produced in rotary kiln systems, yet. The rotary kiln cement production was introduced by Frederik Ransome, as mentioned in an English patent of May 2, 1885 [10]. In the past, the whole cement production process acted in the rotary kiln. This is still rarely the case, particularly for "wet process" that uses raw-meal with a high moisture content mixed with water as a pumpable slurry as represented in Figure 1.2.

Although the choice of the process is mainly determined by the quality of the raw meal, more and more modern cement plants are using the energy saving "dry-process" with cyclone

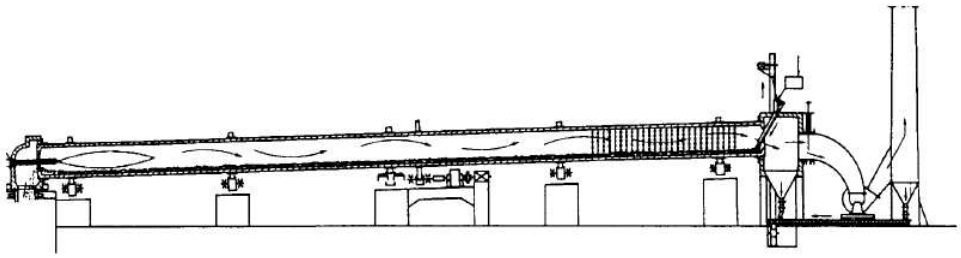

Figure 1.2: Long wet rotary kiln with chains [11].

preheaters.

1.2.2 The modern cement plant : the dry process

In Europe, more than 75 % of cement production is based on dry process [11]. In this process, the limestone (mainly $CaCO_3$) and clay are previously dried, preheated and decarbonized thanks to a cyclone preheater tower.

The first patent concerning the raw mix suspension preheater was applied for by Mr. M. Vogel-Jörgenson, from Frederiksberg in Denmark, patented on July 25, 1934. This represents a decisive development in the heat economy of the cement dry production process. With the preheater, it was possible to obtain a very low flue gas exit temperature of about 330°C, which were not attainable so far. The first four-stage cyclone suspension preheater was introduced into the cement industry in 1951 [10].

The Figure 1.3 represents the whole process. After the quarry extraction and grinding, the limestone is mixed with additional iron and/or alumina oxides. The raw-meal is then injected at the upper part of a cyclone cascade (top right in Figure 1.3) and falls counter-flow of exhaust gas of the rotary kiln before being introduced in it. In modern cement plants a precalciner is added, where up to 60 % of the total cement plant fuel income is injected. The decarbonated meal is then conducted to the rotary kiln.

1.2.3 Chemical reactions

The chemical reactions involved during Portland cement manufacture are a complex series of coupled high temperature reactions. In addition, mineral constitution of raw materials and clinker materials vary in structure and composition, making generalized representation of the reactions involved impossible.

By idealized representation of raw material, clinker materials and reaction pathways, it is possible to simplify the reaction sequence. The reaction sequence involved may be divided into three groups [7]:

- reactions below 1300°C,
- clinkering reactions (1300–1450°C),

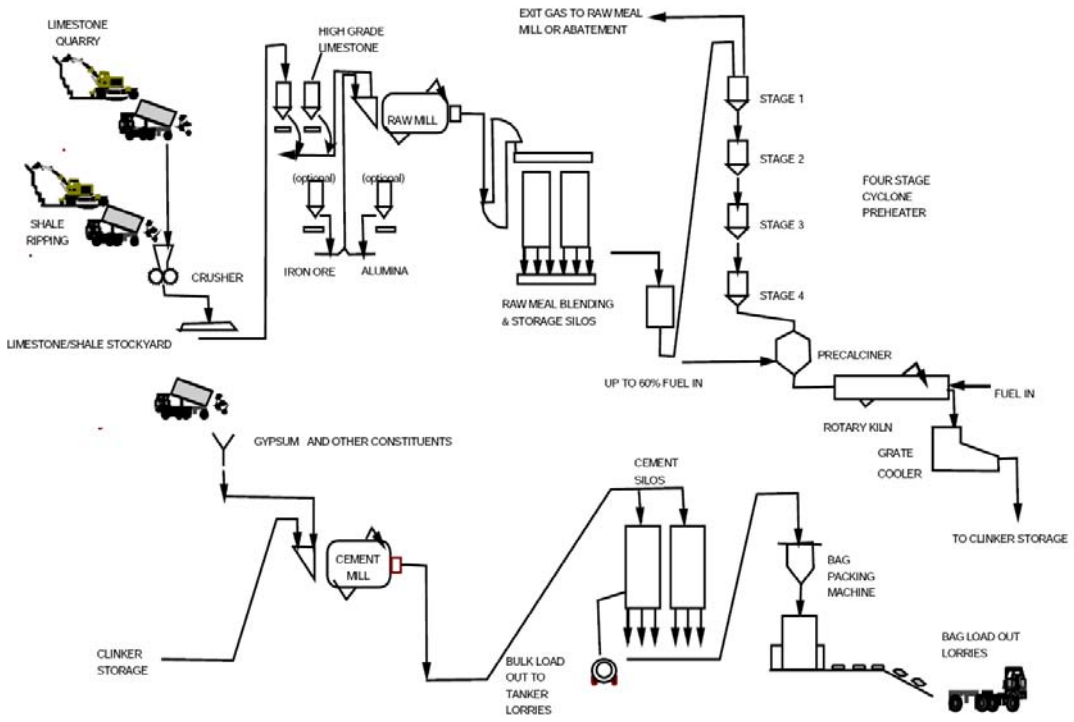

Figure 1.3: Typical precalciner dry process [11].

- reactions during cooling.

Related to the temperatures presented in Figure 1.4, the reactions below 1300°C happen in the preheating tower, the clinkering reactions in the rotary kiln, and reactions during cooling in the following clinker cooler.

1.2.3.1 Reactions below 1300°C – the cyclone preheater

The raw-meal comes into the cyclone preheater, and is heated up to ≈ 1000°C. The reactions begin in this part of the cement plant.

Below 1300°C the main reactions are drying between 100 and 200°C (endothermic), dehydroxylation of clay minerals between 600-800°C (endothermic), calcination at 800-900°C (endothermic) and reactions of calcite ($CaCO_3$) or lime (CaO) with quartz and clay minerals decomposition products (exothermic).

Even if some several exothermic reactions happen, the net enthalpy change is dominated by the endothermic calcination of calcite that proceeds according to Reaction 1.1. The calcination temperature depends on the CO_2 partial pressure, but generally lies in the range 800–900°C. On heating the clay minerals also dissociate into their constituent oxides and water. The main reactions between calcareous and clay mineral constituent oxides are Reactions 1.2, 1.3 and

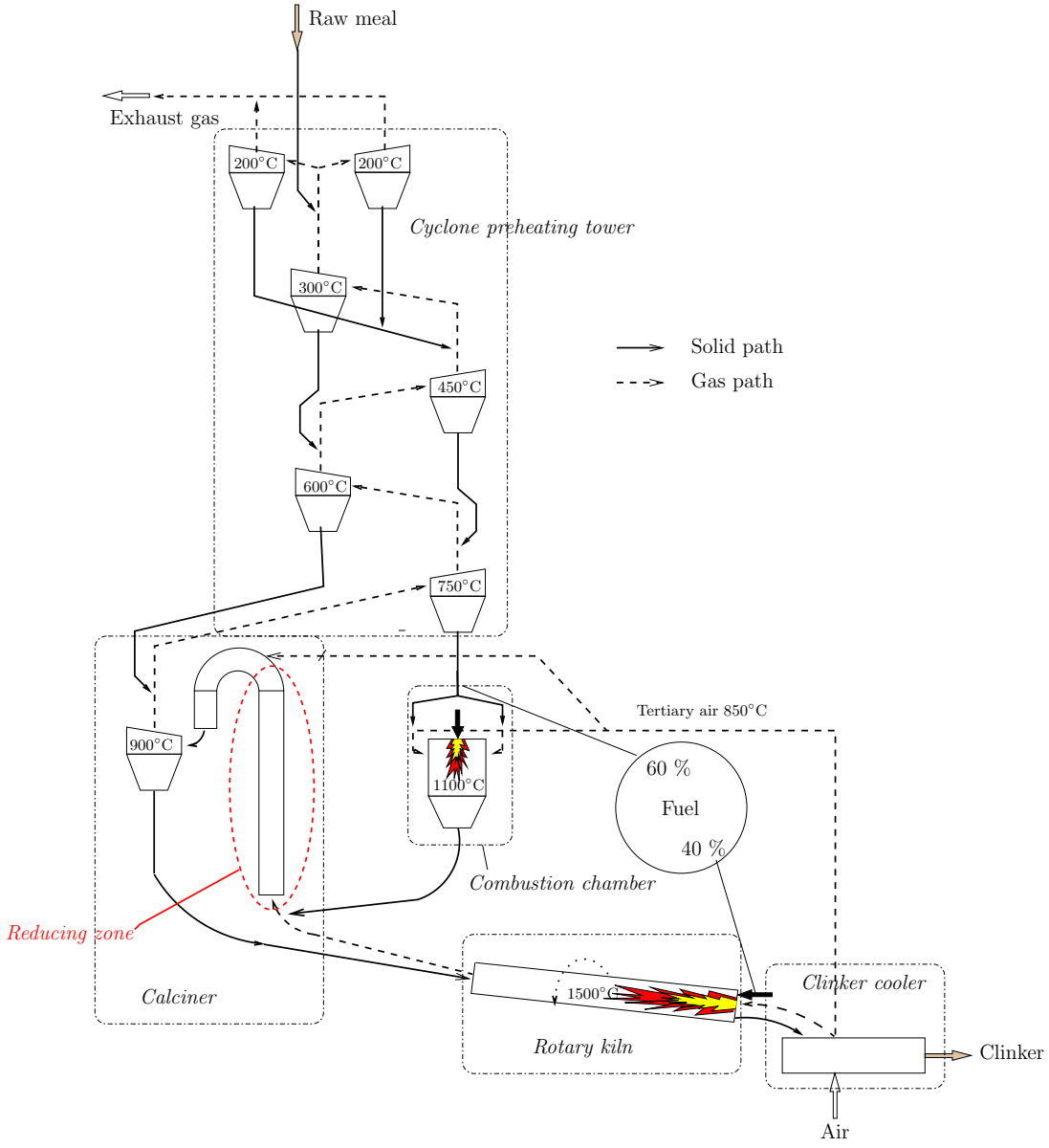

Figure 1.4: Schematic representation of dry line cement plant with a rotary kiln and a precalcination tower.

1.4 [7].

$$\begin{aligned} \mathrm{CaCO_3} &\xrightarrow{\Delta h_1} \mathrm{CaO + CO_2} && (1.1)\\ \Delta h_1 &= +1792\ \mathrm{kJ/kg_{CaCO_3}} \\ 2 \cdot \mathrm{CaO + SiO_2} &\xrightarrow{\Delta h_2} \beta - \mathrm{C_2S} && (1.2)\\ \Delta h_2 &= -734\ \mathrm{kJ/kg_{C_2S}} \\ 3 \cdot \mathrm{CaO} + \alpha - \mathrm{Al_2O_3} &\xrightarrow{\Delta h_3} \mathrm{C_3A} && (1.3)\\ \Delta h_3 &= -27\ \mathrm{kJ/kg_{C_3A}} \\ 4 \cdot \mathrm{CaO} + \alpha - \mathrm{Al_2O_3} + \alpha - \mathrm{Fe_2O_3} &\xrightarrow{\Delta h_4} \mathrm{C_4AF} && (1.4)\\ \Delta h_4 &= -734\ \mathrm{kJ/kg_{C_4AF}} \end{aligned}$$

1.2.3.2 Clinkering reactions – the rotary kiln

The predecarbonated limestone particles get into the rotary kiln where the very high temperature – presented in Figure 1.4 – transforms the meal into clinker.

On heating from 1300 to 1450°C a melt constituting 20–30 % of the solid mass is formed (melt primarily originates from the aluminate and ferrite phase). The material nodulises to form clinker, and most of the CaO present reacts with a large proportion of the belite (C_2S) to form alite (C_3S), according to the endothermic Reaction 1.5.

$$\begin{aligned} \beta - \mathrm{C_2S + CaO} &\xrightarrow{\Delta h_5} \mathrm{C_3S} && (1.5)\\ \Delta h_5 &= +59\ \mathrm{kJ/kg_{C_3S}} \end{aligned}$$

If clinker is underburnt (not adequately thermally processed) it will contain excessive free lime, that leads to unsoundness of concrete (tendency to volume change with time), and low alite content. Overburning (too severe thermal treatment) of clinker results in formation of large crystals. Generally an optimum burning temperature exists. However, generalization is difficult, as factor such as the cooling rate of clinker also are influenced by burning temperature [7].

1.2.3.3 Reactions during cooling – the clinker cooler

Clinker cooling rates influence the crystalline structure of clinker, as well as influencing phase transformations. The resulting effect on cement quality is reflected in soundness, chemical resistance, cement strength and rate of strength development. Cooling rates also influence clinker grindability. Rapid cooling is generally necessary [7].

Chapter 2

Solid combustion

Contents

2.1 The pulverized solid fuels 25

2.1.1 Natural fossil fuel description 25

2.1.2 Petcoke description 29

2.2 The carbonaceous particles combustion 29

2.2.1 The inert heating of the particle 30

2.2.2 The devolatilisation 30

2.2.3 The gas phase reactions : homogeneous oxidation and pollutant chemistry 35

2.2.4 The char oxidation 37

The preceding chapter deals with industrial process. However, it is necessary to perform a precise approach of the scientific aspects of the solid fuel combustion.

In this chapter, a literature review on the pulverized solid fuels and their combustion is proposed. It is divided into two sections: the first one presents the different fuels properties and their differences, and the second one details the mechanisms occurring during their combustion.

2.1 The pulverized solid fuels

In cement plant, the main part of the total energy necessary to yield clinker is provided by the combustion of pulverized solid carbonaceous particles. Coals and petcokes of various qualities are by far the most commonly used fuels, as indicated in Table 1.1 in Chapter 1.

A differentiate description of each type of fuel is proposed in the following sections. Indeed, if the natural fossil fuels are the products of a long time evolution of biomass, petcokes are the residual products of petroleum refinery.

2.1.1 Natural fossil fuel description

Smoot et al. [13] give the following definition for natural fossil fuels :

Coal is a complex sedimentary rock derived from plant remains that underwent peatification and subsequent coalification. Coal originated as peat deposits formed in prehistorical swamps through the accumulation of plant substances whose components underwent differing degrees of chemical decomposition.

The original biomass is mainly composed by water and three vegetal polymers [14] :

- cellulose (40–52 %) that is a glucose polymer,
- hemicellulose (10–30 %) that are complex molecules based on C_6 and C_5 monomer,
- lignin (20–25 %), mix of phenol polymers.

After a long time evolution, the coal composition could be compared to the initial biomass one. Indeed a coal is composed by petrographic constituents, called macerals [13–15] :

- vitrinite (up to 80 % of coal) that is thought to derive mainly from bio-resistant lignin polymers and cellulose (woody or xylem structures).
- liptinite seems to be yielded by polymethylene moieties (up to 10 % in low rank coal) that results from the transformation of leaves, pollen, algae. Liptinite has high O- and H-content and yields mainly volatile matters.
- inertinite results from the decomposition of resistant ligneous part of vegetals.

The progressive transformation of the initial vegetal components into the final fossil fuel is called "coalification". Thus plant remains evolve into peat, lignite, bituminous coal, anthracite and finally in graphite. This process involves the increase of the carbon and the decrease of hydrogen, oxygen and volatile matters contents [13–15]. The "rank" parameter allow the various coals to be classed in function of their coalification degree : a young coal is a low rank coal and has a low carbon content [15]. The Van Krevelen diagram, plotted in Figure 2.1, represents the ratio H/C as a function of O/C (both in mol/mol). The representation is a good illustration of the coal rank parameter. It is interesting for us to locate our fuels among the literature ones.

For example, the U.S. coal classification is principally based on the VM[1] content and the LCV[2]. The different quality of coal are defined in the Table 2.1 from [16].

2.1.1.1 Coal characterization

This notion of coal rank alone could not explain the behavior differences between the different coals during the combustion process. Thus different techniques are employed to obtain useful information.

Proximate analysis The fuel may be analyzed as composed by :

- moisture,

[1] VM : Volatile Matters
[2] LCV : Lower Calorific Value

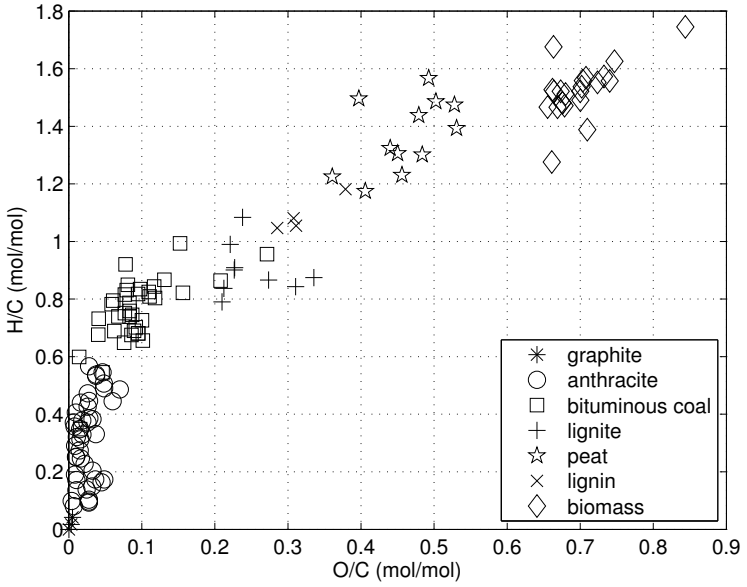

Figure 2.1: Van Krevelen diagram – data coming from the literature [14]

Coal rank	Volatile content	Lower Calorific Value
graphite	VM < 2 w.%	–
anthracite	$2 <$ VM ≤ 14 w.%	–
semi-anthracite	$14 <$ VM ≤ 31 w.%	–
bituminous "low-volatile"	VM > 31 w.%	LCV $\geq 32\,560$ kJ/kg
bituminous "medium-volatile"	–	$26\,750 \leq$ LCV $< 32\,560$ kJ/kg
bituminous "high-volatile"	–	$24\,420 \leq$ LCV $< 26\,750$ kJ/kg
subbituminous	–	$19\,310 \leq$ LCV $< 24\,420$ kJ/kg
lignite	–	LCV $< 19\,310$ kJ/kg

Table 2.1: U.S. coal classification [16]

- ash,
- volatile matters,
- and fixed carbon.

These properties should be determined by following standards.

- The moisture content can be determined by following the french standard NF M03–002 [17]. It consists in measuring the mass loss of the original fuel, set in a drying oven at 110 ± 5°C until no more sample mass variation is measured. In practice the sample is often left 24 h in the oven.
- The volatile matters content is determined by following the standard NF M03–004 [18]. This consists in weighting the char resulting of a 7 min pyrolysis at 900 ± 10°C of 1 g of fuel. The mass loss represents the of volatile matters mass.
- The standard NF M03–003 [19] allows the ash content to be determined. 1 g of fuel in a small quartz tray is set in an oven at 815 ± 10°C for 2 h. The remaining matter is ash.

- Finally, the fixed carbon content is defined by the standard NF M03–006 [20] by the difference to 100 % after subtracting the moisture, ash and volatile matters content, as expressed in 2.1.

$$C_{fix} = 100 - Ash - VM - moist. \tag{2.1}$$

Ultimate analysis The ultimate analysis allows the elementary composition to be determined. A small mass of fuel, precisely weighted, is oxidized in excess of air at high temperature in presence of a solid catalyst. The combustion gases are then analyzed in a gas chromatograph. Thus C, H, N and S elements are then quantified. After subtracting the ash content, oxygen content – O – can be calculated by difference to 100 %.

Petrographic analysis Although no petrographic analysis has been performed in the sequel of this work, it is interesting to mention it. Petrographic microscope allows the macerals composition to be quantified by measuring the reflected intensity of an incident light.

Chemical structural analysis As well in this case, no chemical structural analysis were carried out in this work, but it helps for the better understanding of the phenomena presented later. The purpose of structural analysis is to determine the molecular structure of a fossil fuel [13, 21–23].

The main instruments used to obtain the desired results are ^{13}C-NMR[3] and FTIR[4] spectroscopes. Finally, an hypothetical coal molecule can be drawn as illustrated in Figure 2.2. The structure of this molecule consists in aromatic or hydroaromatic clusters linked by aliphatic bridges.

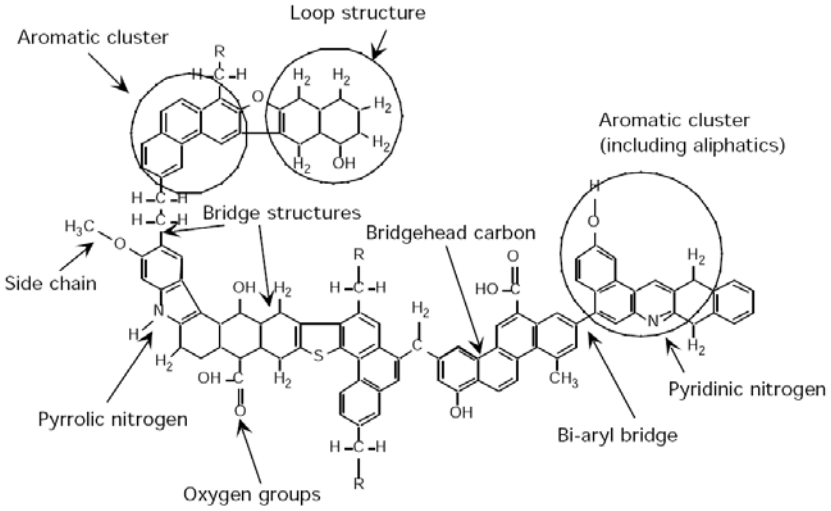

Figure 2.2: Structure of the hypothetical coal molecule [23] adapted from [21].

Physical structural analysis Other physical properties of coal and chars may be determined, such as LCV, heat capacity, thermal conductivity, skeletal and apparent densities, poros-

[3] ^{13}C-NMR : Nuclear Magnetic Resonance of the carbon-13 isotope
[4] FTIR : Fourier Transform InfraRed

ity, specific surface... Those physical parameters have also a great influence on the coal combustion behavior. These measurements will be described in details in the experimental part.

2.1.2 Petcoke description

The petcoke production was extensively described in the thesis of Commandré [24]. Petcoke is the final solid residue of the oil refining process, after the "coker" that is not present on every refinery.

The way to characterize petcoke follows the same methods as for coal characterization. Thus, the physico-chemical properties of petcoke are presented in Table 2.2

LCV daf[5]	33 000 to 35 000	kJ/kg
C	85 ± 5	w.%
H	3.5 ± 1.5	w.%
O	0.5 to 5	w.%
N	0.5 to 1.5	w.%
S	2 to 8	w.%
Ash	0.5 to 5	w.%
VM	8 to 15	w.%
Moisture	< 1	w.%

Table 2.2: Physico-chemical properties of petcoke [24]

The advantages of petcoke compared to coal are its high LCV, low ash content, low moisture absorption, lower explosion risks and a lower price. Whereas the petcoke disadvantages are a the difficulty of combustion due to the low volatile matters content and low char reactivity to O_2 and the high sulfur content that releases pollutants (SO_x) during combustion.

2.2 The carbonaceous particles combustion

Usually the combustion of carbonaceous particles is divided in four parts as shown in Figure 2.3 [15,24]:

- the inert heating,
- the drying,
- the devolatilisation,
- the homogeneous combustion in the gas phase
- and the heterogeneous combustion of the char.

[5]daf : Dry Ash Free basis

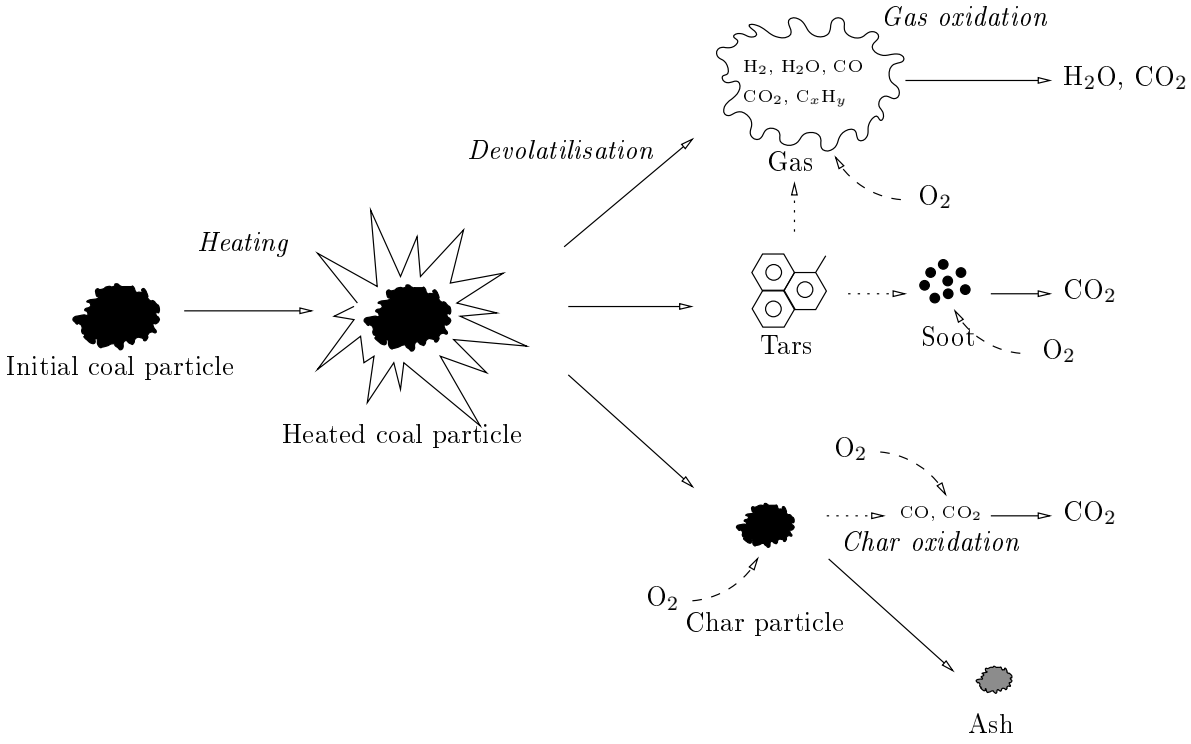

Figure 2.3: Schematic description of the different steps of the combustion of a carbonaceous particle adapted from [14]

2.2.1 The inert heating of the particle

Even if during the heating of the inert heating of the particle no chemical reactions of combustion occur, this step is very important for the later combustion behavior.

Indeed in industrial furnace, the initially cold fuel particle is heated at rates from 10^3 to 10^5 K/s [14, 15, 24, 25]. At such high heating rates, different physico-chemical transformations occur than at slower heating rates. The effect of heating rate is commonly presented by its influence on pyrolysis or char oxidation behaviors [22, 26–28]. These aspects will be detailed in the devolatilisation and char oxidation paragraphs.

To reproduce as close as possible the industrial furnace conditions, a lot of different experimental set-up were used in the literature [22]. The EFR[6] is the most commonly used laboratory device to represent industrial furnaces conditions [14,15,22,24,29]. In such equipment, the fuel particle heating is dominated by convection [15].

2.2.2 The devolatilisation

When the particle reaches a temperature around 600 K [15,24], the fuel thermal decomposition begins : this is the devolatilisation. This extremely fast phenomenon was extensively studied under inert an atmosphere, corresponding to pyrolysis conditions [13–15, 21, 22, 28, 30–32]. The devolatilisation is a very important stage during the combustion process : up to 70 % of the fuel mass can be released at this moment [22]. The pyrolysis yields three different products, in

[6]EFR : Entrained Flow Reactor

different physical state, varying with temperature and coal rank [15,33] :

- gaseous species : CO, CO_2, H_2, H_2O, C_xH_y, N-species (HCN, NH_3) and S-species (SO_2, H_2S),
- liquid species (at ambient temperature) : condensable hydrocarbons, called tars whose molecular weight may reach 2000 g/mol [22],
- and a solid residue : the char. The char physico-chemical properties change widely during the pyrolysis : the carbon content increases, specific surface rises and the particle diameter may increase [15,24].

2.2.2.1 Mechanism and released species

The coal devolatilisation is a very complex process, that occurs mainly in two stages, called primary and secondary pyrolysis, represented in Figure 2.4.

The heat energy income will tend to break the hypothetical coal molecule at its weakest points, called "bridges" in Figure 2.2. This step is the primary pyrolysis that yields tars, CO, CO_2, H_2O or light hydrocarbons. This primary tars have a very similar composition to the initial coal, since they correspond to entire pieces of the initial molecule [13,21].

During the secondary pyrolysis, additional gases like CO, CO_2, H_2, and light hydrocarbons are released from the thermal decomposition of the char residue and of the primary tars [21,22,31, 32]. Serio et al. [32] have shown that the tar overall conversion increases with the temperature up to 60 % at 900°C. Because of the secondary pyrolysis stage, the composition of pyrolysis products changes with temperature [30,34]. Other species like nitrogen or sulfur species are also released during the secondary pyrolysis [23], as shown in Figure 2.4.

The gas species mole fraction measured by Cho et al. [30] during secondary pyrolysis experiments at different temperatures, at high heating rates (10^4 K/s) for three different coals are presented in Figure 2.5. Oil (meaning tars, here) and other hydrocarbons mole fractions, except C_2H_2, decrease with temperature. In an other hand, H_2, CO and C_2H_2 increase with temperature in all case of fuel.

Cai et al. [26] studied the effect of the final temperature and heating rate on devolatilisation products. Their experiments clearly show an increase of the total volatile matters amount with the pyrolysis peak temperature. This is confirmed by Van de Steene [15], whose experimental results are presented in Figure 2.6. He carried out his experiments in the Entrained Flow Reactor in Albi, and studied mass loss during the devolatilisation by measuring the ash content ratio, known as "ash-tracer method".

The tar amount remain constant above 700°C. The heating of the particle is also very sensitive: the quicker the heating, the more volatile matters are devolatilized. Above 1000 K/s, the tar amount levels off [26].

The chars produced during these experiments were analyzed and their reactivity to O_2 [26]. It indicates that the reactivity – strongly correlated to the ratio H/C – decreases with the

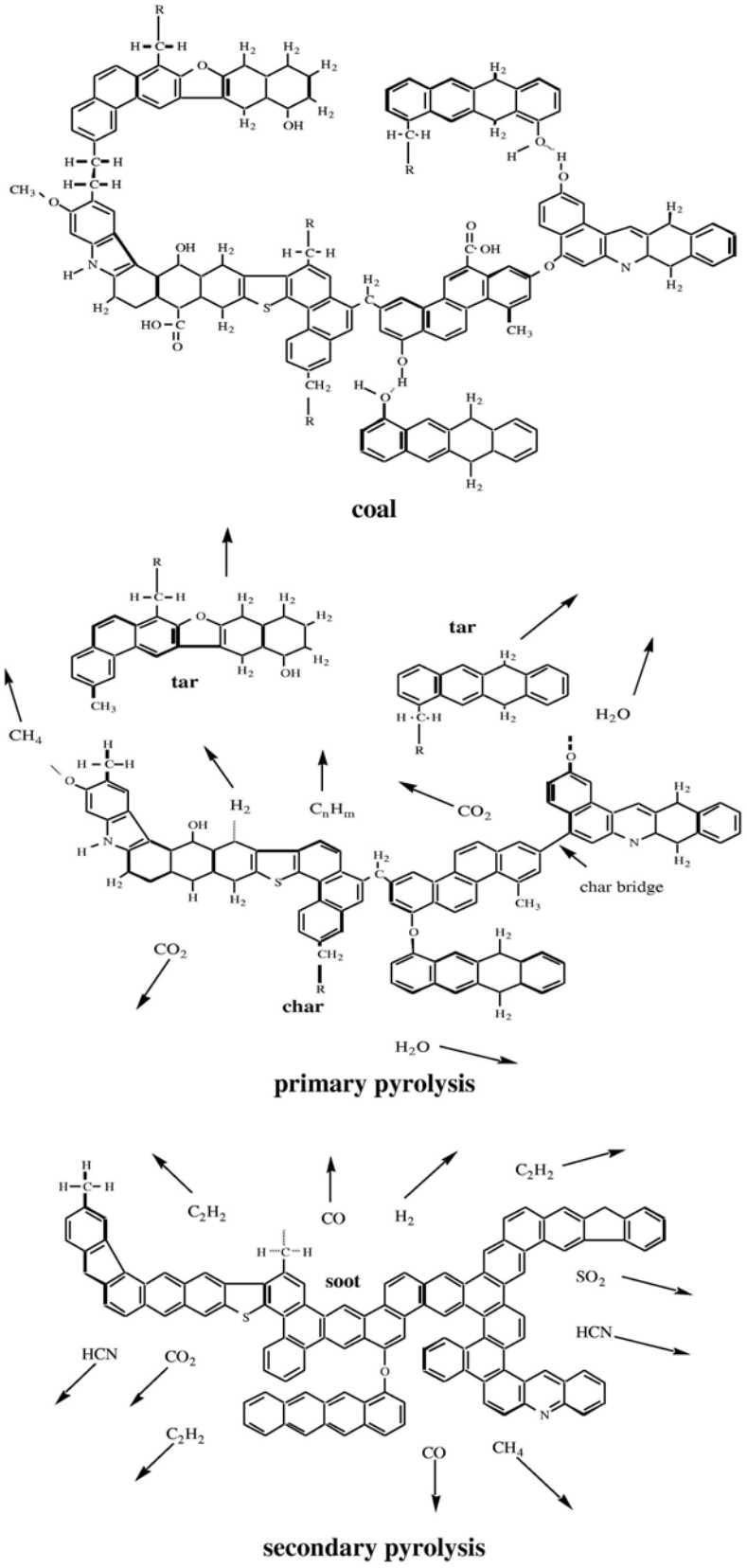

Figure 2.4: Stages of pyrolysis viewed at the molecular level [23] adapted from [21].

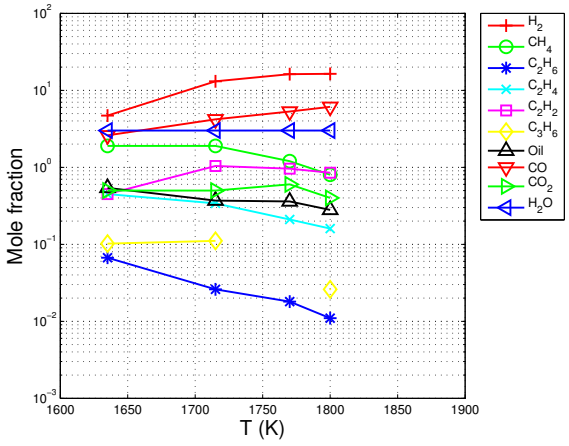

(a)

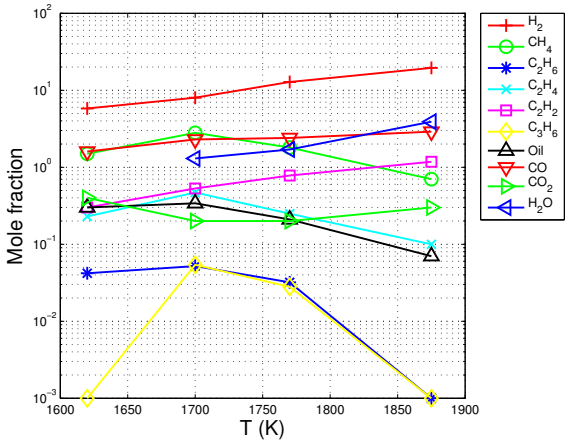

(b)

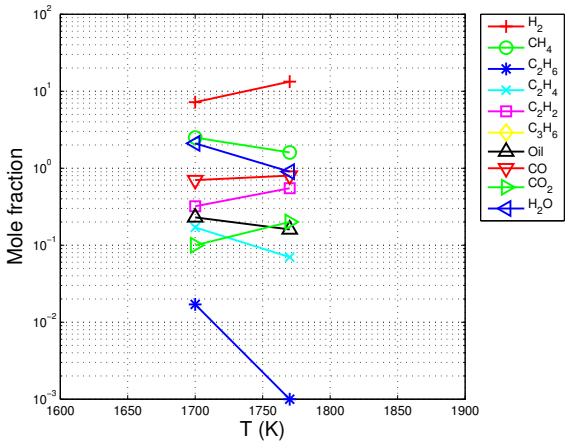

(c)

Figure 2.5: Effect of the secondary pyrolysis temperature and of the coal rank on the released species. Data from Cho et al. [30]. Figures 2.5(a) and 2.5(b) : data from two high-volatile bituminous coals, Figure 2.5(c) data from a low-volatile bituminous coal.

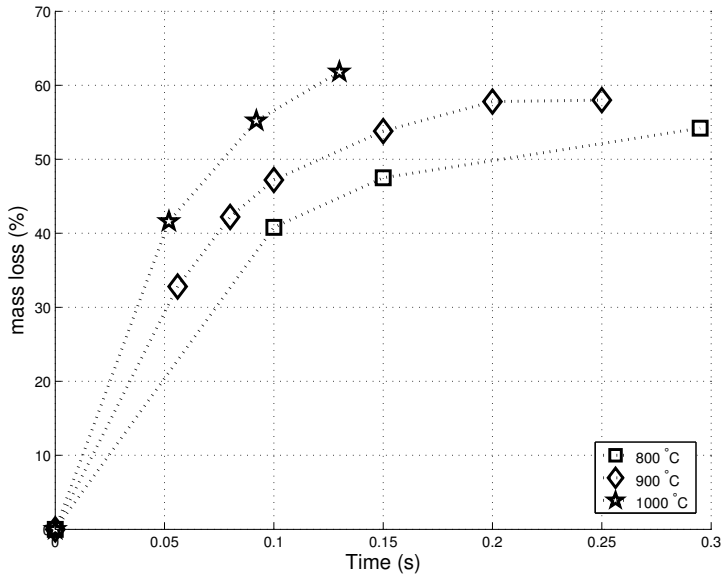

Figure 2.6: Temperature influence on devolatilisation kinetics as a function of the residence time [15]

pyrolysis peak temperature. The high temperature favors an ordering of the carbon structures and consequently a decrease of the char micro-porosity : the thermal annealing. The increase of pyrolysis heating rates increases the chars reactivity up to rates of 1000 K/s. However, Mermoud et al. [35] have shown that the reactivity of chars is highly dependent on the heating rate, whereas the final peak temperature has a lower influence.

2.2.2.2 Devolatilisation modeling

The devolatilisation kinetic aspects are often described by the mass loss rate of the initial coal particle. The kinetics of this mass variation was often modeled by pseudo-Arrhenius laws. The mass balance for a single particle could be written as follows (Eq. 2.2) :

$$\frac{\partial m_{Fuel}}{\partial t} = -\frac{\partial m_{Vol}}{\partial t} - \frac{\partial m_{Char}}{\partial t} \tag{2.2}$$

The simplest approach to model the devolatilisation is to set a constant rate, as expressed in Equation 2.3 :

$$\frac{\partial m_{Fuel}}{\partial t} = K \tag{2.3}$$

The kinetic devolatilisation rate was also modeled by a single pseudo-Arrhenius law (Eq. 2.4 to 2.6) [24,36,37].

$$\frac{\partial m_{Fuel}}{\partial t} = -k_{dev}.m_{Fuel} \tag{2.4}$$

$$\frac{\partial m_{Vol}}{\partial t} = \alpha_{dev}.k_{dev}.m_{Fuel} \tag{2.5}$$

$$k_{dev} = A_{dev}.\exp\left(-\frac{E_{a_{dev}}}{R.T_p}\right) \tag{2.6}$$

where α_{dev} is the volatile matters content.

But to provide a better modeling of these phenomenon, Kobayashi [38] and Ubhayakar [39], developed a "two competing rates" model. Thus, coal will decompose into volatiles matters (VM_1) and char ($Char_1$) because of the first reaction and into VM_2 and $Char_2$ with the second reaction (2.7).

$$\text{Fuel} \longrightarrow \begin{array}{lcll} \alpha_1\,\mathrm{VM}_1 & + & (1-\alpha_1)\,\mathrm{Char}_1 & (1) \\ \alpha_2\,\mathrm{VM}_2 & + & (1-\alpha_2)\,\mathrm{Char}_2 & (2) \end{array} \tag{2.7}$$

As expected from the devolatilisation mechanisms detailed in section 2.2.2.1, the mass loss kinetics are strongly dependent on the heating rate. Indeed, Commandré [24] has shown the great differences between low heating rates of several K/min in TGA[7] experiments and "flash" pyrolysis kinetics in EFR experiments.

A lot of work was done by different authors during the 80's and 90's to model the physical mechanism described in section 2.2.2.1. Solomon and his team proposed an analysis based on the structural analysis of coal. Two models, the Functional Groups (FG) model and the Depolymerization–Vaporization–Cross-linking (DVC) model, were combined in the FG-DVC[8] model [21,31,32]. In this model devolatilisation is separated into two steps: primary pyrolysis that corresponds to the breakage of a macro-molecule giving tars and light gases (CH_4, light aliphatic, H_2O, CO_2) and the secondary pyrolysis that consists in the release of other gas (CH_4, H_2, CO, and HCN). This approach considers the activation energy of the bridges between the different functional groups, taking the cross-linking into account. This FG-DVC model provides a good description of the different products released during the pyrolysis, particularly the ratio between char, tars and volatiles.

Another model, FLASHCHAIN, proposed by Niksa [40], or the Chemical–Percolation–Devolatilization (CPD) model from Fletcher [41] give satisfactory results. They are all based on complex structural data.

2.2.3 The gas phase reactions : homogeneous oxidation and pollutant chemistry

In the gas phase, a large number of chemical reactions happen. The thermal and mass balance is strongly dominated by the oxidation of major species (CO, H_2 and hydrocarbons). However, the pollutants formation, and particularly NO_x, are governed by reactions involving minor species [42].

The volatiles released during the devolatilisation are mostly CO, CO_2, H_2 and hydrocarbons and represent a complex mixture of gases [24,25,28,30]. Those gases may be modeled by a pseudo-molecule $C_xH_yO_zN_nS_s$. This representation is useful to describe globally the gas phase

[7] TGA : Thermo-Gravimetric Analysis
[8] FG-DVC : Functional Group – Depolymerization Vaporization Cross-linking

reactions. In the expression 2.8, λ represents the air excess.

$$\begin{aligned} \mathrm{C}_x\mathrm{H}_y\mathrm{O}_z\mathrm{N}_n\mathrm{S}_s + \lambda\Big(x + \frac{y}{4} - \frac{z}{2} + s\Big)\Big(\mathrm{O}_2 + 3,77\mathrm{N}_2\Big) \longrightarrow x\mathrm{CO}_2 + \frac{y}{2}\mathrm{H}_2\mathrm{O} \\ + \lambda\Big(\frac{n}{2} + 3,77\Big(x + \frac{y}{4} - \frac{z}{2} + s\Big)\mathrm{N}_2\Big) + s\mathrm{SO}_2 + (\lambda - 1)\Big(x + \frac{y}{4} - \frac{z}{2} + s\Big)\mathrm{O}_2 \end{aligned} \tag{2.8}$$

This type of description is also often used to simplify the combustion phenomena, in a first approach. This point of view supposes that only CO_2 and H_2O are the oxidation products of an hydrocarbon.

Different gas phase mechanisms were developed to match the experimental oxidation kinetics. The more simplistic approach is to consider only one reaction. For example, Westbrook and Dryer [43] proposed the following kinetics for ethane oxidation:

$$\mathrm{C}_2\mathrm{H}_6 + \frac{7}{2}\mathrm{O}_2 \longrightarrow 2\mathrm{CO}_2 + 3\mathrm{H}_2\mathrm{O} \tag{2.9}$$

$$\frac{\mathrm{d}\, m_{\mathrm{C}_2\mathrm{H}_6}}{\mathrm{d}\, t} = 1.1 \cdot 10^{12}.\exp\left(\frac{15098}{T}\right) \cdot [\mathrm{C}_2\mathrm{H}_6]^{0.1} \cdot [\mathrm{H}_2\mathrm{O}] \tag{2.10}$$

However, the preceding expressions cannot describe the production of unburnt species and the majority of pollutants. Indeed, the equilibrium observed between CO_2 and CO or between H_2O and H_2 are not taken into account in such global representation and large difference of oxidation kinetics between hydrocarbons [42]. Therefore, authors have built mechanisms with several reactions including the intermediate species CO. In its coal oxidation modeling, Van de Steene [15] used the kinetic parameters determined by [43] for oxidation of methane (CH_4) and benzene (C_6H_6).

In the reality, the reactions involve radical species in a chain of elementary reactions, like the following $\mathrm{OH} + \mathrm{H}_2 \rightleftharpoons \mathrm{H}_2\mathrm{O} + \mathrm{H}$ [42, 44–46]. In this reaction the species OH and H are called "radicals". They have an extremely high reactivity, and therefore a very short life time. These species are essential in the reaction mechanisms and they have to be taken into account to describe correctly the kinetics of the overall conversion of initial species into final oxidized ones.

In order to achieve this, systems of elementary reactions are built [46]. They are called *detailed mechanisms* and may count several hundreds of species and thousands of reactions. The resolution of those non-linear systems is entrust to computers through softwares like the CHEMKIN II package [47, 48]. This aspect will be more detail in the model description, in Chapter 6.

The accurate prediction of the formation/reduction of minor species, such as pollutants, like NO_x, SO_x or CO, it is necessary to model the gas phase reactions with sophisticated kinetic mechanisms, in order to describe correctly the formation/reduction of certain pollutants, like NO_x, SO_x or CO. Indeed, a lot of radicals, like H, OH, HCCO, HCNO have a great influence on the NO_x chemistry [24, 49–55]. This aspect will be more exposed in details in Chapter 3.

2.2.4 The char oxidation

It is often admitted that the carbon residue (char) begins to oxidize when the devolatilisation and the volatiles oxidation are finished. At this step, the O_2 can reach the surface of the char particle. The char is mainly composed by solid carbon, that yields CO and CO_2 during its oxidation through the following reactions:

$$C_s + \frac{1}{2}O_2 \longrightarrow CO \tag{2.11}$$

$$C_s + O_2 \longrightarrow CO_2 \tag{2.12}$$

The fraction of CO released during char oxidation increases with temperature. Arthur [56] proposed the exponential law (Equation 2.13) to describe this behavior :

$$\frac{n_{CO}}{n_{CO_2}} = 2500. \exp\left(-\frac{51843}{RT_p}\right) \tag{2.13}$$

For example, this molar ratio equals 7.5 at 800°C and 26 at 1100°C [15].

The combustion of a solid-fuel particle is an heterogeneous reaction that, apart from the chemical kinetics, always involves several other mechanisms. Hence the process of a heterogeneous reaction may be divided into the steps [46,57]:

- transport of one or more reaction partners,
- adsorption at active sites,
- chemical reaction,
- desorption of the products of the chemical reaction,
- transport of one or more products.

In this sequence, the overall reaction rate is determined by the slowest of these steps. Due to the exponential temperature dependence of surface reaction rates, the chemical reaction is the limiting step at low temperature (Zone I called "chemical" in Figure 2.7), whereas the reaction rates become so fast at high temperature that pore diffusion (Zone II called "internal diffusion" in Figure 2.7) and gas diffusion (Zone III called "external diffusion" in Figure 2.7) become the rate limiting-processes [46,57].

The char oxidation is often modeled by neglecting the porous diffusion limitation, as follows [7,26,58,59]:

$$\frac{\mathrm{d}\, m_{Char}}{\mathrm{d}\, t} = -k_{OxChar}.S_{reac}.P_{O_2}^n \tag{2.14}$$

Smith [60,61] proposed an average char coal oxidation kinetics following Equation 2.14 by collecting a large number of experimental data. This kinetics is presented in Equation 2.15 and Figure 2.8. One can observe a large dispersion – approximately three orders of magnitudes

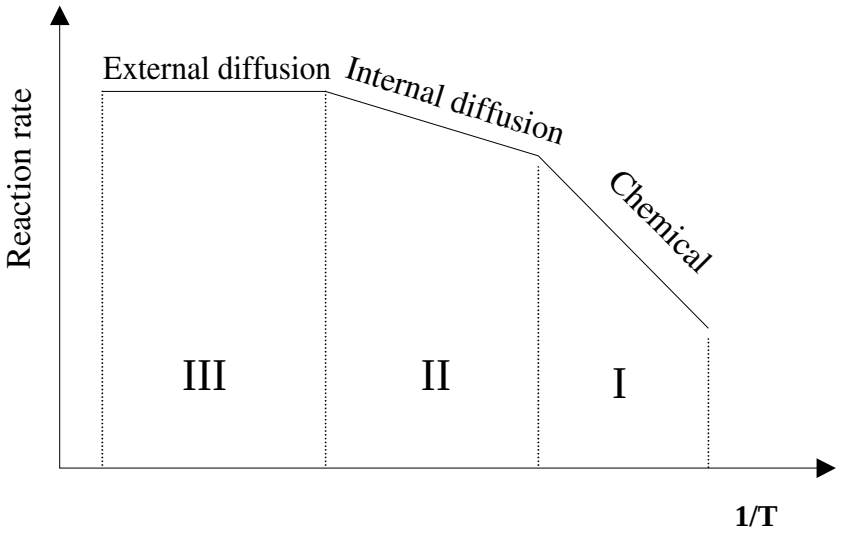

Figure 2.7: Illustration of the three different limitation modes [15,46]

– for the pre-exponential factor k_{OxChar} for different fuels.

$$k_{OxChar} = 3050. \exp\left(-\frac{179400}{RT_p}\right) \tag{2.15}$$

The large dispersion between the experimental values may be due to the difference between fuels. Indeed Tang et al. [62] have shown that the char reactivity decreases with the coal rank. The ashes may also have an influence, since it is well known that the mineral in ash – V, Mo, Mn, Fe, K, Ca... – have catalytic effects [63–65]. Parallel to this, the porous structure changes along the oxidation process [66]. Thus it is very difficult to find universal oxidation kinetics, all the influencing parameters have to be determined experimentally. Moreover, all the chars presented in the Smith study have been produced following different devolatilisation protocol whereas Cai et al. [26] have shown the strong influence of pyrolysis temperature and heating rate on the reactivity.

As it can be seen in Equation 2.14, the reactive surface is a very important parameter in the determination of the char oxidation kinetics. Its measurements could be done following several techniques like BET methods by adsorption of N_2, Ar or CO_2 at the char porous surface, or mercury porosimetry [24,67].

To model the porous diffusion during oxidation of char, Smith [60,61] proposed a reactivity model that allow to describe the coupled diffusion into the porous particle and chemical reaction occurring at the solid porous surface. This model, inspired by Thiele's work on porous catalysts [68], is precisely detailed in [69] and reminded here. As the O_2 comes at the surface of the solid, it diffuses into the porous structure, and oxidizes the carbon. The kinetics of the overall

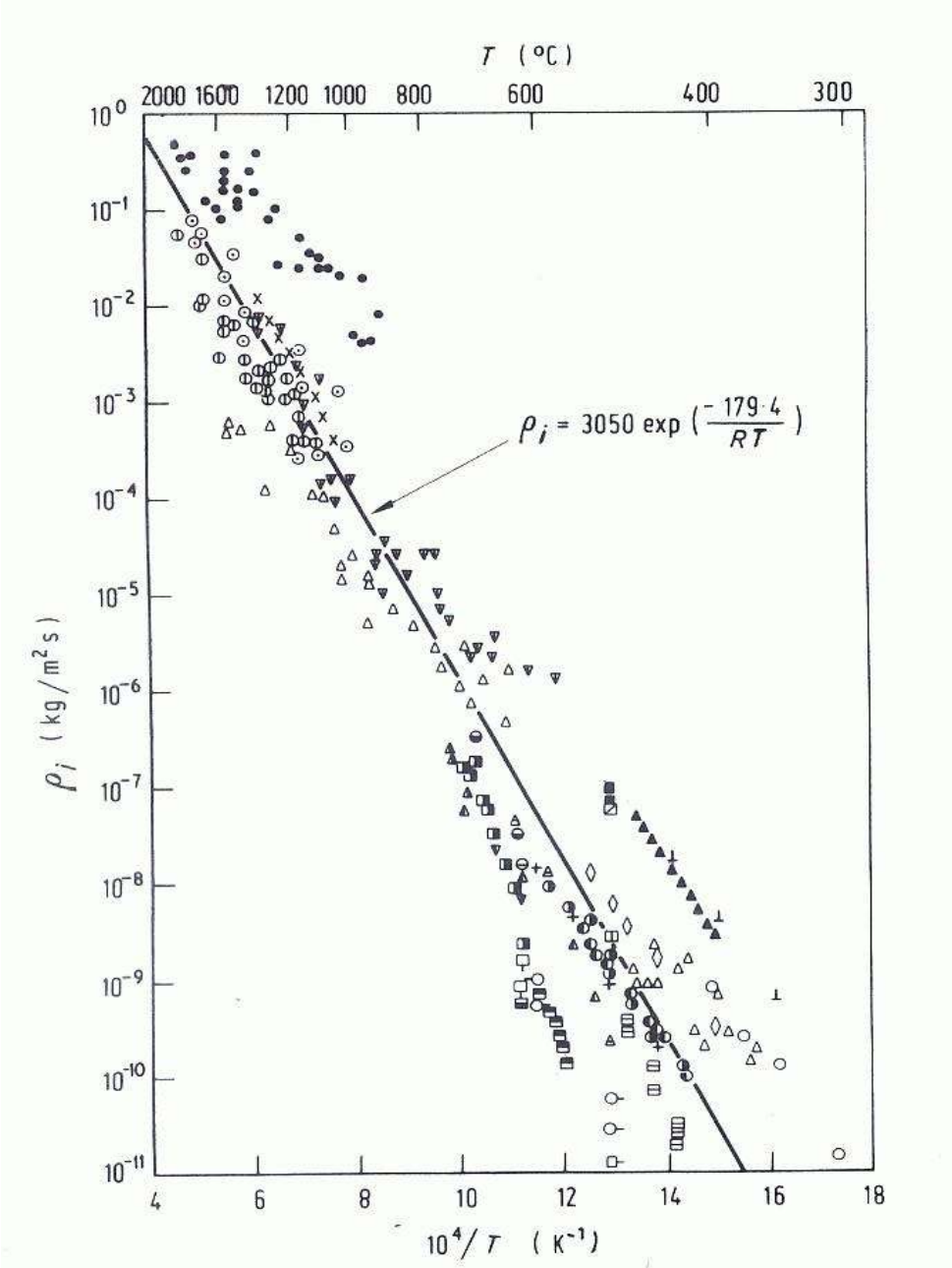

Figure 2.8: Arrhenius kinetic of the char oxidation from Smith [60]. The activation energy is expressed in kJ/mole

heterogeneous reaction can be described through the Equation 2.16:

$$\frac{\mathrm{d}\, m_{Char}}{\mathrm{d}\, t} = -\eta.k_{OxChar}.S_{reac}.P_{\mathrm{O}_2}^{n} \tag{2.16}$$

$$k_{OxChar} = A_{OxChar}.\exp\left(-\frac{E_{a_{OxChar}}}{R.T_p}\right) \tag{2.17}$$

Where A_{OxChar} and $E_{a_{OxChar}}$ are the kinetic constants. S_{reac} is the reactive surface, $S_{reac} = m_p.S_{spe}$. P_{O_2} represents the oxygen partial pressure at the particle surface. n is the order of the reaction. This reaction order, n, in the Equations 2.14 and 2.16 vary in the literature between 0.5 to 1 [7,60,61]. Smith [60] uses a unity value for temperatures greater than 1000 K and 0.5 for lower temperatures.

Assuming a unity reaction order, the effectiveness factor η can then be calculated by means of the pore model [68,69], using pore diameters calculated from the porosity ε, the particle density ρ_p (kg.m^{-3}) and the pore surface area S_{Spe}.

$$d_{pore} = \frac{4.\varepsilon}{\rho_p.S_{Spe}} \tag{2.18}$$

The Knudsen diffusion, D_{Knu} (m^2.s^{-1}), is then

$$D_{Knu} = \frac{d_{pore}}{3}\left(\frac{8.R.T_p}{\pi.M_{\mathrm{O}_2}}\right)^{0.5} \tag{2.19}$$

and the molecular diffusion, D_{mol} (m^2.s^{-1}), is calculated as follow

$$D_{mol} = D_{mol}^{0}.\left(\frac{T+273}{273}\right)^{3/2} \tag{2.20}$$

where M_{O_2} (kg.mol^{-1}) is the molecular mass of O_2 and D_{mol}^{0} the Fick's diffusion coefficient at 273 K for O_2 in N_2 ($D_{mol}^{0} = 1.7 \times 10^{-5}$ m^2.s^{-1}). The effective diffusivity D_{eff} (m^2.s^{-1}) is assumed to be

$$D_{eff} = \frac{\varepsilon}{\tau}.\left(\frac{1}{D_{mol}} + \frac{1}{D_{Knu}}\right)^{-1} \tag{2.21}$$

where τ is the tortuosity. Then the Thiele modulus ϕ and the effectiveness factor η are given by

$$\phi = \frac{d_p}{2}\left(\frac{\beta.S_{Spe}.k_{OxChar}.P_{\mathrm{O}_2,p}}{M_{\mathrm{O}_2}.D_{eff}.[\mathrm{O}_2]_p}\right)^{0.5} \tag{2.22}$$

$$\eta = \frac{3}{\phi}\left(\frac{1}{\tanh\phi} - \frac{1}{\phi}\right) \tag{2.23}$$

where β is the stoichiometry ratio in the reaction between O_2 and C_s (e.g. here $\beta_{\mathrm{O}_2} = \frac{2\times16}{12}$). $P_{\mathrm{O}_2,p}$ is the O_2 partial pressure at the char surface, and $[\mathrm{O}_2]_p$ is its molar concentration (mol/m^3).

Chapter 3

The pollutants formation/reduction : the NO_x chemistry

Contents

3.1 Nitrogen oxides description 41
3.1.1 Health impact 42
3.1.2 Environmental effect 42
3.2 NO_x formation 42
3.2.1 Thermal-NO, or Zeldovich-NO 43
3.2.2 Prompt-NO 43
3.2.3 Fuel NO 43
3.3 NO_x reduction 45
3.3.1 NO_x reduction technologies 45
3.3.2 Gas phase mechanisms 48
3.3.3 Heterogeneous reactions 51

3.1 Nitrogen oxides description

Nitrogen may oxidize in a lot of nitrogen oxides forms, described by the generic term NO_x : mainly NO, NO_2, N_2O, and more occasionally N_2O_3, N_2O_4, N_2O_5. They are naturally present in the atmosphere where they are formed during storms by lightnings or forest and bush fires and also denitrification of nitrate solved in water by bacteria [14, 70].

NO_x are also produced by the human activity, mainly during combustion processes, and represent a strong atmospheric pollution factor, which affects human health and environment, as detailed below. The necessity for NO_x reduction is internationally recognized and effective control technologies have been developed [59]. In the french cement industry, big efforts to reduce NO_x were carried out for several years, allowing the emissions to be reduced of 25 % in 10 years (40 770 tons in 1990 to down 29 760 tons in 2000). Nowadays, the cement plants produce 1.5 % of the french emissions, corresponding to 14 % of the french industrial emissions [9].

The European regulation 2000/76/CE imposes for cement kilns limit values for NO_x fixed at 800 mg/m^3 (STP) for existing plants and 500 mg/m^3 (STP) for new plants. To avoid artificial dilution, this should be measured for O_2 concentration lower than 10 %, in dry air [9].

3.1.1 Health impact

The toxicity of NO is not well known because it oxidizes into NO_2 at ambient temperature. However, NO is aggressive for mucous membranes. NO_2 is strongly oxidant and very aggressive for the respiratory functions. An exposition for more than 15 min at a concentration upper than 5 ppm may cause serious respiratory problems. N_2O is a narcotic gas, formerly used as anesthetic [24, 70].

3.1.2 Environmental effect

N_2O is the most present NO_x in non-polluted atmospheres. It is a greenhouse gas. The global contribution of N_2O to the global warming of the atmosphere is evaluated to 6 % whereas CO_2, CH_4 and CFC are respectively responsible of 49 %, 18 % and 18 % [24, 70]. N_2O is also very stable in the troposphere and may arrive in the stratosphere and so participates to the ozone depletion [14, 24, 46, 70].

Combustion produces mainly NO – 90-95 % of the total amount of NO_x produced – which subsequently oxidizes at ambient temperature into NO_2 [14, 24]. NO_2 is a yellow/brown colored gas, that color the urban polluted atmospheres. Under the sunlight radiations and the presence of unburned hydrocarbons, tropospheric ozone (low-altitude atmospheric layer) and PAN[1] are produced. PAN has a very unpleasant odor and both – ozone and PAN – are very aggressive for lungs : this is photochemical smog phenomenon, encountered in big metropolises in sunny climate (e.g. Los Angeles, Mexico, Athens) [14, 46, 70].

NO and NO_2 also take part into acid rains [71]. This acidity increases the heavy metals solubility, dangerous for health.

3.2 NO_x formation

The nitrogen oxides formation during combustion follows three main routes [24, 46, 72] :

- Thermal-NO, or Zeldovich-NO;
- Prompt-NO;
- Fuel-NO.

[1] PAN : PeroxyAcetylNitrate

3.2.1 Thermal-NO, or Zeldovich-NO

This NO formation mechanism was postulated by Zeldovich in 1946 [46]. Thermal-NO results of the oxidation of N_2 from air through the following mechanism :

$$O + N_2 \overset{k_1}{\rightleftharpoons} NO + N \tag{3.1}$$

$$N + O_2 \overset{k_2}{\rightleftharpoons} NO + O \tag{3.2}$$

$$N + OH \overset{k_3}{\rightleftharpoons} NO + H \tag{3.3}$$

The name of "thermal-NO" is used because of the very high activation energy of the reaction 3.1: 318 kJ/mol, due to the strong triple bond in the N_2-molecule. Thus those reactions are sufficiently fast only at high temperatures (T > 1500°C) [24,45,46,72]. With a flame temperature at about 2000°C, the rotary kiln produces large amounts of thermal-NO [9,10].

3.2.2 Prompt-NO

Fenimore (1970) and Bowman (1973) measured NO concentrations in the vicinity of a flame front higher than the Zeldovich mechanism predictions [24,46]. In this case the N_2 molecule from air is broken by radical CH to yield HCN that reacts further to NO or N_2 [24,45,46,72]. This is the prompt NO formation.

$$CH + N_2 \overset{k_4}{\rightarrow} HCN + N \begin{cases} \nearrow \cdots \rightarrow NO \\ \searrow \cdots \rightarrow N_2 \end{cases} \tag{3.4}$$

Prompt-NO can appear at low temperatures (800°C) in opposition with thermal-NO. Indeed the activation energy for k_4 is much lower (75 kJ/mol) than for thermal-NO (318 kJ/mol) [46] .

3.2.3 Fuel NO

NO-fuel formation mechanism corresponds to the oxidation of the nitrogen constitutive of the fuel itself. This is mainly observed in the case of pulverized fuel combustion, that have always a part of nitrogen in their compounds: at least 0.5 % (kg/kg) of N [24,46,73]. Solid fuel combustion mainly induces the production of Fuel-NO (> 90 % of the overall NO produced during coal combustion) [71–75], resulting from the oxidation of the nitrogen compounds of the fuel. This tendency is further increased in the case of a cement plant calciner: the temperature is low (< 1300°C) and this prevents thermal NO_x formation [24,46].

3.2.3.1 Nitrogen partitioning during pyrolysis

During pyrolysis of a solid fuel, one part of the constitutive N of the fuel is devolatilized and is then oxidized in the gas phase. The other part, remaining in the char, may oxidize during the heterogeneous oxidation or stay in ashes up to 20 % [24]. The repartition of nitrogen during the pyrolysis depends strongly of the coal rank, the temperature and the residence time [14, 41, 74]. At low temperatures (900–1100 K), the main part of the fuel-N is preferentially retained in the char for low rank fuels (60–80 %) [24,27,34,41,74]. The following scheme, in Figure 3.1 represents the nitrogen repartition during the devolatilisation:

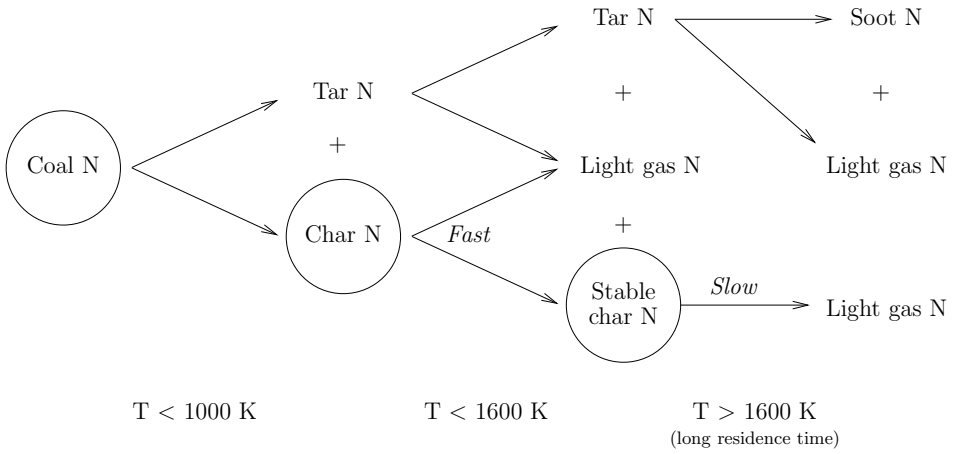

Figure 3.1: Fate of the fuel nitrogen during pyrolysis, from [41].

The N-species released during primary devolatilisation are mainly tars, that can yield light gases during secondary pyrolysis [74]. The light gases released during primary and secondary pyrolysis are mainly HCN, NH_3 and also HNCO [14, 24, 41, 74, 76]. The amount of nitrogen containing volatiles transformed into light gas-phase nitrogen species – HCN and NH_3 – increases with pyrolysis temperature and with decreasing rank of the fuel, up to 60 % for coal [41, 74].

3.2.3.2 Oxidation of N-volatiles

The N-containing volatiles species may be oxidized. At the flame temperature, the nitrogen is rapidly converted into NH and N, further on oxidized into NO while competitively reduced to N_2 according the overall reactions [77]:

$$HCN/NH_3 + O_2 \longrightarrow NO + \cdots \tag{3.5}$$

$$HCN/NH_3 + NO \longrightarrow N_2 + \cdots \tag{3.6}$$

The selectivity between NO and N_2 is principally governed by the fuel/O_2 stoichiometry and the temperature [74, 78]. Other species also present in the combustion system have an influence on the NO formation. CO promotes the oxidation of HCN and NH_3, and also CH_4 and H_2 but in a smaller extent [79].

3.2.3.3 Oxidation of N-char

In combustion systems containing solid fuels such as coal, NO can be both formed and reduced by reactions with the fuel [77]:

$$\text{Char} + O_2 \longrightarrow NO + \cdots \tag{3.7}$$

$$\text{Char} + NO \longrightarrow N_2 + \cdots \tag{3.8}$$

Typically, the overall contribution of NO from char combustion is less than from combustion of the volatiles matters of fuels. However, NO_x formation through char oxidation is less affected by modifications of the combustion conditions than homogeneous NO_x formation/reduction. This makes control of NO_x from heterogeneous formation more difficult [77].

Although it is commonly admitted that NO is the major N-species released during char oxidation, the conversion ratio of N-char into N-species was widely discussed. HCN and HNCO may reach 20 % of the N-char [74]. Visona et al. [80] conclude that assuming the N-char goes either to NO or HCN gives satisfactory results. In most cases, the N-species measured during char oxidation are NO, N_2O, HCN, NH_3 and N_2 [24]. Glarborg et al. [74] precises that for small particles, N-char is oxidized into NO for 75–100 %. Following this repartition, the predictions overestimate the NO concentration. This involves that with increasing particle loading or particle size, reaction of char with NO may serve to efficiently remove NO and reduce the N-char to NO conversion efficiency [24, 74].

3.3 NO_x reduction

The health and environmental effects of NO_x were presented and their formation mechanisms were identified in the preceding sections.

The NO_x reduction techniques are now presented in two steps: first the different industrial techniques are detailed, and then the chemical mechanisms occurring in these processes are reviewed.

3.3.1 NO_x reduction technologies

The NO_x reduction techniques in industrial furnaces may be divided in two categories :

- primary measures, that consist of modifying the combustion conditions to lower the NO_x emissions,
- and secondary measures, consisting in cleaning the flue gas.

3.3.1.1 Primary measures

The principle of primary measures for NO_x reduction is to limit the oxygen concentration and residence time in high temperature zones. The problem is to find the best compromise between

NO_x reduction and combustion efficiency in a short residence time [14].

Recycling flue gas By re-injecting part of the flue gas in the combustion air, the oxygen concentration is lowered. Then the flame temperature is lower and the NO_x concentration is limited [14, 42, 81].

Air staging Following this technique, the oxygen quantity necessary for to the complete combustion is not injected at the main fuel injection: this create a fuel rich mixture where $[O_2]$ is about 85–95 % of the stoichiometry.

The fuel-NO_x formation is lowered: the N-volatiles species are not converted into NO as detailed in paragraph 3.2.3.2. Air is added in cooler zone of the combustion chamber to end the fuel oxidation. This technique is applied for *Low-NOx burners* and *Over Fire Air* installations [14, 42, 81, 82].

Fuel staging or reburning Reburning is among the low-cost and the effective technique that can be used to reduce NO_x from stationary combustion systems [71, 83, 84]. It consists of adding a secondary fuel (10 to 20 % of the total thermal power), frequently natural gas, downstream of the primary burning zone [42, 81], as illustrated in Figure 3.3.1.1, creating a fuel-rich zone that reduces NO_x, by up to 80 % [71]. The unburnt gases are oxidized in the burnout zone by a secondary injection of air: the Over Fire Air. Natural gas is the mostly used as reburning fuel [71].

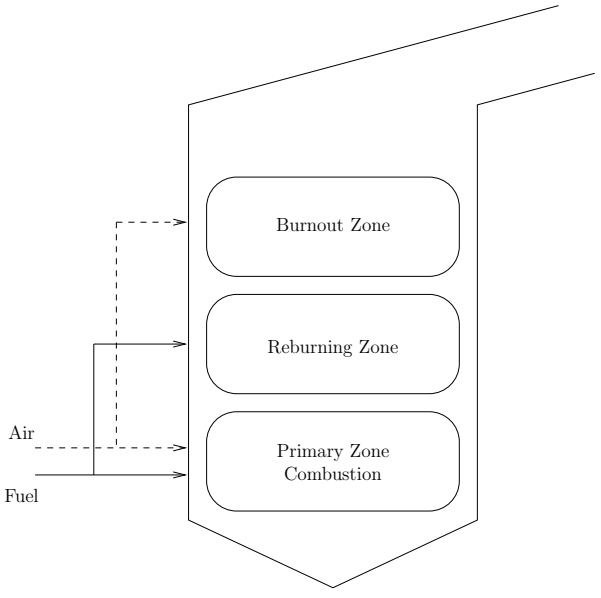

Figure 3.2: Schematic representation of the reburning process, from [42, 71]

Some applications where pulverized coal is used as reburning fuel are presented in the literature [34, 71, 85, 86] showing good NO-reduction efficiency.When pulverized coal is injected, devolatilisation occurs, releasing a large variety of gas species. As presented before, those species are mainly CO, CO_2, H_2, H_2O, CH_4 and other aliphatic or cyclic species and also nitrogen

species, HCN and NH_3 or SO_2. The hydrocarbons species interact with NO and reduce it into N_2. The interactions between NO and the gas species present in the volatile matters (VM) have been widely studied [49–51, 54, 55, 72, 84, 87–89].

NO also reacts with char to form N_2. In the case of coal reburning, the influence of NO reduction at the char surface [67, 75, 90, 91] has to be taken into account. At the present time, the relative contributions of volatile matters and char on the NO reduction process is not fully understood [91, 92]. However, some studies have shown that high-volatile fuels have better reduction abilities than low-volatiles ones [71, 93]. Moreover, Liu et al. [93] also suggest that N-species – HCN and NH_3 – released during pyrolysis could have a positive effect on the NO reduction, in the fuel rich reburning process.

In cement plants, due to the high combustion temperature of the rotary kiln, both thermal and fuel NO are produced there. In the calciner, either in the so-called "combustion chamber" or just downstream of the rotary kiln (cf. Figure 1.4, secondary fuel is injected, creating a fuel-rich zone, also called the "reducing zone". It has been observed that substantial NO reduction occurs in this zone, where the conditions are similar to those of the "reburning" process [24, 58, 59]. These reburning in cement plant calciner is the purpose of the present work.

3.3.1.2 Secondary measures

The secondary measures consist of reducing nitrogen oxides in the combustion flue gas, with or without the use of a catalyst [14].

Selective Catalytic Reduction: SCR The SCR technology is the catalytic reduction of NO_x by ammonia (NH_3). The products of the reduction are N_2 and H_2O. The SCR works in ideal temperature range between 575 and 725 K and allows to obtain NO_x reduction efficiency of 80–90 %. The catalysers are vanadium oxides supported by Titan oxides structures [14, 42].

Using this technology in cement plants requires either catalysts that support the dusty atmosphere, or to reheat the flue gas after de-dusting (energy and investment cost are very high) [9].

Selective Non-Catalytic Reduction: SNCR The SNCR – also called by its first commercial name *Thermal De-NO_x* – is an attractive technology to reduce NO_x because at high temperature (in the range 1100–1300 K) it avoids to use catalysts. The principle is to inject products precursors of NH_i radicals involved in the NO_x destruction mechanism. Those products are ammonia NH_3, urea $(NH_2)_2C{=}O$ and cyanuric acid $(HOCN)_3$.

SNCR is widely used in the world for a large variety of fuels for power-plants. The reduction efficiency can reach 80 % in ideal laboratory conditions but only 40–50 % at industrial scale [42]. In case of the cement industry, several examples exist with the different nitrogen products, also with recovery of ammoniated water from a Kodak plant. The investment for such DeNOx systems in cement plants is comprised between 600 000 € (involving a daily cost 622 €/t_{NO_x} or 1.76 €/$t_{clinker}$) and 1 130 000 € (involving a daily cost 478 €/t_{NO_x} or 0.71 €/$t_{clinker}$) [9].

3.3.1.3 Alternative technologies

The *Advanced Reburning* process corresponds to the addition of nitrogenous gas in the reburning zone, in the Over Fire Air or downstream [42,86,94]. Zamansky et al. [94] proposed to add also sodium to enhance NO-reduction by NH_i radicals. The reduction efficiency can reach 90 %.

3.3.2 Gas phase mechanisms

In this section, the chemical mechanisms involved in the gas phase of an industrial process detailed above are discussed in more details.

3.3.2.1 The reactions involved during SNCR: NO + NH_i

Even if NH_i + NO $\rightleftharpoons$ N_2 + products ($i = 0, 1, 2$) reactions occur, NH_2 is the most reactive species at the SNCR temperatures, from 1100 to 1300 K [83,95].

The NO_x reduction is based on the reaction NH_2 + NO, where NH_2 is formed by the decomposition of the following precursors [42,96]:

- Ammonia – NH_3

$$NH_3 + OH \rightleftharpoons NH_2 + H_2O \quad (3.9)$$
$$NH_3 + O \rightleftharpoons NH_2 + OH \quad (3.10)$$

- Cyanuric acid – $(HOCN)_3$

$$(HOCN)_3 \rightleftharpoons 3\,HNCO \quad (3.11)$$
$$HNCO + H \rightleftharpoons NH_2 + CO \quad (3.12)$$

- Urea – $(NH_2)_2C{=}O$

$$(NH_2)_2C{=}O \rightleftharpoons NH_3 + HNCO \quad (3.13)$$

Then, the reaction between NH_2 and NO follows two paths:

either

$$NH_2 + NO \rightleftharpoons N_2 + H_2O \quad (3.14)$$

or

$$NH_2 + NO \rightleftharpoons NNH + OH \quad (3.15)$$
$$NNH + M \rightleftharpoons N_2 + H + M \quad (3.16)$$

The first path closes the reactions chain, because of the consumption of one radical,

whereas the second path allows the reactions to be entertained through the formation of OH and H radicals [42, 96]. The modeling of SNCR is very sensitive to the branching fraction between these two reaction paths. Indeed, because of the "low" temperature in the SNCR zone, the radical pool is quite poor, and only N-radicals allow the reactivity to be maintained [42].

3.3.2.2 The reactions involved in Natural Gas Reburning

The NG[2] is mainly composed of methane but also small quantities of ethane and propane are present (CH_4 64–98 %, C_2H_6 0.1–14 % and C_3H_8 0.05–8 %) [97]. Even the reburning efficiency to reduce NO_x was widely demonstrated in laboratories and pilot scale experiments since the end of the Seventies [42], the kinetic analysis is more recent [72, 89, 98].

Miller and Bowman [72] proposed a detailed mechanism – many times updated [49–55, 87, 88] – where the NO-reduction occur through the path $NO \rightarrow HCN \rightarrow N_2$. The main hydrocarbon species interacting with NO in the reburn process are the CH_i ($i = 0, 1, 2, 3$) radicals and HCCO. At high temperatures ($> 1000^{\circ}C$), NO is primarily reduced by CH_2, CH and C whereas at lower temperatures CH_3 and HCCO are the predominant species [87–89]. The main reactions involved in reburning are:

$$\begin{aligned}
C + NO &\rightleftharpoons CN + O && (3.17)\\
CH + NO &\rightleftharpoons HCN + O && (3.18)\\
CH_2 + NO &\rightleftharpoons HCN + OH && (3.19)\\
CH_3 + NO &\rightleftharpoons HCN + H_2O && (3.20)\\
&\rightleftharpoons H_2CN + OH && (3.21)\\
HCCO + NO &\rightleftharpoons HCN + CO_2 && (3.22)\\
&\rightleftharpoons HCNO + CO && (3.23)
\end{aligned}$$

Dagaut and his team studied the NO reduction by a wide range of hydrocarbons – from C_1 to C_4 – and built a detailed mechanism that allows the reburning behavior to be predicted [49–53]. He proposed a ranking list in NO-reduction efficiency : methane < NG < ethane ≤ ethylene < acetylene [84]. Dagaut estimates that the main reaction path goes through C_2H_2 and then HCCO [87] as illustrated in Figure 3.3.

3.3.2.3 Other gas phase reactions

Influence of CO Carbon monoxide is a product of a non-complete combustion of hydrocarbons fuels; it is also released during the devolatilisation of solid fuels. The following overall reaction

$$NO + CO \longrightarrow \frac{1}{2}N_2 + CO_2 \qquad (3.24)$$

is very weak in case of small ratio [CO]/[NO], but for high concentrations of CO, the reduction of NO can reach 50% [24].

[2] NG : Natural Gas

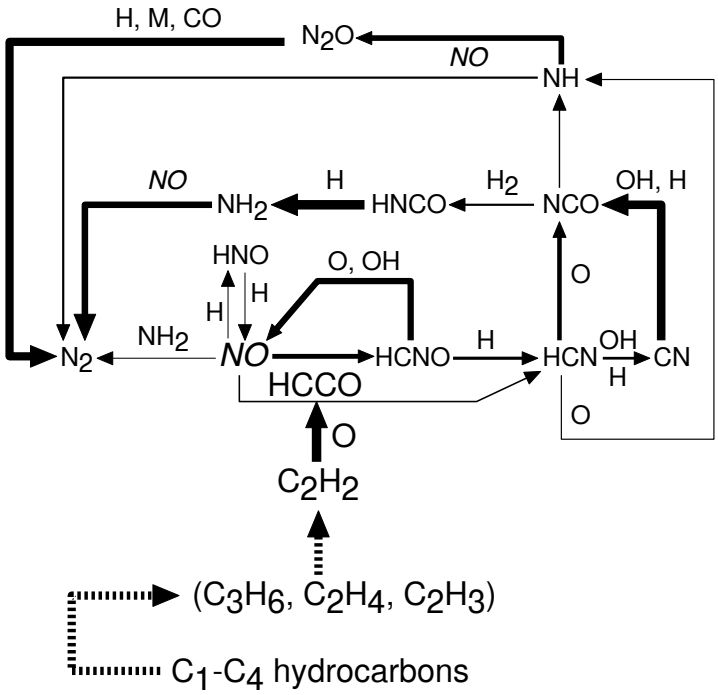

Figure 3.3: Illustration of the main reactions path for NO_x and hydrocarbons interactions [87]

Influence of SO_2 SO_2 is a major atmospheric pollutant released during combustion of coal and heavy fuel oils; it takes part to acid rains [24, 70]. It is released during pyrolysis and char oxidation.

SO_2 is known to limit the NO reduction reactions [54] as well as in case of hydrocarbons oxidation [99]. Indeed, the H radical – very active in NO reduction process – is consumed by SO_2 to yield H_2 in the following termination process

$$\mathrm{H + SO_2 + M} \rightleftharpoons \mathrm{HOSO + M} \tag{3.25}$$

$$\mathrm{HOSO + H} \rightleftharpoons \mathrm{SO_2 + H_2} \tag{3.26}$$

$$\mathrm{HOSO + O_2} \rightleftharpoons \mathrm{HO_2 + SO_2} \tag{3.27}$$

equivalent to

$$\mathrm{H + H + M} \rightleftharpoons \mathrm{H_2 + M} \tag{3.28}$$

and

$$\mathrm{H + O_2 + M} \rightleftharpoons \mathrm{HO_2 + M} \tag{3.29}$$

Dagaut et al. [54] proposes a detailed mechanisms that describe the interaction between NO and C_0 – or H_2 – to C_4 hydrocarbons in presence of SO_2.

3.3.3 Heterogeneous reactions

3.3.3.1 NO reduction by char

The NO molecule can be reduced at the surface of the residual char, following the overall reaction:

$$\mathrm{NO} + \mathrm{C}_s \longrightarrow \frac{1}{2}\mathrm{N}_2 + \mathrm{CO} \tag{3.30}$$

This reaction is slow compared to those in the gas phase but its effect is significant. As in case of heterogeneous oxidation presented in section 2.2.4, the same limitations occur for NO reduction [24,29,67]:

- transport of one or more reaction partners,
- adsorption at active sites,
- chemical reaction,
- desorption of the products of the chemical reaction,
- transport of one or more products.

The reaction between NO_x and coal char were widely studied by different authors. Commandré [24] realized a complete bibliographic review in his PhD, done in the same laboratory as the present work. A summary is presented here.

Aarna and Suuberg [90] made a global review of the different heterogeneous kinetics found in the literature, and proposes a mean reaction kinetics, expressed in Equation 3.32:

$$r_{\mathrm{NO}} = -\eta.k_{\mathrm{NO}}.S_{spe}.m_{Char}.P^{m}_{\mathrm{NO},p} \tag{3.31}$$

$$k_{\mathrm{NO}} = 5.5.10^{6}.\exp\left(-\frac{15939}{T}\right) \qquad \left[\mathrm{g_{NO}.m^{-2}.h^{-1}.atm_{NO}^{-1}}\right] \tag{3.32}$$

The activation temperature $T_a = 15939$ K corresponds to an activation energy of $E_{a_{\mathrm{NO}}} = 133$ kJ.mol^{-1}.

Due to its direct implication in the chemical reaction, the reactive surface determination is a very big issue. Its classical determination is performed through BET method by adsorption of N_2 at the char surface. Commandré et al. [67] have shown that the measurements on the NO reduction by char rates correlate better with the surface area associated with macropores and some mesopores ($>$ 20 nm measured by Hg-porosimetry) than with classical BET areas. They concluded that pores with diameter lower than 20 nm don't participate to the reduction.

The char preparation has also an influence on the NO-reduction kinetics: Commandré et al. [67] found an intrinsic NO reduction kinetics for chars produced under flash conditions in an entrained flow reactor from 50 to 60 times faster than the mean kinetics expressed by Aarna and Suuberg for chars mainly produced in fixed bed or TGA [90].

The comparison of kinetics found in the literature is sometimes difficult due to the different units used by authors to express the kinetic rate constants. Schönnenbeck [29, 100] presents a synthesis of the kinetics of NO reduction by char found in the literature. Even if pre-exponential factors vary, the activation energy proposed by [90] was confirmed by other authors [67, 75, 100]

The NO-reduction by char kinetics is generally accepted to be a first order reaction [24,67, 90]. However, authors found lower reaction order, but always close to the unity: Schönnenbeck found an order of 0.88 [29, 100] and Li et al. [101] propose a reaction order of 0.93.

3.3.3.2 Catalytic reactions

The reduction of NO can be catalyzed by solid (organic or mineral matters). In the next expression 3.33, K symbolizes the catalyst.

$$NO + CO + K \longrightarrow \frac{1}{2} N_2 + CO_2 + K \tag{3.33}$$

Carbon effect The homogeneous reduction of NO by CO presented in the homogeneous reaction paragraph 3.3.2.3 is catalyzed by the presence of char [74, 90, 102].

Mineral catalysts To explain the large differences observed of the intrinsic kinetic rates for NO reduction by char from one fuel to another, authors have studied the catalytic effect of several mineral matters present in coal and petcoke ashes.

Commandré et al. [24, 63] showed that vanadium – V – enhance the NO-reduction by char. He explained the different reactivities between char – factor of 3.5 – through the catalysts presence.

Zevenhoven et al. [102] have shown that calcium – Ca –, sodium – Na – and potassium – K – have positive effect on the heterogeneous NO-reduction, whereas iron – Fe –, aluminum – Al – and sulfur – S – reduce the efficiency of char reduction. Guo et al. [103] also showed an enhancing influence of CaO at high temperature.

Part II

Experimental device, fuels and model description

Résumé de la partie II

Le dispositif expérimental

Les expériences consistant à la détermination des cinétiques des réactions hétérogènes – dévolatilisation, oxydation du char et réduction du NO sur le char – ainsi que celles de reburning ont été menées dans un Réacteur à Flux Entraîné (RFE). Ce réacteur est composé d'un tube en quartz vertical de 8 cm de diamètre intérieur et 2 m de longueur totale. Ce réacteur est chauffé électriquement sur 1,5 m de long à l'aide de trois zones contrôlées en température et respectivement de 0,25, 1 et 0,25 m de longueur (cf. Figure 4.1).

Les gaz constituant l'atmosphère sont préchauffés par des résistances électriques (Figure 4.3), alors que le gaz servant au transport pneumatique des particules est injecté le long de l'axe du réacteur, à l'aide d'une canne d'alimentation refroidie à l'eau. Les débits des gaz sont contrôlés à l'aide de débitmètres régulateurs massiques.

Pour assurer les faibles débits de particules (0,5 à 1,5 g/min), une masse de combustible pulvérisé est précisément pesée sur une balance. Cette masse est ensuite répartie uniformément sur un rail métallique avant d'être déposée sur un tapis roulant se déplaçant à vitesse constante (10 cm/min). Les particules sont dispersées de manière homogène sur la section du réacteur, ce qui permet d'assurer la non interaction entre elles.

Les gaz et les particules – après avoir traversé la zone de réaction – sont échantillonnés à l'aide d'une canne refroidie à l'eau (Figure 4.5). Celle-ci peut être positionnée à différentes distances de l'injection de solide, permettant de prélever les gaz et particules à différents temps de séjour. Une forte proportion (2/3) du débit total du gaz d'atmosphère est prélevée pour assurer la représentativité de l'échantillon et une moyenne des concentrations. Du fait des faibles débits de gaz d'atmosphère utilisés, l'écoulement est laminaire. Ceci permet de calculer le temps de séjour moyen des gaz et des particules par la section échantillonnée dans le four.

Gaz et particules sont ensuite séparés. Les particules sont collectées pour être analysées et les gaz sont conduits vers une série d'analyseurs en continu représentés sur la Figure 4.7. Ces analyseurs sont :

- un analyseur à ionisation de flamme (FID) qui permet de mesurer le méthane, les hydrocarbures totaux et par différence les non-méthaniques;
- une baie d'analyseurs infra rouge à longueur d'onde fixe (NDIR) qui permet de quantifier CO, CO_2, NO et SO_2. Elle est couplée à un analyseur paramagnétique qui permet de

mesurer O_2;

- un catharomètre (TCD) qui détermine la concentration d'H_2 par mesure de conductivité thermique.
- enfin un spectromètre Infra Rouge à Transformée de Fourier (FTIR), qui permet de quantifier NO, NO_2, N_2O, NH_3, HCN, CO, CO_2, CH_4, C_2H_2, C_2H_4, C_2H_6, C_3H_8, C_6H_6 et SO_2.

La préparation et caractérisation des combustibles et des chars

Avant d'être injectés dans le RFE, les combustibles solides sont tamisés pour ne conserver que la tranche granulométrique 30-100 μm. Ainsi les différences de cinétiques observées d'un combustible à l'autre sont uniquement dues aux propriétés du combustible et non à la taille des particules.

Les principales caractéristiques physico-chimiques des combustibles sont mesurées en suivant les normes françaises correspondantes. Ces caractéristiques sont données dans le Tableau 5.1. On remarque que deux combustibles ont un taux de matières volatiles beaucoup plus élevé que les deux autres : le lignite 52 %, le charbon 35 %, l'anthracite 6 % et le petcoke 7 %. Le tracé du diagramme de Van Krevelen (Figure 5.4) permet de situer nos combustibles sur l'échelle des rangs en traçant le rapport H/C en fonction de O/C.

Les chars sont préparés spécifiquement à 900°C sous 3 % d'O_2 pour être réutilisés lors des expériences visant à déterminer les cinétiques des réactions d'oxydation du char d'une part et de réduction du NO sur le char d'autre part. La concentration d'oxygène choisie lors de la production de ces chars est destinée à oxyder les matières volatiles et en particulier des goudrons pour éviter que ceux-ci ne condensent sur les particules. Les chars sont analysés et comparés à ceux obtenus lors de la chauffe lente réalisée en vue de la détermination du taux de matières volatiles.

Les transformations structurales et chimiques lors de la dévolatilisation sont caractérisées à travers des photos prises au Microscope Électronique à Balayage à mode Environnemental (MEBE) dans le Tableaux 5.4 5.5 et de diagrammes comparant les propriétés des chars à celles du combustible initial (Figure 5.5).

Le modèle 1D

Le modèle utilisé pour décrire et interpréter les phénomènes mis en jeu dans le RFE est décrit dans la suite de cette partie. Ce modèle considère une particule sphérique isolée dans un écoulement piston. Il prend en compte les différentes réactions intervenant dans les phénomènes de combustion/reburning.

- Les mécanismes chimiques de la phase gaz (ou réactions homogènes) sont calculés à l'aide de sous-routines du programme CHEMKIN II. Les réactions décrites par le schéma de

Dagaut et al [54] qui compte 145 espèces et 1006 réactions. Outre les interactions NO_x-hydrocarbures, ce schéma prend en compte l'influence du SO_2 sur la chimie des NO_x.

- La perte de masse subie par la particule lors de la pyrolyse est décrite sous la forme d'une simple cinétique du premier ordre.
- Les cinétiques d'oxydation du char et de réduction du NO sur le char (ou réactions hétérogènes) sont elles aussi décrites par des lois d'Arrhenius du premier ordre.

Ce modèle considère deux types d'espèces dégagées : les espèces majoritaires qui sont comptabilisées dans le bilan matière de la particule (CO, CO_2, C_xH_y et H_2) et les espèces minoritaires azotées et soufrées qui sont dégagées proportionnellement à la perte de masse de la particule. Le dégagement de ces espèces est décrit par des coefficients de répartitions qui sont ajustés par confrontation aux données expérimentales spécifiques à chaque réaction hétérogène.

Chapter 4

Presentation of the experimental device

Contents

4.1 The Entrained Flow Reactor (EFR) 59
4.1.1 General description of the EFR 59
4.1.2 The solid fuel feeding 61
4.1.3 The gas flow preheating 61
4.1.4 The reactor furnace 62
4.2 The gas sampling, filtration and analyzing device 63
4.2.1 The sampling 63
4.2.2 The filtration system 66
4.2.3 The gas analysis device 66
4.3 Determination of the residence time 67

4.1 The Entrained Flow Reactor (EFR)

4.1.1 General description of the EFR

The entrained flow reactor was described in Van De Steene and Commandré works [15,24]. It is presented on Figure 4.1. This reactor was designed in order to reproduce the thermal conditions met in an industrial plant, and more particularly in a cement plant precalciner. The maximum operation temperature is 1050°C; the particle and gases residence time can reach 3 seconds.

A gas mixture is previously realized using calibrated mass flow controllers. Then, this mixture is preheated. This gas mixture is the heat and transport vector of the fuel particles inside a 2 m long and 80 mm i.d. tubular quartz reactor. A three-zone electrically heated furnace allows a slightly isothermal flow to be maintained.

The solid fuel particles are injected into the reactor through a water-cooled feeding probe. Then, the reactions occur along the reactor. The gas and solid phases can be collected at different altitudes (z) using a water cooled sampling probe. The gases are forwarded to the analyzers, via a Teflon heated line [24].

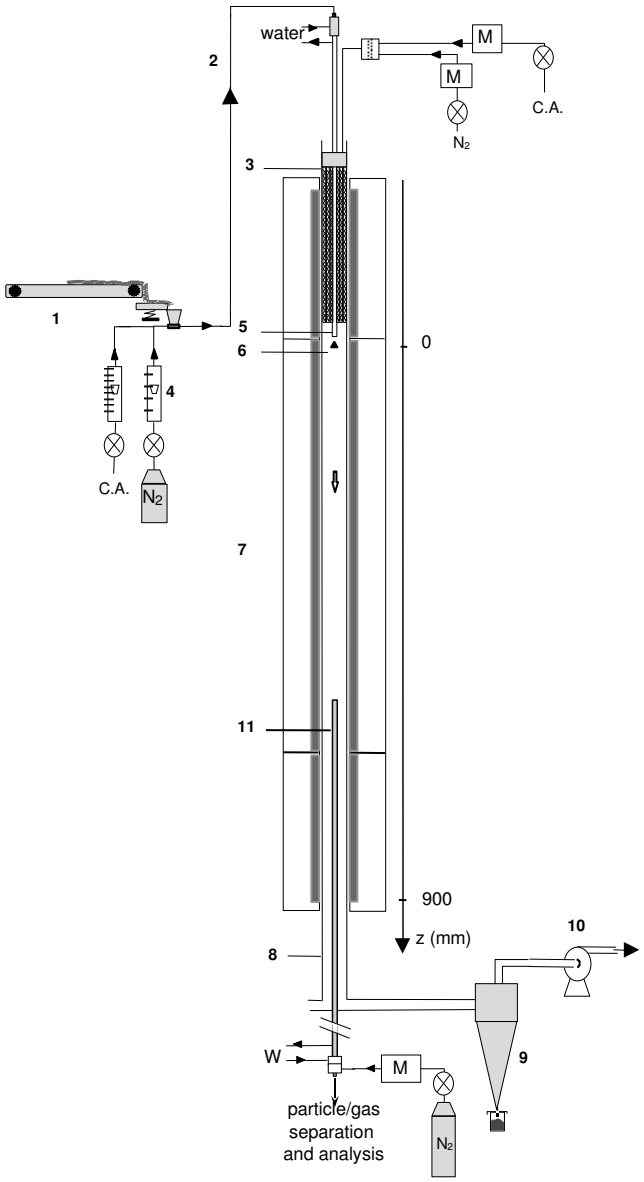

(1)- Conveyor belt, vibrating corridor, ejector;
(2)- Pneumatic transport;
(3)- Electrical preheater;
(4)- Flow meters;
(5)- Water-cooled feeding probe;
(6)- Dispersion dome;
(7)- Three-zone electrical furnace;
(8)- 80mm i.d quartz tube reactor;
(9)- Cyclone collector;
(10)- Exhaust fan;
(11)- Water cooled sampling probe;
W- Water (probes cooling);
M- Mass flow meters and controllers;
N_2- Nitrogen;
C.A.- Compressed Air.

Figure 4.1: Schematic view of the Entrained Flow Reactor of École des Mines d'Albi [15].

4.1.2 The solid fuel feeding

The low particle mass flow rate (0.5–1.5 g/min feeding rate) was ensured by a simple proportioning device consisting of a low velocity conveyor belt (10 cm/min). The belt is fed from separately prepared V-shaped rail along which a precisely weighted quantity of fuel is regularly spread using a calibrated wedge.

The conveyor belt tends to deliver packs (when using sticky powders) ; the flow is perfectly smooth after crossing a vibrating channel (55 cm long in our case). The powder is then driven through a funnel into an injector, and carried to the reactor by pneumatic transport in a 6 mm internal diameter tube using air or N_2. The funnel, the ejector and the pneumatic transport tube are integrated with the vibrating channel, which efficiently suppresses any deposition of the powder between the vibrating corridor and the feeding probe.

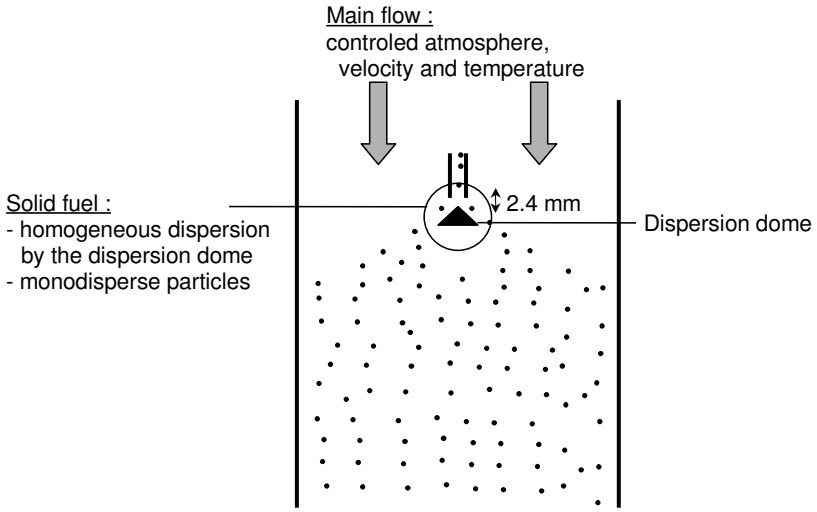

Figure 4.2: Schematic representation of the solid fuel dispersion in the EFR [15, 24].

Particle dispersion in the reactor section – illustrated in Figure 4.2 – is a key to particle non-interaction; for this purpose we used a 10 mm diameter stainless-steel cone located at 2.4 mm below the injection point. The fresh gas sweeping this dispersion device maintains its temperature low enough to avoid fuel sticking [24].

4.1.3 The gas flow preheating

The gas flow will constitute the thermal and chemical environment of the fuel injected into the reactor. The preheater is an assembling of electric resistances, and allows to heat up gases by convective exchange. This electric preheater comprises 12 pairs of spirals resistances which are introduced into 24 silico-aluminous tubes, maintained around a central tube. The tubes positioning is as follows:

- a central silico-aluminous tube maintains the feeding probe in the reactor center. This tube measures 22 mm external diameter and 2,5 mm thickness. It is insulated on its external surface by ceramic wool;

- around the central tube insulator, the 24 silico-aluminous tubes are maintained together by ceramic adhesive, forming two concentric crowns. These tubes are 12 mm in diameter and 2 mm thick.

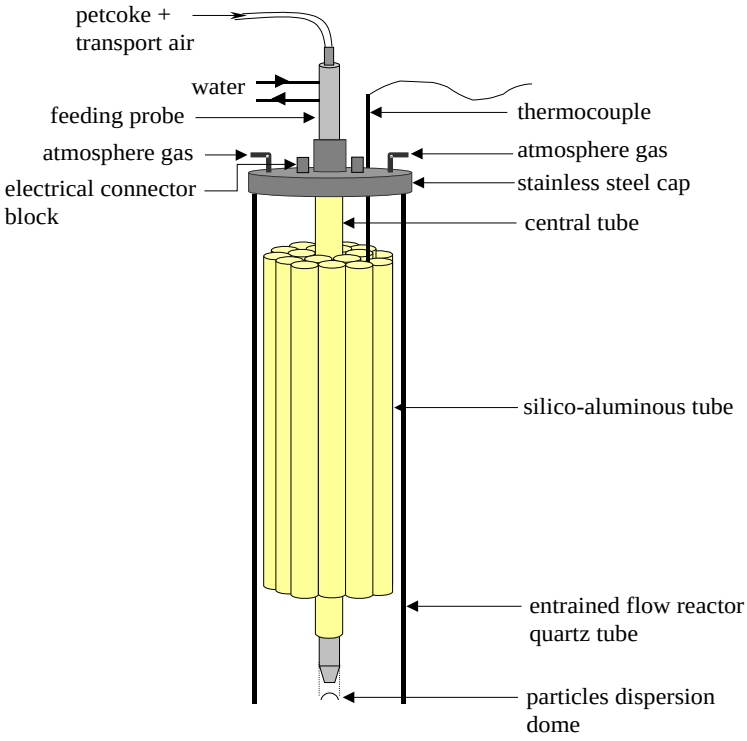

Figure 4.3: Diagram of the electric preheater, with the stainless steel cap and regulation thermocouple introduced into the entrained flow reactor [24].

A descriptive diagram of the electric preheater, that is introduced into the first zone of the electric furnace, is given on Figure 4.3. The power of the electric preheater is 3 kW. The temperature control is carried out thanks to a thermocouple introduced in between the silico-aluminous tubes, that measures the gases temperature at the preheater outlet.

The reactor quartz tube is closed on the top by a stainless-steel cap. This part is centered on the outlet of the quartz tube, and a lip seal ensures the sealing.

4.1.4 The reactor furnace

The quartz reactor is introduced into an 9 kW electric furnace (AET Technologies). The furnace measures 1,65 m in length, and the heated length is 1,5 m. It can reach a maximum temperature of 1050 °C, controlled by three separately heated zones. The first and the third zones measure 25 cm in length, while the central zone is 1 m long.

The thermal profile of the EFR, represented on Figure 4.4 was characterized experimentally, without fuel injection. The furnace and preheater were set at 900°C. This temperature measurements were performed with a temperature probe and were corrected to take the radiation of the furnace wall on thermocouples into account (see Appendix A).

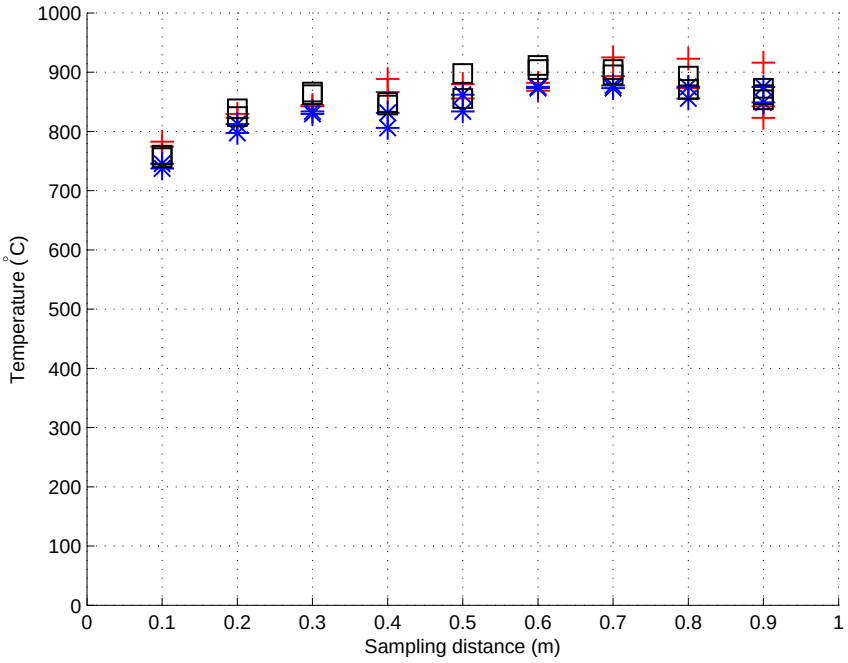

Figure 4.4: Temperature profile of the Entrained Flow Reactor – symbols represent the different thermocouples values – furnace and preheater set-point at 900°C, N_2-transport: 2 l/min (STP) and N_2-atmosphere: 16 l/min (STP).

For low distance to the injection probe, the cold transport flow reduces slightly the flow temperature. Then, the temperature increases and exceeds the set point.

4.2 The gas sampling, filtration and analyzing device

4.2.1 The sampling

Sampling in a gas/solid reactive flow at high temperature is a delicate technique. Indeed, it is necessary to keep the representativeness of the sample, compared to the main flow, and the chemical reactions stopping by a rapid cooling of the samples.

Two different water-cooled probes were used during this work:

- a sampling probe, designed for sampling at different altitudes,
- a collecting probe, designed to collect as much solid as possible.

4.2.1.1 The sampling probe

The sampling probe represented in Figure 4.5 was designed and realized during the PhD of Dr. Van de Steene [15]. This probe, built in stainless-steel, is 1.80 m long, has a 12 mm internal diameter and a 34 mm external diameter. The cooling water is led to the extremity of the probe

by three 1 mm-tubes. A quenching of the reactions may be realized through the injection of cold nitrogen, led to the top of the sampling probe by three other tubes. The external insulation of the sampling probe avoids to disturb the thermal regulation of the furnace.

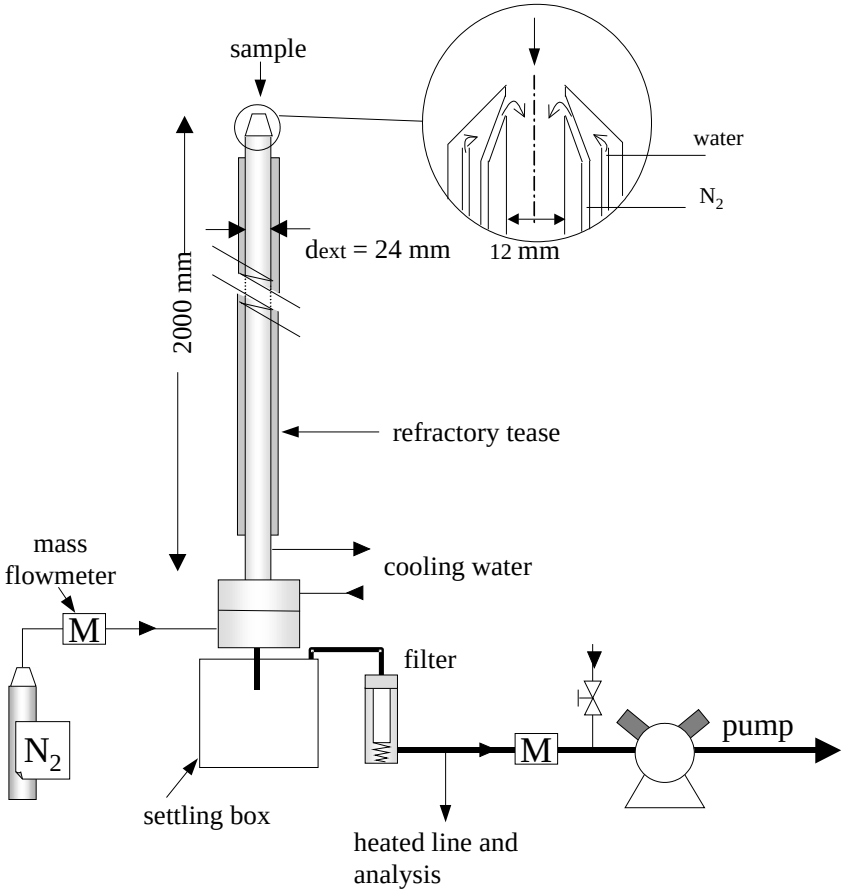

Figure 4.5: The sampling probe description. [24]

4.2.1.2 The collecting probe

The char oxidation and NO reduction by char experiments imply the preparation of several tens of grams of chars. This preparation was performed in the EFR under a controlled atmosphere, and the solids were collected after the desired residence time.

The collecting probe was designed during the PhD of Dr. Commandré [24] to collect the maximum amount of the injected solid. Its external diameter is 60.3 mm, whereas the internal diameter of the EFR equals 80 mm. This water-cooled probe, represented in Figure 4.6, is built in stainless-steel and is composed by 19 vertical tubes that allow to collect and cool down a large part of the solid particles. The conical shape of the top avoids char deposition on the collecting probe.

However, due to its large diameter, this probe may disturb the furnace temperature. Thus, only particle collection at the outlet of the EFR was realized using this probe.

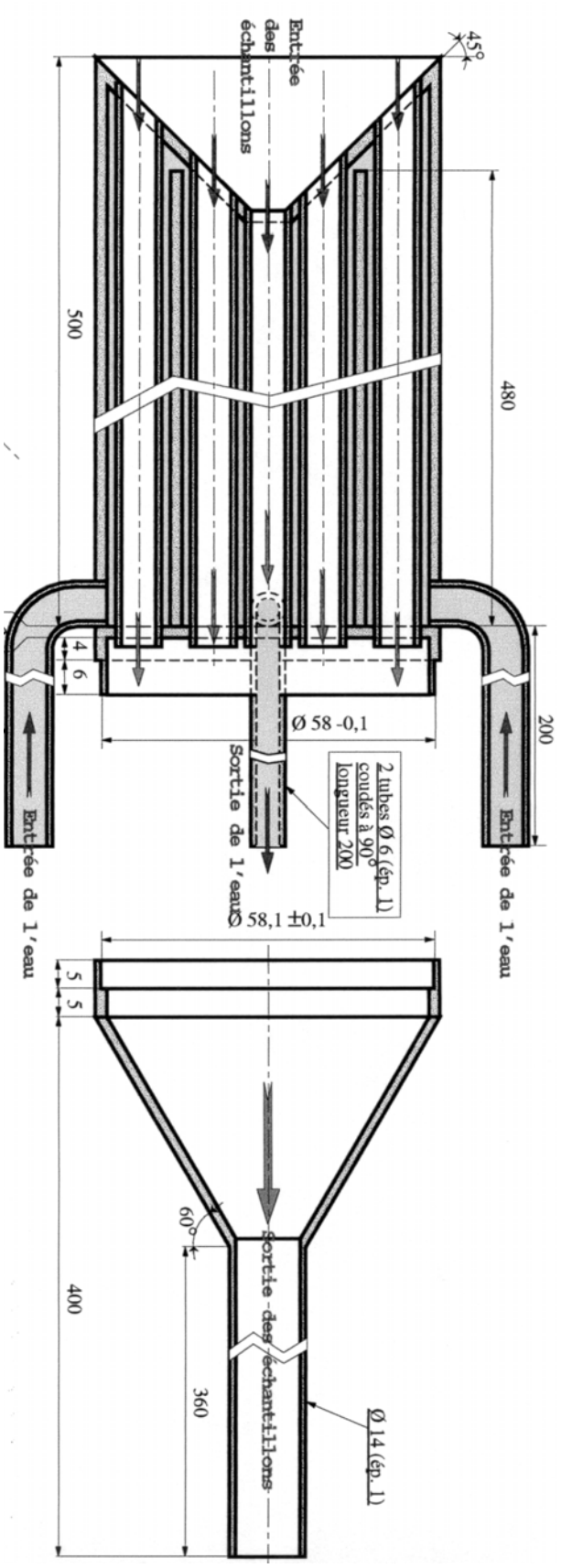

Figure 4.6: The collecting probe description. [24]

4.2.2 The filtration system

The gas analysis is realized after the gas/particles separation represented in Figure 4.5. A settling box is used, where the majority of the solid particles is collected. Downstream the settling box, a glass fiber filter is used to remove the smallest particles. This filter is designed to remove 93 % of the particle larger than 0.01 μm.

4.2.3 The gas analysis device

As we can see in Figure 4.7, the sampled gases will be distributed towards five types of analyzers:

- a COSMA Graphite 655 analyzer, using a Flame Ionization Detector (FID) allows Total HydroCarbon concentrations (THC), Methane (M) and by difference Non-Methane (NM) to be measured,
- a Non Dispersive I.R. (NDIR) SERVOMEX analyzers to quantify CO, CO_2, SO_2, NO and NO_x concentrations ;
- a SERVOMEX paramagnetic analyzer to quantify O_2 ;
- a Thermo Optek NICOLET FTIR analyzer, allows NO, NO_2, N_2O, NH_3, HCN, CO, CO_2, CH_4, C_2H_2, C_2H_4, C_2H_6, C_3H_8, C_6H_6 and SO_2 to be continuously quantified ;
- a SERVOMEX K 1550 Thermal Conductivity Detector (TCD) for hydrogen quantification.

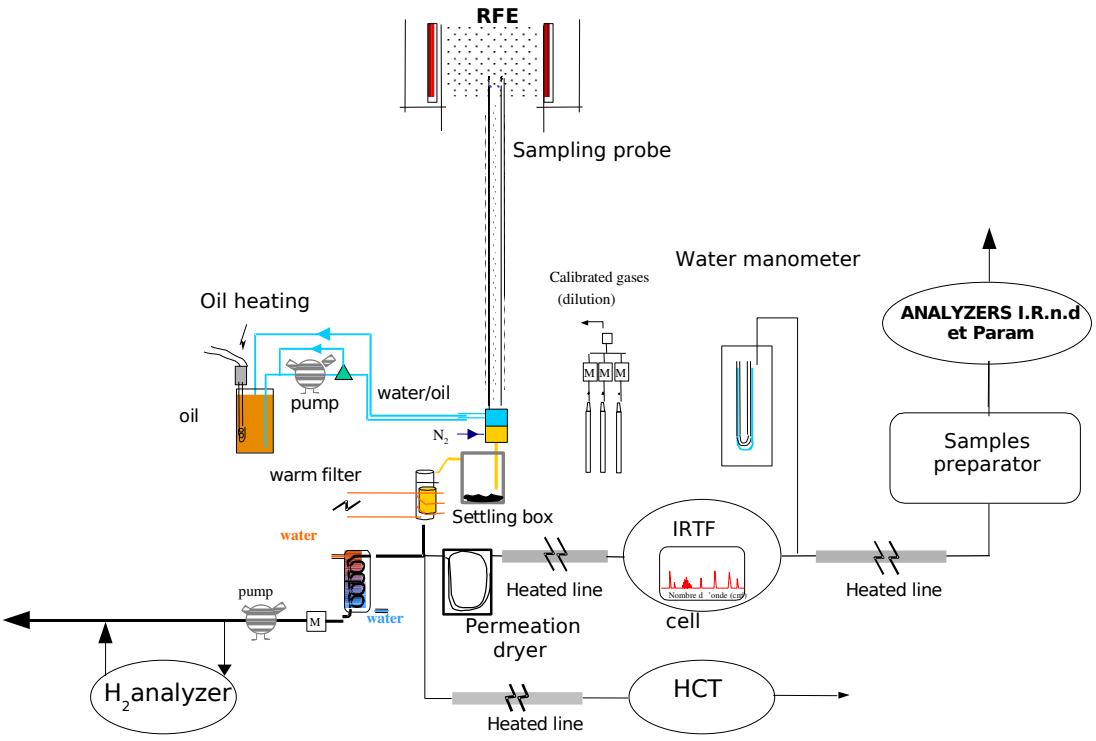

Figure 4.7: Schematic view of the gas analysis device. [24]

Details concerning the principle of the measurement of the different analyzers and their calibration protocol are presented in Appendix C.

4.3 Determination of the residence time

During the experiments, the atmosphere gas introduced into the reactor and the reactor walls were heated to the controlled temperature. The atmosphere gas with controlled concentrations was fed in a total flow rate ($\dot{Q}_{total} = \dot{Q}_{transport} + \dot{Q}_{atmo}$) of 18,55 l/min at STP.

The Reynolds number for an air flow at 1000°C equals only 134 (see Equations 4.2 to 4.1). Thus the flow is fully laminar and has tends toward the theoretical parabolic profile as illustrated in Figure 4.8.

$$Re = \frac{\rho_{air}.\overline{U_{air}}.D}{\mu_{air}} = \frac{0,277.0,287.0,08}{4,76.10^{-5}} = 134 \quad (4.1)$$

with

$$\rho_{air} = \frac{\overline{M_{air}}.P}{R.T} = \frac{29.10^{-3}.101325}{8,314.1273} = 0,277\,\mathrm{kg/m^3} \quad (4.2)$$

$$\mu_{air}(1000°C) = 5 \times 10^{-7}.T^{0.6372} = 4,76 \times 10^{-5}\,\mathrm{kg/m.s} \quad (4.3)$$

$$\overline{U_{air}} = \frac{\dot{Q}_{total}}{S} = \frac{18,55[\mathrm{l/min\ (STP)}]}{60000.\pi.0,08^2}.\frac{1273}{273} = 0,287\,\mathrm{m/s} \quad (4.4)$$

In Equations 4.1 and 4.2, ρ_{air} is the air density, $\overline{M_{air}}$ the air molecular mass, P the pressure, R the ideal gas constant, T the gas temperature, μ_{air} is the air viscosity, $\overline{U_{air}}$ is the mean velocity and S is the cross sectional area of the reactor.

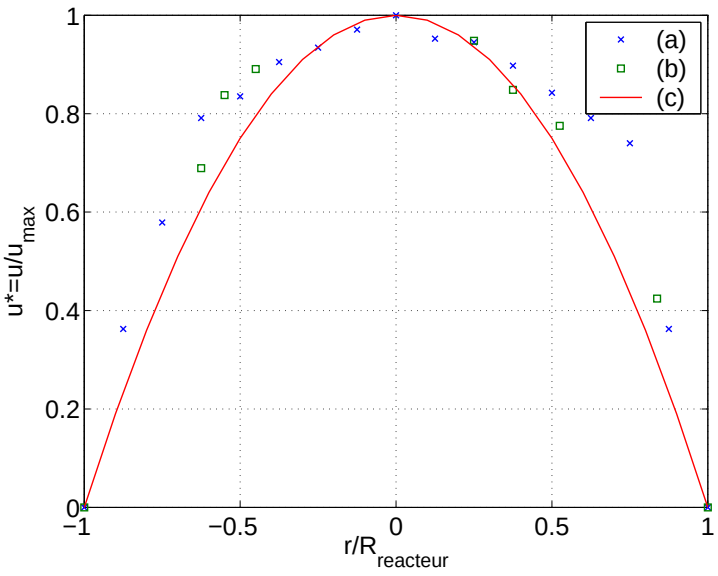

Figure 4.8: Dimensionless velocity profile $u^* = u/U_{max}$ over a reactor section (distance to the injection probe z = 1500 mm) : (a) Cold flow hot wire measurements, (b) Hot flow (700°C) Laser Doppler Anemometry (LDA) measurements, (c) Theoretical parabolic velocity profile in a cylinder.

To achieve satisfactory averaging of the concentrations over a cross section of the reactor, the total flow at the suction of the sampling probe was 12 l/min (STP) out of the 18.55 l/min (STP). Thus, the mean velocity of the sampled gases is different from the mean velocity of the total flow, as illustrated in Figure 4.9.

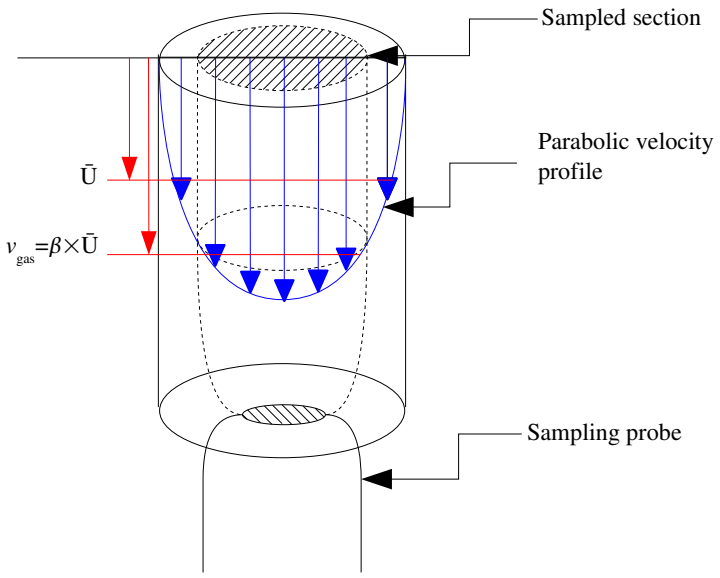

Figure 4.9: Representation of the mean velocities of the total gas flow and the sampled gas flow.

The ratio β of the mean velocity of the sampled section v_{gas} over the mean velocity of the total flow $\bar{U}$ is evaluated to $\beta = v_{gas}/\bar{U} = 1,6$. The detailed calculation is presented in Appendix B.

Because of their density higher than that of the gas have a different velocity than gas. The sliding velocity v_{slide} of particles relative to the gas can be calculated with the Stokes law for a particle smaller than 300 μm [15] :

$$v_{slide} = g.d_p^2.\frac{(\rho_{part} - \rho_{gas})}{18.\mu_{gas}} \tag{4.5}$$

Here g is the gravity acceleration, d_p the particle diameter, ρ_{part} the particle density, ρ_{gas} the gas density and μ_{gas} the gas viscosity.

Finally the gas residence time, Δt_{gas}, and the particle residence time, Δt_{part}, can be

calculated by following Equations 4.6 and 4.8.

$$\Delta t_{gas} = \frac{z}{v_{gas}} \tag{4.6}$$

$$v_{part} = v_{slide} + v_{gas} \tag{4.7}$$

$$\Delta t_{part} = \frac{z}{v_{part}} \tag{4.8}$$

$$z = \text{sampling distance to particle injection}$$

Chapter 5

Preparation and characterization of the fuels and chars

Contents

5.1 Introduction 71

5.2 Physico-chemical analysis methods 72

5.2.1 The proximate analysis 72

5.2.2 The ultimate analysis 73

5.2.3 The physical properties 73

5.3 Preparation and characterization of fuels 73

5.3.1 Particle size calibration 73

5.3.2 Physico-chemical analysis of the fuels 73

5.4 Preparation and characterization of the chars 75

5.4.1 "Flash" chars production 75

5.4.2 "Flash" chars physico-chemical analysis 76

5.4.3 Reference fixed bed chars characterization 77

5.5 Discussion 77

5.5.1 Fuels properties 77

5.5.2 Chars properties 78

5.1 Introduction

To realize this work, four different fuels were supplied by Polysius AG. Three of them represent natural fossil fuels of different ranks: a lignite, a coal and an anthracite. A petcoke was also studied. These four fuels represent the major energy income in the cement industry.

The preparation and the characterization of these fuels is related in the following sections of this chapter.

One purpose of the present work is to characterize independently the heterogeneous kinetic parameters of char reactions, i.e. char oxidation and NO reduction at the char surface. Both production and characterization of the chars are also detailed in this chapter.

5.2 Physico-chemical analysis methods

Both fuels and chars were characterized following the same protocol, detailed in the next paragraph. The physico-chemical analysis performed for our fuels and chars are divided into three parts detailed below:

- the proximate analysis (moisture, ash, volatiles and char contents)
- the ultimate analysis (composition in C, H, O, N and S elements),
- and the physical properties (density and calorific value).

The results of theses analyzes are presented in Tables 5.1 to 5.3.

5.2.1 The proximate analysis

The proximate analysis means the determination of the macroscopic characteristics of a carbonaceous fuel :

- the moisture content,
- the ash content,
- the volatile content,
- the fixed carbon.

The proximate analysis was carried out by following the french standard, describe in section 2.1.1.1:

The moisture content moist. in Table 5.1, was measured following the NF M 03-002 [17] by quantifying the mass loss of the fuel left 24 hours in a drying oven at 110 ± 5°C.

The ash content , Ash in Table 5.1, was measured following the NF M 03-003 french standard. The ash content measurement consists in the weighting of the rest of 1 g of fuel oxidized during 2 hours at 815°C under air atmosphere.

The volatile matters content VM in Table 5.1, was measured following the NF M 03-004 french standard. The volatile content is the mass loss after 7 min soak pyrolysis at 900°C of 1 g of dry fuel. The char residue is stored to be used as a reference char, further called Fixed Bed char.

The "fixed carbon" C_{fix} in Table 5.1, value is calculated by difference to 100 %, as follows 5.1 :

$$C_{fix} = 100 - Ash - VM - moist. \tag{5.1}$$

5.2.2 The ultimate analysis

The ultimate analysis was realized by a chromatograph analyzer NA 2100 Protein of CEInstruments. The oxygen content is calculated by difference, after subtracting the other elements and ash contents.

5.2.3 The physical properties

The lower calorific value, LCV, were measured with a IKA Analysentechnik C5003 Control calorific bomb.

The skeletal density, ρ_{pycno} was measured by a Micromeritics Accupyc 1330 Helium pycnometer.

5.3 Preparation and characterization of fuels

5.3.1 Particle size calibration

Prior to any analysis or experiment, the four fuels previously ground by Polysius were sieved. Only the fraction 30-100 μm was selected:

- the upper limit is representative of that used in industrial furnaces,
- the lower limit is imposed by the EFR pneumatic transport (presented in Chapter 4) problems: the injection probe often stocks when particles smaller than 30 μm are injected.

After this treatment, the particle size was similar for the four fuels, and would not be responsible for any difference observed along the combustion/reburning process.

The separation of the particles smaller than 30 μm is performed by pneumatic sieving, whereas the particles bigger than 100 μm are excluded by manual sieving. A second pneumatic sieving at 30 μm is realized to ensure a reliable 30-100 μm selection. The procedure followed to select the desired particles size is represented in Figure 5.1

5.3.2 Physico-chemical analysis of the fuels

The fuel physico chemical analyzes are presented in Table 5.1. The preceding section 5.2 details the measuring techniques. All the values reported in this table are mean values of series of at least three measurements. This repeatability is realized to ensure a good representativity of the main sample.

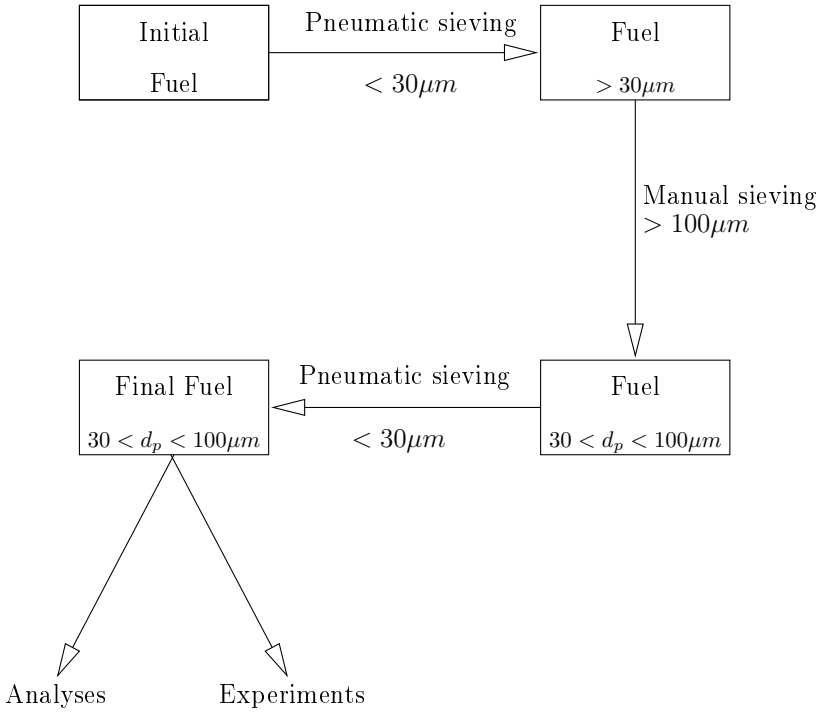

Figure 5.1: Particle size calibration procedure.

	Proximate analysis				Ultimate analysis						
Fuel Name	moist. [w.%]	VM [w.%]	Ash [w.%]	C_{fix} [w.%]	C [w.%]	H [w.%]	N [w.%]	S [w.%]	O [w.%]	LCV [kJ/kg]	ρ_{pycno} [kg/m^3]
Lignite	4.73	51.50	8.66	35.11	59.28	5.07	0.42	1.72	24.85	26702	1420
Coal	3.46	34.76	11.60	50.18	65.27	4.77	1.71	0.45	16.20	25917	1410
Anth.	0.63	5.503	6.32	87.55	84.91	2.75	1.12	0.46	4.44	30765	1280
Petcoke	1.82	6.84	0.5	90.84	83.30	1.85	1.59	5.93	6.83	32759	1580

Table 5.1: Fuel physico-chemical analysis. The values for fixed carbon (C_{fix}) in proximate analysis and O-atoms in ultimate analysis were both calculated by difference to 100 %.

Lignite and coal have similar physico-chemical analyzes: their proximate and ultimate analyzes are close and correspond to low rank coal. They have a high volatile matters and high oxygen content. Their LCV are low compared to those of Anthracite and Petcoke. However, anthracite and petcoke have also similar analyzes, with low VM and O-contents.

Lignite has a lower N-content than the three other fuels, that have similar values. The S content is low for coal and anthracite, with 0.5 %, while petcoke has almost 6 % of sulfur.

5.4 Preparation and characterization of the chars

5.4.1 "Flash" chars production

The chars injected in the EFR to determine the kinetic parameters for char oxidation and NO reduction at the char surface were themselves produced in the EFR. Indeed, their physico-chemical properties strongly depend on their production conditions, particularly heating rate. Thus, before the determination of the kinetics of char reactions (char oxidation and NO char reduction experiments), the chars were produced as follows.

- The total atmosphere gas flow rate in the EFR was 18.55 L/min (STP) and contained 3 $\%O_2$,
- the fuel particle feeding rate was 1.5 g_{Fuel}/min transported by a 2.55 L/min (STP) nitrogen flow,
- the atmosphere temperature was set to 900°C,
- the char particles were then collected after a particle residence time of 2 s.

The 3 % oxygen concentration was set to oxidize the volatile matters, particularly tars, and prevent them from condensing at the char surface. This phenomenon was observed experimentally by Pillet [14] and suggested by Solomon et al [22]. In the literature, the total mass of VM released during high heating rates pyrolysis is classically 1.5 to 2 times greater than the value measured during standard tests [15]. Pillet [14] found lower factor around 1 and explained that the tar or soot condensation at the char surface disturbs the ash tracer method, classically used for the VM quantification.

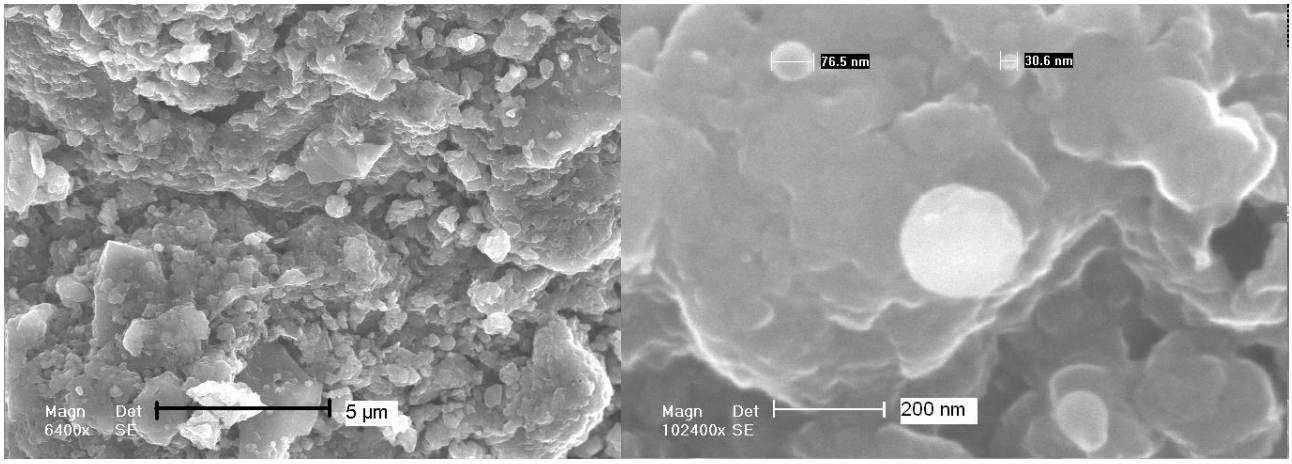

(a) (b)

Figure 5.2: Lignite char: ESEM photographs of tar condensation at the char surface.

In our case, tar condensation at the char surface was also observed in case of pyrolysis under pure nitrogen of high-volatile fuels (lignite and coal). The ESEM[1] photographs in Fig-

[1]ESEM : Environmental Scanning Electron Microscope

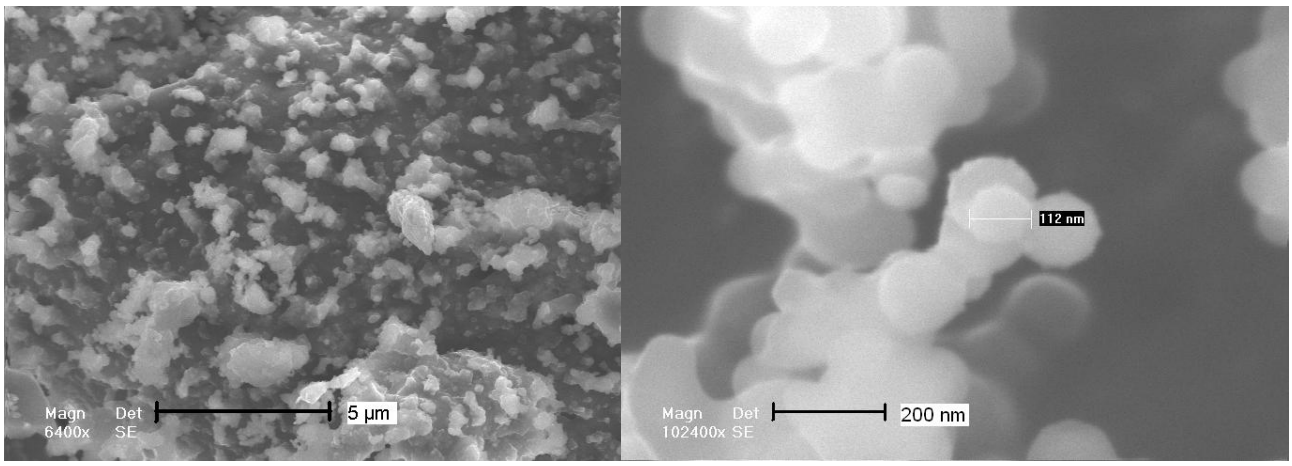

(a) (b)

Figure 5.3: Coal char: ESEM photographs of tar condensation at the char surface.

ures 5.2 and 5.3 clearly show spherical particles of several nanometers, that are typical of soot aggregates [14].

Due this observation, it was decided to set the concentration of oxygen to 3 $\%O_2$. This char production protocol was successfully applied by Commandré et al [24,63,67].

5.4.2 "Flash" chars physico-chemical analysis

The physico-chemical properties of the collected chars are presented in Table 5.2. Due to the small quantities of char available, the char ash content, necessary to evaluate the O-content, was measured using Thermo-Gravimetric (TG) devices under air. The final temperature was set to 815°C, as in normalized test and the sample was left more than 1 hour at this temperature.

		Ultimate analysis					Physical properties		
Fuel Name	Ash [w.%]	C [w.%]	H [w.%]	N [w.%]	S [w.%]	O [w.%]	ρ_{pycno} [kg/m^3]	ε [%]	S_{Spe} [m^2/g]
Lignite	16.33	65.47	1.35	0.93	2.36	13.46	1760	-	123
Coal	17.48	71.18	1.2	1.97	0.16	8.03	1700	68.18	4.4
Anth.	7.42	86.01	1.87	1.00	0.36	4.72	1950	14.2	27.5
Petcoke	1.61	88.37	1.31	1.52	6.23	0.96	1630	3.4	3.7

Table 5.2: "Flash" chars physico-chemical analysis. The values for O-atom proportions were calculated by difference to 100 %.

The specific surface, S_{Spe}, was measured using the N_2-BET method with a Micromeritics Gemini device. The porosity, ε, was determined with Hg-porosimetry, thanks to the Micromeritics Autopore III 9420. Note that the porosity of lignite char could not be measured because the highly porous and fragile sample was crushed by high pressure of mercury during its measurement.

Using the total specific surface - as measured from BET using N_2 – to characterize the char reactive surface is the classical reference method, despite it is known that the total porous surface is not the actual reactive surface [35]. Nevertheless, this is open to research to determine the actual reactive surface of a porous carbon. The determining parameter is the product $A.S$, where A is classically fitted by confrontation of the model to experiments.

5.4.3 Reference fixed bed chars characterization

The char residue obtained after the 7 min soak pyrolysis in an oven at 900 °C described above (cf. NF M 03-004: french standard to characterize the volatiles content) were also characterized in terms of their physico-chemical analysis. The char chemical analysis was determined using the same method as detailed in case of "Flash" chars. The char ash content, necessary to evaluate the O-content, was measured following the french standard NF M 03-003. The results of theses analyzes are presented in Table 5.3.

		Ultimate analysis					Physical properties		
Fuel Name	Ash [w.%]	C [w.%]	H [w.%]	N [w.%]	S [w.%]	O [w.%]	ρ_{pycno} [kg/m^3]	ε [%]	S_{Spe} [m^2/g]
Lignite	18.38	75.28	1.68	1.25	1.89	1.41	1910	59.68	343.0
Coal	17.21	72.04	1.11	1.43	0.55	10.46	1890	53.31	10.4
Anth.	6.54	86.67	1.54	1.06	0.46	3.73	-	-	6.49
Petcoke	0.68	85.80	0.71	1.27	4.64	6.90	1810	41.16	9.82

Table 5.3: Fixed Bed chars physico-chemical analysis. The values for O-atom proportions were calculated by difference to 100 %.

5.5 Discussion

5.5.1 Fuels properties

As we can see in Table 5.1, two of these fuels, – lignite and coal – have a high volatile content (51.5 and 34.8 w.% respectively), whereas anthracite and petcoke are very low-volatile fuels (5.5 and 6.8 w.%). Coal has the highest ash content (11.6 w.%), whereas petcoke has a very low one (0.5 %); anthracite and lignite have ash content values of 6.3 and 8.7 w.% respectively.

The nitrogen content of the fuels is comprised between 1.1 and 1.7 w.%, apart from lignite where N-content is low: 0.4 %. The two high-volatile fuels have a high oxygen content: 24.9 w.% for lignite and 16.2 w.% for coal, whereas anthracite and petcoke contain 4.4 and 6.8 w.% oxygen only respectively.

The Van Krevelen diagram, presented in Chapter 2 is completed in Figure 5.4 with the properties of the four studied fuels. They are all well situated in the zone of their own rank. The rank notion – time evolution of the sedimentary rock – doesn't mean anything for petcoke, but

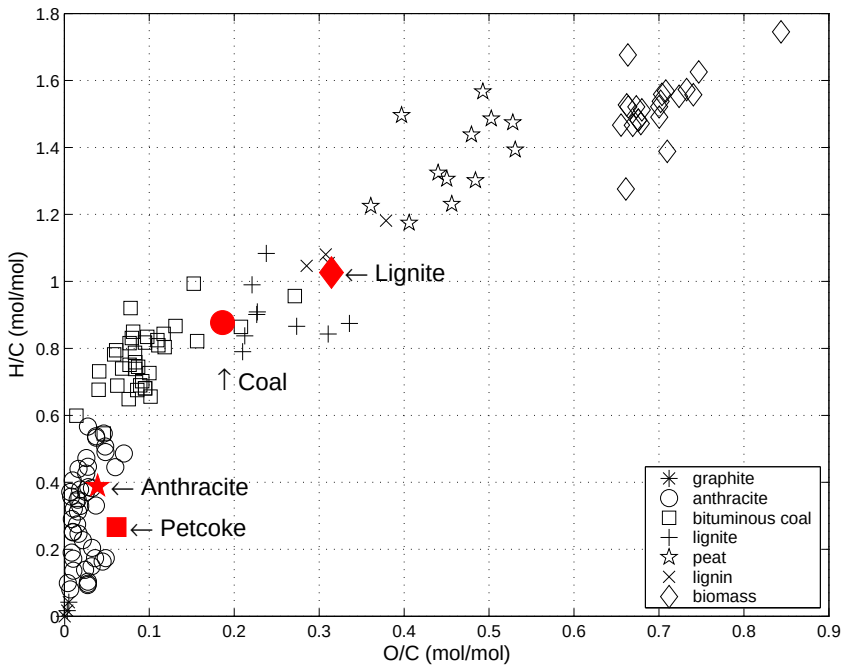

Figure 5.4: Van Krevelen diagram – fuel for the present work (◇ Lignite, ○ Coal, ☆ Anthracite and □ Petcoke) superposed with data from the literature [14]

it is interesting to compare it with anthracite coal. The studied Petcoke has a higher oxygen content than the anthracite.

5.5.2 Chars properties

5.5.2.1 Chars analyzes

For all chars (Flash and Fixed Bed ones), the ash content is greater than the fuel one. One should be careful with the char ash content comparison between char types in Tables 5.2 and 5.3. Indeed, the values were not determined following the same experimental protocol. However one remarks that the ash content of flash chars is higher than that for soak pyrolysis, except for lignite. This implies that a larger amount of volatiles matters was released during flash pyrolysis.

Significant amount of elements other than C were still present in the chars during analysis. This is classically observed whatever the char preparation conditions. Indeed, chars prepared from the same fuels by heating for 7 min at 900°C in soak conditions exhibit ultimate analysis similar to the flash chars. Moreover, during char devolatilisation experiments, no more volatile matters are formed after 1 s residence time as shown in Figures 7.1 to 7.4 in Chapter 7, indicating that devolatilisation was over. The probable explanation for this is that most H and O found during char analysis were not present just after char production, but were captured from the atmosphere in the time period between char production and char analysis [22].

5.5.2.2 ESEM pictures

Representative ESEM[2] pictures of the initial fuel and of the two types chars – i.e. generated either in "Flash" or in fixed bed conditions – are collected in Tables 5.4 and 5.5 for each fuel.

Lignite and coal chars have a more porous aspect than petcoke and anthracite ones. In case of coal, the flash pyrolysis seems to create spongious and bubble-like structures. However, only careful conclusion could be done with such pictures. Indeed, the pore size influencing the porosity and the BET-specific surface are still invisible at this length scale.

Specific surface is very high for chars of lignite and anthracite, and low for chars coal and petcoke.

5.5.2.3 The fate of the different fuel constituents

Thanks to the results presented above (i.e. fuel, fixed-bed char and "Flash" char analysis), one can study the fate of carbon, nitrogen and sulfur in the chars. Due to the uncertainties mentioned above about the determination of O and H in the chars, the fate of these species will not be considered here. A reference median line ($y = x$) is also plotted in Figures 5.5. If an experimental point is placed on this line then the release in VM of the considered atoms was proportional to the mass of the fuel during devolatilisation.

As expected, it appears in Figure 5.5(a) that carbon is concentrated in chars. Indeed, all the symbols are located above the median line, particularly in case of lignite in fixed bed chars.

The char nitrogen symbols in Figure 5.5(b) are distributed on the two sides of the median line. In case of lignite, both fixed bed and flash chars concentrate the N-elements. In case of coal, the nitrogen is concentrated in flash chars, whereas it is more released in the volatiles matters in case of fixed bed pyrolysis. For petcoke and anthracite, nitrogen in the char is proportionally released to the mass loss : the char-nitrogen is equal to initial fuel-nitrogen.

Sulfur evolution on the figure 5.5(c). The sulfur content in the char is almost equal to the original sulfur content in the fuel. The analysis are on the median line, according to results of Commandré et al. [104]. The sulfur content of chars seems also to be independent of the devolatilisation heating rate. Indeed, whatever fixed bed devolatilisation or flash devolatilisation, the values are quite equal.

In Figure 5.5(d), the chars skeletal density is plotted in function of the initial fuel one. It increases obviously during pyrolysis and more sensitively after low heating rates.

[2]ESEM : Environmental Scanning Electron Microscope

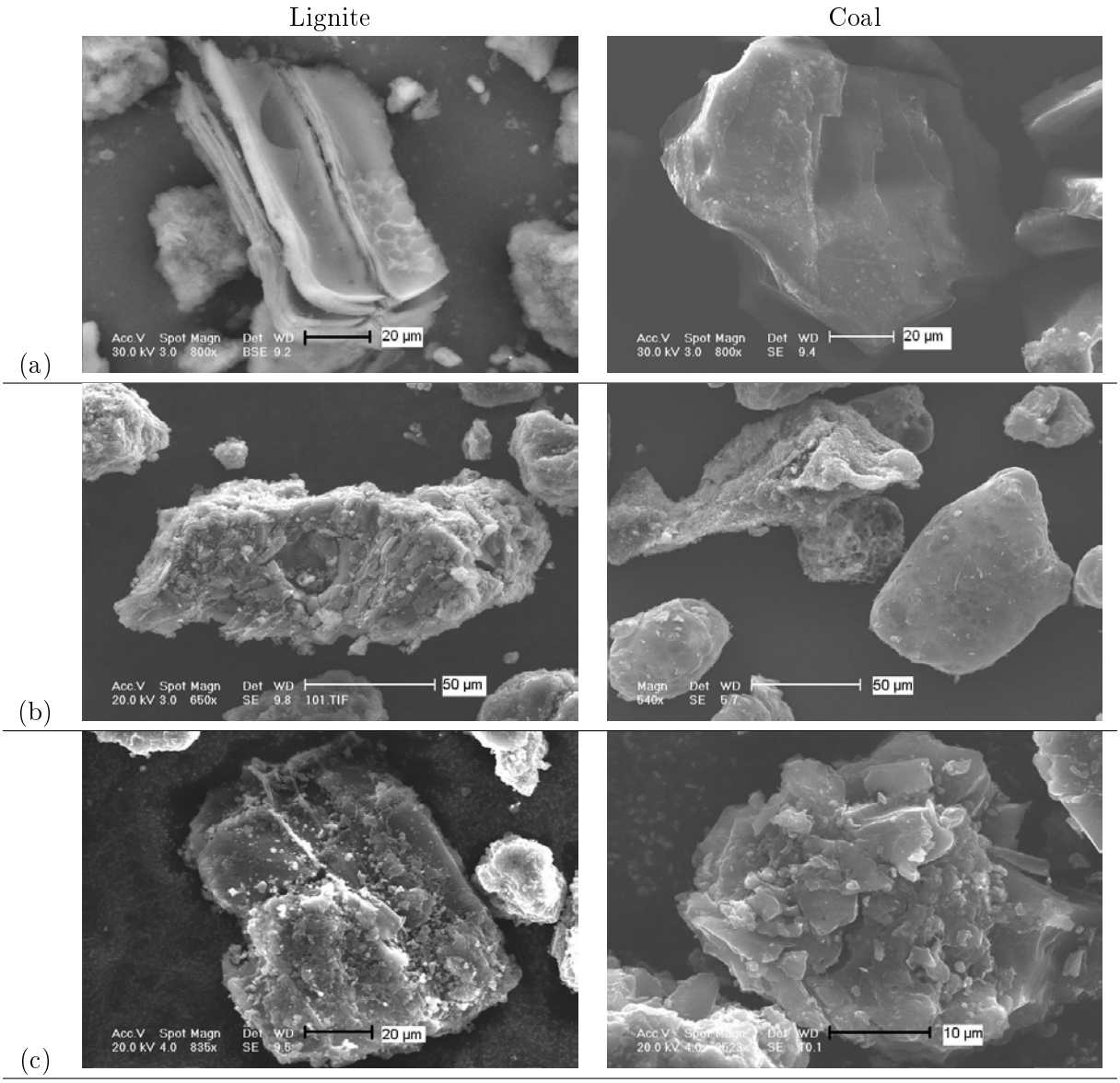

Table 5.4: Lignite and Coal: ESEM pictures of the fuels (a), the "Flash" chars (b) and the fixed bed chars (c).

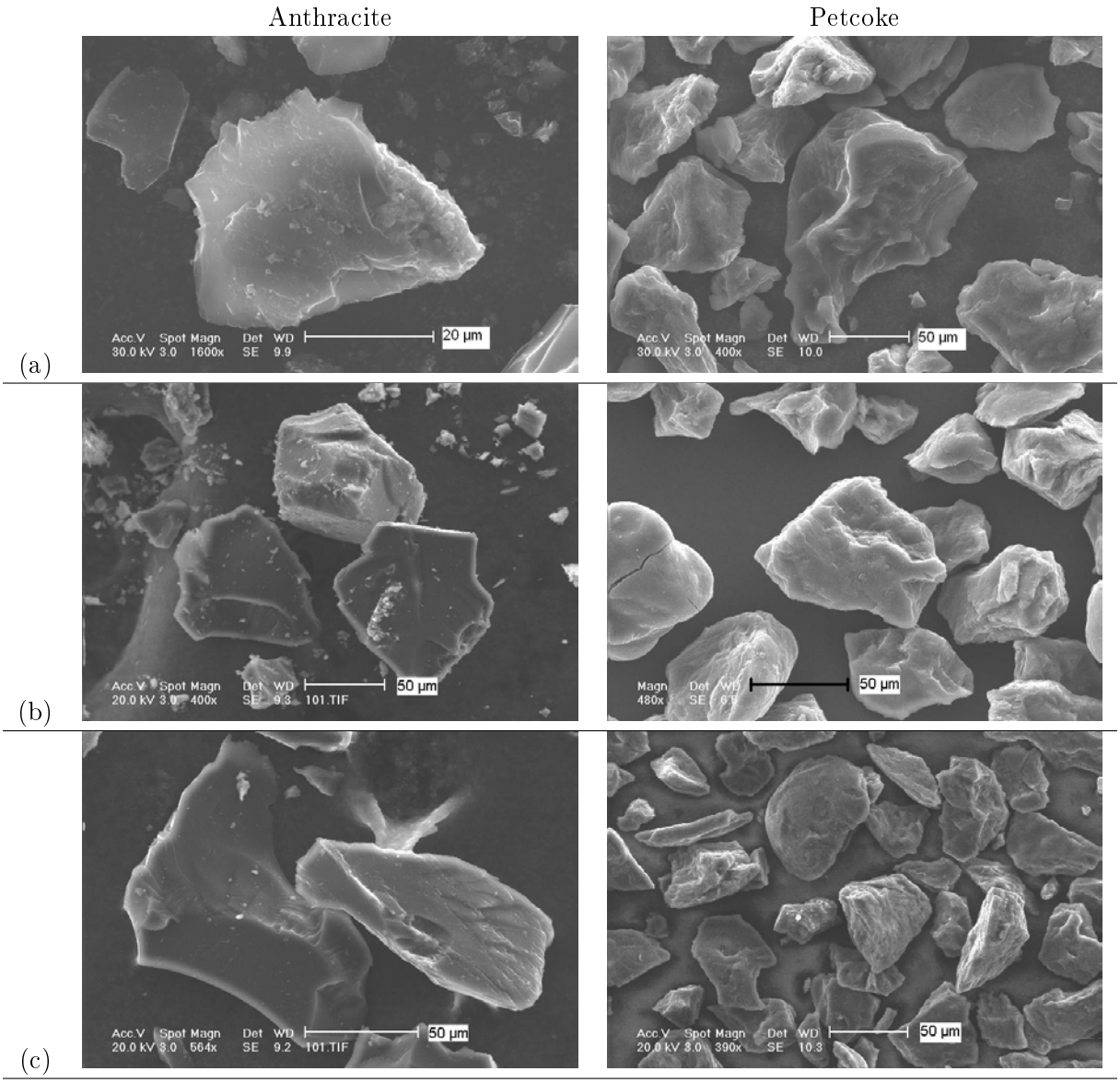

Table 5.5: Anthracite and Petcoke: ESEM pictures of the fuels (a), the "Flash" chars (b) and the fixed bed chars (c).

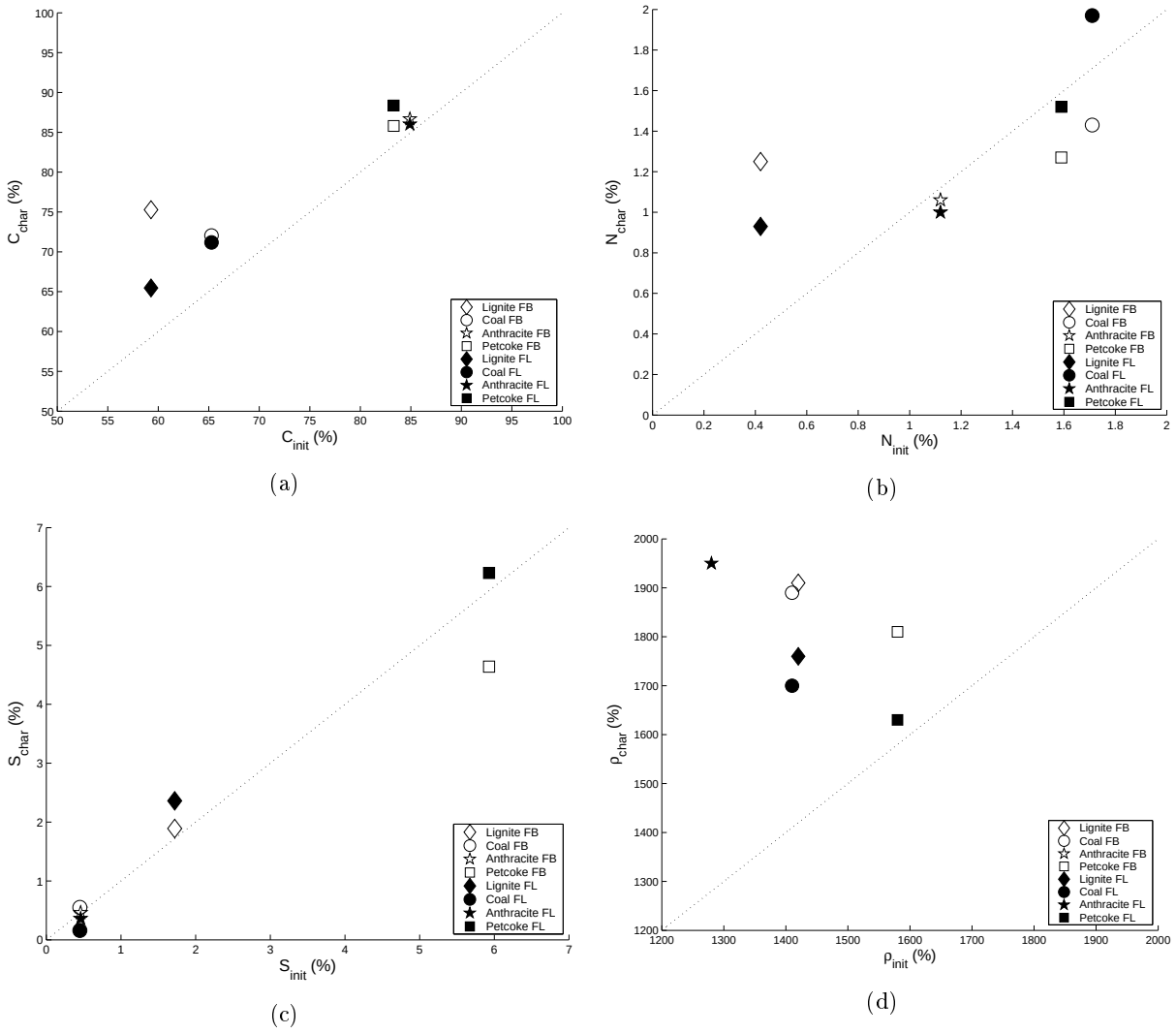

Figure 5.5: Effect of the heating rate during pyrolysis on the release of : carbon (Figure 5.5(a)), nitrogen (Figure 5.5(b)), sulfur (Figure 5.5(c)) and skeletal density (Figure 5.5(d))–FB = Fixed Bed (open symbols), FL = FLash (close symbols).

Chapter 6

The Entrained Flow Reactor model

Contents

6.1 Introduction 83
6.2 Model description 83
6.2.1 Main assumptions 84
6.2.2 Particle properties 85
6.2.3 Devolatilisation 85
6.2.4 Char heterogeneous reactions 89
6.2.5 Gas phase reactions 92
6.2.6 Heat transfers 94
6.3 Numerical integration 95

6.1 Introduction

The model used in the present work is based on a thermochemical model developed successively by Van de Steene and Commandré [15, 24, 105] to describe the combustion of powdered fuels in Entrained Flow Reactor (EFR) conditions (laminar flow) and was improved for this work.

It takes into account the thermal and chemical mechanisms involved during the combustion/reburning of solid particles. The formation and reduction mechanisms for fuel NO, prompt NO, and thermal NO are modeled.

The particle devolatilisation and the released gaseous species are taken into account. The gas phase reactions are computed by CHEMKIN II [47] subroutines that are called by the main program. The char oxidation and NO reduction by char reactions are also computed, taking into account the gas diffusion outside and inside the porous particle.

6.2 Model description

The model is based on a Lagrangian approach. Indeed, the whole flow is simulated considering a single particle and the gas volume that can be associated with it. This particle and gas volume

sample represent an elementary part of the EFR's flow. The model simulates the time evolution of this sample. Figure 6.1 is a representation of the considered geometric model.

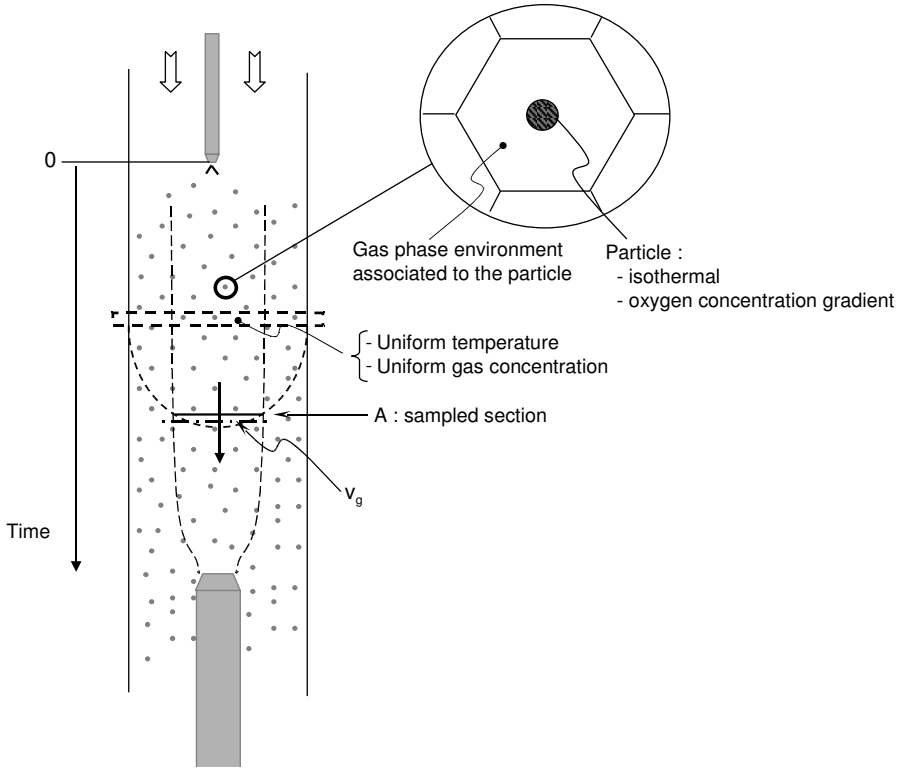

Figure 6.1: Schematic description of the modeled geometry.

The initial gas volume element surrounding the particle is fixed by the ratio of solid and gas flows injected in the EFR.

At each time step, the particle is composed of initial fuel, char (except at $t = 0$), nitrogen, sulfur, oxygen, and ash. The particle temperature is computed through a heat balance including conductive heat exchange with the gas phase, radiative heat exchange with the furnace wall and heat source terms from heterogeneous reactions. Its initial temperature is estimated to be 50°C.

The surrounding gas temperature is computed through a heat balance that includes the heat exchange with the reactor wall by convection, the heat exchange with the particle by conduction and heat source terms from gas phase reactions.

At the beginning of the simulation, the gas are only composed of N_2, O_2 and NO (hanging on the type of modeled experiments). It is further enriched by gases released during pyrolysis. Chemical reactions take place in the gas phase.

The initial N- and S-contents of the fuel are released either during pyrolysis or char oxidation, as different gaseous species (HCN, NH_3, NO, NO_2, N_2O, and SO_2).

6.2.1 Main assumptions

- the particle is supposed spherical and isothermal,

- the thermal properties of the particle are supposed homogeneous and isotropic,
- the particle diameter is not supposed to change during the reactions; a constant diameter of 65 μm is taken at the mean size of the 30–100 μm fraction selected for the experiments,
- the specific surface is supposed to be constant along time and is taken equal to that measured by BET method after the flash char production in the EFR.
- the slip velocity between gas and particle is neglected,
- the gas concentrations and temperature are homogeneous in the particle environment.

The next paragraphs give details about each part of the model.

6.2.2 Particle properties

The particle composition is initially described in terms of C, H, O, N, S and ash percentages. The mass of each component is computed during the chemical reactions at each time step. N and S are released through different gas species both during pyrolysis and char oxidation, proportionally to the mass loss: the mass fractions of N and S in the char do not change along the process. This repartition of these atoms is carried out using partitioning coefficients as detailed further.

The heat capacity of the particles, char and ashes are respectively set to 1200, 1900 and 1900 J.kg^{-1}.K^{-1} respectively, for all fuels. The tortuosity of the porous particle is assumed to be equal to 4.

6.2.3 Devolatilisation

Because the purpose of this work was not to achieve such a fine description of the devolatilisation mechanisms as presented in FG-DVC, FLASHCHAIN or CPD models (see Section 2.2.2.2), but to describe correctly the VM release observed during experiments, the devolatilisation kinetics was described using a simple mathematical model: the mass loss is described through a single pseudo Arrhenius law. Indeed, although a large number of publications show that coal devolatilisation should be modeled with more detailed models [13, 21, 22, 31–33], other authors used this rough assumption because of its simplicity and its relatively good accuracy with global experimental results [24, 106].

Hence, the devolatilisation kinetics is assumed to follow a single pseudo-Arrhenius law (Equation 6.2):

$$\frac{\partial m_{Fuel}}{\partial t} = -k_{dev}.m_{Fuel} \tag{6.1}$$

$$k_{dev} = A_{dev}.\exp\left(-\frac{E_{a_{dev}}}{R.T_p}\right) \tag{6.2}$$

The fuel mass, m_{Fuel}, is assumed to devolatilize into a volatile matters mass fraction,

α_{dev}, and into the char residual mass fraction, $1 - \alpha_{dev}$ (see Equations 6.1 and 6.3).

$$\frac{\partial m_{Vol}}{\partial t} = \alpha_{dev}.k_{dev}.m_{Fuel} \quad (6.3)$$

$$\frac{\partial m_{Char}}{\partial t} = (1 - \alpha_{dev}).k_{dev}.m_{Fuel} \quad (6.4)$$

In this model, tars – that represent approximately half the mass of volatile matters – were assumed to have the same composition as char, and to behave as the char residue during regarding their oxidation and participation to NO chemistry. Also H and O atoms that are not recovered during analysis of pyrolysis gases were assumed to form water, i.e. not to play a role in the pollutants chemistry. These assumptions remain weak points in the proposed approach, and should motivate further research in these domains. However, it has been checked that assuming that the remaining O-atoms are released into H_2O affects the prediction by the for NO mole fraction in reburning conditions by less than 6 %.

Thus the volatile matters modeled are assumed to be composed of

- major species – carbon oxides (CO, CO_2), hydrogen, and hydrocarbons (CH_4, C_2H_2, C_2H_4, C_2H_6 and C_3H_8) (Figure 6.2),
- minor species – nitrogen species (NO, N_2O, NH_3, HCN), and SO_2.

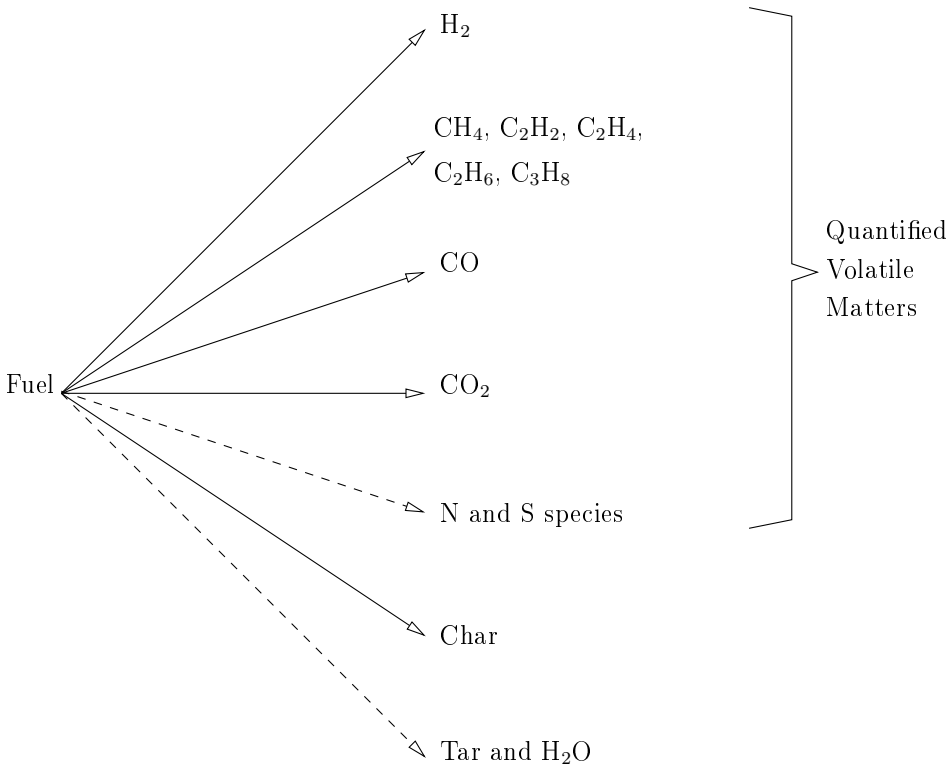

Figure 6.2: Mass distribution of fuel during devolatilisation.

- At first, the mass of N or S containing species is calculated.

  Establishing the N mass balance described in Figure 6.3 the mass of each N containing

can be calculated first through the partition coefficient α_N that distinguishes between N in volatile species and N remaining in the char.

- volatile N is distributed among NO, N_2O, HCN and NH_3 thanks to the partitioning coefficients η_v, β_v, δ_v and ε_v respectively. Their values were determined by fitting the model to experimental values. The N balance is closed through γ_v, assuming that the remaining N atoms are converted to N_2.

- N in char and tars is distributed among NO, NO, HCN and NH_3 resulting from later char oxidation thanks to the partitioning coefficients η_c, β_c, δ_c and ε_c respectively. Again the N balance is closed thanks to γ_c, assuming that the remaining N is converted to N2.

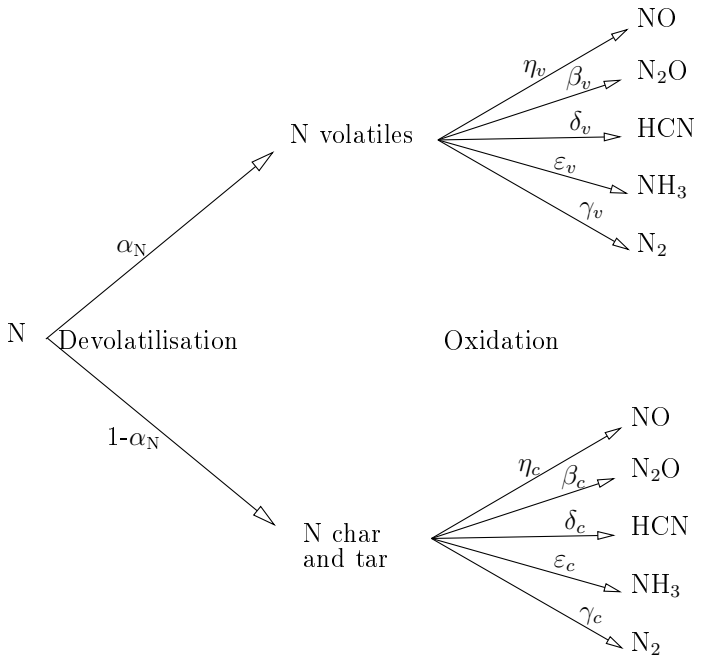

Figure 6.3: Nitrogen distribution through devolatilisation and char oxidation.

The mass balance for S species proposed in Figure 6.4 assumes that part of the fuel sulfur is released during devolatilisation to form SO_2 only. The partitioning coefficient is determined by fitting the model with devolatilisation experiments. The S atoms remaining in char and tar are converted later on to SO_2, along the char oxidation reaction.

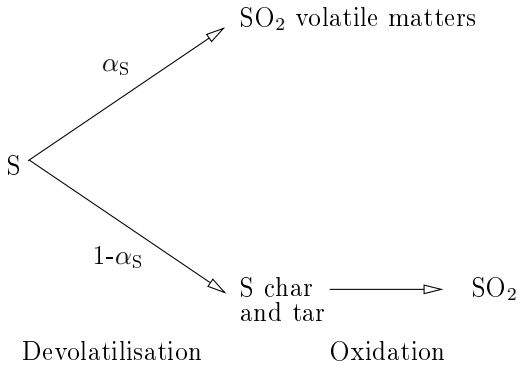

Figure 6.4: Sulfur distribution through devolatilisation and char oxidation.

- A mass balance for O atoms represented in Figure 6.5 is then established. The O atoms are supposed to devolatilize into CO and CO_2, with the partitioning coefficients $\alpha_{O\rightarrow CO}$ and $\alpha_{O\rightarrow CO_2}$ respectively, both determined by fitting the model with devolatilisation experiments. A negligible amount of O is used to form N and S containing species; the remaining O atoms are omitted, which is equivalent to converting them into H_2O as detailed previously.

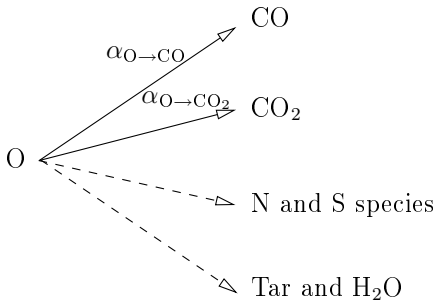

Figure 6.5: Oxygen distribution through devolatilisation.

- The mass of the last volatile species can be calculated from the H balance as illustrated in Figure 6.6. H atoms are released as hydrocarbons, i.e. CH_4, C_2H_2, C_2H_4, C_2H_6, C_3H_8 and H_2, with the partitioning coefficients $\alpha_{H\rightarrow CH_4}$, $\alpha_{H\rightarrow C_2H_2}$, $\alpha_{H\rightarrow C_2H_4}$, $\alpha_{H\rightarrow C_2H_6}$, $\alpha_{H\rightarrow C_3H_8}$ and $\alpha_{H\rightarrow H_2}$, respectively. These partitioning coefficients are set by fitting the model with pyrolysis experiments. A negligible amount of H is used to form N and S containing species; the remaining H atoms are omitted, which is equivalent to converting them into H2O.

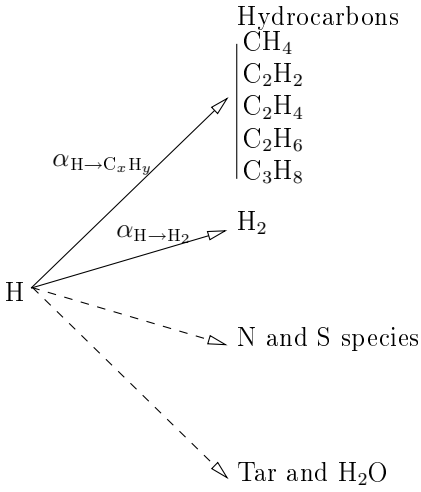

Figure 6.6: Hydrogen distribution through devolatilisation.

- Finally, the mass balance for C established in Figure 6.7 enables to calculate the mass of char. The mass of tar is included in the mass of char, as discussed previously.

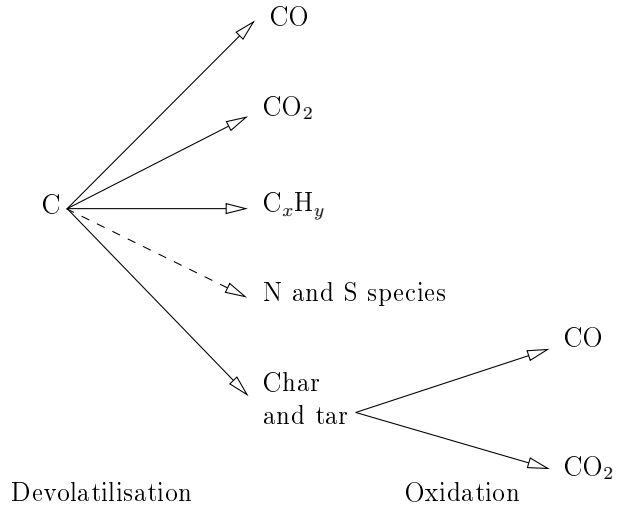

Figure 6.7: Carbon distribution through devolatilisation and char oxidation.

Each volatile species are supposed to be released proportionally to the total mass of volatile matters released, as illustrated in the example case of CO in Equation 6.5.

$$\frac{\partial m_{\mathrm{CO}}}{\partial t} = \alpha_{\mathrm{O}\rightarrow\mathrm{CO}} \cdot \frac{m_{\mathrm{O},fuel}}{m_{Fuel}} \cdot \frac{M_{\mathrm{CO}}}{M_{\mathrm{O}}} \cdot \frac{\partial m_{\mathrm{Vol}}}{\partial t} \tag{6.5}$$

where $m_{\mathrm{O},fuel}$ is the oxygen mass in the fuel, m_{Fuel} is the mass of fuel, M_{CO} and M_{O} are the molar mass of CO and O respectively.

6.2.4 Char heterogeneous reactions

Both char oxidation and NO reduction are calculated in this numerical model.

6.2.4.1 Char oxidation

The char oxidation reaction into CO and CO_2 is represented by the following reaction 6.6.

$$C_s + \left(1 - \frac{fr_{CO}}{2}\right) O_2 \longrightarrow fr_{CO}\,CO + (1 - fr_{CO})\,CO_2 \tag{6.6}$$

where fr_{CO} is the mole fraction of CO released during char oxidation, determined following Arthur's law [56] presented in Eq. 6.7, already presented in section 2.2.4.

$$\frac{n_{CO}}{n_{CO_2}} = 2500.\exp\left(-\frac{51\,843}{RT}\right) \tag{6.7}$$

This ratio equals 7.5 at 800°C and 26.5 at 1100°C. Thus the char is mainly oxidized into CO in the studied temperature range.

The thermal energy released during char oxidation is provided to the particle following the next expression:

$$\Delta H = fr_{CO}.\Delta H_{C\rightarrow CO} + (1 - fr_{CO}).\Delta H_{C\rightarrow CO_2} \tag{6.8}$$

The kinetics of the char oxidation is modeled following a single pseudo-Arrhenius law 6.10:

$$\frac{\partial\, m_{Char,Ox}}{\partial\, t} = -\eta.k_{OxChar}.S_{spe}.m_{Char}.P_{O_2,p}^{n} \tag{6.9}$$

$$k_{OxChar} = A_{OxChar}.\exp\left(-\frac{E_{a_{OxChar}}}{RT_p}\right) \tag{6.10}$$

where m_{Char} is the mass of char in the considered volume element (kg), η is the effectiveness factor (dimensionless), S_{spe} the specific pore surface area (m^2/kg), $P_{O_2,p}$ is the O_2 partial pressure at the char surface (Pa_{O_2}) and n is the reaction's order, assumed to be equal to 1 in this work. A_{OxChar} is the pre-exponential factor of the kinetic law ($kg_{C_s}.m^{-2}.s^{-1}.Pa_{O_2}^{-1}$) and $E_{a_{OxChar}}$ is the activation energy for char oxidation (J/mol).

During the char oxidation, the particle mass decreases while the particle diameter remains constant: the porosity increases.

The mass transfer limitations concerning the particles have to be evaluated, both externally and internally.

Internal mass transfer Within the particles, the effective diffusion coefficients for calculating effectiveness factors were estimated by means of the standard pore model developed by Smith [60,61] and detailed in section 2.2.4.

External mass transfer For external transfer, the O_2 diffusion outside the particle is modeled by the following transfer law:

$$\phi_{O_2} = k_m.A_p.\left([O_2]_{env} - [O_2]_p\right) \tag{6.11}$$

Here, ϕ_{O_2} is the oxygen consumed by the particle (mol/s), k_m is the transfer coefficient (m/s), A_p is the external area of the particle ($A_p = \pi.d_p^2$ in m^2) and $[O_2]_{env}$ is the bulk O_2 concentration. ϕ_{O_2} is calculated thanks to the reaction 6.6 as follows:

$$\phi_{O_2} = \frac{\partial m_{Char,Ox}}{\partial t}.\frac{1}{M_C}.\left(1 - \frac{fr_{CO}}{2}\right) \tag{6.12}$$

The transfer coefficient k_m is calculated thanks to the Sherwood number (Equation 6.13). $Sh = 2$ means that only the Fick's diffusion – and not the convection – is taken into account. This assumption was validated by Van de Steene [15]. D_{mol} is calculated here at the mean value between the bulk and the particle temperatures.

$$Sh = \frac{k_m.d_p}{D_{mol}} = 2 \tag{6.13}$$

Minor species During char oxidation, minor species – SO_2 and nitrogen species (NO, N_2O, NH_3, HCN) – are also released. In the model these species are assumed to be released proportionally to the char mass loss rate. Respectively, the α_S and the η_c, β_c, δ_c, ε_c and γ_c partitioning coefficients make it possible to describe the release of these species (see Figures 6.3 and 6.4). For example, the Equation 6.14 describe the NO release during char oxidation.

$$\frac{\partial m_{NO}}{\partial t} = (1 - \alpha_N).\eta_c.\frac{m_{N,char}}{m_{Char}}.\frac{M_{NO}}{M_N}.\frac{\partial m_{Char,Ox}}{\partial t} \tag{6.14}$$

where $m_{N,char}$ is the nitrogen mass in the char, m_{Char} is the mass of char, M_{NO} and M_N are the molar mass of NO and N respectively and $\frac{\partial m_{Char,Ox}}{\partial t}$ is the mass of char oxidation rate.

6.2.4.2 NO reduction at the char surface

The NO reduction at the char surface (Reaction 6.15) is calculated through a first order Arrhenius kinetic law.

$$C_s + NO \longrightarrow CO + \frac{1}{2}N_2 \tag{6.15}$$

$$\frac{\partial m_{Char,NO}}{\partial t} = -\eta.k_{NO}.S_{spe}.m_{Char}.P_{NO,p}^m \tag{6.16}$$

$$k_{NO} = A_{NO}.\exp\left(-\frac{E_{a_{NO}}}{RT_p}\right) \tag{6.17}$$

The internal and external mass transfer are specifically computed for NO reduction by char reaction, as in case of char oxidation.

6.2.5 Gas phase reactions

The gas phase reactions, including nitrogen and sulfur chemistry, are treated with the Dagaut et al. scheme (145 species, 1006 reactions) [54]. This detailed mechanism, presented in Appendix D allows oxidation of the volatile matters and interactions between NO and hydrocarbons (from C_0 to C_4) to be correctly described, taking the influence of SO_2 into account. The reaction rates and energy source terms are treated by CHEMKIN II [47] software subroutines that are called by the main program.

A chemical reaction may be written on a general form as in expression 6.18. The summations in Equation 6.18 are for all chemical species in the system, but only species that appear as reactants or products will have non-zero stoichiometric coefficients $\nu_{i,r}$. Hence, species that are not involved will drop out of the equation.

$$\sum_{i=1}^{N} \nu'_{i,r} \mathcal{M}_i \underset{k_{b,r}}{\overset{k_{f,r}}{\rightleftharpoons}} \sum_{i=1}^{N} \nu''_{i,r} \mathcal{M}_i \tag{6.18}$$

where

$$\begin{aligned} N &= \text{number of chemical species in the system} \\ \nu'_{i,r} &= \text{stoichiometric coefficient for reactant } i \text{ in reaction } r \\ \nu''_{i,r} &= \text{stoichiometric coefficient for product } i \text{ in reaction } r \\ \mathcal{M}_i &= \text{symbol denoting species } i \\ k_{f,r} &= \text{forward rate constant for reaction } r \\ k_{b,r} &= \text{backward rate constant for reaction } r \end{aligned}$$

Then the reaction rate $k_{f,r}$ may be calculated with the Arrhenius law as follows 6.19.

$$k_{f,r} = A_{f,r}.T^{\beta_r}.\exp\left(-\frac{E_{a_{f,r}}}{R.T}\right) \tag{6.19}$$

where $A_{f,r}$ and $E_{a_{f,r}}$ are respectively pre-exponential factor and activation energy, and β_r is the temperature exponent. These parameters are given in detailed kinetic schemes.

The molar rate of creation/destruction of species i in reaction r, $\hat{R}_{i,r}$, is given by the equation 6.20

$$\hat{R}_{i,r} = \left(\nu''_{i,r} - \nu'_{i,r}\right)\left(k_{f,r}\prod_{i=1}^{N}[C_{i,r}]^{\nu'_{i,r}} - k_{b,r}\prod_{i=1}^{N}[C_{i,r}]^{\nu''_{i,r}}\right) \tag{6.20}$$

where

$$\begin{aligned} C_{i,r} &= \text{molar concentration of each reactant and product species } i \text{ in reaction } r \ \left[\text{mol.m}^{-3}\right] \\ \nu'_{i,r} &= \text{forward rate exponent for each reactant and species } i \text{ in reaction } r \\ \nu''_{i,r} &= \text{backward rate exponent for each reactant and species } i \text{ in reaction } r \end{aligned} \tag{6.21}$$

The production rate $\hat{R}_i$ of the ith species can be written as a summation of the molar rate of production for all the N_R reactions involving the ith species:

$$\hat{R}_i = \sum_{r=1}^{N_R} \hat{R}_{i,r} \tag{6.22}$$

Equation 6.18 is valid for both reversible and non-reversible reactions. For non-reversible reactions, the backward rate constant, $k_{b,r}$, is simply omitted. When not, the backward rate constants are calculated as follows:

$$k_{b,r} = \frac{k_{f,r}}{K_{c_r}} \tag{6.23}$$

$$K_{c_r} = K_{p_r} \left(\frac{P_{atm}}{RT}\right)^{\sum_{i=1}^{N} \nu_{i,r}} \tag{6.24}$$

$$K_{p_r} = \exp\left(\frac{\Delta S_r^0}{R} - \frac{\Delta H_r^0}{RT}\right) \tag{6.25}$$

The heat release or consumption during the reactions need also to be computed because of its influence on the system temperature and therefore on the kinetics. For the reaction r between the species i, the enthalpy and the entropy variations are calculated by the next expressions:

$$\Delta H_r^0 = \sum_{i=1}^{N} \left(\nu''_{i,r} - \nu'_{i,r}\right) H_i^0 \tag{6.26}$$

$$\Delta S_r^0 = \sum_{i=1}^{N} \left(\nu''_{i,r} - \nu'_{i,r}\right) S_i^0 \tag{6.27}$$

The species standard state properties, like enthalpy H_i^0 and entropy S_i^0, are calculated in function of the temperature using polynomial fits to the specific heats at constant pressure (the superscript ^{0} refers to the standard-state pressure 1 atm):

$$\frac{Cp_i^0}{R} = \sum_{n=1}^{P} a_{n,i}.T^{(n-1)} \tag{6.28}$$

Other thermodynamic properties are given in terms of integrals of the specific heats. First

the standard state enthalpy is given by

$$H_i^0 = \int_0^T Cp_i^0 dT \tag{6.29}$$

so that

$$\frac{H_i^0}{RT} = \sum_{n=1}^{P} \frac{a_{n,i}.T^{(n-1)}}{n} + \frac{a_{P+1,i}}{T} \tag{6.30}$$

where the constant of integration $a_{P+1,i}.R$ is the heat formation at 0 K. This constant is evaluated from knowledge of the standard heat of formation at 298 K, since the polynomial representations are usually not valid down to 0 K.

The standard-state entropy is written as

$$S_i^0 = \int_0^T \frac{Cp_i^0}{T} dT \tag{6.31}$$

so that

$$\frac{S_i^0}{R} = a_{1,i} \ln T + \sum_{n=2}^{P} \frac{a_{n,i}.T^{(n-1)}}{n-1} + a_{P+2,i} \tag{6.32}$$

where the constant of integration $a_{P+2,i}.R$ is evaluated from knowledge of the standard entropy at 298 K [47].

6.2.6 Heat transfers

6.2.6.1 Particle mass balance

The particle mass is computed through the following mass balance:

$$\frac{\partial m_p}{\partial t} = -\frac{\partial m_{Vol}}{\partial t} + \frac{\partial m_{Char,Ox}}{\partial t} + \frac{\partial m_{Char,\mathrm{NO}}}{\partial t} \tag{6.33}$$

In the Equation 6.33, the decrease of the particle mass is computed as the sum of the mass lost during the pyrolysis (m_{Vol}), the char oxidation $m_{Char,Ox}$ and the NO reduction by char $m_{Char,NO}$.

6.2.6.2 Particle thermal balance

The particle temperature is calculated through the following thermal balance:

$$Cp\frac{\partial m_p T_p}{\partial t} = h_p A_p \left(T_{env} - T_p\right) + \epsilon_p A_p \sigma_0 \left(T_f^4 - T_p^4\right) + \sum_{solids} \frac{\partial m_i}{\partial t} \Delta h_{r,het} - \sum_{gas} \dot{m}_i cp_i T_p \tag{6.34}$$

In the right member, the first term represent the heat exchange by the particle by con-

duction/convection. The h_p coefficient is calculated through a Nusselt number correlation.

$$Nu_p = \frac{h_p d_p}{\lambda_g} = 2 \tag{6.35}$$

Van de Steene [15] has shown that only conduction has to be taken into account, thus $Nu_p = 2$.

The second term represent the radiative heat transfer between the furnace wall and the particle ($\sigma_0 = 5.67 \times 10^{-8}$ W.m^{-2}.K^{-4} is the Boltzmann constant and ϵ_p is the particle emissivity). The third term represent the heterogeneous reactions enthalpy and the fourth term is enthalpy transported by the gaseous species leaving the particle. The enthalpy flux of the gas entering the porous particle is neglected.

6.2.6.3 Environment mass balance

The environment mass is computed through the following mass balance:

$$\frac{\partial m_{env}}{\partial t} = \sum_{i=1}^{N} \frac{\partial m_i}{\partial t} \tag{6.36}$$

$$\frac{\partial m_i}{\partial t} = \sum_{r_{het}=1}^{N_{R_{het}}} \left(\frac{\partial m_i}{\partial t} \right)_{r_{het}} + \sum_{r=1}^{N_R} \left(\frac{\partial m_i}{\partial t} \right)_r \tag{6.37}$$

The variation of the mass of the particle surrounding environment m_{env} is computed as the sum of the mass variation of each species m_i. The species mass variation is the result either of heterogeneous reactions r_{het} – devolatilisation, char oxidation and NO reduction at the char surface – or of gas phase reaction r.

6.2.6.4 Environment thermal balance

The bulk/environment temperature is computed through the thermal balance:

$$\frac{\partial m_{env} C_{env} T_{env}}{\partial t} = h_p A_p (T_p - T_{env}) + h_{fe} m_{env} (T_f - T_{env}) + \sum_{gas} \hat{R}_i H_i + \sum_{gas} \dot{m}_i C_p T_p \tag{6.38}$$

Here, $h_{fe} m_{env} (T_f - T_{env})$, represent the heat exchanged between the furnace and the environment. This flux is simply described through an heat exchange coefficient that was adjusted to fit the temperature profile: $h_{fe} = 16000$ W.kg^{-1}.K^{-1} [24].

6.3 Numerical integration

All the equations (particle's mass and heat balance equations, gas phase heat balance equations, and the gas phase chemistry equations) are time integrated simultaneously with the help of the Gear algorithm, that can solve "stiff" ODE systems [107]. The whole model is included in a FORTRAN 77 program.

Part III

Characterization of the elementary heterogeneous reactions and detailed analysis of the reburning by solid fuels

Résumé de la partie III

L'objectif principal de ce travail est la modélisation du processus de reburning au charbon. Dans ce cas, toutes les réactions décrites sur la Figure 1 se déroulent simultanément : dévolatilisation, oxydation du char, réactions en phase gazeuse et réduction du NO sur le char.

Il s'agit donc dans un premier temps de caractériser individuellement ces réactions hétérogènes : déterminer les paramètres cinétiques ainsi que les gaz dégagés lors des réactions. Trois différents types d'expériences ont ainsi été conduits à trois températures différentes : 800, 900 et 1000°C. Ces expériences ont ensuite été modélisés et les résultats du modèle calés sur les résultats expérimentaux.

Caractérisation des réactions hétérogènes élémentaires

pyrolyse sous 100 % de N_2. Le combustible est injecté dans le RFE. L'échantillonnage est réalisé à différents temps de séjour. Les espèces gazeuses sont analysées à chaque température.

Les paramètres cinétiques de la pyrolyse sont adaptés pour reproduire la vitesse de dégazage et les coefficients de répartition sont ajustés pour que les prédictions du modèle (lignes) correspondent le mieux possible aux symboles des expériences sur les Figures 7.1 à 7.4 (fraction molaire).

Il apparaît que l'hydrogène est l'espèce gazeuse la plus concentrée en volume dans les produits de pyrolyse mesurés. CO et CO_2 sont aussi très concentrés dans les gaz. Parmi les hydrocarbures, CH_4 est l'espèce la plus présente, alors que C_2H_2 et C_2H_4 sont souvent du même ordre de grandeur.

Oxydation du char. Du char préalablement préparé est injecté sous une atmosphère contenant 3 % d'O_2 complété en N_2. Les expériences ont été réalisées aux trois températures expérimentales. Gaz et particules sont échantillonnés après un temps de séjour de 2 s.

Ceci permet de caler les paramètres cinétiques de la réaction hétérogène d'oxydation. Les valeurs numériques sont présentées dans le Tableau 7.1, alors que la Figure 7.11(a) représente la consommation d'O_2 en fonction de la température, et la Figure 7.11(b) le diagramme d'Arrhenius correspondant. Les coefficients de partage pour les espèces dégagées lors de l'oxydation du char sont ajustés pour reproduire au mieux les valeurs expérimentales.

Réduction du NO sur le char. Du char préalablement préparé est injecté sous une atmosphère contenant 880 ppm de NO complété en N_2. Le prélèvement des gaz est effectué après un temps de séjour des particules de 2 s. Ce type d'expérience permet de déterminer les paramètres cinétiques de la réaction de réduction du NO sur le char en calant la concentration de NO calculée sur celle mesurée. Les valeurs numériques sont présentées dans le Tableau 7.1 et les Figures 7.14(a) et 7.14(b) représentant respectivement la consommation de NO et le diagramme d'Arrhenius correspondant.

Étude de la situation de reburning

Expériences et modélisations Une série d'expériences a été menée : il s'agit de la situation représentant le reburning. Pour ceci nous avons injecté du combustible sous 1,5 % d'O_2 et 880 ppm de NO (complété en N_2). Ce type d'expérience reproduit les conditions rencontrées dans la zone réductrice d'un précalcinateur de cimenterie. Pour ces expériences, l'échantillonnage est uniquement réalisé après un temps de séjour de 2 s dans le RFE.

La consommation de NO est représentée sur la Figure 8.1. On observe une forte différence entre les combustibles à fort taux de matières volatiles – lignite et charbon – et les autres. De plus, la réduction de NO augmente avec la température.

Lors de sa modélisation, aucun paramètre n'a été ajusté. La variation totale du NO est représentée aux trois températures pour les quatre combustibles comme la somme des différentes contributions sur les Figures 8.6: NO produit lors de la dévolatilisation, NO réduit dans la phase gazeuse, NO réduit sur le char et NO produit lors de l'oxydation du char. De même, l'évolution temporelle calculée à 1000°C est tracée sur les Figures 8.7 et 8.8.

Il apparaît que la réduction du NO dans la phase gazeuse est du même ordre de grandeur que la réduction sur le char après un temps de séjour des particules de 2 s. La réduction du NO sur le char croît continuellement avec la température alors que la réduction dans la phase gazeuse présente des singularités en fonction de la température pour les combustibles à forte teneur en matières volatiles : la réduction du NO est plus faible à 900°C dans le cas du lignite et du charbon qu'à 800 et 1000°C.

Cette dernière constatation s'explique par la grande complexité des mécanismes en compétition dans la phase gazeuse. Une étude détaillée de la chimie dans la phase gazeuse pour ces deux combustibles – lignite et charbon – permettra de mieux comprendre les mécanismes mis en cause.

Étude détaillée de la chimie en phase gazeuse Une étude détaillée de la chimie se déroulant dans la phase gazeuse a donc été entreprise dans le cas des deux combustibles cités précédemment. Cette démarche a pour but de déterminer les mécanismes réactionnels mis en jeux et l'identification des principales voies réactionnelles.

L'analyse des voies réactionnelles ne peut être conduite qu'à un instant précis. Une fois la modélisation du réacteur menée à son terme (cf. Chapitre 8), les fractions molaires des 145 espèces ainsi que la température des gaz est exportée vers le programme PSR de

CHEMKIN II. Ce programme modélise un réacteur parfaitement mélangé. Un temps de séjour extrêmement faible au sein de PSR est imposé ($\tau = 1 \times 10^{-10}$ s) pour éviter que les concentrations et la température n'évoluent. Ainsi, seuls les taux de réactions instantanés sont calculés et permettent de déterminer les chemins réactionnels prépondérants.

Cinq modélisations du réacteur dans les conditions de reburning ont donc été la source de cette étude : charbon à 800, 900 et 1000°C et lignite à 800 et 1000°C. Les dates pour conduire l'étude détaillée sont choisis après l'analyse des taux de formation de NO sur les Figures 8.9 à 8.13. Dans trois cas, une seule date a été choisie pour mener l'étude, alors que dans les deux derniers cas, trois dates sont étudiées du fait des phases successives de consommation puis reformation et enfin consommation du NO observées.

Finalement, il apparaît que plusieurs mécanismes interviennent dans la réduction homogène du NO. Ainsi, les hydrocarbures interviennent par le biais des réactions de reburning lorsque la température des gaz dépasse 1000°C. Pour les températures inférieures, la réduction de NO en N_2 est dominée par les réactions mettant en jeu le NH_3 dégagé lors de la pyrolyse : il s'agit de mécanismes de la SNCR. Dans le cas du lignite, la forte concentration en CO contribue légèrement à réduire le NO en N_2.

Une étude de sensibilité a été menée (Figure 8.28) pour étudier l'influence de la teneur en azote du combustible sur l'efficacité du reburning. Ainsi il est remarquable de noter que plus la teneur en azote du combustible est élevée, plus la réduction du NO dans la phase gazeuse est efficace.

Chapter 7

Characterization of the elementary heterogeneous reactions

Contents

7.1 Devolatilisation 103
7.1.1 Experimental and modeling protocol 103
7.1.2 Results 106
7.2 Char oxidation 115
7.2.1 Experimental and modeling protocol 115
7.2.2 Results 115
7.3 NO Reduction by char 122
7.3.1 Experimental and modeling protocol 122
7.3.2 Results 122
7.4 Concluding synthesis 124

In this chapter, the elementary heterogeneous reactions – i.e. devolatilisation, char oxidation and NO reduction by char – are characterized independently.

For each case, specific experiments and modelings are performed to fit the kinetic parameters and species quantities. This is the preliminary step before the complete experiments and modelings of the complex reburning situation, presented in Chapter 8.

The results of experiments and modelings for each heterogeneous reaction are presented below.

7.1 Devolatilisation

7.1.1 Experimental and modeling protocol

The following experiments were performed at 800, 900, and 1000°C, under pure N_2 atmosphere:

- to determine the variety of species released during devolatilisation and to quantify them.

- to achieve the determination of the kinetic parameters of the devolatilisation reaction.

For this type of experiments, the particle mass flow was set to 1.5 g/min for each fuel and the total flow rate in the reactor was 18.55 l/min (STP), distributed between the pneumatic transport flow – 2.55 l/min (STP) and the preheated flow – 16 l/min (STP) of pure N_2. The gases and particle were sampled after different residence time, i.e. sampling probe altitude.

The pyrolysis experiments were then modeled. The devolatilisation kinetics was determined by adjusting the pre-exponential factor A_{dev} so that the modeled total mass of devolatilized species matches the experimental values. The activation energy $E_{a_{dev}}$ of the pseudo-Arrhenius law used for devolatilisation kinetics was kept constant to 110 kJ/mol, corresponding to a value commonly found in the literature [15, 24, 38, 108].

During the devolatilisation modeling, the partitioning coefficients for oxygen between CO/CO_2 and the distribution for all the other volatile species – major species (hydrogen or hydrocarbons) or minor species (N- and S-containing species) – (see Chapter 6) are set to fit the experimental data during the pyrolysis experiments. For each fuel, only one pair of pyrolysis kinetic parameters – A_{dev} and $E_{a_{dev}}$ – is used for all temperature, whereas all the other partitioning coefficients are adjusted at each temperature. All the parameters relative to the devolatilisation process are presented in Table 7.1.

	Name	Unit	Lignite			Coal			Anthracite			Petcoke		
	T	°C	800	900	1000	800	900	1000	800	900	1000	800	900	1000
Particle properties	C	w.%	$100-H-O-N-S-Ash$			$100-H-O-N-S-Ash$			$100-H-O-N-S-Ash$			$100-H-O-N-S-Ash$		
	H	w.%	5.07			4.77			2.75			1.85		
	O	w.%	24.9			16.2			4.44			6.83		
	N	w.%	0.42			1.71			1.12			1.59		
	S	w.%	1.72			0.45			0.46			5.93		
	Ash	w.%	8.66			11.6			6.32			0.5		
	ρ_p	$kg.m^{-3}$	550			697			1200			1000		
	ρ_{sol}	$kg.m^{-3}$	1760			1700			1950			1630		
	S_{Spe}	$m^2.g^{-1}$	123			4.4			27.5			3.7		
Devolatilisation	α_{dev}	$kg_{VM}.kg^{-1}_{Fuel}$	0.309	0.157	0.274	0.0977	0.167	0.180	0.0032	0.0161	0.028	0.0068	0.013	0.0254
	A_{dev}	s^{-1}		$7.41{\cdot}10^5$			$3.67{\cdot}10^5$			$3.41{\cdot}10^5$			$1.19{\cdot}10^5$	
	$E_{a_{dev}}$	$kJ.mol^{-1}$		110			110			110			110	
	$\alpha_{O\rightarrow CO}$	-	0.130	0.141	0.301	0.112	0.224	0.226	0.008	0.044	0.075	0.022	0.039	0.101
	$\alpha_{O\rightarrow CO_2}$	-	0.526	0.133	0.134	0.055	0.066	0.064	0.020	0.041	0.051	0.041	0.069	0.070
	$\alpha_{H\rightarrow H_2}$	-	0.036	0.037	0.262	0.048	0.133	0.357	0.013	0.111	0.347	0.012	0.065	0.263
	$\alpha_{H\rightarrow CH_4}$	-	0.075	0.059	0.094	0.094	0.145	0.145	0.006	0.046	0.059	0.001	0.002	0.005
	$\alpha_{H\rightarrow C_2H_2}$	-	0.003	0.002	0.008	0.002	0.010	0.019	$5{\cdot}10^{-5}$	$1{\cdot}10^{-4}$	$2{\cdot}10^{-4}$	$6{\cdot}10^{-5}$	$2{\cdot}10^{-4}$	$3{\cdot}10^{-4}$
	$\alpha_{H\rightarrow C_2H_4}$	-	0.058	0.046	0.084	0.045	0.061	0.030	$3{\cdot}10^{-4}$	$8{\cdot}10^{-4}$	$4{\cdot}10^{-4}$	$7{\cdot}10^{-4}$	$5{\cdot}10^{-4}$	$5{\cdot}10^{-4}$
	$\alpha_{H\rightarrow C_2H_6}$	-	0.006	0.047	0	0.013	0.010	0	0	0	0	0	$3{\cdot}10^{-5}$	0
	$\alpha_{H\rightarrow C_3H_8}$	-	0	0	$4{\cdot}10^{-4}$	0.001	0.001	0	0	$5{\cdot}10^{-4}$	0	$2{\cdot}10^{-4}$	$5{\cdot}10^{-4}$	$7{\cdot}10^{-4}$
	Minor species													
	α_S	-	0.157	0.157	0.157	0.2	0.4	0.4	0.004	0.07	0.07	0.01	0.01	0.01
	α_N	-		0.47		0.23	0.23	0.37		0.24			0.71	
	η_v	-	0	0	0	0	0	0	0	0	0	0	0	0
	β_v	-	0.002	0.002	0.025	0.009	0.009	0.005	0.008	0.008	0.008	0.001	0.003	0.003
	δ_v	-	0.054	0.054	0.269	0.052	0.391	0.541	0.000	0.005	0.042	0.001	0.005	0.017
	ε_v	-	0	0	0.068	0.021	0.035	0.087	0.013	0.042	0.125	$4{\cdot}10^{-4}$	0.002	0.011
	γ_v	-	$1-\eta_v-\beta_v-\delta_v-\varepsilon_v$			$1-\eta_v-\beta_v-\delta_v-\varepsilon_v$			$1-\eta_v-\beta_v-\delta_v-\varepsilon_v$			$1-\eta_v-\beta_v-\delta_v-\varepsilon_v$		
Char oxidation	A_{OxChar}	$kg_{C_s}.m^{-2}.s^{-1}.atm^{-1}$	$4.26\cdot10^5$			$3.41\cdot10^5$			$9.31\cdot10^2$			$3.12\cdot10^4$		
	$E_{a_{OxChar}}$	$kJ.mol^{-1}$	179.4			179.4			179.4			179.4		
	Minor species													
	η_c	-	0.75	0.75	0.75	0.75	0.3	0.75	0.75	0.75	0.75	0.075	0.15	0.15
	β_c	-	#	#	#	#	#	#	#	#	#	#	#	#
	δ_c	-	#	#	#	#	#	#	#	#	#	#	#	#
	ε_c	-	#	#	#	#	#	#	#	#	#	#	#	#
	γ_c	-	$1-\eta_c-\beta_c-\delta_c-\varepsilon_c$			$1-\eta_c-\beta_c-\delta_c-\varepsilon_c$			$1-\eta_c-\beta_c-\delta_c-\varepsilon_c$			$1-\eta_c-\beta_c-\delta_c-\varepsilon_c$		
NO red.	A_{NO}	$mol_{\text{NO}}.m^{-2}.s^{-1}.atm^{-1}$	$2.01\cdot10^4$			$2.98\cdot10^4$			$3.90\cdot10^2$			$2.71\cdot10^3$		
	$E_{a_{\text{NO}}}$	$kJ.mol^{-1}$	133			133			133			133		

Table 7.1: Heterogeneous reactions parameters used in the model.

7.1.2 Results

7.1.2.1 Released species

We have plotted in Figures 7.1 to 7.4 the time evolution of the mole fraction of VM during experiments at 800, 900, and 1000°C for the lignite, the coal, the anthracite and the petcoke together with the modeled mole fractions. The values under 10 ppm – represented by the bold black dashed line – should not be considered since they are below the detection limit of the analyzers.

The temperature evolution of the species mole fractions after a particle residence time of 2 s is plotted in Figures 7.5 and 7.6. In most of cases the concentrations of released species increase with the temperature. It appears that H_2 becomes the main species released in mole during pyrolysis above 900°C in all cases. CO and CO_2 are also important, as well as CH_4 which is always the major hydrocarbon species. Other species are mainly hydrocarbons like C_2H_2 and C_2H_4. One should note that even under pure nitrogen condition, reactions happen: in all cases, at 1000°C, C_2H_4 mole fraction decreases in time whereas H_2 and C_2H_2 ones increase.

SO_2 is measured, and its concentration increases with temperature. Nitrogen species, like HCN and NH_3 are also released, whereas no presence of NO_x (out of N_2O traces below the detection limit) was measured in this pyrolysis conditions. These results are in close agreement with other experimental results presented in the literature [13,21,22,25,31–33].

Elements balance The partitioning coefficients adjusted for pyrolysis and presented in Table 7.1 allow the element balance to be done for devolatilisation.

Oxygen balance One can note that the proportion of O-atoms released into CO increases with the temperature in all cases, whereas the oxygen pyrolyzed into CO_2 increases between 800 and 900°C and stabilizes above for coal, anthracite and petcoke. In case of lignite $\alpha_{O\rightarrow CO_2}$ decreases first and stay constant between 900 and 1000°C. However, a large part of the O-atoms is not retrieved in the pyrolyzed species. It is assumed to be water.

Hydrogen balance The fraction of H-atoms released into H_2 increases with the temperature in all cases. It is also the case for the other hydrocarbon species CH_4, C_2H_2 and C_2H_4. The behavior observed for C_2H_6 and C_3H_8 should be carefully interpreted because of their measured concentration below the detection limit.

Nitrogen balance The coefficient α_N was determined using the chars ultimate analysis, presented in Table 5.2. In case of coal, it was adjusted afterward at 1000°C, to avoid the sum of the η_v, β_v, δ_v and ε_v to be greater than unity.

One remarks that the fraction of N-atoms released into HCN and NH_3 – δ_v and ε_v respectively – increases with the temperature. η_v always equals zero, because no NO was measured during pyrolysis, as mentioned above.

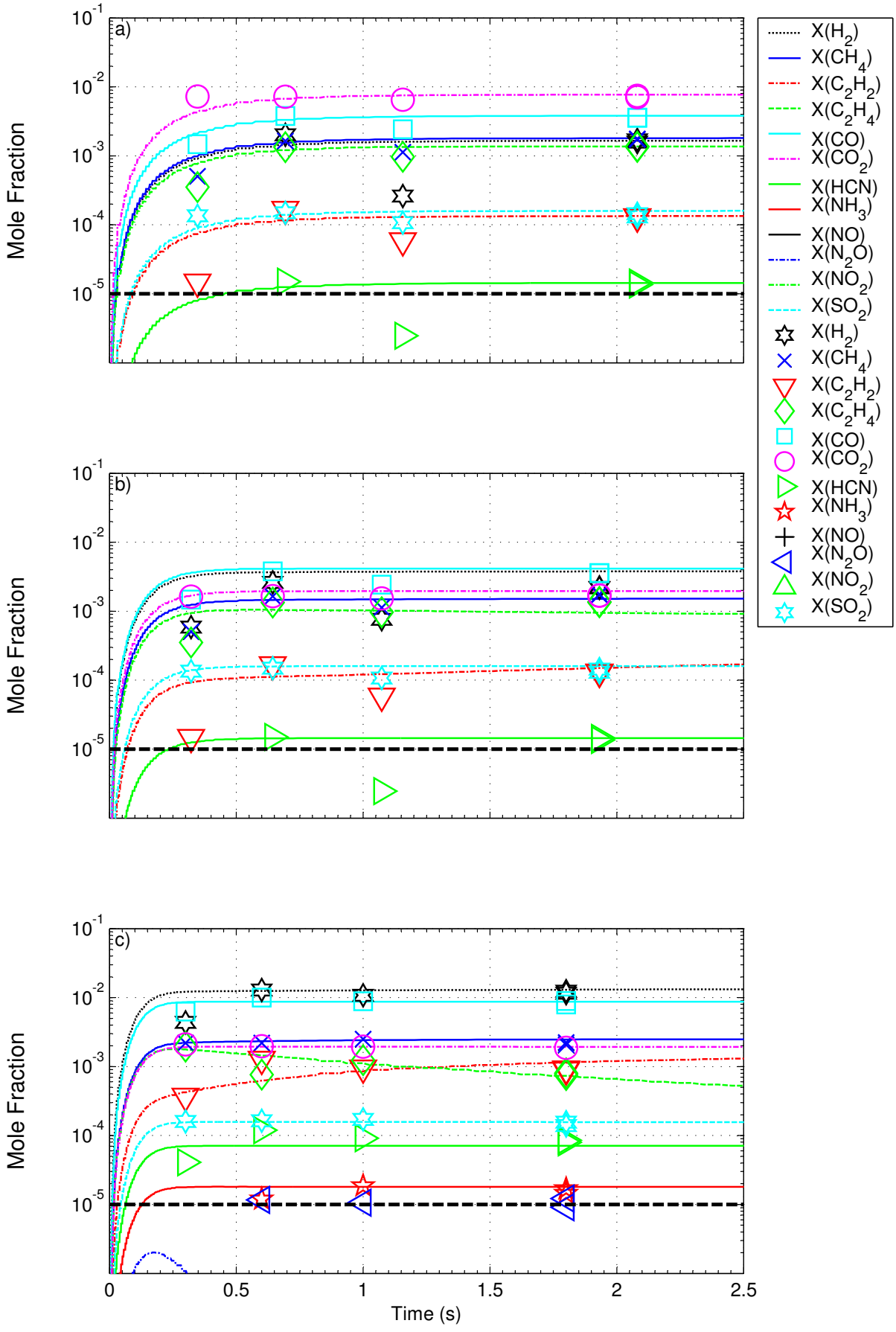

Figure 7.1: Lignite devolatilisation: measured (symbols) and calculated (lines) mole fraction profiles at 800 (a), 900 (b), and 1000°C (c) as a function of particle residence time.

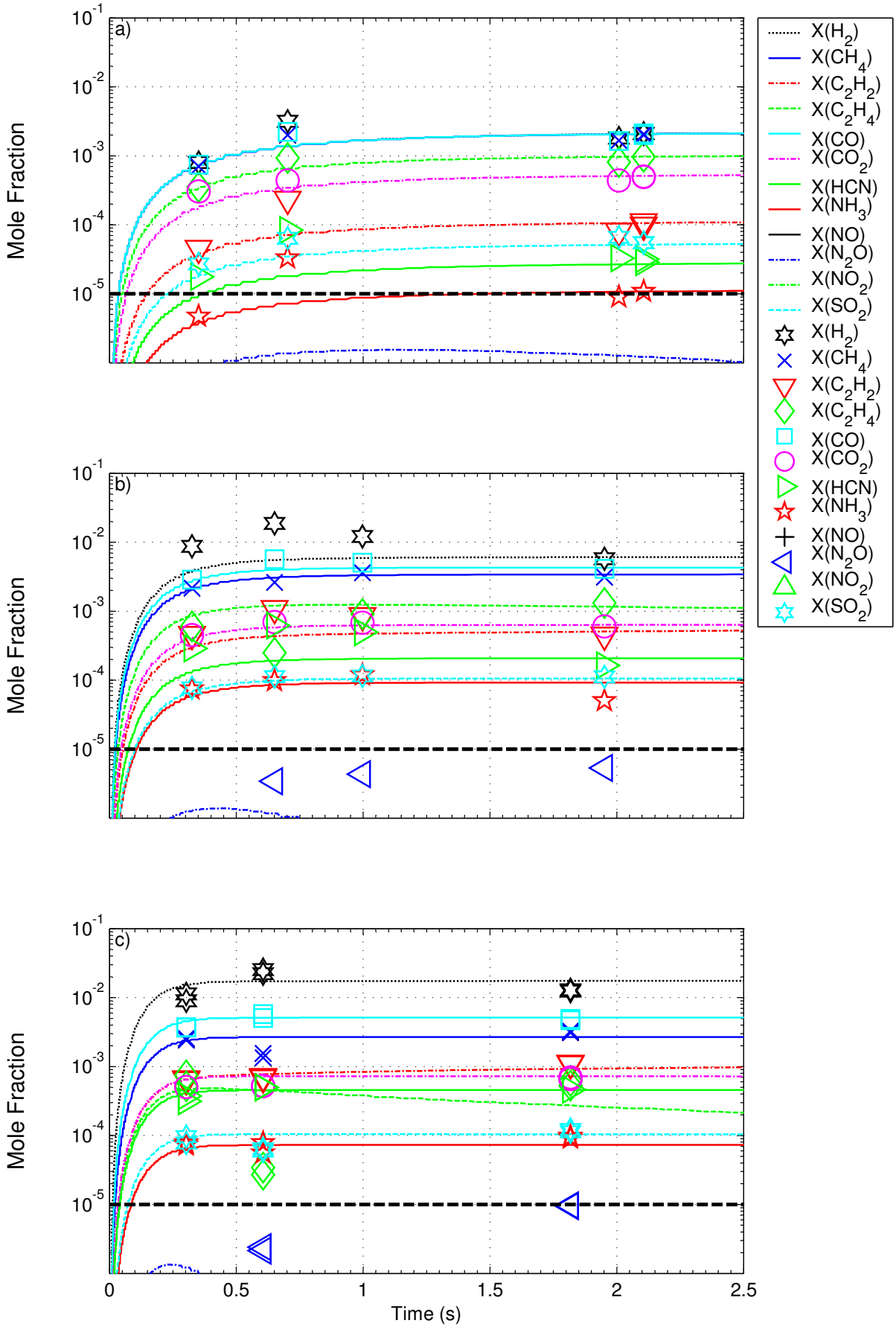

Figure 7.2: Coal devolatilisation: measured (symbols) and calculated (lines) mole fraction profiles at 800 (a), 900 (b), and 1000°C (c) as a function of particle residence time.

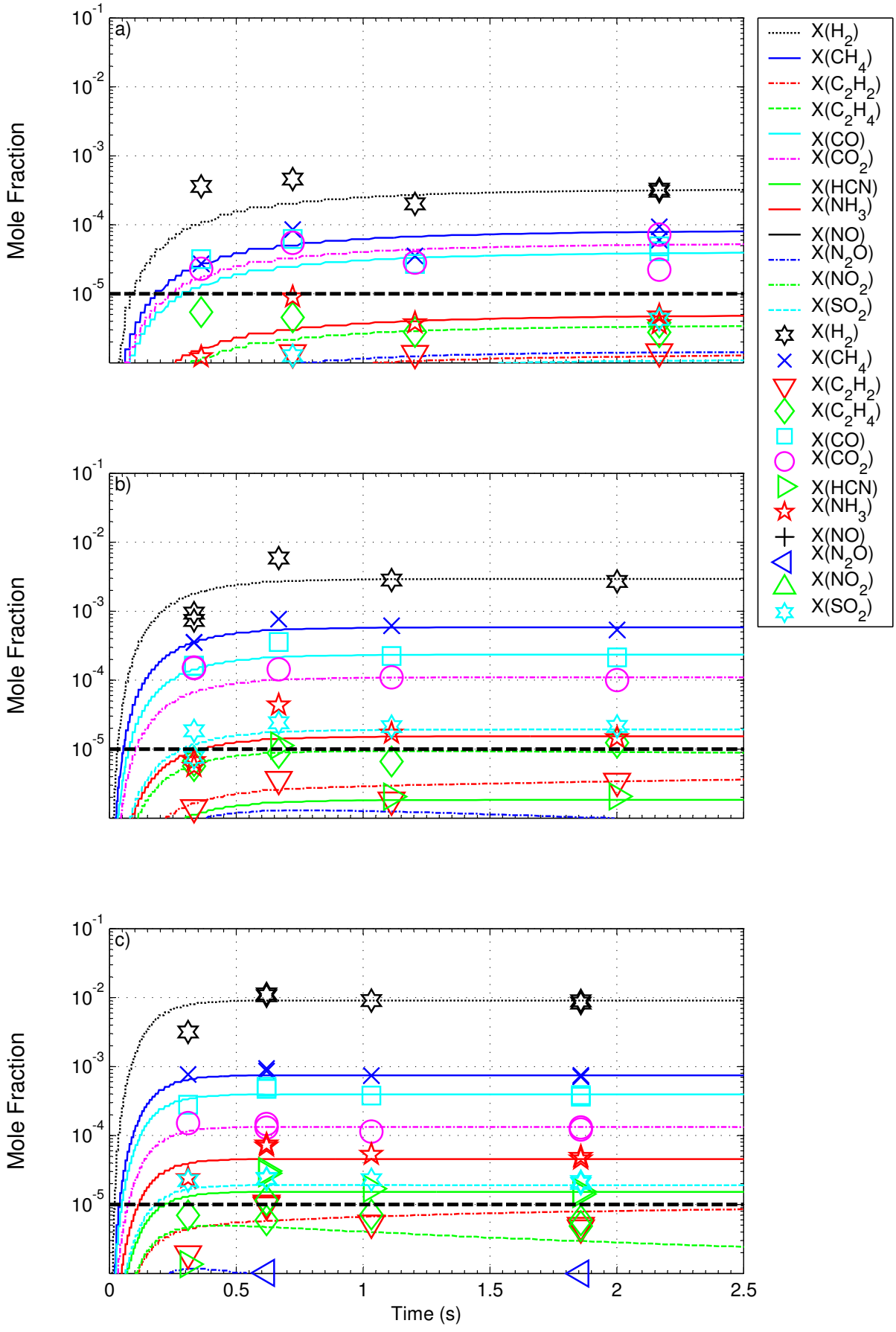

Figure 7.3: Anthracite devolatilisation: measured (symbols) and calculated (lines) mole fraction profiles at 800 (a), 900 (b), and 1000°C (c) as a function of particle residence time.

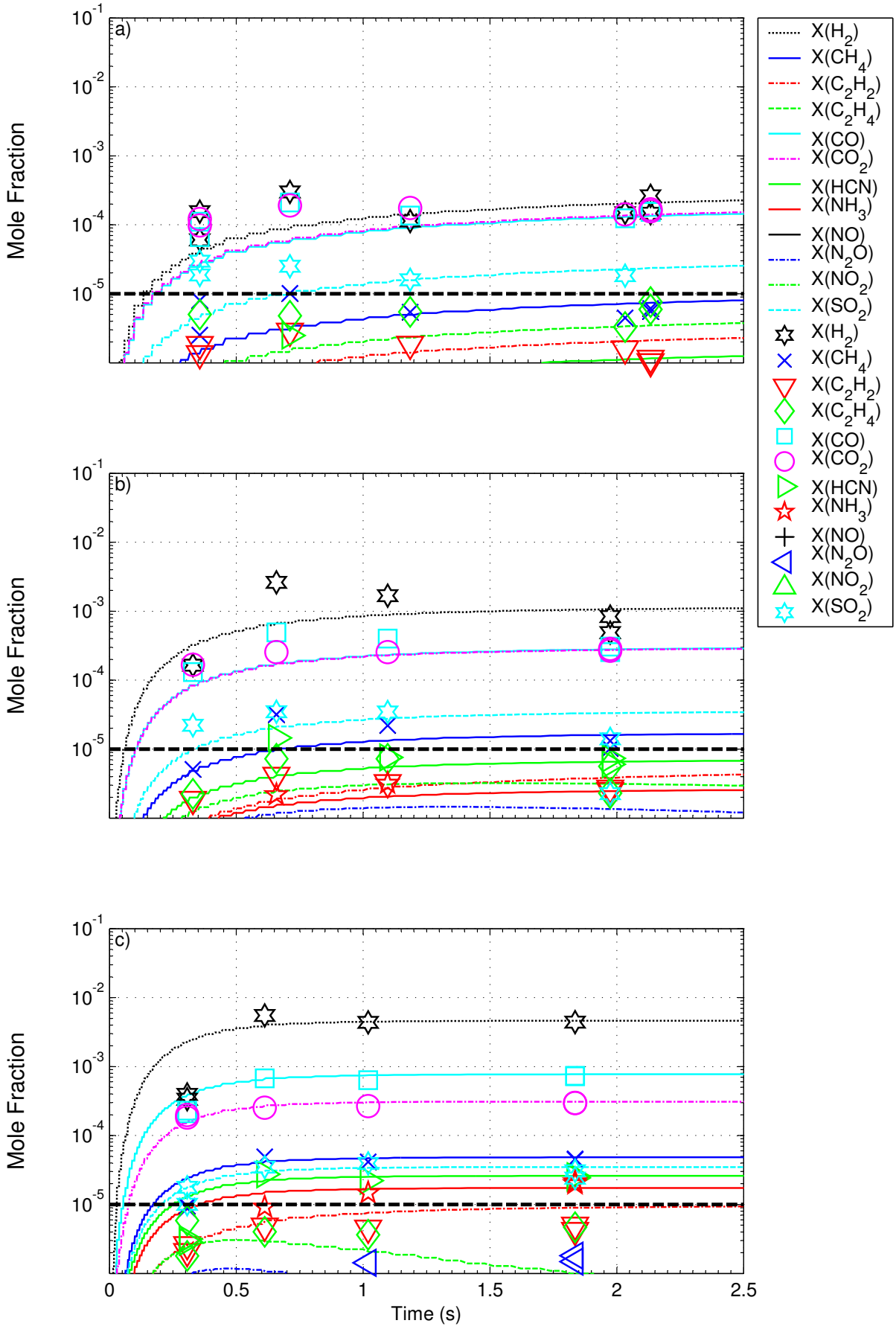

Figure 7.4: Petcoke devolatilisation: measured (symbols) and calculated (lines) mole fraction profiles at 800 (a), 900 (b), and 1000°C (c) as a function of particle residence time.

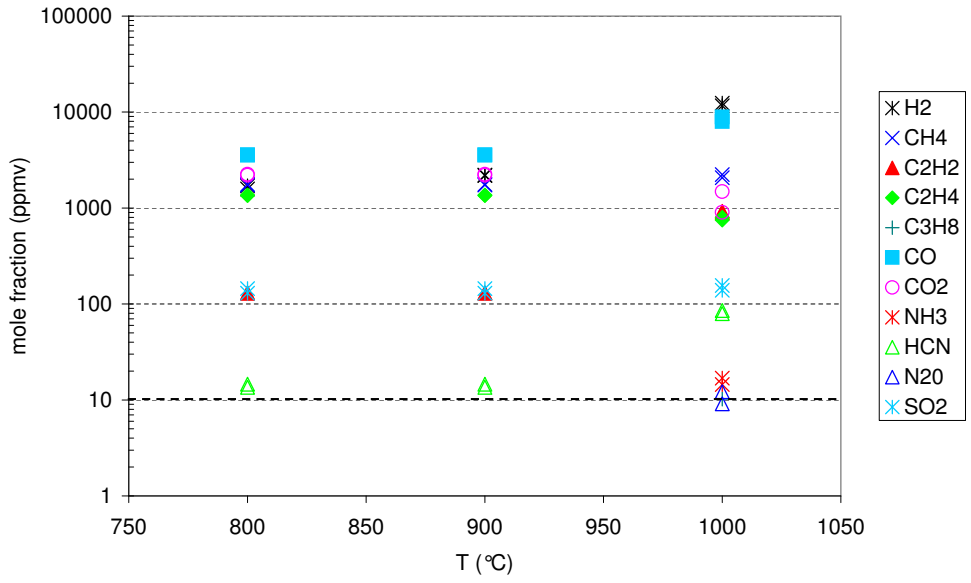

(a)

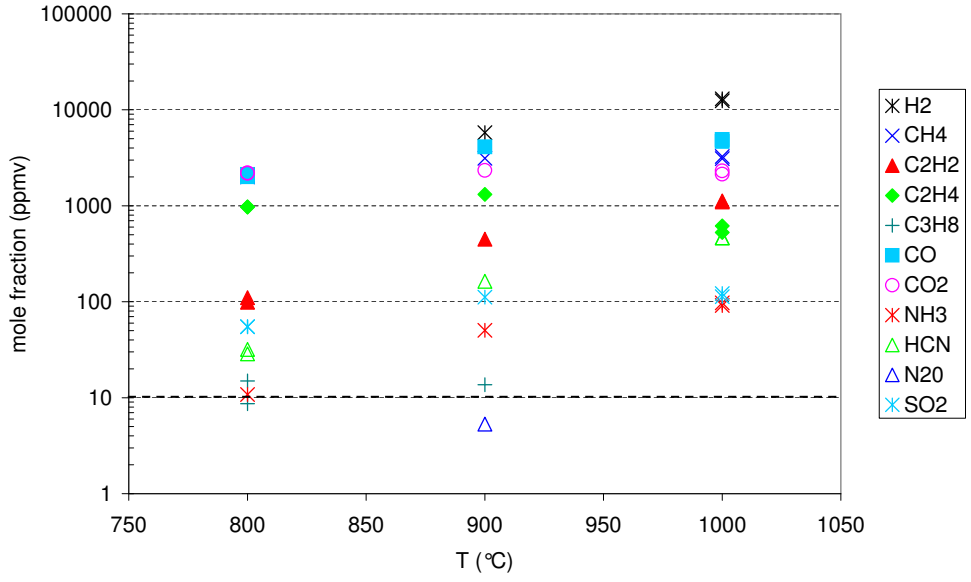

(b)

Figure 7.5: Fuels devolatilisation (7.5(a) Lignite and 7.5(b) Coal): temperature evolution of the analyzed species after 2 s residence time.

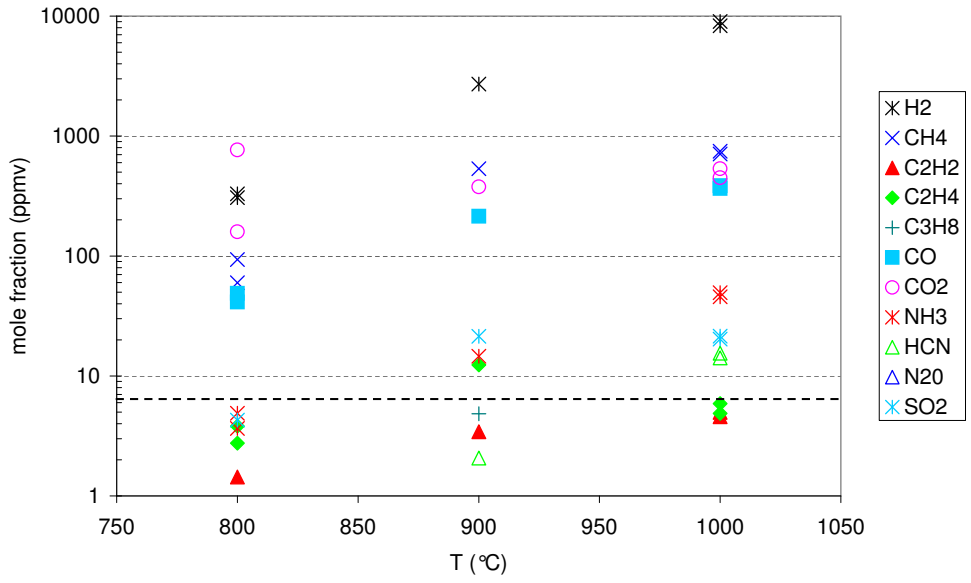

(a)

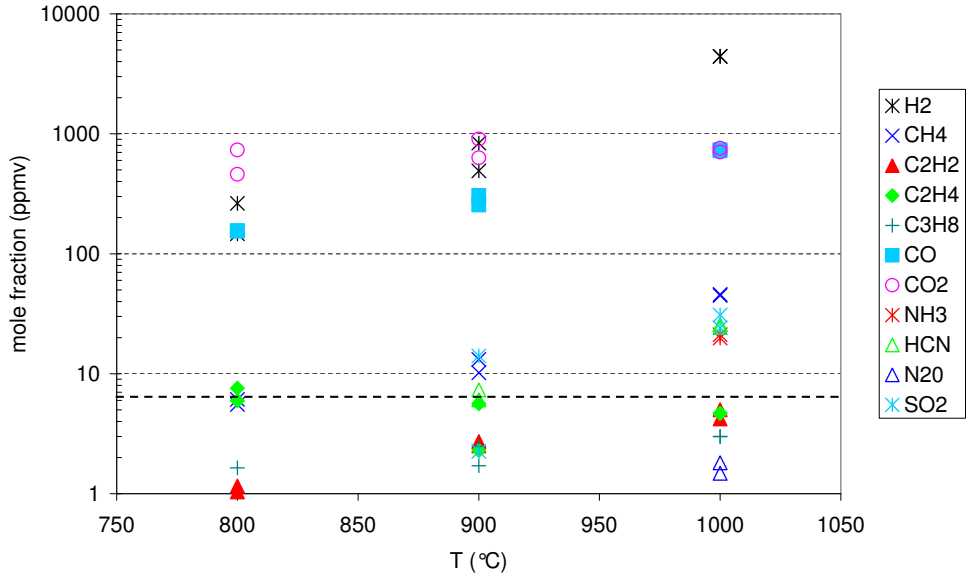

(b)

Figure 7.6: Fuels devolatilisation (7.6(a) Anthracite and 7.6(b) Petcoke): temperature evolution of the analyzed species after 2 s residence time.

7.1.2.2 Devolatilisation kinetics

The traditional ash tracer method was not used here to determine the pyrolysis progress because the ash and volatile contents of several fuels – i.e. Petcoke, Anthracite – are too low (see Table 5.1). As a consequence, the kinetic parameters were derived from the time variation of the total mass of volatile matters analyzed during the experiments, which is equivalent to the ash tracer approach.

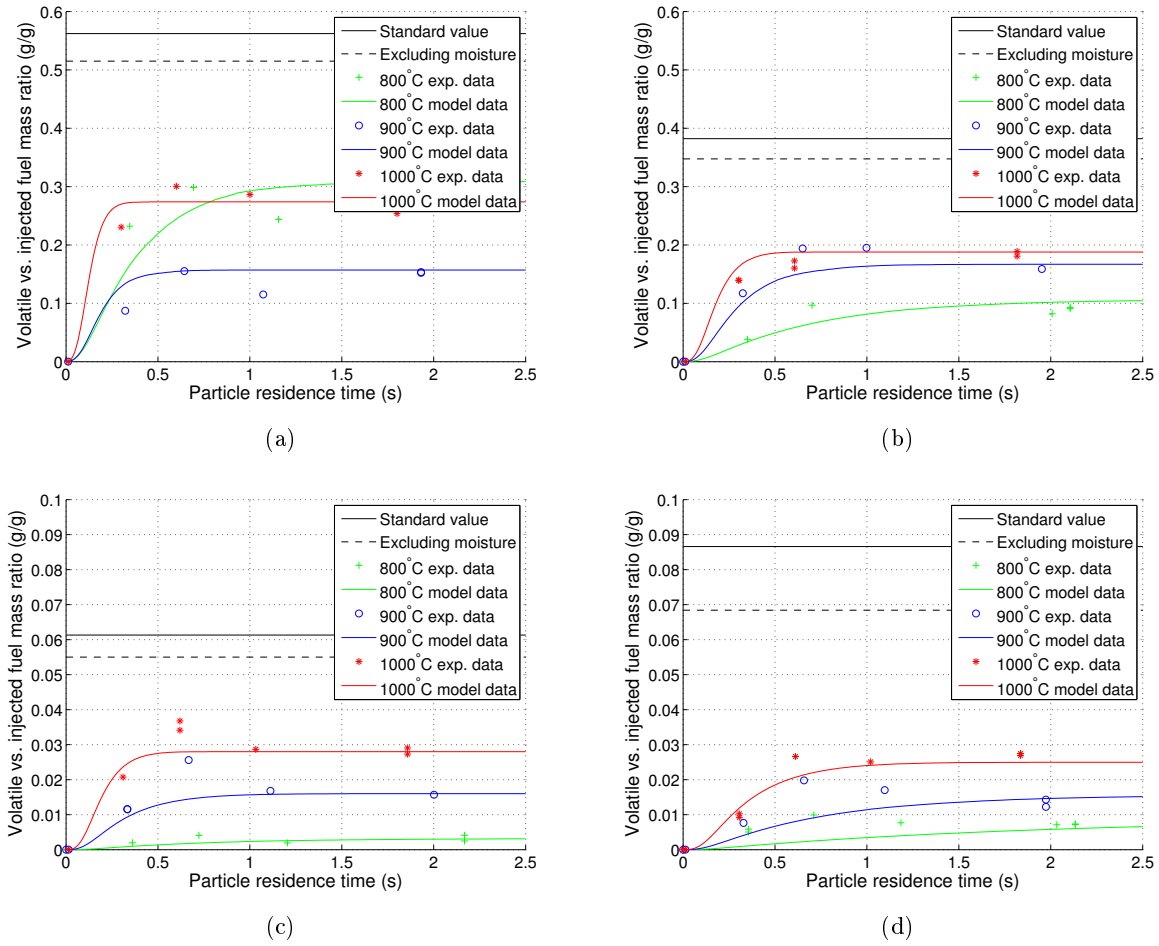

Figure 7.7: Fuels devolatilisation (7.7(a) Lignite, 7.7(b) Coal, 7.7(c) Anthracite, and 7.7(d) Petcoke): time evolution of the sum of measured gas masses normalized to the initial fuel mass flow at different temperatures. Symbols $(+, \circ, *)$: experiment values; colored lines: mathematical fit; black lines: standard test values.

The total mass flow rate for all the VM analyzed has been calculated and plotted for the four fuels in Figure 7.7. It should be noted that the data are normalized to the initial fuel mass flow rate injected into the EFR. The full scale in ordinate is 0.6 g_{VM}/g_{Fuel} for Figures 7.7(a) and 7.7(b), and 0.1 g_{VM}/g_{Fuel} for Figures 7.7(c) and 7.7(d).

The amount represented on these diagrams as a straight black line corresponds to the standard VM content; it is always larger than the sum of the species analyzed. This is due to the fact that several species, such as tars and water, were not measured in the experimental device. The results indicate that half or more of the VM mass was not identified despite the

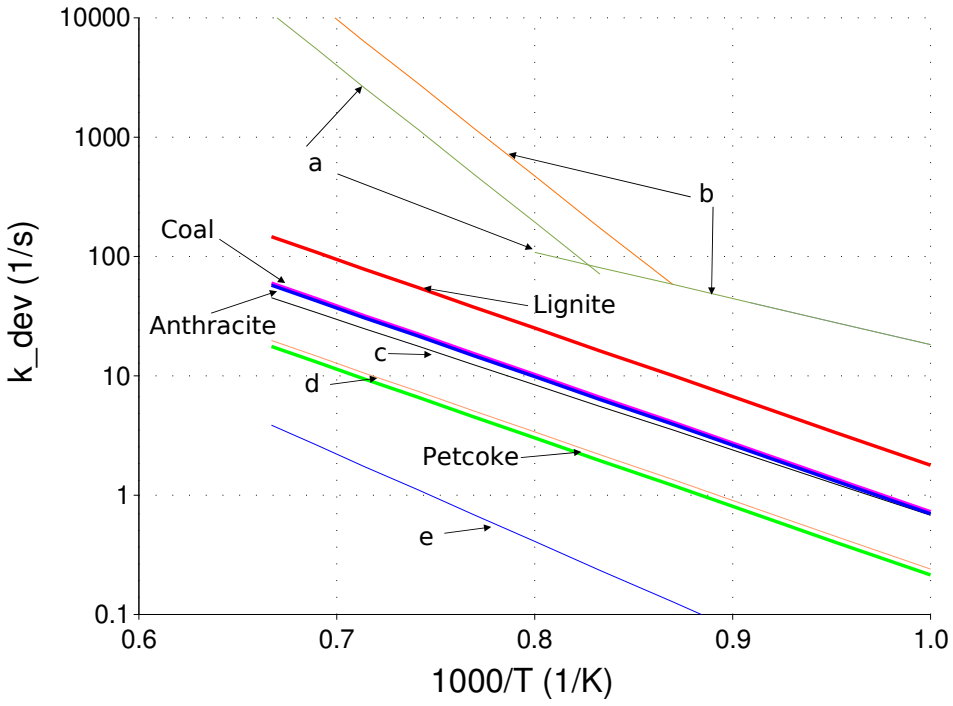

Figure 7.8: Comparison between the determined devolatilisation kinetics for the four fuels and kinetics from the literature: (a): Van de Steene – Coal [15], (b): Ubhayakar – Coal [39], (c): Kobayashi – Coal [38], (d): Commandré – Petcoke [24], and (e): Gat – Coal [108]

large number of species analyzed in this work. In the following, tars are assumed to have the same composition (C, N , S) as char, and to have the same reactivity as char in the oxidation and NO reduction reactions. For the low VM content fuels – anthracite and petcoke – the final mass of VM released increases when the devolatilisation temperature increases from 800 to 1000°C. Surprisingly, this typical behavior is not retrieved in the case of the high VM content of lignite.

The devolatilisation kinetic parameters are presented in Table 7.1. They show that the rate of devolatilisation increases from petcoke to anthracite, coal, and lignite, which is in agreement with the literature [22,24]. The pyrolysis kinetics of lignite is twice that of coal and anthracite and more than six time quicker than petcoke's. The values for lignite pyrolysis kinetic parameters are close to those reported by Dupont [109] about biomass flash devolatilisation. The Arrhenius diagram for this kinetic parameters compared to kinetics from the literature [15,24,38,108] are plotted in Figure 7.8.

7.2 Char oxidation

7.2.1 Experimental and modeling protocol

The char oxidation

- is responsible for the formation of gaseous N-species
- consumes char residue, that itself reduces some NO in the gas phase.

Its reaction kinetics has to be known. Chars were previously produced by pyrolyzing the fuels at 900°C under 3 % O_2 as described in section 5.4. Chars were re-injected into the EFR and samples were taken after a 2 s particle residence time.

The total atmosphere gas flow rate in the reactor and its distribution between pneumatic transport and preheated atmosphere flow are the same as that in pyrolysis experiments case. The oxygen concentration was set to 3 %. This value of 3 % O_2 was selected to obtain high enough fuel burnout for accurate determination to be reached, on the base of O_2 consumption measurements.

Because of their high reactivities, coal and lignite chars were injected at the feeding rate of 0.5 g/min, whereas petcoke and anthracite were fed at the rate of 1.5 g/min.

The pre-exponential factor, A_{OxChar} in Equation 6.10 in the model, is adjusted through a minimization of the difference between the experimental results obtained at the three temperatures 800, 900, and 1000°C and model computed values. The activation energy, $E_{a_{OxChar}}$, was kept constant to the Smith value: 179,4 kJ.mol^{-1} [61].

7.2.2 Results

The mole fractions of the analyzed species evolution in function of temperature are plotted in Figures 7.9 and 7.10. The CO_2 mole fraction increases, whereas CO decreases with the temperature in all cases. As well as SO_2, NO also increases with the temperature. Otherwise, all the other measurement are below the detection limit of 10 ppm.

One purpose of these experiments was to set the values of the partitioning coefficients for the char oxidation, η_c, β_c, δ_c and ε_c. Due to the low experimental values, we are unable to set precisely these partitioning coefficients, except for NO. However, they do not play a great role in the complete reburning modelings, where the char burnout is negligible, as illustrated in Figures 8.4 and 8.5: it was checked that no sensitive variations of the final NO mole fraction was found when those coefficients are set to zero. Consequently, the coefficients impossible to be properly adjusted are replaced by the symbol # in the Table 7.1.

The experimental and modeling results after parameter fitting are compared in Figures 7.11(a) and 7.11(b). The kinetic parameters derived are summarized in Table 7.1.

The lignite char is the most reactive one; anthracite char is the least reactive char (see Figure 7.11(a)). Coal and lignite chars, which were fed at the feeding rate of 0.5 g/min, consumed

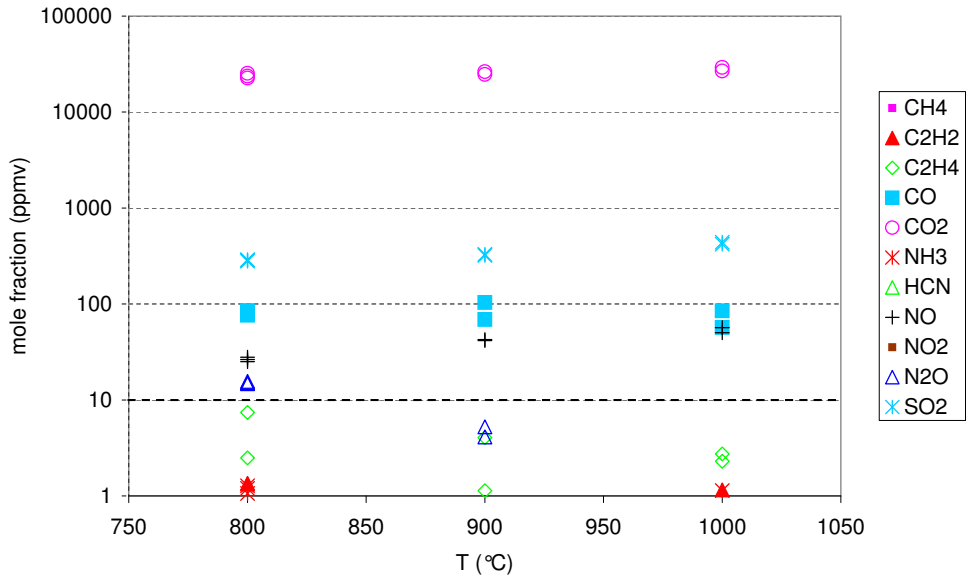

(a)

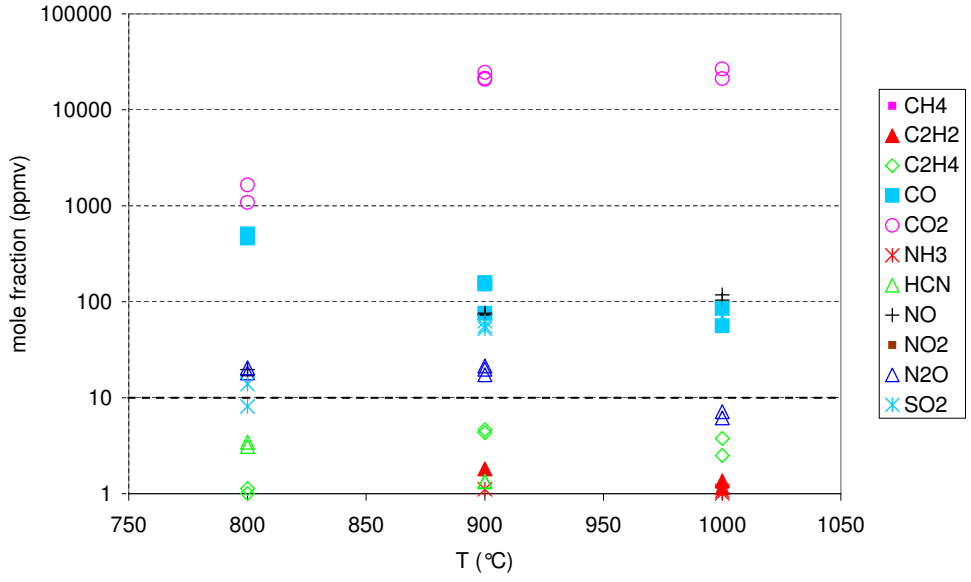

(b)

Figure 7.9: Chars oxidation (7.9(a) Lignite and 7.9(b) Coal): temperature evolution of the analyzed species after 2 s residence time.

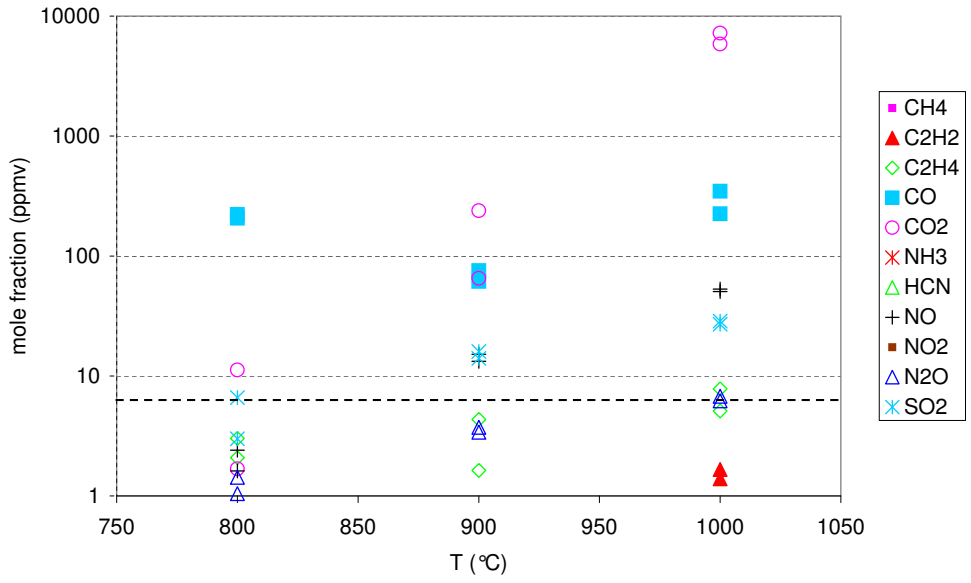

(a)

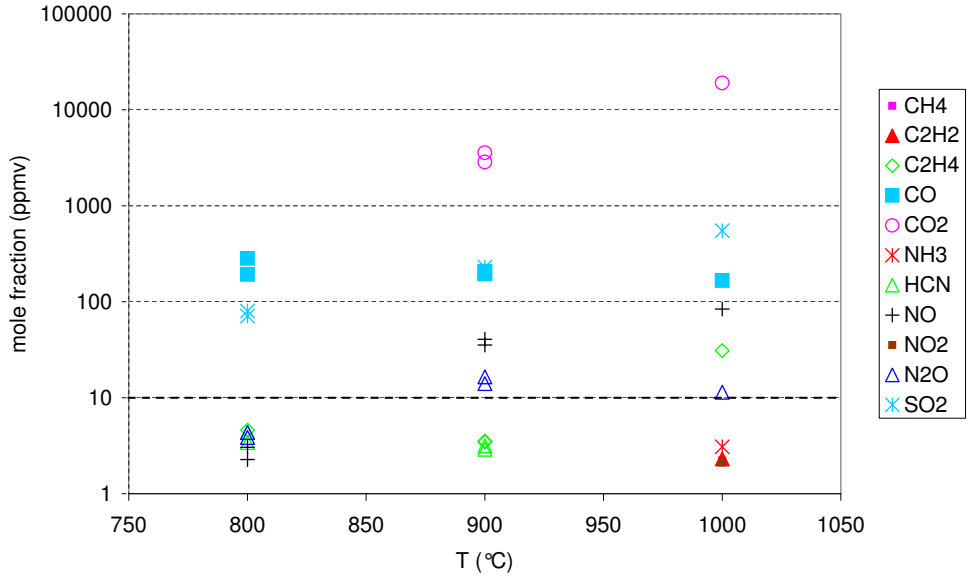

(b)

Figure 7.10: Chars oxidation (7.10(a) Anthracite and 7.10(b) Petcoke): temperature evolution of the analyzed species after 2 s residence time.

more oxygen than anthracite and petcoke chars, injected at a higher rate of 1.5 g/min. The Arrhenius diagram presented in Figure 7.11(b) shows that the reactivity of coal char is two orders of magnitude higher than that of anthracite char; the reactivity plotted in this diagram is specific surface based. Thus lignite and petcoke are superposed. The Smith kinetics is also plotted to compare with the literature. The values from the present work are well dispersed around the Smith average correlation.

Once kinetic parameters are fitted, it is possible, from the results of the model, to analyze the char combustion process in more details. The modeled gas and particle temperatures are plotted in the left hand side graphs of the Figures 7.12 and 7.13 in case of experiments at 1000°C. The temperature of the particles remains very close to that of the atmosphere gas. They reach a peak temperature around 0.5 s residence time, but the temperature increase as compared with the furnace temperature remains small. Additionally, char oxidation progress variables – char dimensionless mass, char burnout – defined as the ratio of the mass loss to the char initial mass – and Thiele effectiveness – are also plotted in the center graphs of Figures 7.12 and 7.13. The char oxidation for lignite is highly limited by porous diffusion, as shown by the relative Thiele effectiveness. High volatile fuels – lignite and coal – which have the more reactive chars, show char burnout of more than 80 and 70 % for lignite and coal respectively, whereas low volatile fuels – anthracite and petcoke – have much lower char burnouts, both below 10 %. The time evolution for O_2, CO and CO_2 mole fractions are plotted in the right hand side graphs of the Figures 7.12 and 7.13. Experimental values are added and show a close agreement between the model and experimental data. This confirms that the use of the Arthur's law, presented in Equation 6.7 in Chapter 6 is adequate.

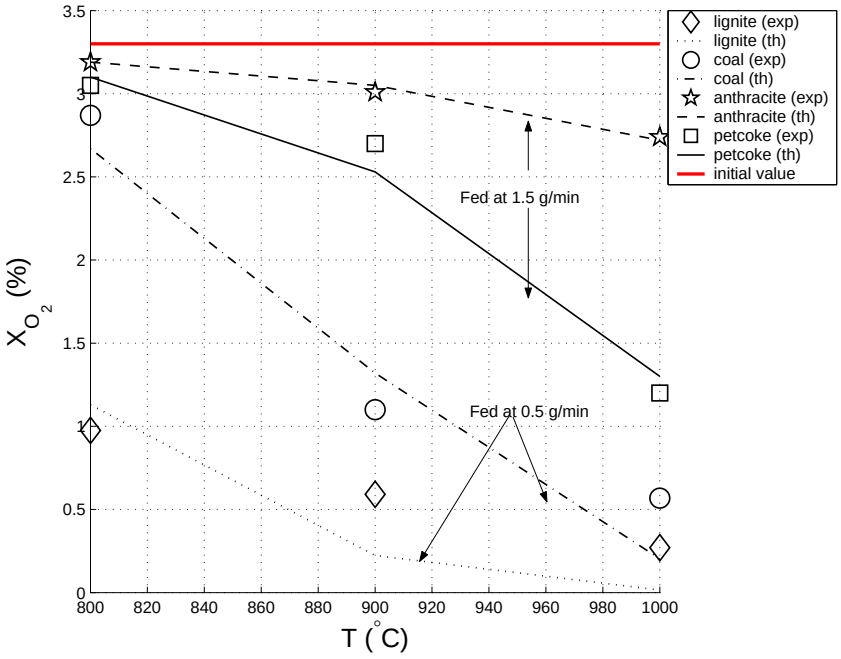

(a)

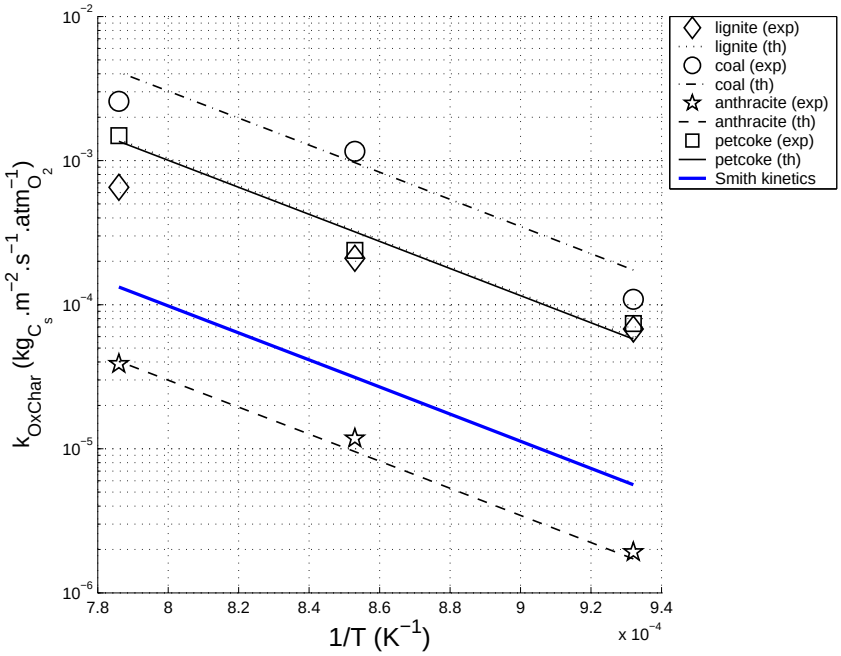

(b)

Figure 7.11: O_2 mole fraction decrease vs. temperature (Figure 7.11(a)) and the corresponding Arrhenius diagram (Figure 7.11(b)) – symbols correspond to experiments while lines are calculated values. Smith kinetics is plotted from [60]

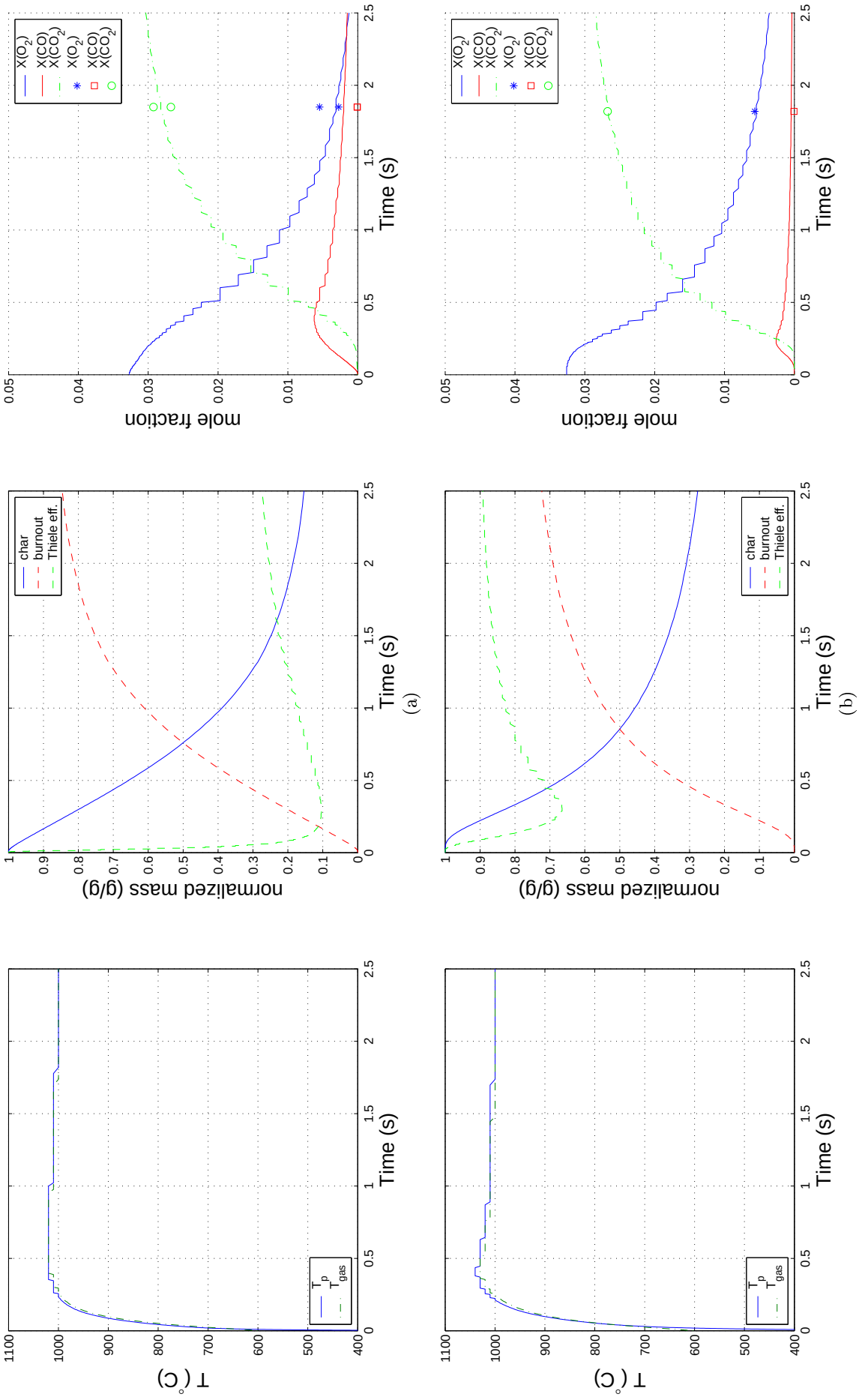

Figure 7.12: Chars oxidation (7.12(a) Lignite and 7.12(b) Coal) at 1000°C: time evolution of gas and particle temperatures (left), of reaction progress – i.e. char mass, burnout, and Thiele effectiveness – (center) and of experimental – symbols – and modeled – lines – of O_2, CO and CO_2 mole fractions (right).

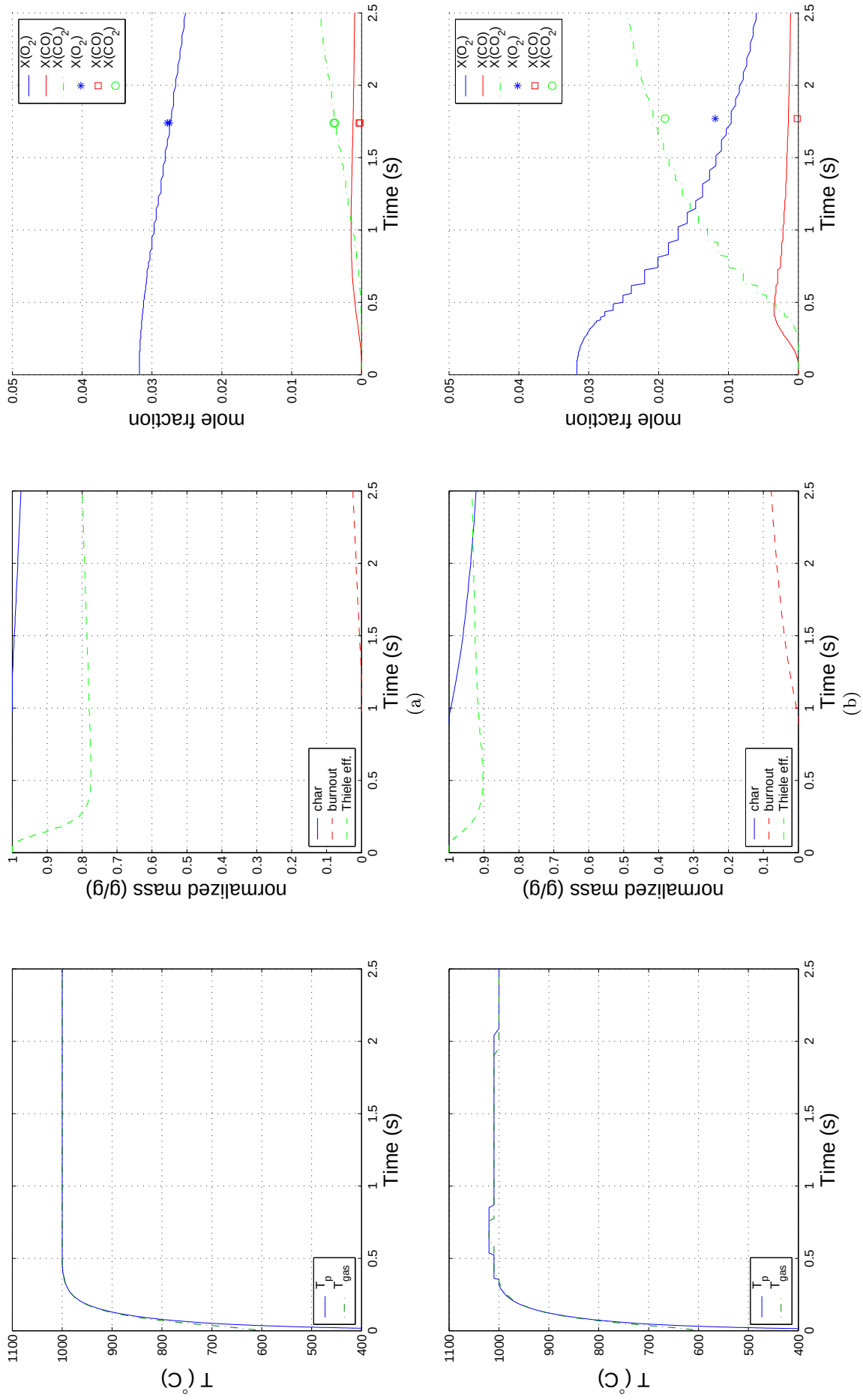

Figure 7.13: Chars oxidation (7.13(a) Anthracite and 7.13(b) Petcoke) at 1000°C: time evolution of gas and particle temperatures (left), of reaction progress – i.e. char mass, burnout, and Thiele effectiveness – (center) and of experimental – symbols – and modeled – lines – of O_2, CO and CO_2 mole fractions (right).

7.3 NO Reduction by char

7.3.1 Experimental and modeling protocol

The chars were produced as described in section 5.4 and were re-injected into the EFR in an atmosphere containing 880 ppm NO in N_2. The particle and gases were sampled after a particle residence time of 2 s.

The transport and the atmosphere preheated gas flow rate are the same as that in corresponding pyrolysis and char oxidation experiments.

The chars were fed at the rate of 1.5 g/min for coal, anthracite and petcoke chars. Lignite char was injected with a 0.5 g/min feeding rate, because of its high reactivity.

The NO reduction by chars experiments were then modeled. The decrease of the NO mole fraction along the EFR enables the Arrhenius parameters for this heterogeneous reaction to be determined. In the minimization process, only the pre-exponential factor A_{NO} was adjusted to fit the the experimental NO concentration. The activation energy $E_{a_{\mathrm{NO}}}$ was kept constant at 133 kJ.mol^{-1}; this value was outlined by Aarna et al. [90] after averaging of a large number of experimental data. This value was confirmed by [67, 75].

7.3.2 Results

The experimental results and modeled values are plotted in terms of NO mole fraction decrease and an Arrhenius diagram in Figures 7.14(a) and 7.14(b). The kinetic parameters derived are presented in Table 7.1. A close agreement between the calculated values and the experimental results was found for all fuels (see Figure 7.14). The average kinetics proposed by Aarna et al. [90] is plotted for comparison with literature. The surface related kinetic constants of the present work are up to three orders of magnitude quicker than that of Aarna et al. However, the activation energy initially outlined by Aarna is once again confirmed.

The lignite char is the most reactive one; petcoke and anthracite chars are less reactive (see Figure 7.14(a)). The specific surface related reactivity presented in an Arrhenius diagram in Figure 7.14(b) shows that two orders of magnitude separate the reactivities of coal and anthracite chars.

It is interesting to note that the reactivities for NO reduction by char and char oxidation reactions are in the same order: the coal char is the most reactive in both cases – oxidation or NO reduction – and anthracite is the slowest.

During the NO reduction by char modeling, a temperature increase of less than 1°C was observed. Moreover, the char burnout was always very low: below 1 %.

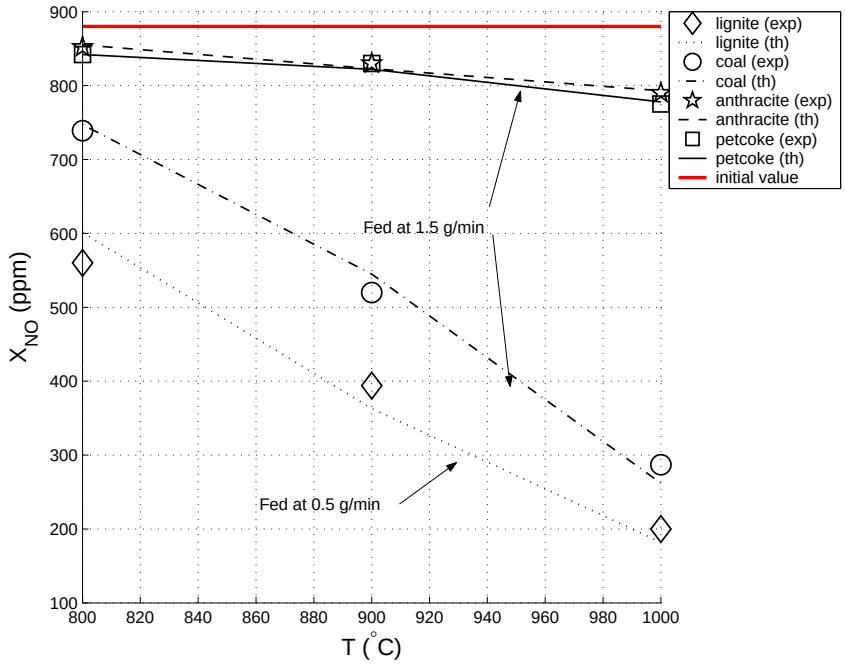

(a)

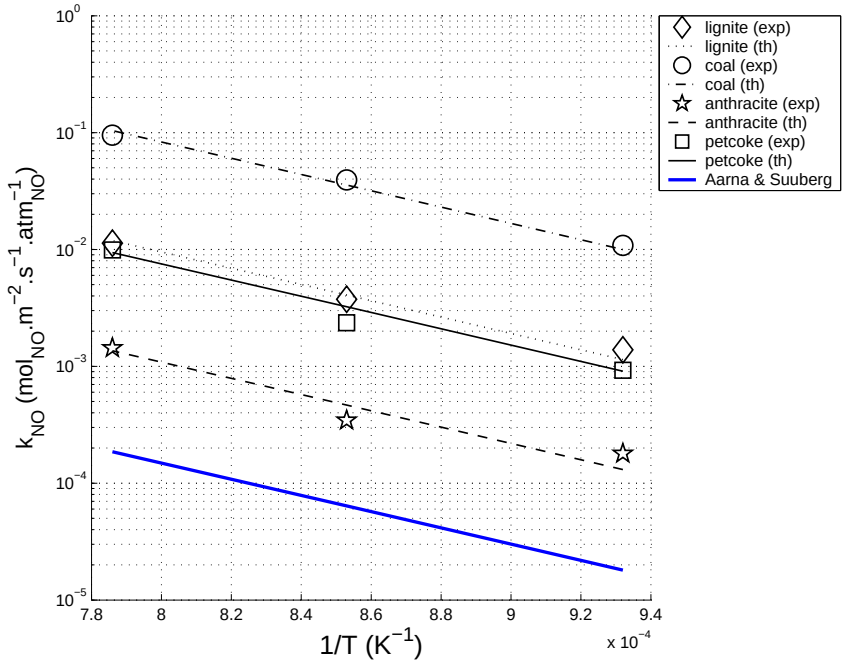

(b)

Figure 7.14: NO mole fraction decrease vs. temperature (Figure 7.14(a)) and the corresponding Arrhenius diagram (Figure 7.14(b)) – symbols correspond to experiments while lines are calculated values. Aarna kinetics is plotted from [90]

7.4 Concluding synthesis

- The first experiments, where the fuels were pyrolyzed under 100 % N_2, made it possible to quantify the variety of the species released and the kinetics of the devolatilisation reaction. This was achieved at three temperatures: 800, 900, and 1000°C.

  The lignite, that has the lower rank and higher volatile matters amount, has the highest devolatilisation kinetics. Although they are greatly different fuels, coal and anthracite have similar pyrolysis kinetic parameters; petcoke is the slowest.

- Secondly, the char oxidation kinetics were characterized by running experiments under 3 % O_2, and the release of N- and S-containing gas species were characterized.

  One observe here that lignite and coal chars have much higher char oxidation reactivity than anthracite and petcoke one.

Table 7.2: Reactivity of chars for oxidation: $A_{O_2} \times S_{spe}$.

Fuel Name	$A_{OxChar} \times S_{spe}$ $[s^{-1}.atm_{O_2}^{-1}]$
Lignite	$5.24 \cdot 10^7$
Coal	$1.54 \cdot 10^6$
Anthracite	$2.56 \cdot 10^4$
Petcoke	$1.15 \cdot 10^5$

The values presented in Table 7.2 represent the product of the pre-exponential factor A_{O_2} (presented in Table 7.1) of the Arrhenius law for char oxidation by the reactive surface S_{spe} (presented in Table 5.2), that is more representative of the intrinsic reactivity of chars than A_{O_2} alone, which is surface related. They show clearly the very large difference of reactivity between lignite and anthracite chars : a factor of more than 2000 differentiates the two values.

- Thirdly, the char NO reduction reaction was investigated experimentally. The kinetic parameters were determined by adjusting the kinetic parameters to match the experimental values. As in case of char oxidation, the product of A_{NO} (presented in Table 7.1) by the reactive surface S_{spe} (presented in Table 5.2) is presented in Table 7.3. Note that A_{NO} is converted in terms of consumed carbon to be compared with A_{OxChar}. The reactivity of lignite char is about 250 times larger than petcoke chars.

Table 7.3: Reactivity of chars for NO reduction: $A_{NO} \times S_{spe}$.

Fuel Name	$A_{NO} \times S_{spe}$ $[s^{-1}.atm_{NO}^{-1}]$
Lignite	$2.96 \cdot 10^4$
Coal	$1.57 \cdot 10^3$
Anthracite	$1.28 \cdot 10^2$
Petcoke	$1.20 \cdot 10^2$

$A_{\mathrm{NO}} \times S_{spe}$ is plotted in function of $A_{\mathrm{O}_2} \times S_{spe}$ in Figure 7.15. The reference line $y = \frac{x}{1000}$ is also plotted. Char oxidation and NO reduction by char reactions are clearly correlated; a char that oxidizes rapidly reduces NO efficiently. One remarks that $A_{\mathrm{NO}} \times S_{spe} \ll A_{\mathrm{O}_2} \times S_{spe}$ by a factor of about 1000.

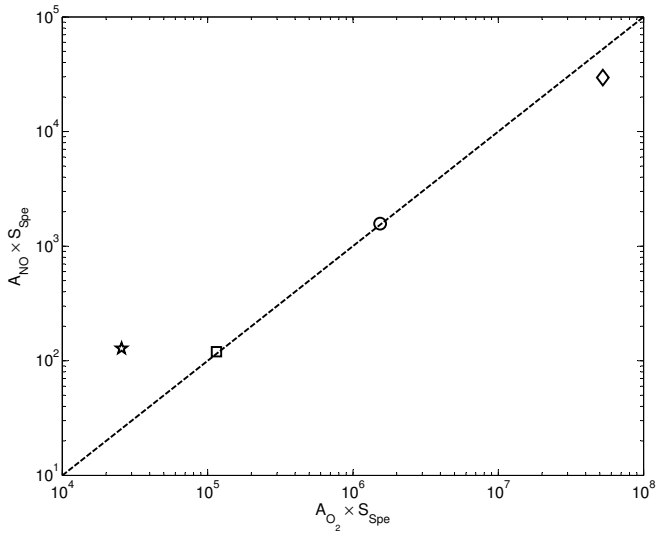

Figure 7.15: $A_{\mathrm{NO}} \times S_{spe}$ in function of $A_{\mathrm{O}_2} \times S_{spe}$. $\diamond$ Lignite, $\circ$ Coal, $\stackrel{\star}{\sim}$ Anthracite, and $\square$ Petcoke.

After the preceding considerations, it appears that the lower the rank of the fuel studied in this work, the higher the reactivity in both the heterogeneous elementary reactions of char oxidation and NO reduction by char. This observation should be carefully considered. Indeed, only four fuels have been characterized, and no statistical or general interpretation is possible.

Chapter 8

Detailed analysis of the reburning conditions

Contents

8.1 Experiments and modelings of reburning with solid fuels 128

8.1.1 Experimental and modeling protocol 128

8.1.2 Results 128

8.1.3 Synthesis 136

8.2 Detailed analysis of the gas phase reactions 140

8.2.1 Introduction 140

8.2.2 Choice of the dates 140

8.2.3 Identification of the pathways in gas phase reactions 147

8.2.4 Results and discussion 147

8.2.5 Discussion 170

8.2.6 Synthesis 172

In the Chapter 7, the elementary heterogeneous reactions were characterized independently. The model parameters for each reaction were adjusted to fit the experimental data. They are all summarized in Table 7.1.

This chapter focuses on the complete reburning conditions, where all the reactions happen simultaneously. Results of the experiments and of the modelings that were carried out are presented in the following sections.

In order to explain surprising gas phase behavior, a detailed analysis of the homogeneous reactions was also performed for high volatile fuels (lignite and coal).

8.1 Experiments and modelings of reburning with solid fuels

8.1.1 Experimental and modeling protocol

Reburning experiments were first carried out with the four fuels, at the three furnace temperatures 800, 900, and 1000°C, with a particle residence time of 2 s. 1.5 g/min of original fuel was fed into the EFR. The total atmosphere gas flow rate was 18.55 l/min (STP); the composition was 1.5 % O_2 and 880 ppm NO.

These experiments aimed at reproducing all the thermochemical phenomena occurring in the reducing zone of a calciner together. Then, the reburning experiments were modeled using the kinetic parameters and partitioning coefficients as determined previously. At this stage, no parameters were adjusted. The results were compared to experimental data.

8.1.2 Results

8.1.2.1 Experiments

The measured NO consumption after 2 s for the four fuels at the three experimental temperatures was plotted in Figure 8.1. This consumption is expressed as the difference between the initial and the final NO mole fractions in the gas phase. It appears clearly that lignite and coal are more efficient in reducing NO than low volatile fuels. Lignite is the most efficient NO reducer, whereas anthracite is the least.

The NO reduction capability increases with temperature for all fuels, but not with comparable sensitivities: for instance, the NO reduction capacity of lignite varies much less with temperature than the NO reduction capacity of coal.

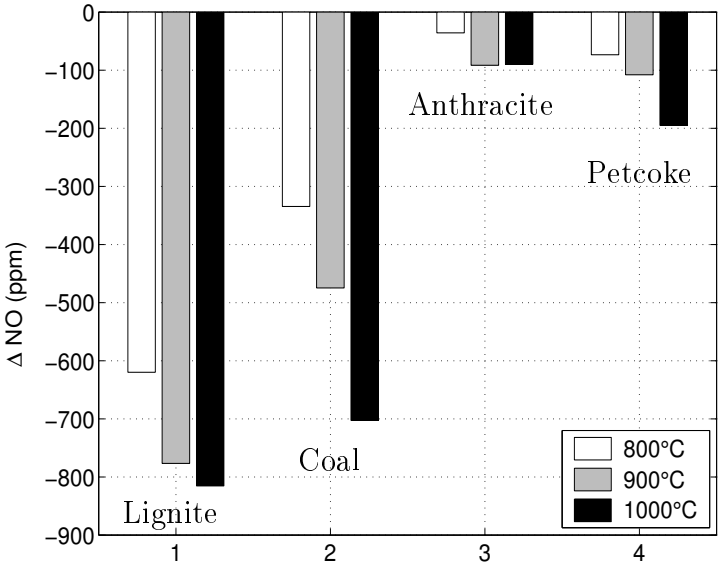

Figure 8.1: Experimental NO reduction during reburning experiments at 800, 900, and 1000°C for the four fuels. Initial atmosphere composed of 1.5 % O_2 and 880 ppmv NO

In the following, the experimental temperature of 1000°C is chosen to present some results because the chemical reactions are more active at this temperature. Thus the variations of the species concentrations are larger and more chemical mechanisms occur. Moreover, this allow to extrapolate these results to other process at higher temperatures than cement plant calciners.

It is of particular interest to observe the composition of the gas phase for pyrolysis and for reburning experiments (at 1000°C) that are plotted together in Figures 8.2 and 8.3. One can see that, in the case of high volatile fuels – lignite and coal –, the gas phase composition is relatively similar between pyrolysis (inert atmosphere, named Type 1 in figures) and reburning experiments (in the presence of 1.5 % O_2 and 880 ppm NO, named Type 4 in figures). In the case of low volatile fuels – petcoke and anthracite –, hydrocarbons are no longer present in the gas phase at the end of reburning experiments. These hydrocarbons have been oxidized and the gaseous atmosphere is different from the pyrolysis atmosphere. The reburning reactions cannot be more detailed without numerical modeling.

Another very interesting result clearly appears comparing Figures 8.2 and 8.3 : the hydrocarbons have lower mole fraction in the case of the low-volatile fuels that high-volatile fuels, whatever the experiment type. The concentration of ethylene (C_2H_4) and acetylene (C_2H_2) are much lower for anthracite (ca. 7 ppm), and petcoke (ca. 7 ppm) than for lignite (ca. 1000 ppm) and coal (ca. 600 and 1000 ppm) under pyrolysis conditions. As demonstrated previously, these C_2 hydrocarbons are very efficient reburning fuels [49, 50, 84, 96, 98]. Ammonia is also released through the pyrolysis of the four fuels at a concentration of ca. 20-100 ppm. Since these levels are much lower than that of the NO used here (880 ppm), the reduction of NO by ammonia should not be efficient [96, 110].

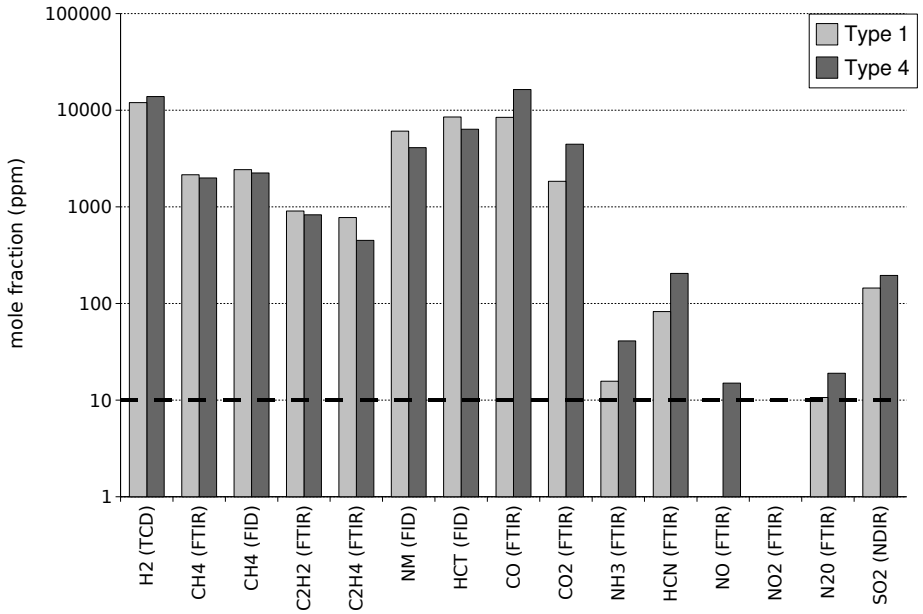

(a)

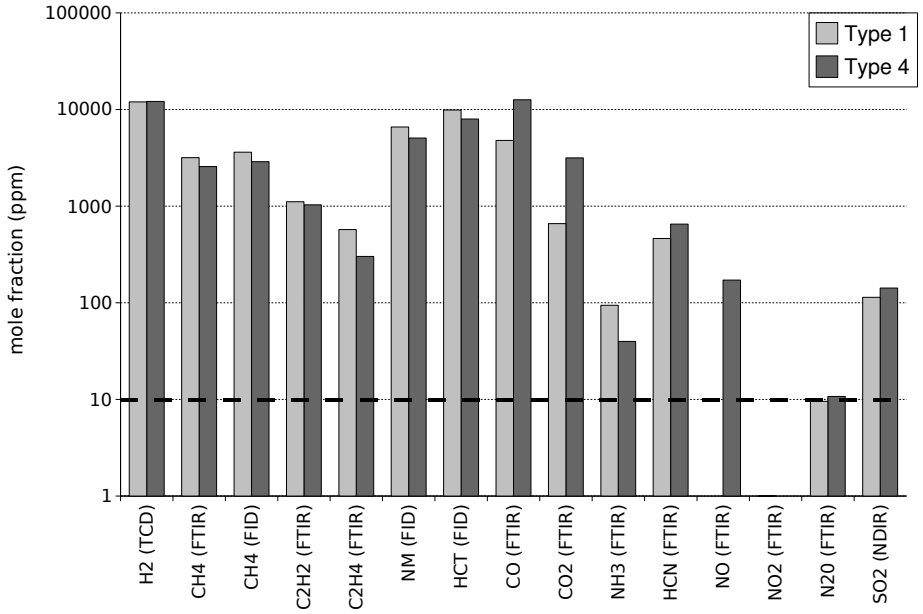

(b)

Figure 8.2: Composition of the gas phase for two different experiment types: Type 1 – pyrolysis experiments, Type 4 – reburning experiments (Lignite 8.2(a) and Coal 8.2(b)) at 1000°C. NM : non-methane hydrocarbons, HCT : total hydrocarbons. The dashed line represents the detection limit.

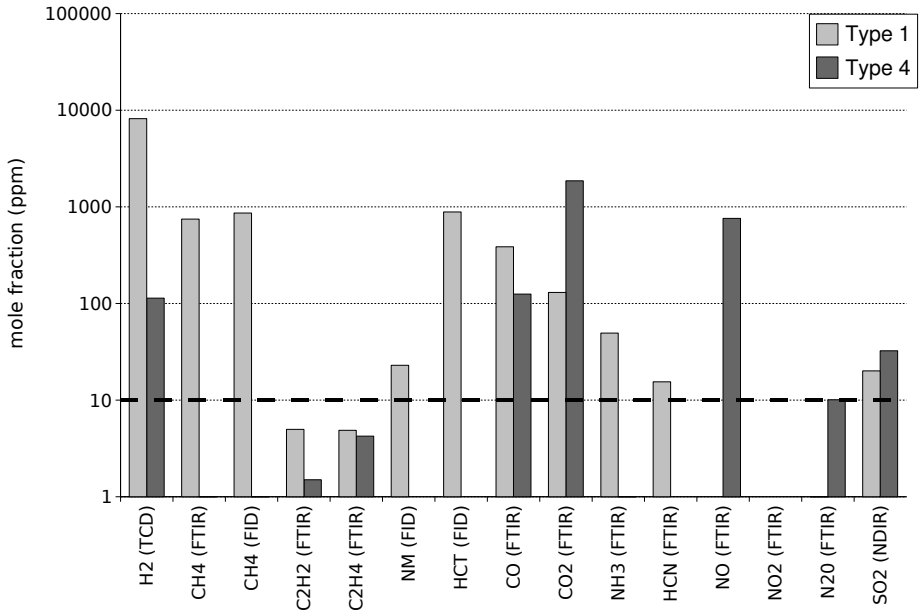

(a)

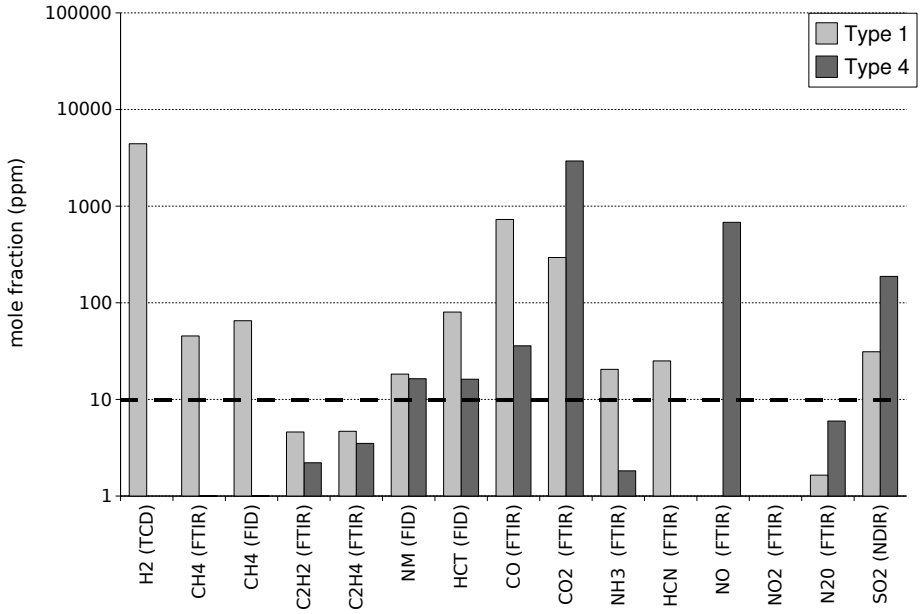

(b)

Figure 8.3: Composition of the gas phase for two different experiment types: Type 1 – pyrolysis experiments, Type 4 – reburning experiments (Anthracite 8.3(a) and Petcoke 8.3(b)) at 1000°C. NM : non-methane hydrocarbons, HCT : total hydrocarbons. The dashed line represents the detection limit.

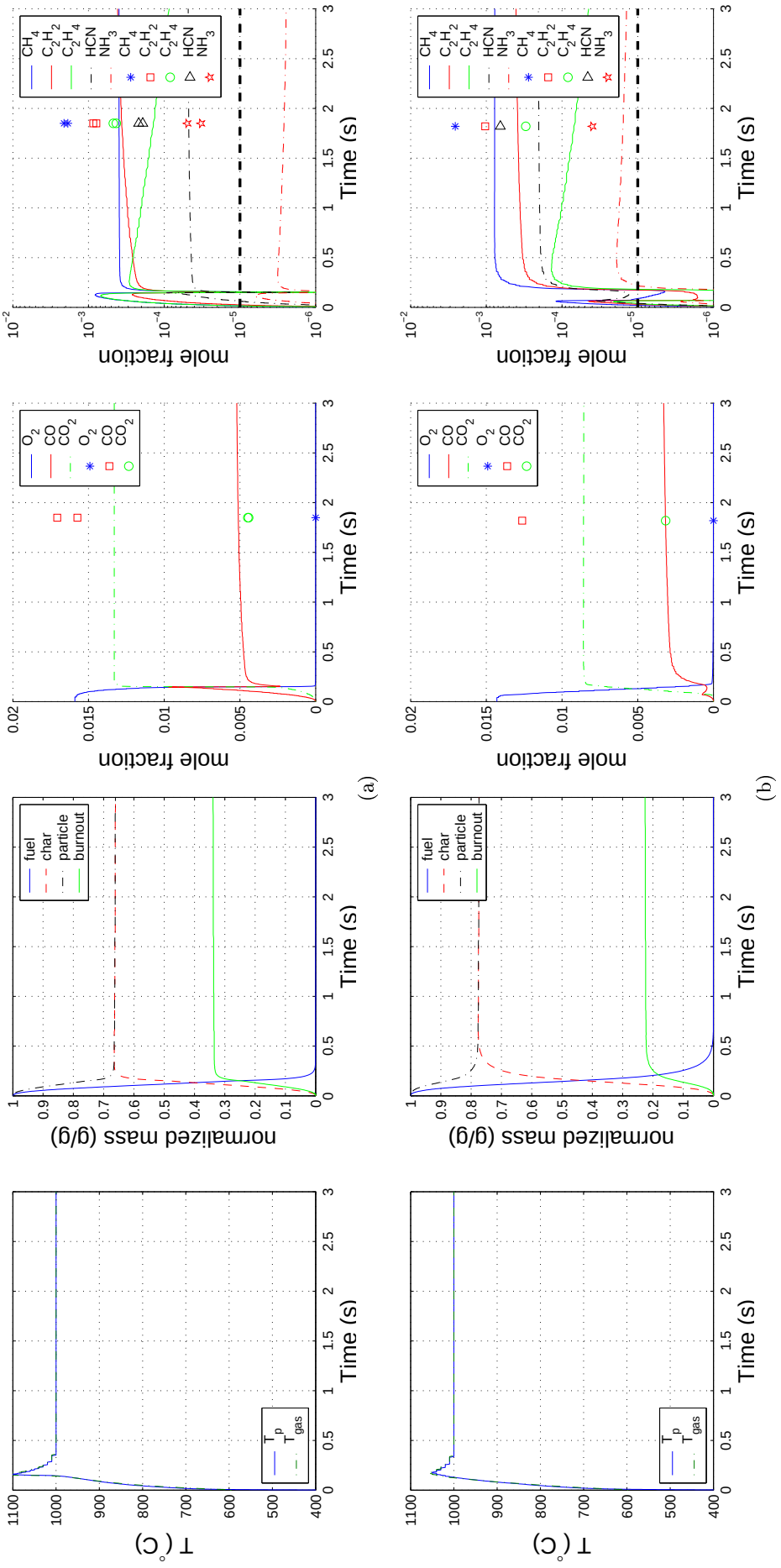

Figure 8.4: Reburning conditions (8.4(a) Lignite and 8.4(b) Coal) at 1000°C: time evolution of gas and particle temperatures (left), of reaction progress – i.e. fuel, char and particle mass and particle burnout – (center left) and of experimental (symbols) and modeled (lines) of O_2, CO and CO_2 mole fractions (center right) and CH_4, C_2H_2, C_2H_4, HCN and NH_3 mole fractions (right).

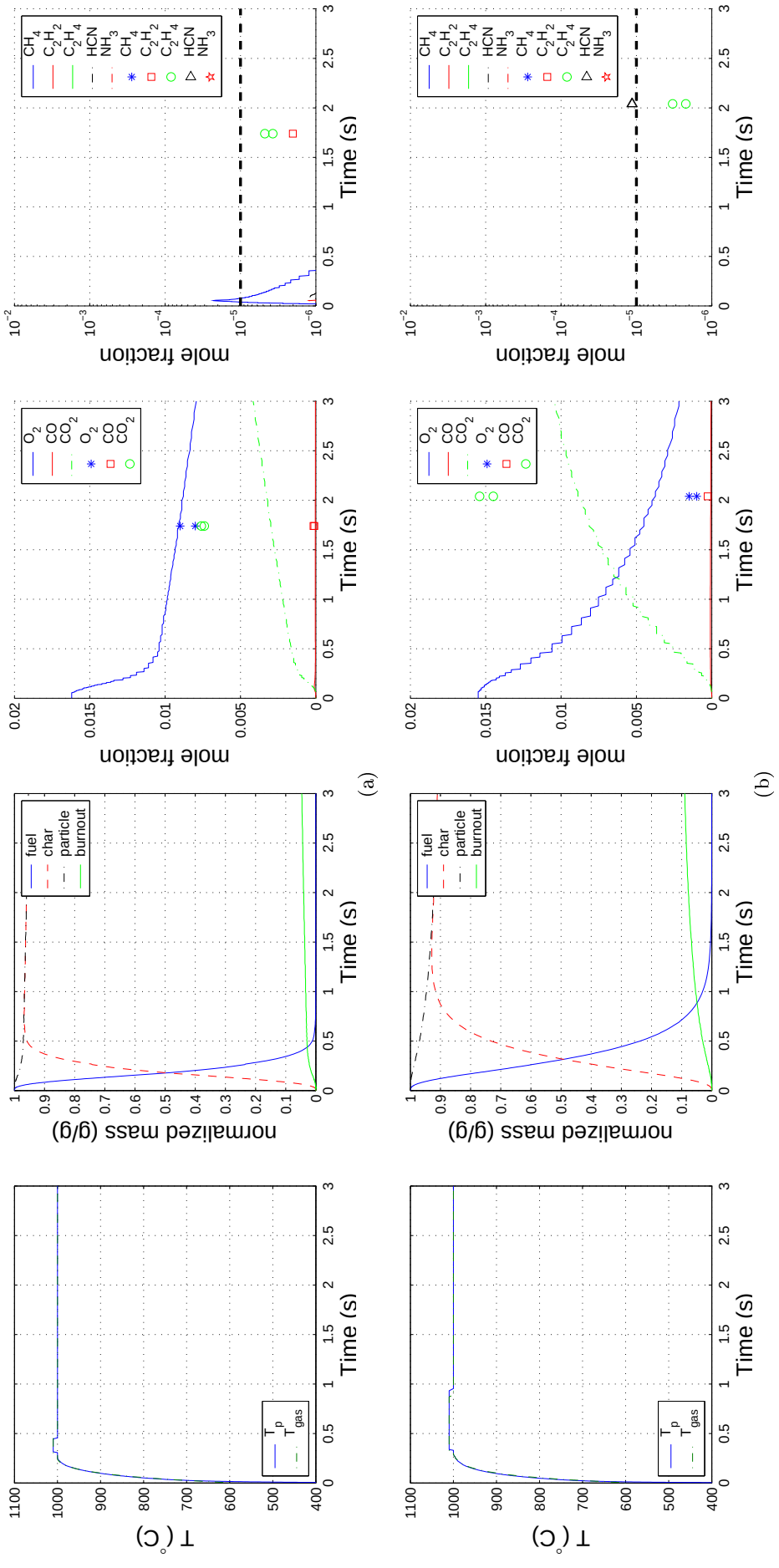

Figure 8.5: Reburning conditions (8.5(a) Anthracite and 8.5(b) Petcoke) at 1000°C: time evolution of gas and particle temperatures (left), of reaction progress – i.e. fuel, char and particle mass and particle burnout – (center left) and of experimental (symbols) and modeled (lines) of O_2, CO and CO_2 mole fractions (center right) and CH_4, C_2H_2, C_2H_4, HCN and NH_3 mole fractions (right).

8.1.2.2 Modeling

Thermo-chemical predictions The modeled gas and particle temperatures are plotted in the left hand side graphs of the Figures 8.4 and 8.5 in the case of furnace temperatures set at 1000°C. In the case of lignite and coal (see Figures 8.4(a) and 8.4(b)), gases and particles reach peak temperatures of 1050°C for coal and 1100°C for lignite, around 0.25 s residence time. In the case of anthracite and petcoke in Figures 8.5(a) and 8.5(b), the peak temperature is much lower than that of high volatile fuels, and it located around 0.5 s.

Additionally to these temperatures, solid reaction progress variables – fuel, char and particle (defined as the sum of fuel and char) dimensionless mass and particle burnout – are also plotted in the center-left graphs of the Figures 8.4 and 8.5. One can remark that the mass decrease of char due to oxidation is very low for all fuels. After devolatilisation (when fuel mass equals zero), the particle burnout as reached a stable value, whereas in the case of low-volatiles fuels, O_2 concentration is not null. This is due to the slow char oxidation reaction.

The time evolution for O_2, CO, and CO_2 mole fractions are plotted in the center-right graphs of the Figures 8.4 and 8.5, and mole fractions evolution of CH_4, C_2H_2, C_2H_4, HCN, and NH_3 are represented on right hand side graphs. Due to the undetermined VM mass during pyrolysis experiments, the prediction of the major species O_2, CO, and CO_2 is not as accurate as in the preceding char oxidation case. The fact that the model overestimates CO_2 and underestimates CO, CH_4, C_2H_2, C_2H_4, HCN, and NH_3 in case of lignite and coal, in Figures 8.4(a) and 8.4(b) respectively, indicates that the real gas mixture is more fuel-rich than that modeled. In the case of low-volatile fuels (anthracite and petcoke in Figures 8.5(a) and 8.5(b) respectively), the model underestimates the O_2 consumption and the CO_2 mole fraction. This may be explained, once again, by the non quantified species released during pyrolysis. They are oxidized into CO_2 and not CO because of the remaining O_2. The hydrocarbons and N-species in the right hand side graphs are all below 1 ppmv.

NO predictions The modeled final total NO variation is represented in Figure 8.6 together with the contributions of each homogeneous and heterogeneous phenomena, at the three experimental temperatures. The values of total NO final variation determined experimentally are also plotted, using symbols. Several experiments were repeated, which explains the presence of several symbols.

Although differences were observed for species concentrations (see Figures 8.4 and 8.5), a relatively close agreement between the computed and the experimental values was obtained. The model, without adjusting anymore parameter, is able to describe the large differences in NO reduction capacity of the four fuels. Nevertheless, the computation seems to underestimate the NO reduction in most cases (Figure 8.6). This could be due to the fact that the model does not take into account a quantity of non-measured species that may influence the NO reduction process, particularly tars. The model is now used for a detailed analysis of the contribution of each phenomena to the formation or reduction of NO during the reburning process.

First, one remarks that the contribution of the NO formed during the devolatilisation is negligible. This is directly induced by the fact that no NO was measured during the pyrolysis

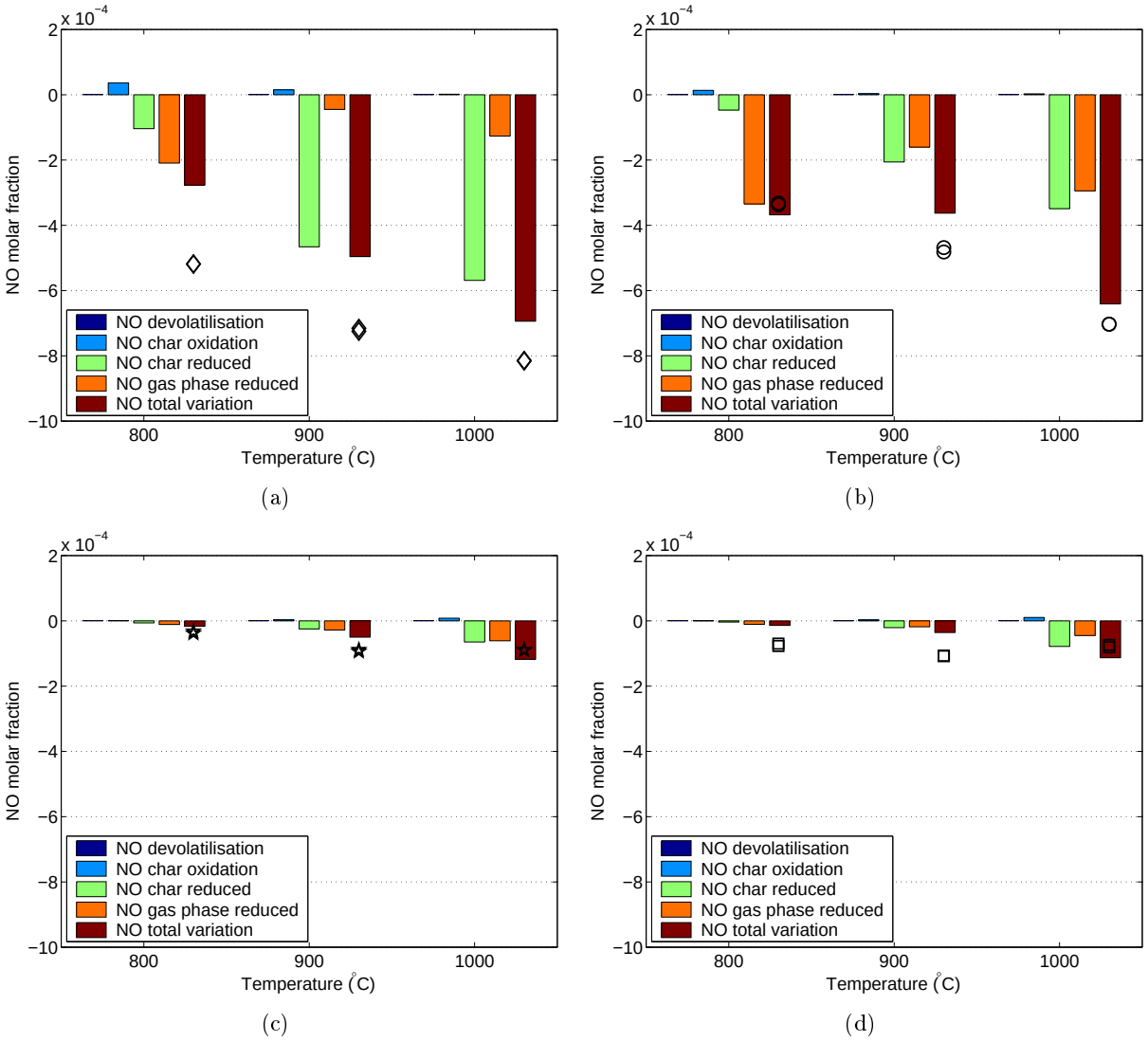

Figure 8.6: Total NO mole fraction variation in the gas phase as the sum of NO from devolatilisation, NO from the char oxidation, NO reduced on the char and NO from the gas phase reactions for the three experiments temperatures (Experimental values: ◇ Lignite 8.6(a), ○ Coal 8.6(b), ☆ Anthracite 8.6(c) and □ Petcoke 8.6(d)).

experiments. Then, the contribution of NO released during the char oxidation is low compared to the other phenomena. This directly correlated to the very small char consumption observed in Figures 8.4 and 8.5. The NO reduction by char is very important. It is the dominating phenomenon in the case of lignite and coal at 900 and 1000°C (see Figures 8.6(a) and 8.6(b) respectively). The NO reduction occurring in the gas phase is the second dominant phenomenon.

Due to the direct influence of temperature on Arrhenius kinetics, the reduction of NO by char increased with temperature in all cases (Figures 8.6). The gas phase reduction contribution increased slightly for low-volatile fuels with temperature, whereas the tendency is difficult to interpret in the case of lignite and coal. One can see a decrease at 900°C for coal and lignite. In the case of lignite, one may recall that the total volatile mass analyzed at 900°C was approximately half that measured at 800 or 1000°C (Figure 7.7(a)). This has an influence here.

It can also be noticed that the quantity of NO produced during the char oxidation surprisingly decreases with increasing temperatures for lignite and coal (see Figures 8.6(a) and 8.6(b) respectively); it increases as can be expected anthracite and petcoke (Figures 8.6(c) and 8.6(d)). This is due to the fact that, for lignite and coal, the particles are less oxidized with increasing temperature. The explanation is that oxygen reacts with the highly reactive gases present in the surroundings of the particle before oxidizing the char.

The non-monotonic behavior of the homogeneous NO reduction observed for lignite and coal is the result of complex competitive phenomena in the gas phase and at the char surface. This will be investigated in the Section 8.2.

The model predicts that NO reduction capability for each fuel would increase with temperature, as observed experimentally. Except for coal between 800 and 900°C, where the NO total variation remains constant. In this case, although NO reduction by char increases, the gas phase NO reduction decreases.

Figures 8.7 and 8.8 represent the time evolution of the total NO mole fraction in the gas phase, and the contribution of gas phase reactions and heterogeneous reactions in forming/reducing NO, at 1000°C. It can be observed from these Figures that the homogeneous (gas phase) reduction process starts early (0.05-0.1 s) and then stabilizes, whereas char NO reduction starts later on (0.1-0.5 s) but then always increases.

For coal, anthracite and petcoke, the gas phase NO reduction after 2 s particle residence time is of the same order of magnitude as the char reduction.

In the case of lignite, the homogeneous reduction starts very early but reaches a peak value, NO is then reformed to stabilizes after 0.15 s. This surprising behavior will be analyzed in details in the Section 8.2. The majority of NO decrease is due to heterogeneous reduction.

8.1.3 Synthesis

The NO reduction during solid fuels reburning was successfully modeled for a lignite, a coal, an anthracite and a petcoke. The different phenomena involved simultaneously in the NO formation/reduction process were characterized and quantified. This allowed to specify the NO reduction capacities of the four solid fuels used for the present work.

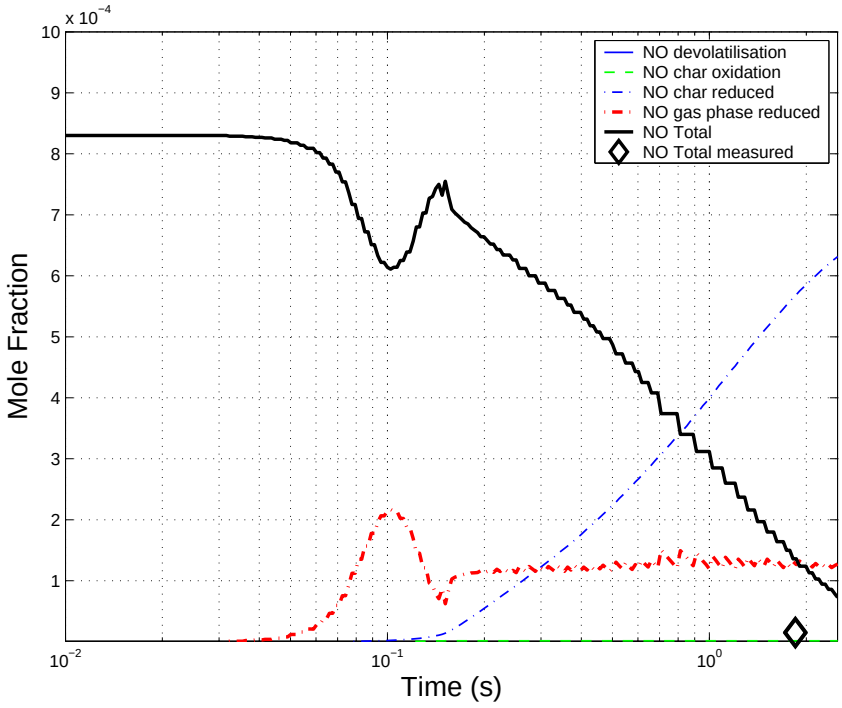

(a)

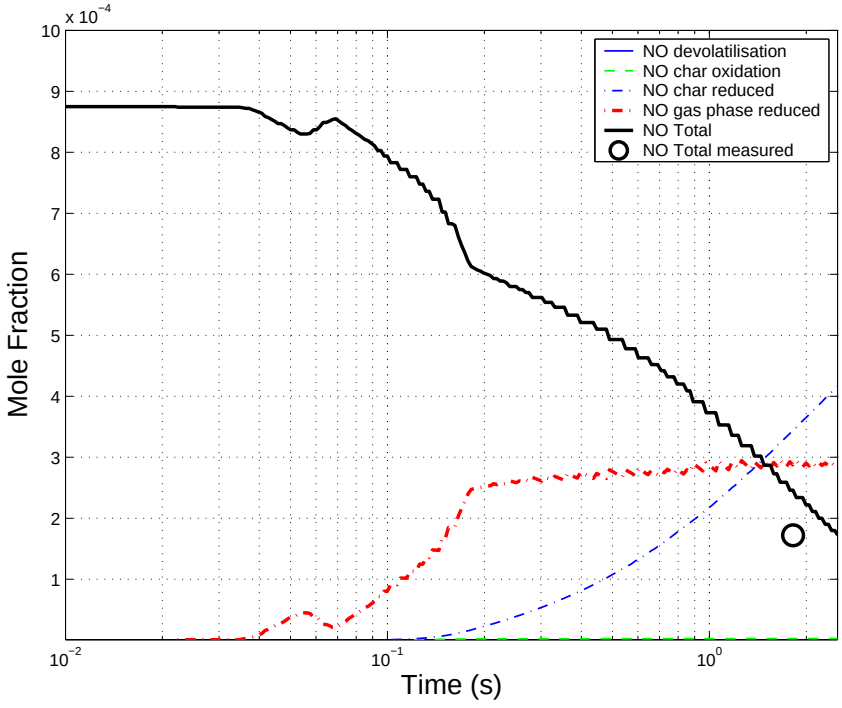

(b)

Figure 8.7: Variation of total NO mole fraction in the gas phase as the sum of NO from the char oxidation, NO from the gas phase reactions, NO from the devolatilisation and NO reduced on the char at 1000°C as a function of particle residence time (Lignite 8.7(a), Coal 8.7(b)). $\diamond$ and $\circ$ are experimental values for total NO.

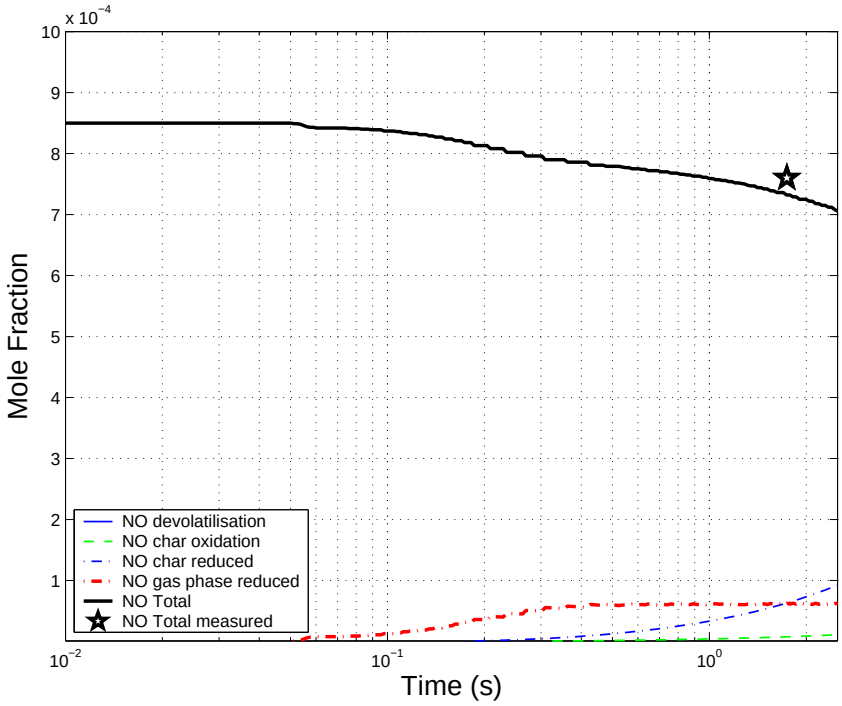

(a)

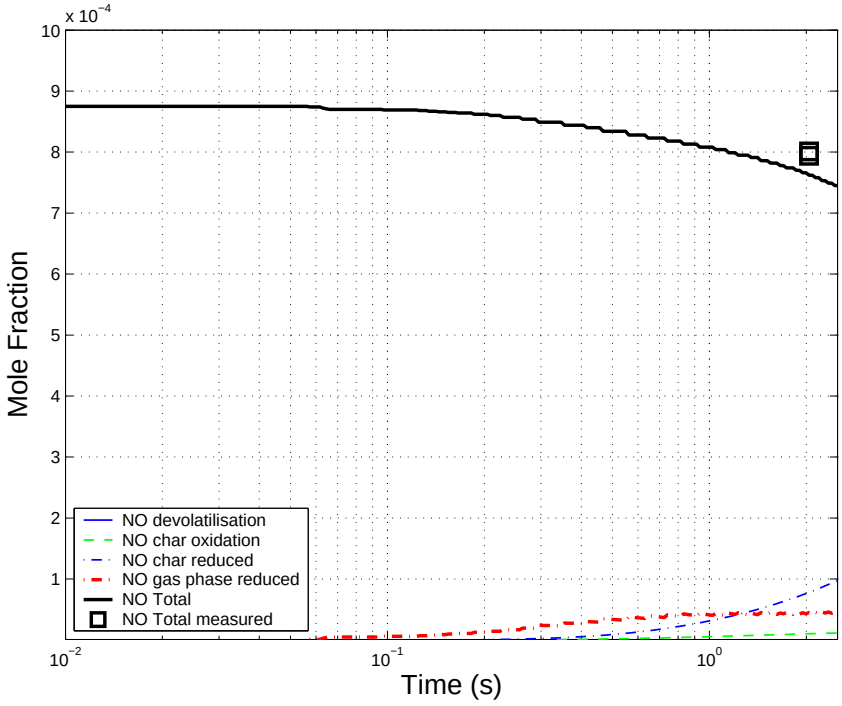

(b)

Figure 8.8: Modeled variation of total NO mole fraction in the gas phase as the sum of NO from the char oxidation, NO from the gas phase reactions, NO from the devolatilisation and NO reduced on the char at 1000°C as a function of particle residence time (Anthracite 8.8(a) and Petcoke 8.8(b)). ☆ and □ are experimental values for total NO.

The experiments were undertaken to represent the reburning conditions encountered in a cement plant calciner: injection of fuels under ca. 1 % O_2 and ca. 880 ppm NO. The "global" NO reduction was quantified.

Lignite it is the most efficient NO reducer. This is due to a number of phenomena.

- It has the highest volatile content,
- the highest char porous surface
- and the highest char NO reduction reactivity.

Anthracite, is the worst NO-reducer; this can be explained by

- its low volatile content,
- its low char NO reduction reactivity.

Coal, which also has a high volatile content and a high char reactivity, reduces NO efficiently. Petcoke is comparable to anthracite regarding its low efficiency in reducing NO.

All the experiments described above were modeled for the four fuels at the three experimental temperatures: 800, 900, and 1000°C. A satisfactory description of each experiment was achieved.

The model, made it possible to analyze the complex situation of reburning. The results clearly indicate that at short residence time, homogeneous reduction is the most efficient mechanism. After 2 s, the char reduction mechanism becomes more significant. Thus, for three fuels, coal, anthracite, and petcoke, homogeneous reduction is comparable with heterogeneous reduction. In the case of lignite, char is more efficient in reducing NO than gas phase reactions.

However, in the case of lignite and coal, the amount of NO reduced by gas phase reactions is not monotonic with temperature : one can see a clear and surprising decrease between the quantities reduced at 800°C and that reduced at 900°C for both coal and lignite. This question will be explored in detail in the next section.

8.2 Detailed analysis of the gas phase reactions

8.2.1 Introduction

In the preceding chapter, a modeling of the reburning using four fuels was performed, taking both homogeneous and heterogeneous mechanisms into account. The results indicate that gas phase reactions largely contribute to NO reduction. Moreover, two surprising results were observed:

- the reduction of NO by homogeneous reactions is not always monotonic regarding the reaction temperature.
- lignite produces more VM than coal, but reduces less NO in the gas phase,
- the time evolution of the NO reduced in the gas phase for coal at 900°C and lignite at 1000°C present unexplained variations.

The purpose of the present chapter is to clarify these issues through a detailed analysis of the gas phase reactions mechanisms. Indeed, since gas phase reactions were computed using detailed chemistry (145 species, 1006 reactions), the identification of the main pathways leading to the formation or destruction of NO requires an accurate examination of the computations.

The detailed gas phase reactions analysis was limited here to the high-volatile fuels, i.e. lignite and coal. Lignite and coal have a high volatile content: 56 and 38 w.% respectively. The nitrogen content of coal – 1.71 w.% – is more than four times higher than that of lignite – 0.42 w.% –, contrary to the sulfur content that is high for lignite – 1.72 w.% – and low for coal – 0.45 w.%.

In the case of lignite, one may recall that the total volatile mass analyzed at 900°C was approximately half that measured at 800 or 1000°C (see section 7.1). This should have an influence here. Because of this, the gas phase reactions for coal reburning will be examined at 800, 900 and 1000°C, whereas the lignite gas phase reactions will be examined only at 800 and 1000°C.

8.2.2 Choice of the dates

As a synthesis of the previous results from the model, we have plotted for each fuel in Figures 8.9 to 8.13 the time evolution of variables that we estimate important to describe the thermochemical system evolution along time:

- gas and particle temperature;
- total NO mole fraction as the sum of NO produced by char oxidation, NO reduced by char and NO reduced in the gas phase;
- NO formation rate in the gas phase;
- hydrocarbons mole fraction;

- CO, CO_2, HCN, NH_3 and SO_2 mole fraction
- and H, OH, HCCO, CH_2 and CH_3 radicals.

The NO formation rate in the gas phase diagram was plotted after a slight smoothing of the data to avoid the numerical oscillations appearing through the derivation of the NO mole fraction. When dashed is negative (below $\frac{\mathrm{d}X_{\mathrm{NO}}}{\mathrm{d}t} = 0$), this means NO is reduced through gas phase mechanisms.

From these results, we will select a number of dates at which detailed analysis of gas phase reactions will be carried out.

In the case of coal

- with the furnace at 800°C (Figure 8.9), even if the gas and particle temperature and the species concentration show a monotonic evolution, one observes a maximum value of the NO reduction rate around $t = 0.4$ s. This date was selected for the detailed chemical analysis.
- with the furnace at 900°C, all the profiles in Figure 8.10 show strong variations. The NO formation rate present peak values: at $t = 0.15$ s NO is reduced in the gas phase, at $t = 0.25$ s NO is formed and at $t = 0.35$ s NO is reduced again. The temperatures reach a peak value of 1000°C around $t = 0.35$ s. At this time, the different gas mole fractions vary a lot, showing a strong decrease of hydrocarbons, CO and HCN whereas CO_2 increases and radicals reach a peak concentration. The three dates $t = 0.15$, 0.25 and 0.35 s were retained to perform the detailed chemical analysis.
- with the furnace at 1000°C (Figure 8.11), small oscillations of the NO formation rates appear at very short dates. These are of small amplitudes, whereas a large NO reduction zone, correlated with hydrocarbons decrease and radicals high concentrations exists between 0.07 and 0.16 s. The detailed chemical analysis will be carried out at $t = 0.15$ s.

In the case of lignite

- with the furnace at 800°C, the monotonic evolution of the profiles and the minimum value observed in Figure 8.12 recalls the coal at 800°C case. The date retained for the detailed chemical analysis was $t = 0.4$ s.
- with the furnace at 1000°C, NO is successively reduced, formed and reduced again, as observed in Figure 8.13. A first NO reduction occurs for dates lower than 0.1 s. Between 0.1 and 0.15 s, NO is formed in the gas phase, and then a new reduction period appears. The selected dates for the detailed chemical analysis are $t = 0.09$ s, $t = 0.12$ s and finally $t = 0.16$ s.

All the selected dates are marked by a vertical black line in Figures 8.9 to 8.13.

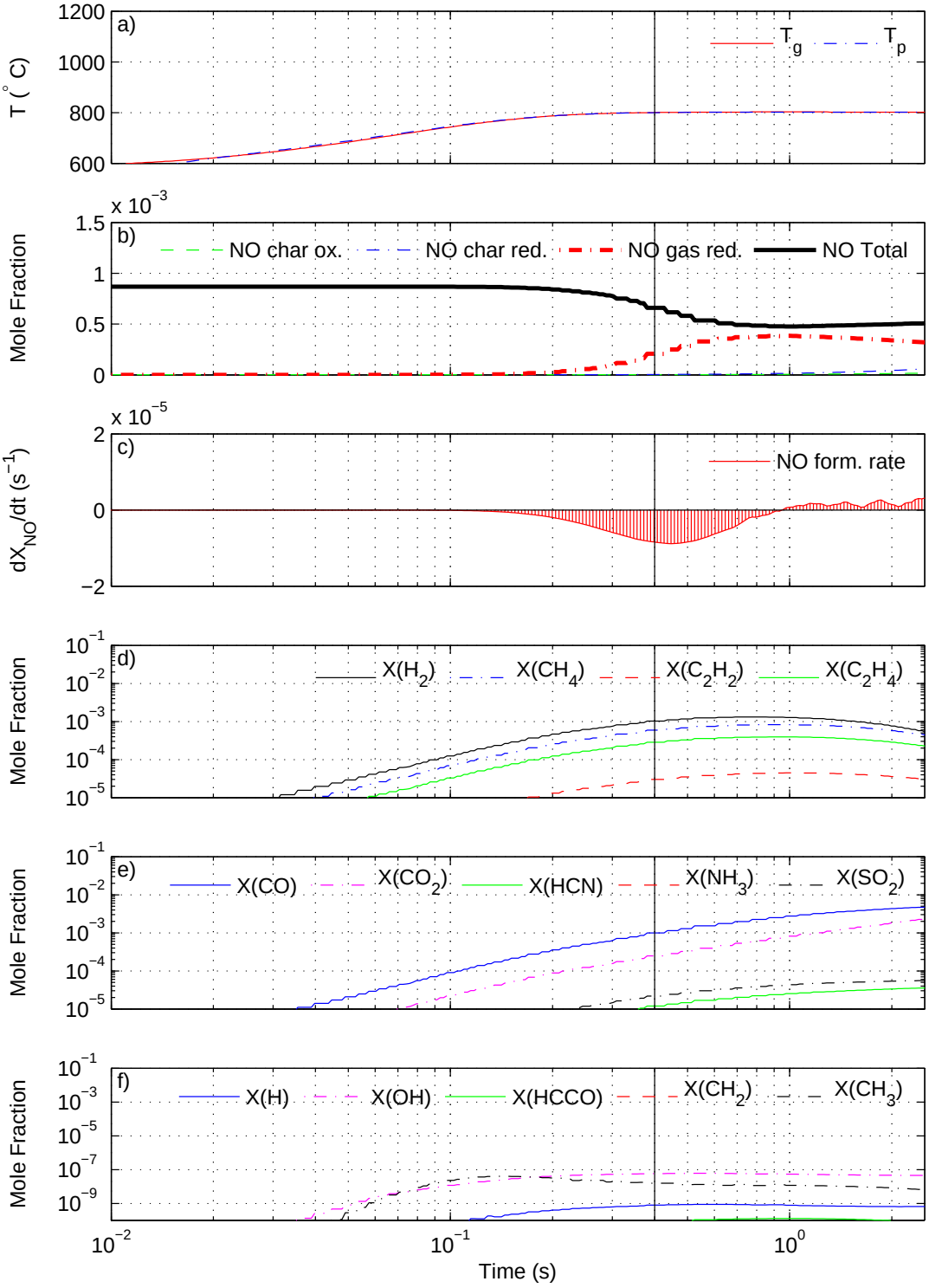

Figure 8.9: Synthesis of the model; Coal, furnace at 800°C : Time evolutions of (a) – gas, T_g, and particle, T_p, temperature. (b) – total NO as the sum of NO produced by char oxidation, NO reduced by char and NO reduced in the gas phase. (c) – NO form rate in the gas phase. (d) – Hydrocarbons. (e) – CO, CO_2, HCN, NH_3 and SO_2. (f) – radicals.

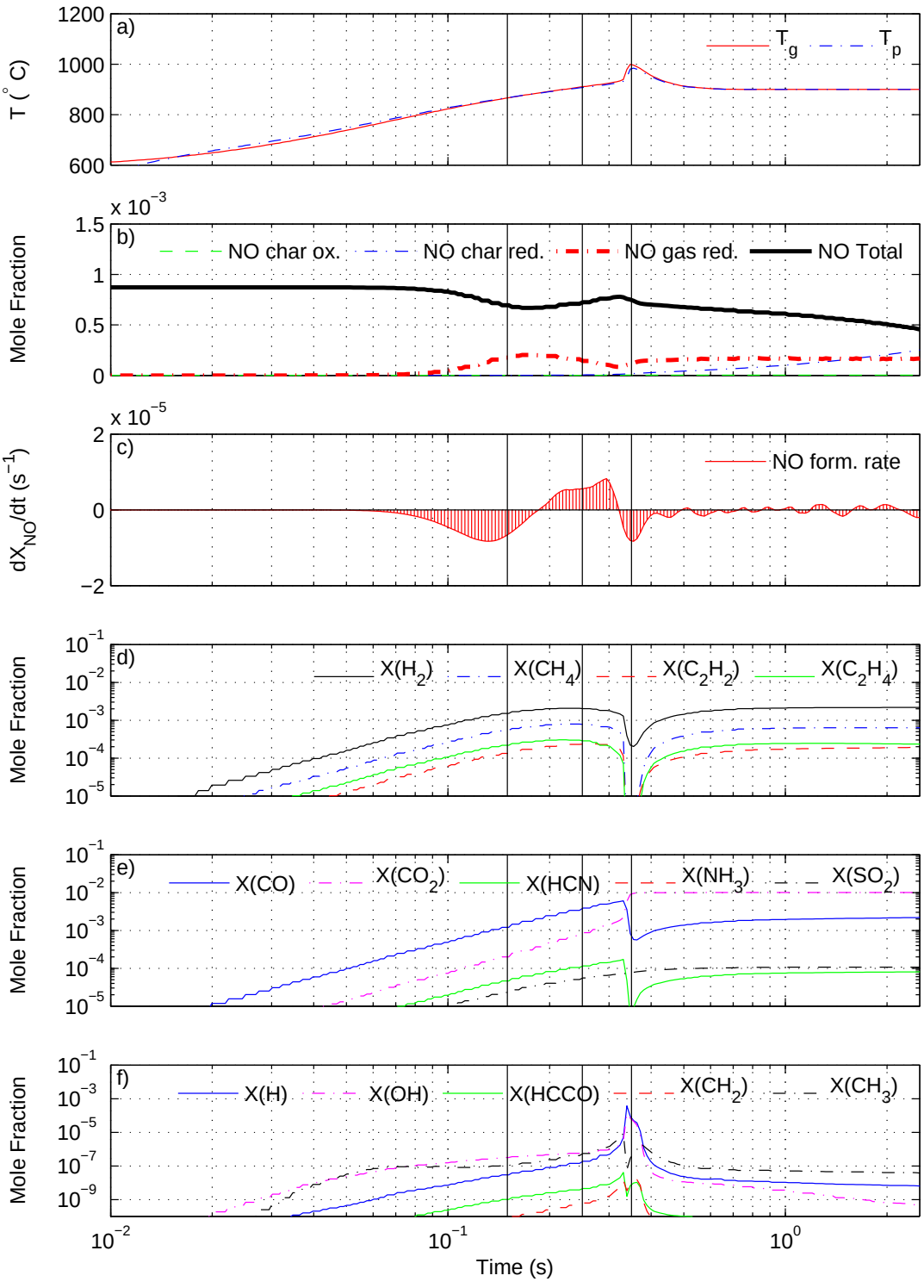

Figure 8.10: Synthesis of the model; Coal, furnace at 900°C : Time evolutions of (a) – gas, T_g, and particle, T_p, temperature. (b) – total NO as the sum of NO produced by char oxidation, NO reduced by char and NO reduced in the gas phase. (c) – NO form rate in the gas phase. (d) – Hydrocarbons. (e) – CO, CO_2, HCN, NH_3 and SO_2. (f) – radicals.

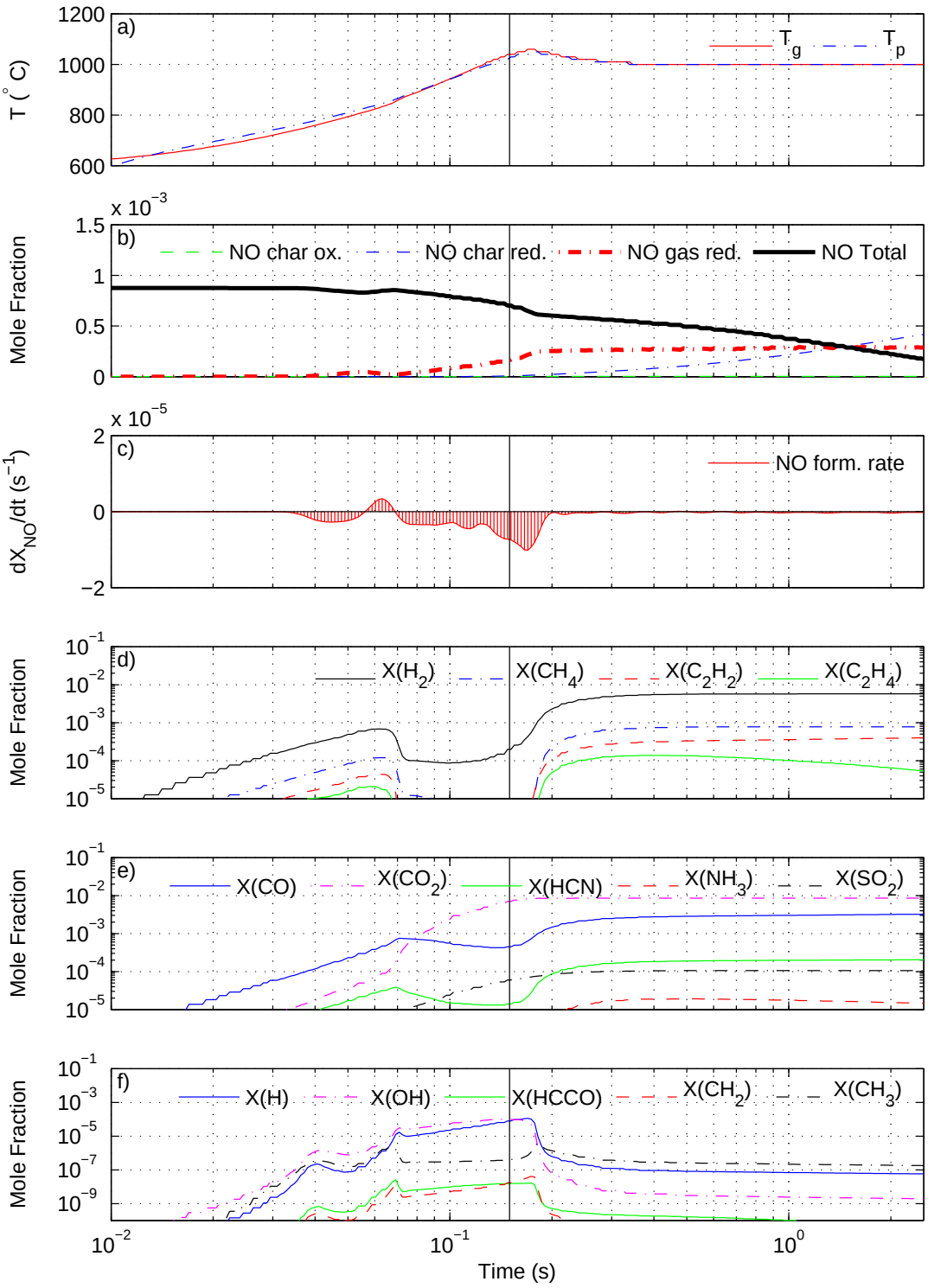

Figure 8.11: Synthesis of the model; Coal, furnace at 1000°C : Time evolutions of (a) – gas, T_g, and particle, T_p, temperature. (b) – total NO as the sum of NO produced by char oxidation, NO reduced by char and NO reduced in the gas phase. (c) – NO form rate in the gas phase. (d) – Hydrocarbons. (e) – CO, CO_2, HCN, NH_3 and SO_2. (f) – radicals.

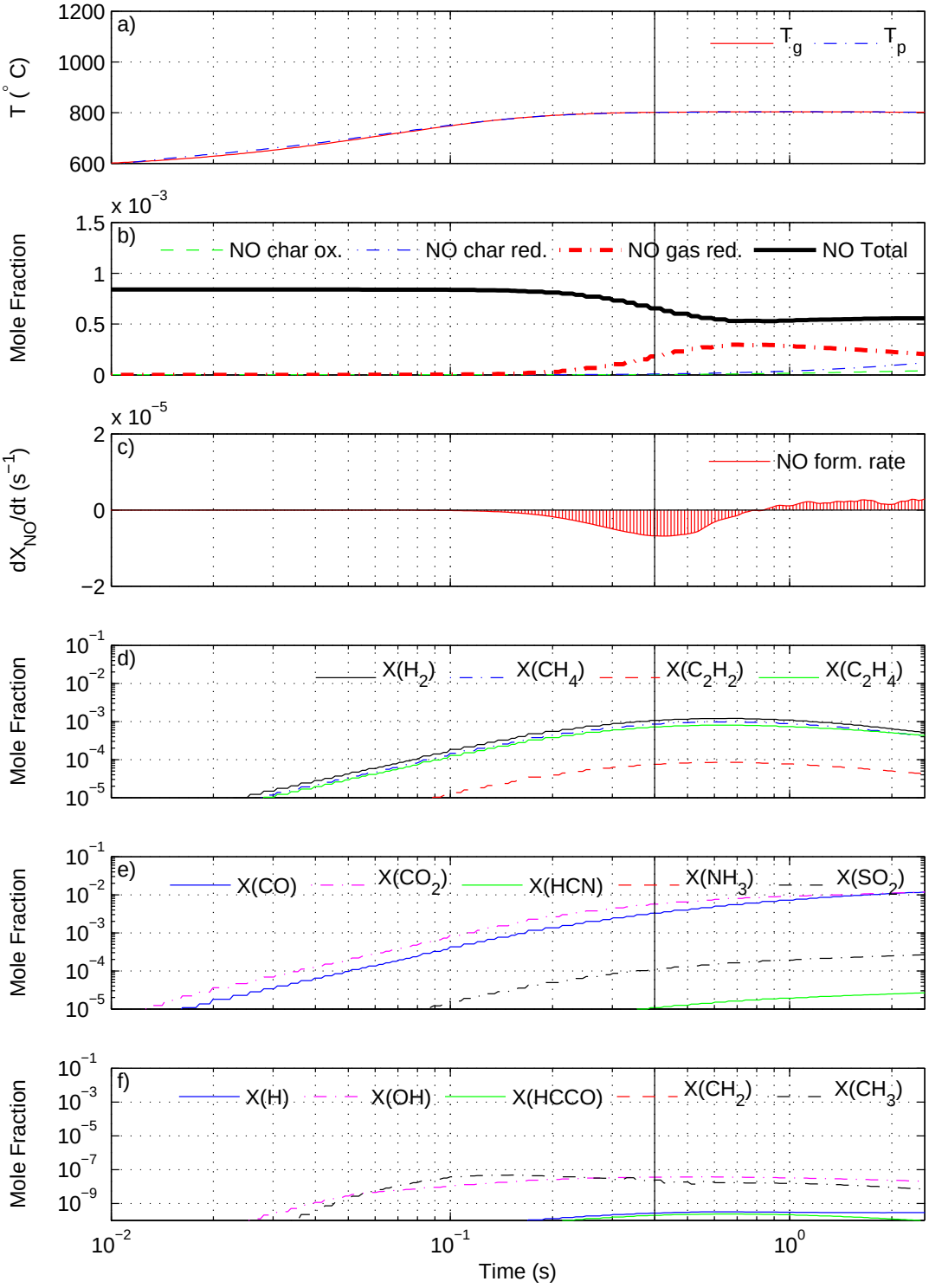

Figure 8.12: Synthesis of the model; Lignite, furnace at 800°C : Time evolutions of (a) – gas, T_g, and particle, T_p, temperature. (b) – total NO as the sum of NO produced by char oxidation, NO reduced by char and NO reduced in the gas phase. (c) – NO form rate in the gas phase. (d) – Hydrocarbons. (e) – CO, CO_2, HCN, NH_3 and SO_2. (f) – radicals.

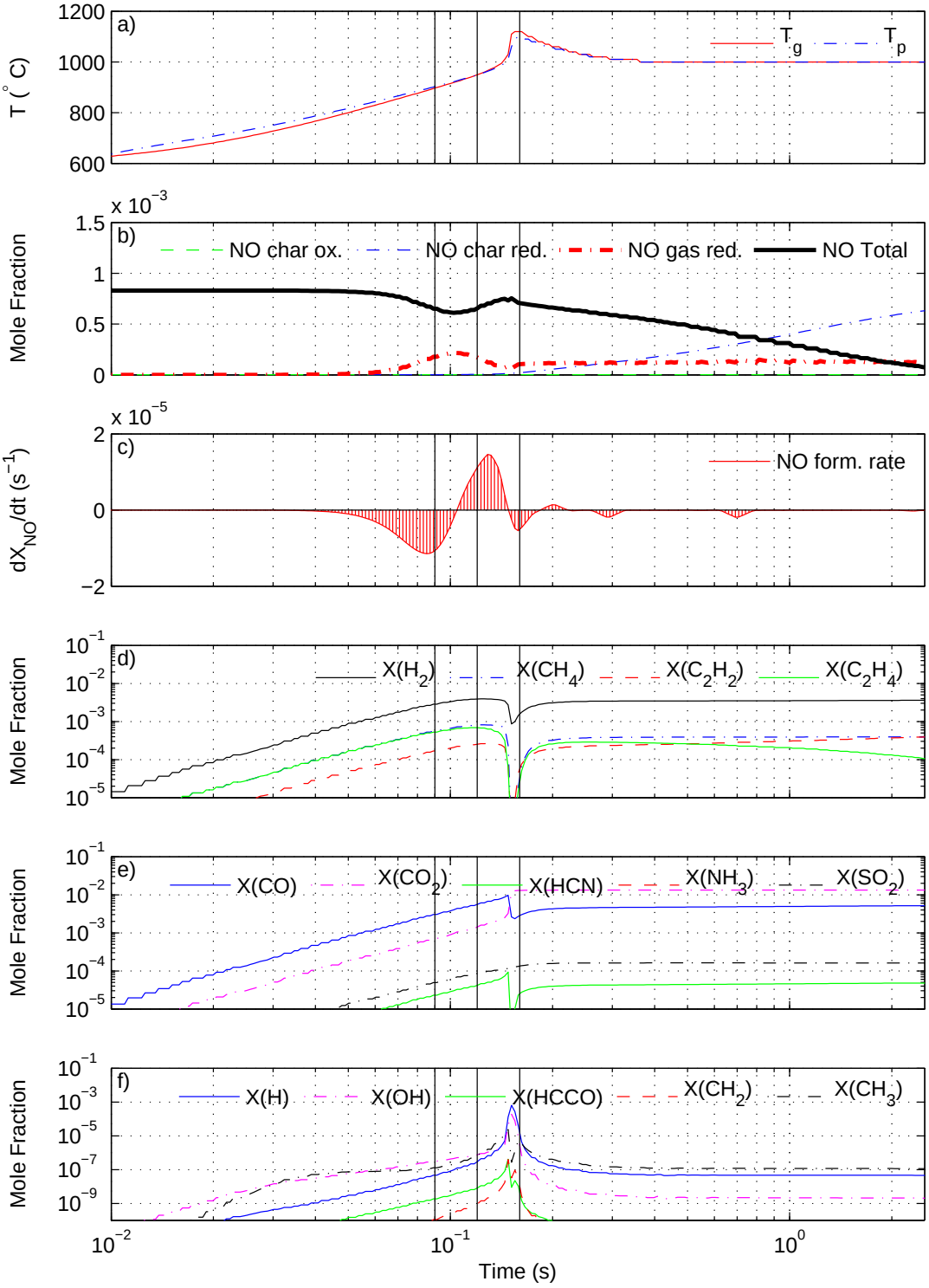

Figure 8.13: Synthesis of the model; Lignite, furnace at 1000°C : Time evolutions of (a) – gas, T_g, and particle, T_p, temperature. (b) – total NO as the sum of NO produced by char oxidation, NO reduced by char and NO reduced in the gas phase. (c) – NO form rate in the gas phase. (d) – Hydrocarbons. (e) – CO, CO_2, HCN, NH_3 and SO_2. (f) – radicals.

8.2.3 Identification of the pathways in gas phase reactions

The method used to identify the main reaction paths is the following. At a chosen date, the mole fraction, X_i, and the gas temperature, T_g, are exported to the PSR program of the CHEMKIN II package [47]. These T_{gas} and X_i represent here the initial conditions of the PSR modeling. A very short residence time is set in PSR (here $\tau = 1 \times 10^{-10}$ s) to avoid the X_i to have a sensible change. Nevertheless, the reaction rates are calculated. By enabling the AROP option, all the rates of consumption/production are saved in an output file. Then, by following the species involved in the NO reactions, the main reaction paths will be drawn and interpreted.

8.2.4 Results and discussion

In the following paragraphs some conventions are used to simplify the text. They are listed below:

- (RXXX) is the reaction index in the mechanism of Dagaut et al. [54], presented in Appendix D and (-RXXX) means that the reverse reaction occurs.
- ROC(YY) and ROP(YY) mean the normalized rates of consumption and of production respectively of the species YY, for a given reaction.

In the main reaction paths representations, drawn by following one by one the involved species in the NO chemistry, the width of arrows is related to the normalized consumption of the species at the beginning of the arrow. Only normalized consumption rates larger than 0.01 are drawn.

The species in a box are the ones that were quantified in the experimental work.

In the main reaction paths, the symbol MEALL appears. It means methylallyle, i.e. CH_3-CH-CH-CH_2.

8.2.4.1 Gas phase reactions for coal

Coal, reactor at 800°C : For coal with the reactor at 800°C, the date of $t = 0.4$ s was chosen to perform the detailed chemical analysis. At this time, the gas has reached the final temperature at 800°C (Figure 8.9).

The main reaction paths for coal at 800°C, for a date of 0.4 s are represented in Figure 8.14. It shows that NO reacts following three main mechanisms:

- the conversion into NO_2, HNO or HONO. These species are mostly recycled into NO.
- the conversion into HCN, and then N_2 by reacting with hydrocarbonated radicals HCCO, CH_2 and CH_3. These reactions are the reburning reactions.
- the conversion into N_2, by reacting with NH_2 or NNH. These are the SNCR (Selective Non Catalytic Reduction) reactions.

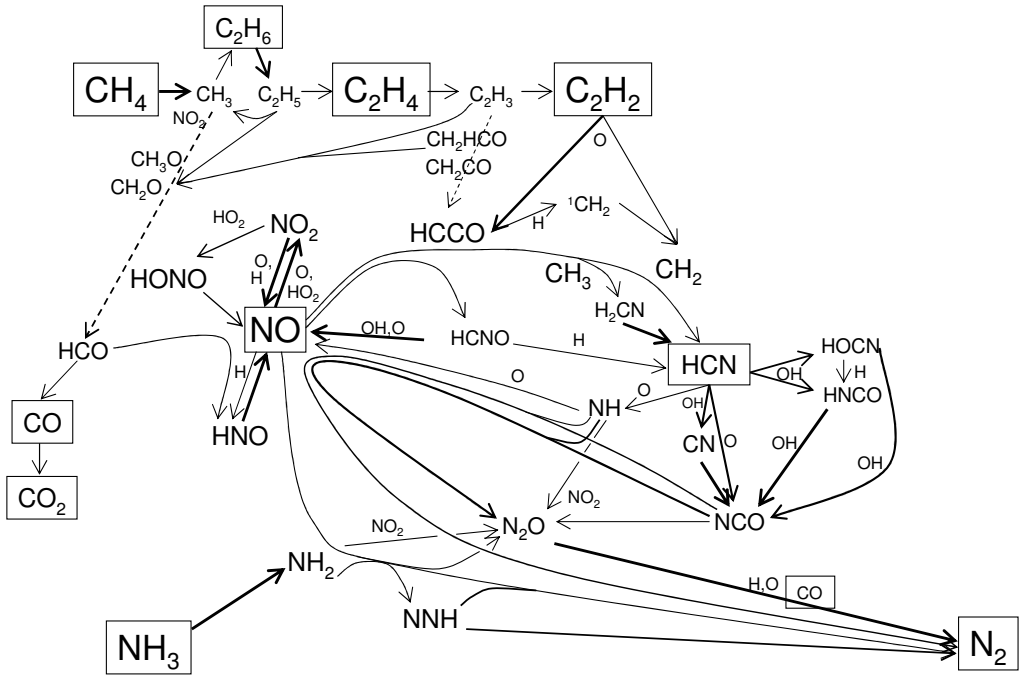

Figure 8.14: Main reaction paths for coal at 800°C, $t = 0.15$ s. Boxes represent the gases initially present or released during devolatilisation.

NO balance:

The total NO consumption rate reaches 2.06×10^{-6} s^{-1} whereas its total production rate is 1.14×10^{-6} s^{-1}, meaning a net consumption rate of NO of $\frac{\mathrm{d}\, X_{\mathrm{NO}}}{\mathrm{d}\, t} = -9.16 \times 10^{-6}$ s^{-1}.

The examination of all the reactions consuming NO, listed below, enables to identify the main NO conversion mechanism. It indicates that the reaction (R140) represents more than 98 % of the total NO consumption; it yields NO_2.

The NO_2 and HONO – that is exclusively produced by NO_2 – recycling into NO represents 99 % of the total production rate of NO. However, the NO is mostly converted into NO_2 at the net conversion rate of 8.90×10^{-7} s^{-1} that corresponds to 97,6 % of the net NO consumption rate.

HNO produced by reactions (R143) and (R959) is entirely recycled into NO. Thus, the last 2.4 % of the net NO consumption rate are due to reburning reactions (R168) and (R169) and to the consumption of NO by NH_2 (R101).

$NH_2 + NO$	$\rightleftharpoons$	$N_2 + H_2O$	ROC(NO) = -0.002	(R101)
$NO + HO_2$	$\rightleftharpoons$	$NO_2 + OH$	ROC(NO) = -0.982	(R140)
$NO + HCO$	$\rightleftharpoons$	$HNO + CO$	ROC(NO) = -0.009	(R143)
$HCCO + NO$	$\rightleftharpoons$	$HCNO + CO$	ROC(NO) = -0.003	(R168)
$HCCO + NO$	$\rightleftharpoons$	$HCN + CO_2$	ROC(NO) = -0.001	(R169)
$CH_3O + NO$	$\rightleftharpoons$	$CH_2O + HNO$	ROC(NO) = -0.001	(R959)

N_2 balance:

Because of the very high activity of the reactions involving NO_2, HONO and HNO, the other mechanisms hardly show up. Thus, to have a better understanding of the reactions that reduce NO into N_2 a balance of N_2 is further performed. It is also of high interest to identify the reactions leading to N_2, which is the final stage of the NO reduction.

First, one observes that the total N_2 consumption rate ($\frac{\mathrm{d}\,X_{N_2}}{\mathrm{d}\,t} = 4.21 \times 10^{-18}$ s^{-1}) is negligible compared to its production rate (5.83×10^{-9} s^{-1}). The reactions yielding N_2 – listed below – are dominated by reactions involving NH_2 or its derivative NNH. These reactions – (R101), (R116) and (R117) – contribute for more than 95 % to the formation of N_2. Nitrous oxide (N_2O) is responsible for 4.2 % of the N_2 production, following (R156) and (R160).

$N + NO$	$\rightleftharpoons$	$N_2 + O$	ROP(N_2) = 0.005	(-R78)
$NH_2 + NO$	$\rightleftharpoons$	$N_2 + H_2O$	ROP(N_2) = 0.849	(R101)
$NNH + M$	$\rightleftharpoons$	$N_2 + H + M$	ROP(N_2) = 0.035	(R116)
$NNH + NO$	$\rightleftharpoons$	$N_2 + HNO$	ROP(N_2) = 0.067	(R117)
$N_2O + M$	$\rightleftharpoons$	$N_2 + O + M$	ROP(N_2) = 0.003	(R156)
$N_2O + CO$	$\rightleftharpoons$	$N_2 + CO_2$	ROP(N_2) = 0.039	(R160)
$NCO + NO$	$\rightleftharpoons$	$CO_2 + N_2$	ROP(N_2) = 0.002	(R217)

It is of high interest to understand the fate of the intermediate species, responsible of the N_2 formation. Thus, the NH_2 radical is entirely produced by NH_3, whereas N_2O is formed by NH_2 for more than 82 % through reactions (R102) and (R109), listed below. HNO produces 3.3 % of N_2O through reactions (R130) and (R131). The species resulting from the reburning process – NH and NCO – are responsible for 14 % of the formation of N_2O through the reactions (R91), (R93), (R216) and (R219).

$NH + NO$	$\rightleftharpoons$	$N_2O + H$	ROP(N_2O) = 0.012	(R91)
$NH + NO_2$	$\rightleftharpoons$	$N_2O + OH$	ROP(N_2O) = 0.003	(R93)
$NH_2 + NO$	$\rightleftharpoons$	$N_2O + H_2$	ROP(N_2O) = 0.012	(R102)
NH_2+NO_2	$\rightleftharpoons$	$N_2O + H_2O$	ROP(N_2O) = 0.813	(R109)
$2HNO$	$\rightleftharpoons$	$N_2O + H_2O$	ROP(N_2O) = 0.022	(R130)
$HNO + NO$	$\rightleftharpoons$	N_2O+OH	ROP(N_2O) = 0.011	(R131)
$NCO + NO$	$\rightleftharpoons$	$N_2O + CO$	ROP(N_2O) = 0.070	(R216)
$NCO + NO_2$	$\rightleftharpoons$	CO2+N_2O	ROP(N_2O) = 0.055	(R219)

Finally, the reburning mechanism, identified in the Figure 8.14, are overall responsible for a normalized production of N_2 lower than 1 %.

Synthesis:

At 800°C, for coal at a date of $t = 0.4$ s, the SNCR mechanisms dominates the NO to

N_2 reduction process. However, at this temperature, the NO is mostly converted into NO_2 as represented in Figure 8.15. Thus, the effective NO_x reduction should be considered as sum of NO + NO_2. Then, for coal at 800°C, it appears that the modeled coal reburning is not very efficient.

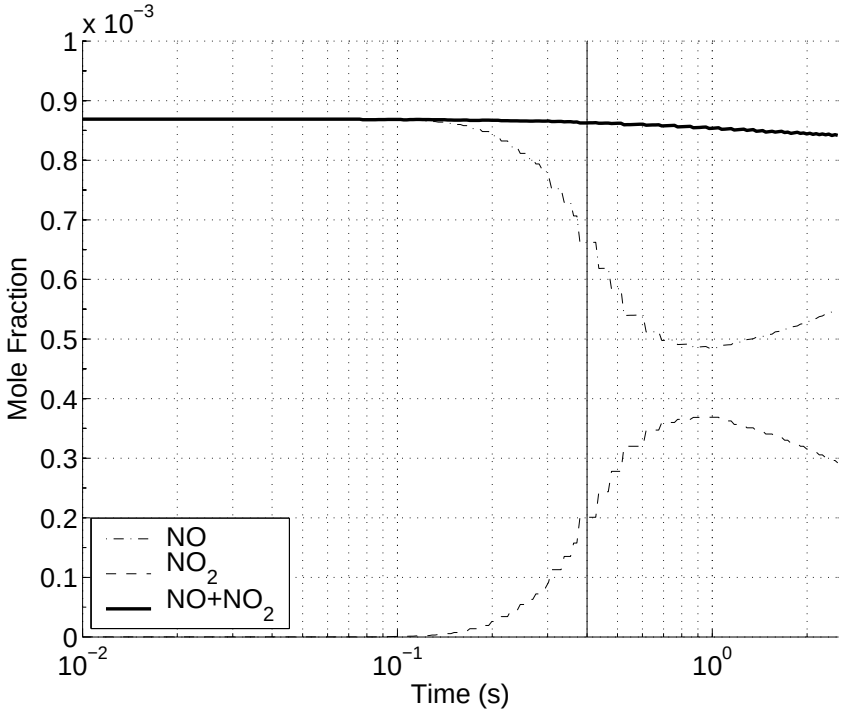

Figure 8.15: Coal at 800°C : Time evolution for NO (only gas phase variations), NO_2 and the sum NO + NO_2.

Coal, reactor at 900°C : For coal at 900°C, due to the oscillations observed in Figure 8.10, three dates were chosen: $t = 0.15$, 0.25 and 0.35 s.

Date of $t = 0.15$ s After this date, the gas temperature reaches 867°C.

The main reaction paths for coal – reactor temperature at 900°C – represented in Figure 8.16, is very similar to that already depicted in the case of coal at 800°C in Figure 8.14. The same mechanisms – i.e. conversion/recycling through NO_2, HONO and HNO, reduction through reburning reactions with hydrocarbonated radicals and SNCR reaction with NH_2 and NNH – happen in this case.

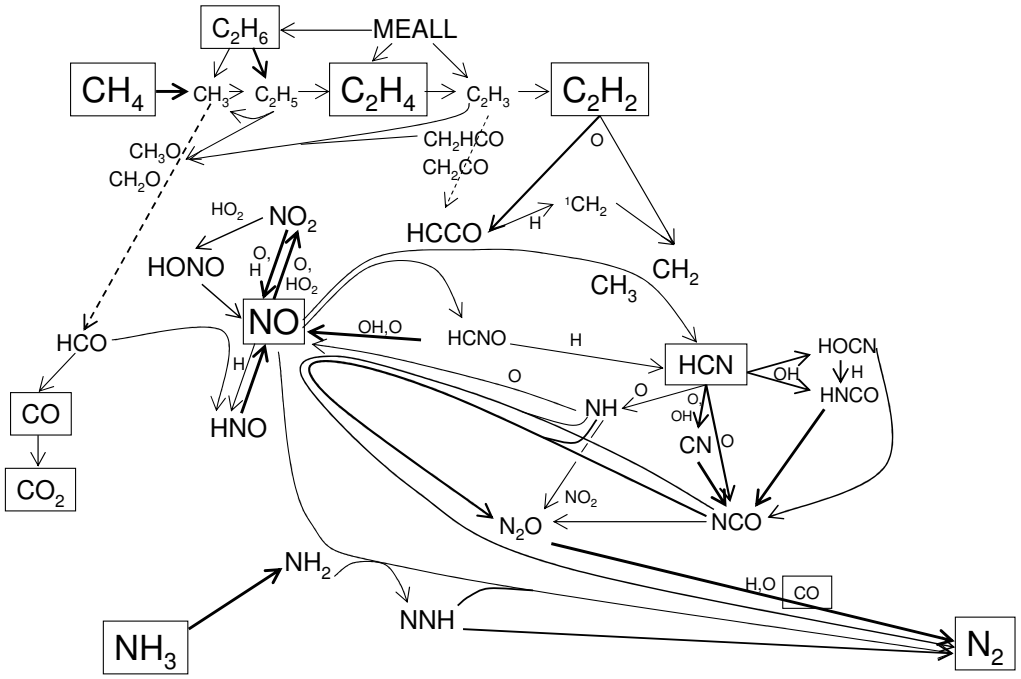

Figure 8.16: Main reaction paths for coal at 900°C, $t = 0.15$ s. Boxes represent the gases initially present or released during devolatilisation.

NO balance:

At this date, the NO is mainly consumed: the total rate of consumption of NO is 1.09×10^{-5} s^{-1} whereas its production rate is 8.91×10^{-6} s^{-1}. Thus the net rate of consumption of NO equals $\frac{\mathrm{d}\,X_{\mathrm{NO}}}{\mathrm{d}\,t} = -1.95 \times 10^{-6}$ s^{-1}.

A balance for NO shows that the NO is mostly converted into NO_2 through reaction (R140), presented above, that represents 98 % of the total NO consumption rate. NO_2 is recycled into NO; this reaction represents 99 % of the total NO production rate. The net production rate of NO_2 reaches 1.89×10^{-6} s^{-1}, i.e. 97 % of the net consumption rate of NO.

The time evolution of NO, NO_2 and their sum is plotted in Figure 8.17. The final NO

reduction correspond to the total NO_x reduction.

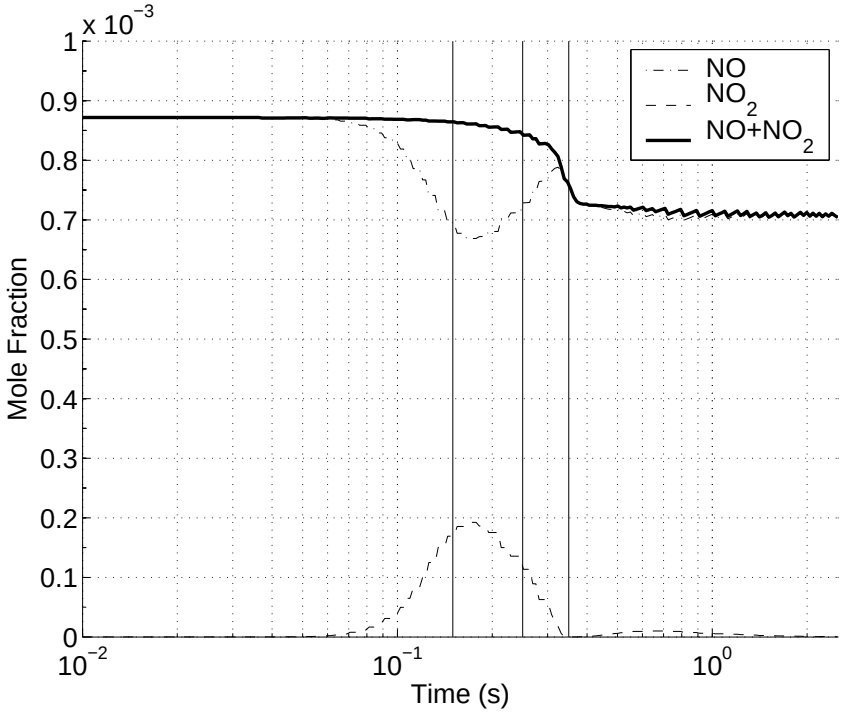

Figure 8.17: Coal at 900°C : Time evolution for NO (only gas phase variations), NO_2 and the sum NO + NO_2.

The last 3 % of net consumption rate of NO are distributed between reburning reactions with HCCO – (R168) and (R169), presented above – for a contribution of 2 % to the NO net depletion, and reaction with NH_2 (R101).

The efficiency of reburning NO consumption is minored by reactions (R171) and (R172) that oxidize HCNO into NO. Finally the efficiency of NO consumption via reburning – efficiency defined as the ratio between the net consumption rate of NO through reburning reactions and the total NO consumption by reburning reactions – reaches only 36 %.

$$HCNO + O \rightleftharpoons NO + HCO \qquad ROP(NO) = 0.001 \quad (R171)$$

$$HCNO + OH \rightleftharpoons NO + CH_2O \qquad ROP(NO) = 0.006 \quad (R172)$$

N_2 balance:

From a balance on N_2, it can be established that the reactions producing N_2, listed below, are dominated by reactions involving NH_2 and NNH – (R101), (R116) and (R117) – for more than 96 %. NNH, involved in (R116) and (R117), is entirely produced by the reaction (R100).

N_2O is responsible for only 1 % of the total N_2 production rate. N_2O is produced through reactions involving NH radical (sum of (R91) and (R93) contribution: $ROP(N_2O) = 0.116$), reactions involving NCO (sum of (R216) and (R219) contribution: $ROP(N_2O) = 0.512$). Added to (R217) ($ROP(N_2) = 0{,}020$), these reburning reactions contribute only for 2.5 % of the N_2 formation

$N + NO$	$\rightleftharpoons$	$N_2 + O$	$ROP(N_2) = 0.002$	(-R78)
$NH + NO$	$\rightleftharpoons$	$N_2 + OH$	$ROP(N_2) = 0.003$	(R92)
$NH_2 + NO$	$\rightleftharpoons$	$N_2 + H_2O$	$ROP(N_2) = 0.863$	(R101)
$NNH + M$	$\rightleftharpoons$	$N_2 + H + M$	$ROP(N_2) = 0.047$	(R116)
$NNH + NO$	$\rightleftharpoons$	$N_2 + HNO$	$ROP(N_2) = 0.054$	(R117)
$N_2O + M$	$\rightleftharpoons$	$N_2 + O + M$	$ROP(N_2) = 0.001$	(R156)
$N_2O + CO$	$\rightleftharpoons$	$N_2 + CO_2$	$ROP(N_2) = 0.009$	(R160)
$NCO + NO$	$\rightleftharpoons$	$CO_2 + N_2$	$ROP(N_2) = 0.020$	(R217)

Synthesis:

The SNCR is the main mechanism governing the reduction of NO into N_2. But, as in the case of coal with the furnace at 800°C, the NO is mostly converted into NO_2.

Date of $t = 0.25$ s At the date of $t = 0.25$ s, the gas temperature has reached 910°C. At this time, Figure 8.10 clearly shows that NO is formed.

The main reaction paths for coal, reactor temperature at 900°C, depicted in Figure 8.18.

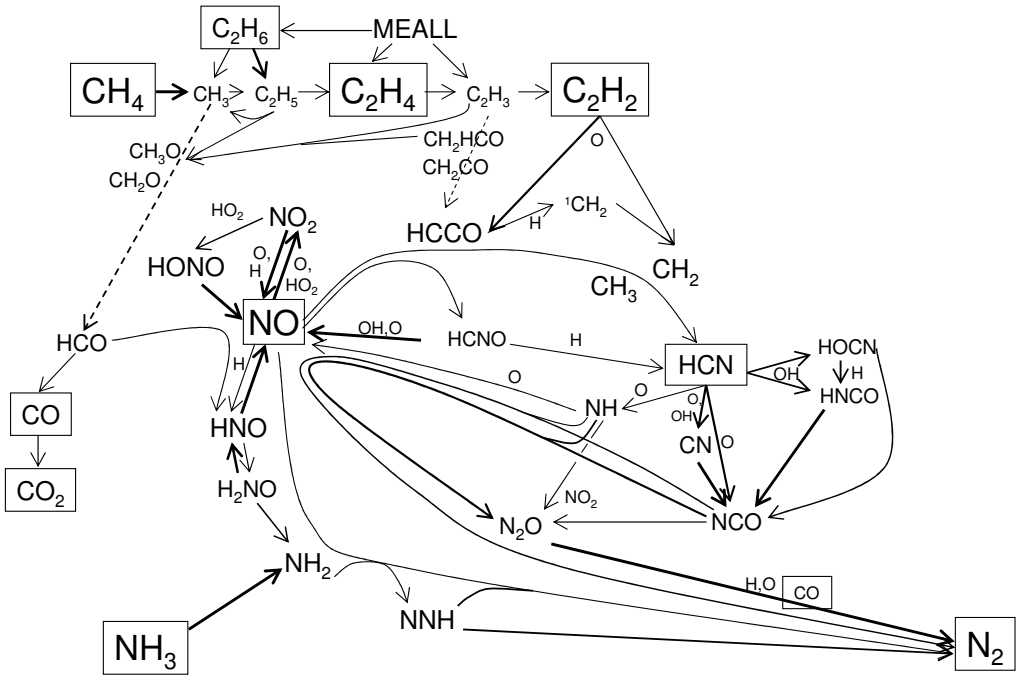

Figure 8.18: Main reaction paths for coal at 900°C, $t = 0.25$ s. Boxes represent the gases initially present or released during devolatilisation.

NO balance:

The NO balance indicates a total NO production and consumption rates of 3.22×10^{-5} and 3.15×10^{-5} s^{-1} respectively; the net production rate of NO is $\frac{\mathrm{d}\,X_{\mathrm{NO}}}{\mathrm{d}\,t} = +7.77 \times 10^{-7}$ s^{-1}.

At this time, NO is still mainly consumed to form NO_2 through (R140) (ROC(NO) = 0.965), but the reactions converting NO_2 into NO are now dominating. Hence, the NO_2 is now reduced into NO, since the net NO production rate due to NO_2 reaches 9.71×10^{-7} s^{-1}.

HNO is entirely recycled into NO. The difference between the net NO production rate and the production rate due to NO_2 is explained by the NO consumption by NH_2 through (R101) (ROC(NO) = 0.002) and by HCCO through reactions (R168) and (R169) (ROC(NO) = 0.014). Here, the reburning efficiency, defined above, reaches only 30 %.

N_2 balance:

The N_2 balance indicates that N_2 is globally produced at this date (its consumption rate is negligible compared to its production rate).

The production through the SNCR reactions (R101), (R116) and (R117) is still dominating with a global ROP(N_2) = 0.864. N_2O contributes to the N_2 formation for 5.8 % through reactions (R155), (R156) and (R160). NCO forms directly N_2 by (R217) (ROP(N_2) = 0.060) and NH contributes also to this positive balance for 1.2 % through (R92).

In contradiction with the preceding cases, 80.5 % of N_2O is formed by reactions involving intermediate species of the reburning process NH and NCO, through (R91), (R93), (R216) and (R219) defined above. Finally, the total reburning contribution to the NO to N_2 conversion reaches now 11.9 %.

Date of $t = 0.35$ s At the date of $t = 0.35$ s, the gas phase temperature reaches 996 °C. The NO formation rate plotted in Figure 8.10 indicates that NO is globally consumed at this time.

The main reaction paths for coal, with the reactor temperature set at 900°C for $t = 0.35$s, is depicted in Figure 8.19.

NO balance:

The number of reactions consuming NO, listed below, increases. The total NO consumption and production rates reach 2.30×10^{-5} and 2.43×10^{-5} s^{-1} respectively. The net NO consumption rate equals $\frac{d X_{NO}}{d t} = -1.25 \times 10^{-6}$ s^{-1}.

One remarks that the conversion of NO into NO_2 became less important than for shorter dates (ROC(NO) = -0.107), whereas the participation of HNO and HONO to the total consumption of NO increased to 65.3 and 8.3 % respectively. Here, HONO and NO_2 are entirely recycled into NO. In the case of HNO, 99.5 % is recycled into NO and 0.5 % is converted into H_2NO that produces further NH_2.

The reburning reactions (R162), (R164), (R165), (R168) and (R169) represent 5.5 % of the total NO consumption. The reactions involving NH and NCO represent a net consumption of NO of 2.49×10^{-7} and 1.83×10^{-7} s^{-1} respectively. Finally, the reburning reactions represent 50 % of the net consumption rate of NO, whereas NH and NCO are respectively responsible for 20 and 14.6 % of the NO depletion. N and NH_2 contribute for 4.4 % and 11 % of the NO consumption respectively.

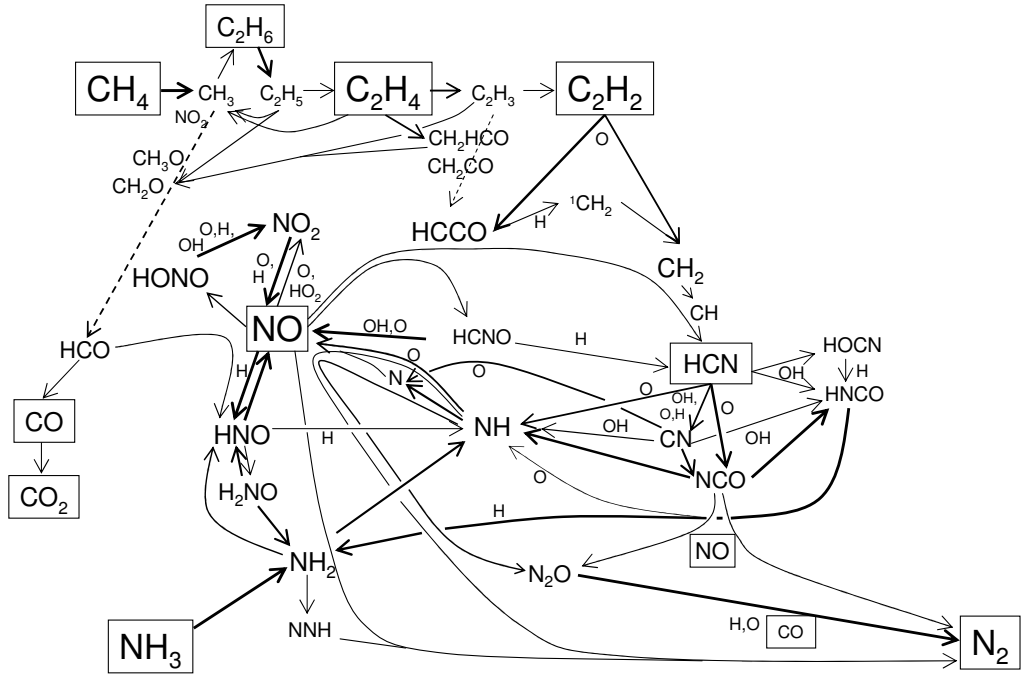

Figure 8.19: Main reaction paths for coal at 900°C, $t = 0.35$ s. Boxes represent the gases initially present or released during devolatilisation.

N + NO	$\rightleftharpoons$	N_2 + O	ROC(NO) = −0.002	(-R78)
NH + NO	$\rightleftharpoons$	N_2O + H	ROC(NO) = −0.009	(R91)
NH + NO	$\rightleftharpoons$	N_2 + OH	ROC(NO) = −0.003	(R92)
NO + HO_2	$\rightleftharpoons$	NO_2 + OH	ROC(NO) = −0.107	(R140)
NO + OH + M	$\rightleftharpoons$	HONO + M	ROC(NO) = −0.083	(R141)
NO + H + M	$\rightleftharpoons$	HNO + M	ROC(NO) = −0.641	(R142)
NO + HCO	$\rightleftharpoons$	HNO + CO	ROC(NO) = −0.012	(R143)
NO + O + M	$\rightleftharpoons$	NO_2 + M	ROC(NO) = −0.070	(-R147)
CH + NO	$\rightleftharpoons$	HCN + CO	ROC(NO) = −0.003	(R162)
CH_2 + NO	$\rightleftharpoons$	HCN + OH	ROC(NO) = −0.006	(R164)
CH_2 + NO	$\rightleftharpoons$	HCN0 + H	ROC(NO) = −0.010	(R165)
HCCO + NO	$\rightleftharpoons$	HCNO + CO	ROC(NO) = −0.027	(R168)
HCCO + NO	$\rightleftharpoons$	HCN + CO_2	ROC(NO) = −0.009	(R169)
NCO + NO	$\rightleftharpoons$	N_2O + CO	ROC(NO) = −0.005	(R216)
NCO + NO	$\rightleftharpoons$	N_2 + CO_2	ROC(NO) = −0.004	(R217)

N_2 balance:

The N_2 balance shows that the N_2 consumption rate is negligible compared to its production rate. The reactions that produce N_2 are listed below.

The reactions involving NH_2 and NNH – (R101), (R117), (R118) and (R119) – represent

22.3 % of the N_2 formation rate. The N radical, that is mainly produced by NH, is responsible for 7.4 % of the N_2 formation rate throusf (-R78), whereas NH contributes for 11.5 % by (R92) and N_2O 46 % by (R155)+(R157)+(R160).

$N + NO$	$\rightleftharpoons$	$N_2 + O$	$ROP(N_2) = 0.074$	(-R78)
$NH + NO$	$\rightleftharpoons$	$N_2 + OH$	$ROP(N_2) = 0.115$	(R92)
$NH_2 + NO$	$\rightleftharpoons$	$N_2 + H_2O$	$ROP(N_2) = 0.186$	(R101)
$NNH + NO$	$\rightleftharpoons$	$N_2 + HNO$	$ROP(N_2) = 0.031$	(R117)
$NNH + H$	$\rightleftharpoons$	$N_2 + H_2$	$ROP(N_2) = 0.004$	(R118)
$NNH + OH$	$\rightleftharpoons$	$N_2 + H_2O$	$ROP(N_2) = 0.002$	(R119)
$N_2O + H$	$\rightleftharpoons$	$N_2 + OH$	$ROP(N_2) = 0.443$	(R155)
$N_2O + O$	$\rightleftharpoons$	$N_2 + O_2$	$ROP(N_2) = 0.015$	(R157)
$N_2O + CO$	$\rightleftharpoons$	$N_2 + CO_2$	$ROP(N_2) = 0.002$	(R160)
$NCO + NO$	$\rightleftharpoons$	$CO_2 + N_2$	$ROP(N_2) = 0.127$	(R217)

Here, N_2O is produced through (R91) for 64.4 % and through (R216) for 33.7 %. NH is formed by HNO for 9.8 %, NH_2 for 6.7 % and HCN and its derivative (HNCO, CN and NCO) for 83.5 %. NH_2 is produced by NH_3 (28.2 %), HNCO (45.1 %), HCN (0.9 %), and finally H_2NO (25.9 %).

Synthesis:

The addition of all the different species contributions allow to conclude that more than 80 % of the N_2 formation occurs through reburning mechanism, around 11 % is due to the contribution of HNO (through the formation of H_2NO and NH) and 7 % is due to the contribution of NH_3.

Coal, reactor at 1000°C : The chosen date for coal at 1000°C is $t = 0.15$ s. At this time, the gas temperature has reached 1040°C (see Figure 8.11).

For coal in reburning experiments conditions, with the reactor temperature at 1000°C, the main reaction paths represented in Figure 8.20 is very similar to that depicted in the case of coal with a reactor temperature of 900°C, for $t = 0.35$ s in Figure 8.19.

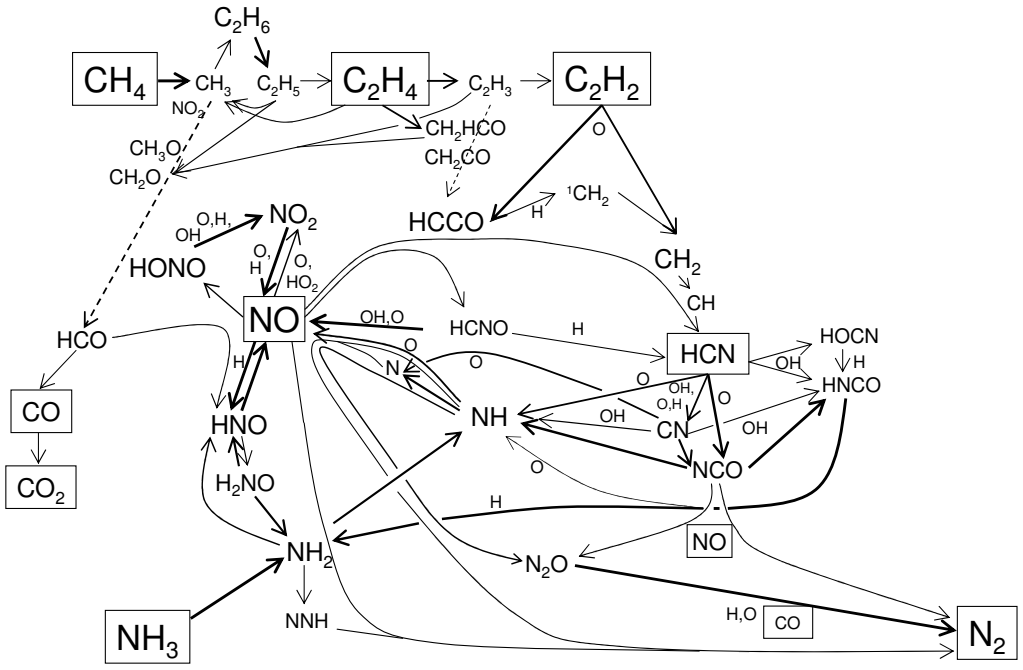

Figure 8.20: Main reaction paths for coal at 1000°C, $t = 0.15$ s. Boxes represent the gases initially present or released during devolatilisation.

NO balance:

In these conditions, NO is consumed : the total rate of consumption of NO is 4.26×10^{-5} s^{-1} whereas its production rate equals 3.80×10^{-5} s^{-1}. Thus the net consumption rate of NO is $\frac{\mathrm{d}\, X_{\mathrm{NO}}}{\mathrm{d}\, t} = -4.52 \times 10^{-6}$ s^{-1}.

In this case the reactions that consume NO are listed below. The reactions that yield NO_2, HNO and HONO represent more than 88 % of the total NO consumption through (R140), (R141), (R142), (R143) and (-R147). These species recycle completely into NO. They do not influence the total NO balance.

The reburning reactions (R162), (R164), (R165), (R168) and (R169) represent 4.2 % of the NO consumption. The reactions involving NH – (R91) and (R92) – and NCO – (R216) and (R217) – represent 1.2 and 1.8 % of the total consumption of NO respectively. Finally, the reburning reactions represent more than 33 % of the net consumption rate of NO, whereas NH and NCO are respectively responsible for 18.4 and 15.3 % of the NO depletion. N and NH_2

contribute for 7.6 % and 25.5 % of the NO consumption respectively.

N + NO	$\rightleftharpoons$	N_2 + O	ROC(NO) = −0.007	(-R78)
NH + NO	$\rightleftharpoons$	N_2O + H	ROC(NO) = −0.009	(R91)
NH + NO	$\rightleftharpoons$	N_2 + OH	ROC(NO) = −0.003	(R92)
NH_2 + NO	$\rightleftharpoons$	NNH + OH	ROC(NO) = −0.001	(R100)
NH_2 + NO	$\rightleftharpoons$	N_2 + H_2O	ROC(NO) = −0.012	(R101)
NNH + NO	$\rightleftharpoons$	N_2 + HNO	ROC(NO) = −0.001	(R117)
CH + NO	$\rightleftharpoons$	HCN + O	ROC(NO) = −0.002	(R162)
CH_2 + NO	$\rightleftharpoons$	HCNO + H	ROC(NO) = −0.004	(R164)
CH_2 + NO	$\rightleftharpoons$	HCN + OH	ROC(NO) = −0.007	(R165)
HCCO + NO	$\rightleftharpoons$	HCNO + CO	ROC(NO) = −0.022	(R168)
HCCO + NO	$\rightleftharpoons$	HCN + CO_2	ROC(NO) = −0.007	(R169)
NCO + NO	$\rightleftharpoons$	N_2O + CO	ROC(NO) = −0.010	(R216)
NCO + NO	$\rightleftharpoons$	CO_2 + N_2	ROC(NO) = −0.008	(R217)

In this case, the necessity to use net balance is obvious. Indeed, either products of reburning reactions are recycled into NO through reactions (R171) and (R172), or the species involved in the NO reduction into N_2 or N_2O may themselves oxidize into NO – see (R80), (R81), (R86), (R88) and (R224).

N + O2	$\rightleftharpoons$	NO + O	ROP(NO) = 0.001	(R80)
N + OH	$\rightleftharpoons$	NO + H	ROP(NO) = 0.002	(R81)
NH + OH	$\rightleftharpoons$	NO + H_2	ROP(NO) = 0.006	(R86)
NH + O	$\rightleftharpoons$	NO + H	ROP(NO) = 0.013	(R88)
HCNO + O	$\rightleftharpoons$	NO + HCO	ROP(NO) = 0.017	(R171)
HCNO + OH	$\rightleftharpoons$	NO + CH2O	ROP(NO) = 0.010	(R172)
NCO + O	$\rightleftharpoons$	NO + CO	ROP(NO) = 0.010	(R224)

N_2 balance:

The following three reactions are responsible for more than 50 % of the N_2 formation. This shows the high importance of N_2O in the N_2 formation.

N_2O + H	$\rightleftharpoons$	N_2 + OH	ROP(N_2) = 0.477	(R155)
N_2O + O	$\rightleftharpoons$	N_2 + O_2	ROP(N_2) = 0.031	(R157)
N_2O + CO	$\rightleftharpoons$	N_2 + CO_2	ROP(N_2) = 0.001	(R160)

The reactions (-R78), (R92) and (R101) between NO and N-species contribute to 36.4 % of the N_2 production. Reaction (R217) – between NCO (product of reburning, through HCN) and NO – yields 10.7 % of the N_2 formation.

The important species N_2O is mainly produced by NH – 65.5 % through (R91) – and by NCO – 32.8 % through (R216). NH seems to be a very important species in the NO reduction process, either to yield N_2 (R92) or to produce N_2O (R91). Thus the mechanism of formation of NH is of high interest; it is presented in the following five reactions:

$NH_2 + O$	$\rightleftharpoons$	$NH + OH$	ROP(NH) = 0.021	(R95)
$NH_2 + OH$	$\rightleftharpoons$	$NH + H_2O$	ROP(NH) = 0.028	(R98)
$NH_2 + H$	$\rightleftharpoons$	$NH + H_2$	ROP(NH) = 0.048	(R99)
$HCN + O$	$\rightleftharpoons$	$NH + CO$	ROP(NH) = 0.245	(R192)
$NCO + H$	$\rightleftharpoons$	$NH + CO$	ROP(NH) = 0.644	(R213)

NH is mainly – ≈ 89 % – produced by HCN and NCO. These are intermediate species of the reburning process; HCN is also released during the devolatilisation. A smaller part – 9.7 % – of NH is produced by NH_2 that comes directly from NH_3.

Synthesis:

Finally, the reburning path dominates the NO reduction process in the gas phase. By adding the different contributions, the NO reduction through the HCN path represents around 85 % of the reduction, whereas NH_3 ($\rightarrow NH_2$) contributes around 12.5 % of the total destruction of NO. HNO ($\rightarrow H_2NO \rightarrow NH_2$) is responsible for 1.5 % of the NO depletion.

The time evolution of NO, NO_2 and their sum is plotted in Figure 8.21. In this case, the observed NO depletion corresponds to the total NO_x depletion.

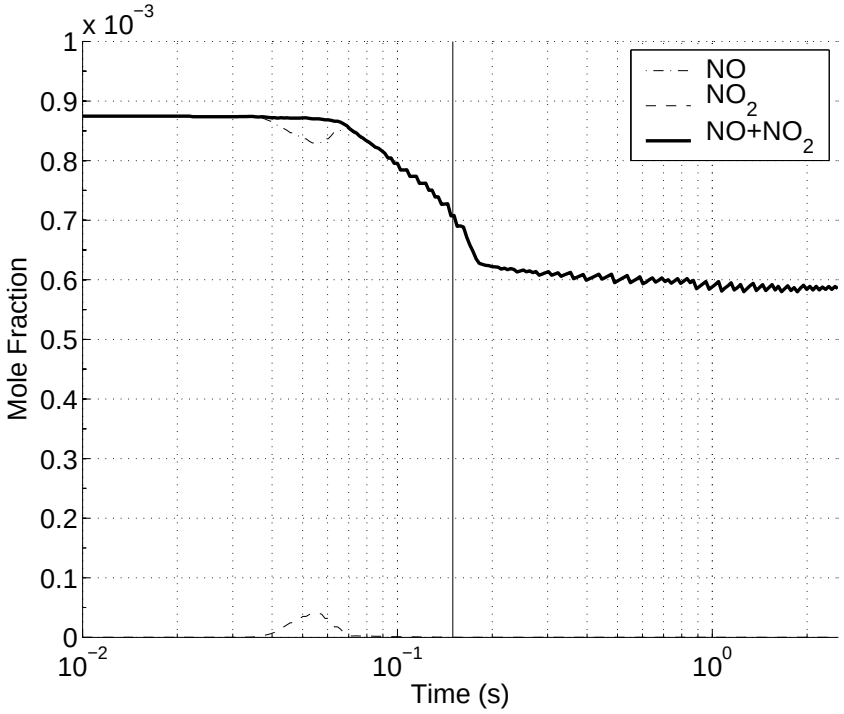

Figure 8.21: Coal at 1000°C : Time evolution for NO (only gas phase variations), NO_2 and the sum NO + NO_2.

Coal gas phase analyzes summary At 800°C, for coal at a date of $t = 0.4$ s, the SNCR mechanisms dominates the NO to N_2 reduction process. However, at this temperature, the NO is mostly converted into NO_2.

In the case of the furnace temperature set at 900°C and at

- time of 0.15 s, the gas phase is at 867°C. The strong influence of NH_2 shows that the

mechanisms governing NO reduction into N_2 (more than 96 %) is that involved in the SNCR process. However, most of the consumed NO is converted into NO_2.

- time of 0.25 s, the gas reaches now 910°C. NO is globally produced by the reconversion of NO_2, produced at shorter date. The formation of N_2 is still dominated by the reactions involved in the SNCR process (86.4 %), but the reburning reactions influence increases to reach 11.9 %.
- After 0.35 s, the gas temperature has reached a peak temperature at 996°C. NO is consumed through reburning mechanisms for more than 80 %. The HNO contribution reach 11 %; NH_3 through SNCR reactions only participates for 7 %.

With the reactor temperature at 1000°C, the reburning path dominates the NO reduction process. The NO reduction through the HCN path represents around 85 % of the reduction, whereas NH_3 ($\rightarrow NH_2$) contributes around 12.5 % of the total destruction of NO.

8.2.4.2 Gas phase reactions for lignite

Lignite, reactor at 800°C For lignite with the reactor temperature set at 800°C, a date of $t = 0.4$ s was chosen to perform the detailed chemical analysis. At this time, the gas has reached the final temperature of 800°C (see Figure 8.12.

The main reaction paths for lignite at 800°C, for a date of 0.4 s are represented in Figure 8.22.

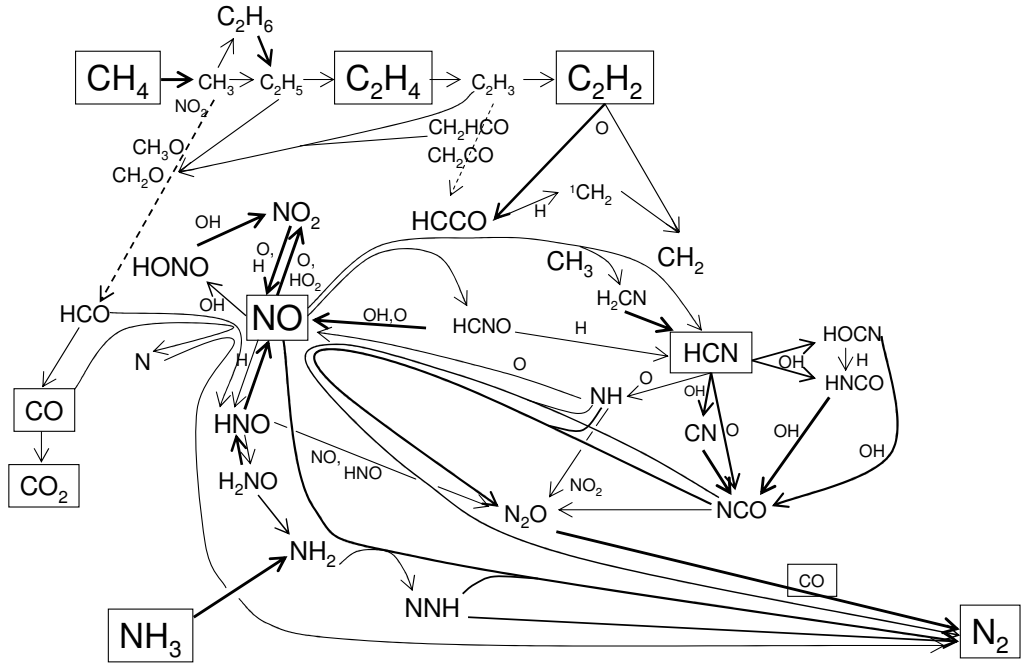

Figure 8.22: Main reaction paths for lignite at 800°C, $t = 0.4$ s. Boxes represent the gases initially present or released during devolatilisation.

NO balance:

NO is globally consumed: the total rate of consumption of NO is 1.82×10^{-6} s^{-1} whereas its total production rate is 1.21×10^{-6} s^{-1}. Thus, the NO net consumption rate equals $\frac{\mathrm{d}\,X_{\mathrm{NO}}}{\mathrm{d}\,t} = -6.17 \times 10^{-7}$ s^{-1}.

The case of lignite at 800°C presents some similarities with coal at the same furnace temperature : NO is mostly converted into NO_2 through reaction (R140). The net rate of NO consumption for this reaction equals 6.05×10^{-7} s^{-1} that corresponds to 98 % of the NO net consumption rate. HNO produced by reactions (R143) and (R959) is entirely recycled into NO.

Thus, the last 2 % of the net NO consumption rate are due to reburning reactions (R168) and (R169) and to the consumption of NO by NH_2 (R101).

$NO + HO_2$	$\rightleftharpoons$	$NO_2 + OH$	ROC(NO) = -0.978	(R140)
$NO + HCO$	$\rightleftharpoons$	$HNO + CO$	ROC(NO) = -0.009	(R143)
$HCCO + NO$	$\rightleftharpoons$	$HCNO + CO$	ROC(NO) = -0.008	(R168)
$HCCO + NO$	$\rightleftharpoons$	$HCN + CO_2$	ROC(NO) = -0.003	(R169)
$CH_3O + NO$	$\rightleftharpoons$	$CH_2O + HNO$	ROC(NO) = -0.002	(R959)

N_2 balance:

The N_2 consumption rate is negligible compared to its production rate. The reactions yielding N_2 are listed below. They are dominated by the reaction (R160) involving N_2O. NH_2 and NNH contribute here for 9.1 % of the N_2 production rate. The N radical is responsible for 24.8 % of the formation of N_2, whereas NCO is involved for 2.3 % through (R217).

$N + NO$	$\rightleftharpoons$	$N_2 + O$	ROP(N_2) = 0.248	(-R78)
$NH_2 + NO$	$\rightleftharpoons$	$N_2 + H_2O$	ROP(N_2) = 0.081	(R101)
$NNH + M$	$\rightleftharpoons$	$N_2 + H + M$	ROP(N_2) = 0.005	(R116)
$NNH + NO$	$\rightleftharpoons$	$N_2 + HNO$	ROP(N_2) = 0.005	(R117)
$N_2O + M$	$\rightleftharpoons$	$N_2 + O + M$	ROP(N_2) = 0.014	(R156)
$N_2O + CO$	$\rightleftharpoons$	$N_2 + CO_2$	ROP(N_2) = 0.622	(R160)
$NCO + NO$	$\rightleftharpoons$	$CO_2 + N_2$	ROP(N_2) = 0.023	(R217)

The NH_2 radical is entirely produced by NH_3. The reactions producing N_2O are listed below: the species resulting from the reburning process – NH and NCO – are responsible for more than 60 % of the formation of N_2O through the reactions (R91), (R93), (R216) and (R219), whereas N_2O is formed by NH_2 for only 3.2 % through reaction (R109). HNO produces 29.4 % of N_2O through reactions (R130) and (R131). Here again, the N radical has a non negligible influence : it contributes for 6.5 % of the formation rate of N_2O

$N + NO_2$	$\rightleftharpoons$	$N_2O + O$	ROP(N_2O) = 0.065	(R79)
$NH + NO$	$\rightleftharpoons$	$N_2O + H$	ROP(N_2O) = 0.050	(R91)
$NH + NO_2$	$\rightleftharpoons$	$N_2O + OH$	ROP(N_2O) = 0.032	(R93)
NH_2+NO_2	$\rightleftharpoons$	$N_2O + H_2O$	ROP(N_2O) = 0.032	(R109)
$2HNO$	$\rightleftharpoons$	$N_2O + H_2O$	ROP(N_2O) = 0.201	(R130)
$HNO + NO$	$\rightleftharpoons$	N_2O+OH	ROP(N_2O) = 0.093	(R131)
$NCO + NO$	$\rightleftharpoons$	$N_2O + CO$	ROP(N_2O) = 0.330	(R216)
$NCO + NO_2$	$\rightleftharpoons$	CO2+N_2O	ROP(N_2O) = 0.218	(R219)

In the present case, the production of N radical is only due to the reaction: $CO + NO \rightleftharpoons CO_2 + N$ (-R249).

Synthesis:

Finally, the reburning reactions are overall responsible of a normalized production of N_2 around 42 %. At 800°C, for lignite after a date of $t = 0.4$ s, the NO to N_2 reduction process

- the SNCR reactions are responsible for 10 %,
- the CO ($\rightarrow$ N) for 29 %
- and HNO for 19 %.

However, at this temperature, the NO is mostly converted into NO_2 as represented in Figure 8.23.

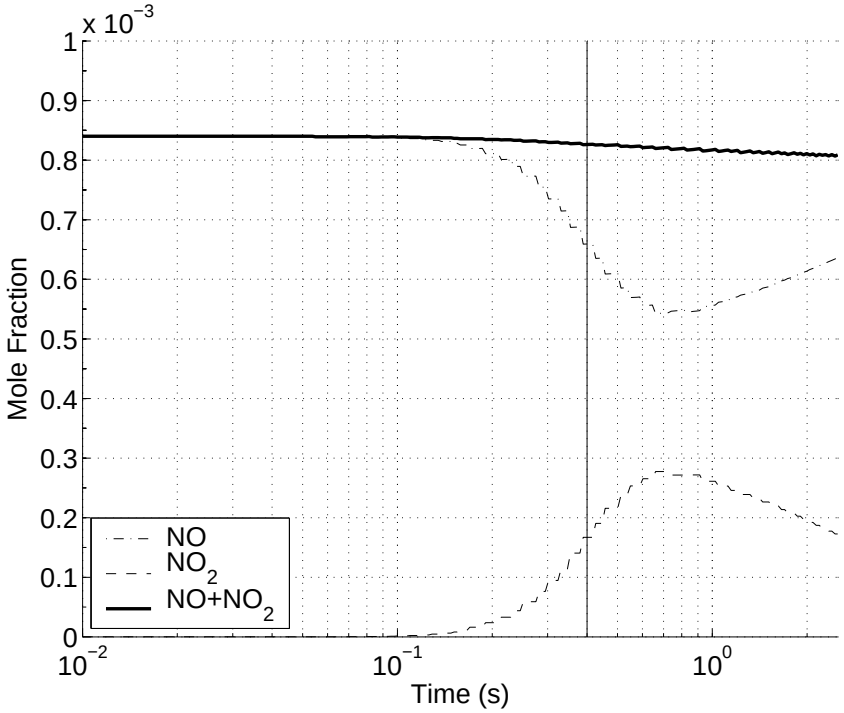

Figure 8.23: Lignite at 800°C : Time evolution for NO (only gas phase variations), NO_2 and the sum NO + NO_2.

Lignite, reactor at 1000°C : For lignite, with the reactor temperature set at 1000°C, three dates were chosen: $t = 0.09$, 0.12 and 0.16 s due to the oscillations observed in Figure 8.13.

Date of $t = 0.09$ s For lignite at 1000°C and a date of 0.09 s, the gas temperature equals 895°C.

The main reaction paths for this case, i.e. lignite with EFR at 1000°C and $t = 0.09$ s, are represented in Figure 8.24. They are very similar to those already depicted in the case of coal at 800°C (Figure 8.14).

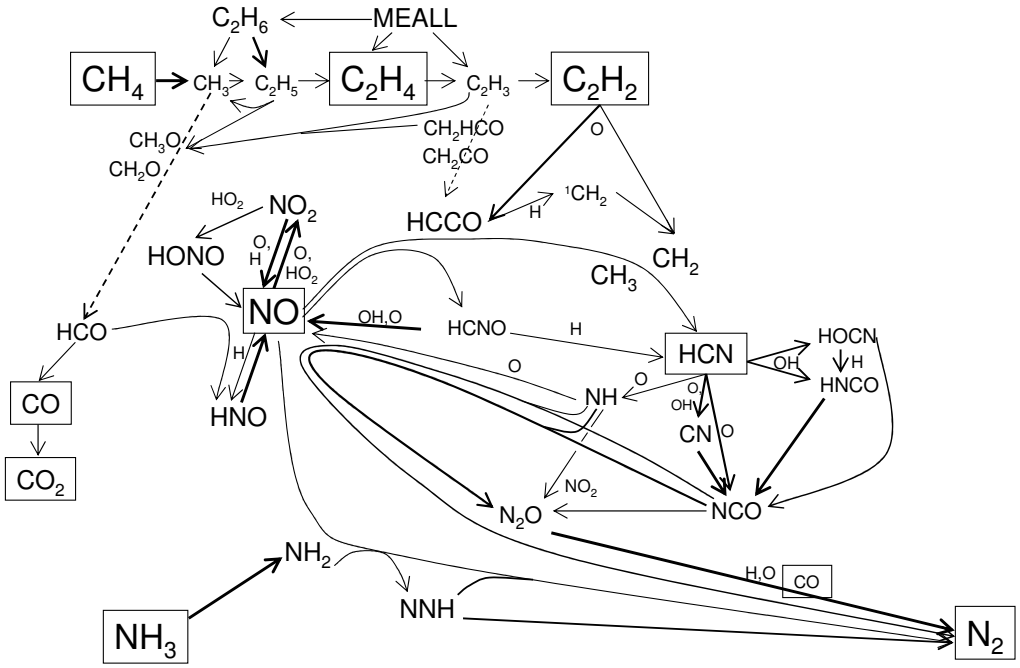

Figure 8.24: Main reaction paths for lignite at 1000°C, $t = 0.09$ s. Boxes represent the gases initially present or released during devolatilisation.

NO balance:

The NO is globally consumed : the total rate of consumption of NO is 1.85×10^{-5} s^{-1} whereas its production rate is 1.30×10^{-5} s^{-1}. Thus the net consumption rate reaches $\frac{\mathrm{d}\,X_{\mathrm{NO}}}{\mathrm{d}\,t} = -5.46 \times 10^{-6}$ s^{-1}.

The NO is mostly converted into NO_2 through reaction (R140) that represents 98 % of the total NO consumption rate. Even if NO_2 is recycled into NO (99 % of the total NO production rate), the net rate of NO_2 production reaches 5.37×10^{-6} s^{-1}, i.e. 98 % of the net NO consumption rate.

The last 2 % of net consumption rate of NO are distributed between reburning reactions (R168) and (R169) – 1.3 % of the net NO depletion – and NH_2 reduction (R101) for 0.7 %

of the net NO consumption. The efficiency of reburning NO consumption is minored by reactions (R171) and (R172) that oxidize HCNO into NO. Finally the efficiency of reburning NO consumption is 45 % only.

HCNO + O	$\rightleftharpoons$	NO + HCO	ROP(NO) = 0.001	(R171)
HCNO + OH	$\rightleftharpoons$	NO + CH_2O	ROP(NO) = 0.006	(R172)

N_2 balance:

The balance on N_2 reveals that the reactions producing N_2 are dominated by NH_2 and NNH reactions (R101), (R116) and (R117) for more than 96 %. NNH, involved in (R116) and (R117), is entirely produced by the reaction (R100). N_2O is only responsible for 1 % of the N_2 production. N_2O is produced through reactions (R91) and (R93) (ROP(N_2O) = 0.116), (R216) and (R219) (ROP(N_2O) = 0.512). Added to (R217) (ROP(N_2) = 0,020), these reburning reactions contribute only for 2.5 % of the N_2 formation

N + NO	$\rightleftharpoons$	N_2 + O	ROP(N_2) = 0.002	(-R78)
NH + NO	$\rightleftharpoons$	N_2 + OH	ROP(N_2) = 0.003	(R92)
NH_2 + NO	$\rightleftharpoons$	N_2 + H_2O	ROP(N_2) = 0.863	(R101)
NNH + M	$\rightleftharpoons$	N_2 + H + M	ROP(N_2) = 0.047	(R116)
NNH + NO	$\rightleftharpoons$	N_2 + HNO	ROP(N_2) = 0.054	(R117)
N_2O + M	$\rightleftharpoons$	N_2 + O + M	ROP(N_2) = 0.001	(R156)
N_2O + CO	$\rightleftharpoons$	N_2 + CO_2	ROP(N_2) = 0.009	(R160)
NCO + NO	$\rightleftharpoons$	CO_2 + N_2	ROP(N_2) = 0.020	(R217)

Date of $t = 0.12$ s The gas temperature reaches 950°C.

The main reaction paths for this case, i.e. lignite with EFR at 1000°C and $t = 0.12$ s, is represented in Figure 8.25. They are very similar to that already depicted in the case of coal at 900°C in Figure 8.18.

NO balance:

The NO consumption and production rates equal 5.68×10^{-5} and 6.10×10^{-5} s^{-1} respectively. Then, the net production rate of NO is $\frac{d X_{NO}}{d t} = +4.20 \times 10^{-6}$ s^{-1}.

As in the case of coal with the reactor temperature set at 900°C, the NO initially converted into NO_2 during the first NO consumption zone in Figure (8.13) is recycled into NO.

Even if NO_2 is the main product during NO consumption, its balance shows a global conversion into NO at the rate of 4.59×10^{-6} s^{-1}. The difference observed between this value and the total NO production rate (6.10×10^{-5} s^{-1}) is due to the NO consumption by NH_2 – through the reaction (R101) – and HCCO – through (R168) and (R169).

N_2 balance:

In the N_2 balance, the decomposition of the reactions conducting to the final stage of the NO reduction indicates that NH_2 and NNH – both exclusively from ammonia – are responsible for more than 92 % of the N_2 formation rate.

The last percents are distributed between N_2O – through (R155), (R156) and (R160) for 5.4 % – and NCO – through (R217) for 1.4 %. Note that NH_2 is also involved in the formation

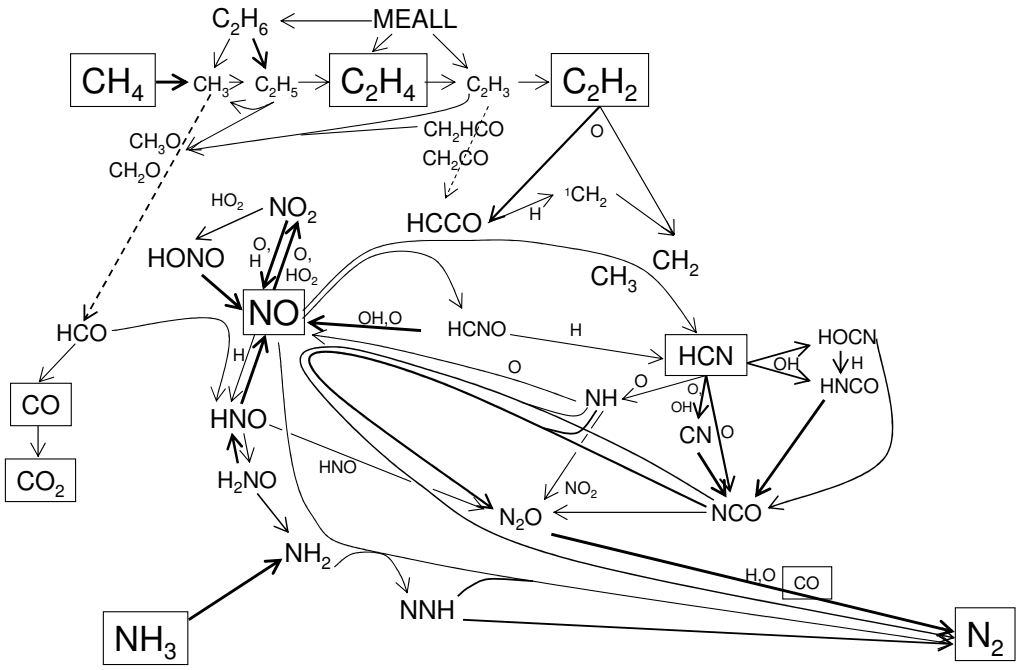

Figure 8.25: Main reaction paths for coal at 1000°C, $t = 0.12$ s. Boxes represent the gases initially present or released during devolatilisation.

of N_2O, either directly or by the intermediate NH radical.

Date of $t = 0.16$ s After a date of 0.16, the gas has reached a peak temperature at 1115°C.

The main reaction paths for lignite at 1000°C for a date of $t = 0.16$ s are illustrated in Figure 8.26.

NO balance:

At this time, the NO is globally consumed : the consumption and production rate reach 8.30×10^{-7} and 5.26×10^{-7} s^{-1} respectively. Then, the net consumption rate of NO equals $\frac{\mathrm{d}\,X_{\mathrm{NO}}}{\mathrm{d}\,t} = -3.04 \times 10^{-7}$ s^{-1}.

The main part of the total NO consumption rate – more than 51 % – is due to the formation of HNO and NO_2. These species are almost entirely recycled into NO and do not participate to the NO net depletion. Indeed, a small fraction (about 1 %) of the total HNO is converted into H_2NO and further to NH_2, and another fraction – 1.2 % – to NH. The reactions that consume NO are listed below.

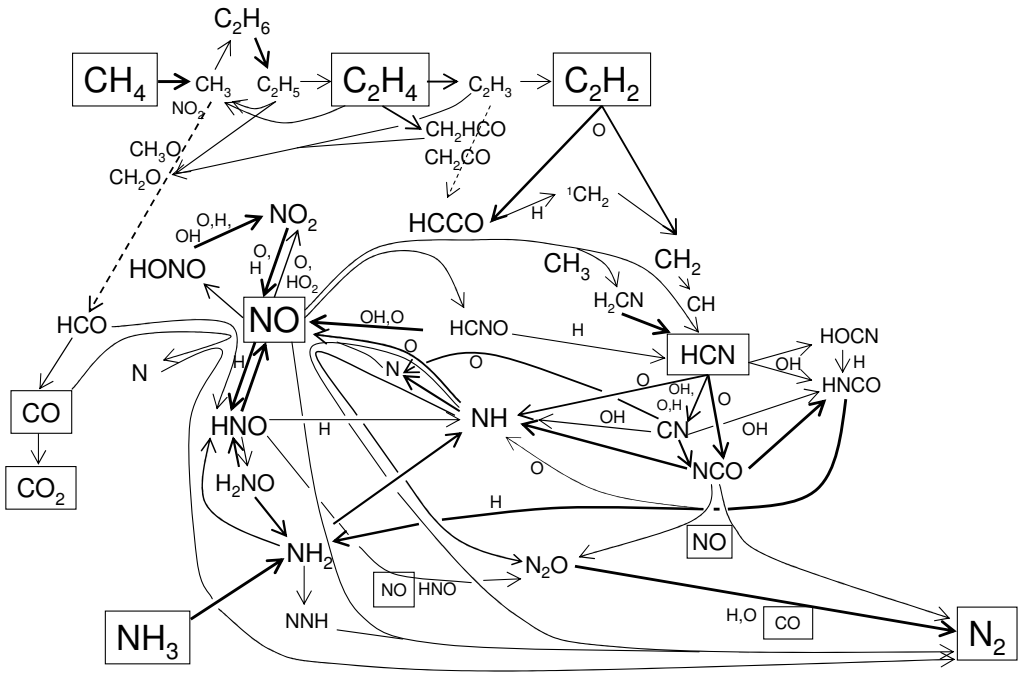

Figure 8.26: Main reaction paths for lignite at 1000°C, $t = 0.16$ s. Boxes represent the gases initially present or released during devolatilisation.

N + NO	$\rightleftharpoons$	N_2 + O	ROC(NO) = −0.002	(-R78)
NH + NO	$\rightleftharpoons$	N_2O + H	ROC(NO) = −0.004	(R91)
NH + NO	$\rightleftharpoons$	N_2 + OH	ROC(NO) = −0.002	(R92)
NH_2 + NO	$\rightleftharpoons$	NNH + OH	ROC(NO) = −0.003	(R100)
NH_2 + NO	$\rightleftharpoons$	N_2 + H_2O	ROC(NO) = −0.032	(R101)
NNH + NO	$\rightleftharpoons$	N_2 + HNO	ROC(NO) = −0.001	(R117)
CH_2 + NO	$\rightleftharpoons$	HCNO + H	ROC(NO) = −0.026	(R164)
CH_2 + NO	$\rightleftharpoons$	HCN + OH	ROC(NO) = −0.050	(R165)
CH_3 + NO	$\rightleftharpoons$	HCNO + H	ROC(NO) = −0.107	(R166)
CH_3 + NO	$\rightleftharpoons$	HCN + OH	ROC(NO) = −0.107	(R167)
HCCO + NO	$\rightleftharpoons$	HCNO + CO	ROC(NO) = −0.100	(R168)
HCCO + NO	$\rightleftharpoons$	HCN + CO_2	ROC(NO) = −0.033	(R169)
NCO + NO	$\rightleftharpoons$	N_2O + CO	ROC(NO) = −0.001	(R216)
CO + NO	$\rightleftharpoons$	N + CO_2	ROC(NO) = −0.002	(-R249)

Here, the reburning reactions (R164) to (R169) represent more than 88 % of the NO net depletion, when reactions involving NH_2 and NNH – (R101) and (R117) – are responsible for 8.5 % of the NO consumption rate. NH contributes for 1.4 % through reaction (R91) and (R92). It is interesting to note that CO consumes 1 % of NO through the chain reactions (-R249) and (-R78).

HNO through H_2NO contributes to the NH_2 formation for more than 22 %. The rest of the NH_2 formation is provided by NH_3. HNO is also involved in the formation of NH for more than 89 %. The remaining NH formation percents come from HCN (and NCO) for more than 12 % and NH_2 for 5 %.

N_2 balance:

The N_2 balance indicates, that total contribution of NH_3 to the NO reduction into N_2 is about 35 %; the part attributed to reburning mechanisms is equal to 30 %. Finally the HNO participation to the NO conversion into N_2 represents 34 % of the whole formation. CO is responsible for 3 %.

Because of its influence in the direct reduction of NO through (R92) and the production of N_2O, NH is the central species of the NO reduction for lignite at 1000°C. NH_2 contributes also to the reduction of NO.

The time evolution of NO, NO_2 and their sum is plotted in Figure 8.27. It indicates that the final NO consumption represents the effective NO_x reduction.

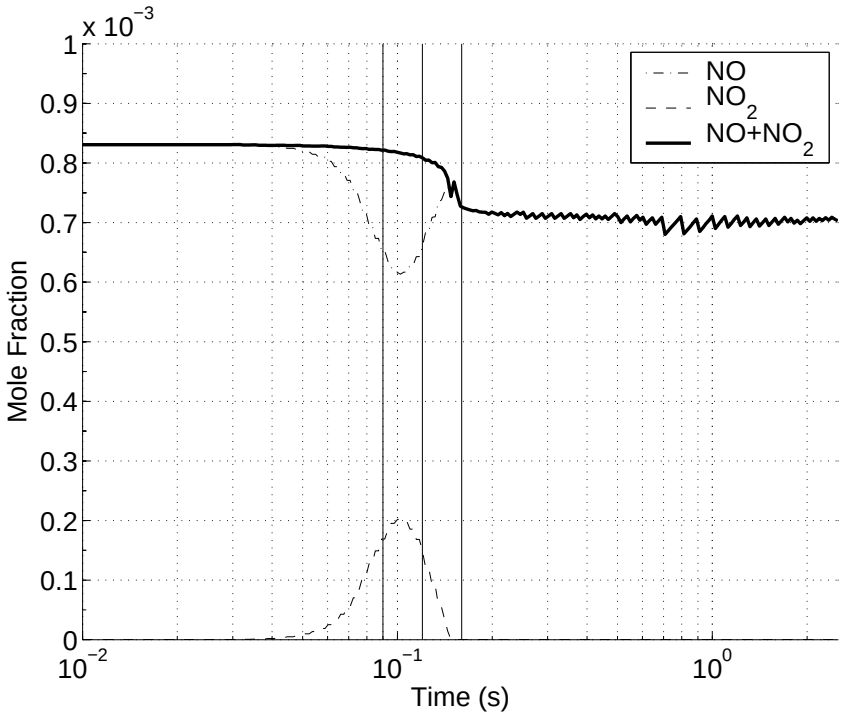

Figure 8.27: Lignite at 1000°C : Time evolution for NO (only gas phase variations), NO_2 and the sum NO + NO_2.

Lignite gas phase analyzes summary At 800°C, for lignite at a date of $t = 0.4$ s, the NO to N_2 reduction process is due to

- the SNCR mechanisms are responsible for 10 %;
- the CO ($\rightarrow$ N) for 29 %;
- and HNO for 19 %.

The reburning reactions are overall responsible for a normalized production of N_2 around 42 %. However, at this temperature, the NO is mostly converted into NO_2, as represented in Figure 8.23.

In the case of lignite with the reactor at 1000°C, the three dates chosen to perform the detailed chemical analysis results are comparable with the case of coal with the furnace at 900°C.

- Indeed, at $t = 0.09$ s, the gas phase temperature is 895°C. Here the NO is mostly converted into NO_2, i.e. 98 % of the net NO depletion. The rest of the NO consumption corresponds to the NO reduction into N_2, dominated by SNCR mechanisms (more than 95 %).
- At the time of 0.12 s, the temperature is at 950°C and the NO_2 recycled to NO. Even if NO is globally produced, the reduction of NO to N_2 occurs and his still dominated – 92 % – by SNCR mechanisms.
- Finally, at the third date, $t = 0.16$ s, NO depletion is due to for 35 % to NH_3, 34 % to HNO, 30 % to reburning mechanisms and 3 % to CO.

Compared to coal reaction paths, in the case of lignite a new mechanism appears: the reduction of NO by CO. Indeed CO is more concentrated in the case of lignite than in the case of coal. This CO results both from devolatilisation or from char oxidation and NO reduction by char (higher kinetic rates). This observation of the CO influence for high concentrations confirms those of Commandré [24] related in Chapter 3.

8.2.5 Discussion

8.2.5.1 Chemical interpretations

The equivalence ratio, ϕ, defined for the oxidation of the mixture of measured gas released during the pyrolysis can be calculated by the ratio of the mole fraction of oxygen necessary to oxidize the mixture of measured gases at the end of the pyrolysis in stoichiometric condition, $X_{O_2,St}$, to the initial oxygen mole fraction $X_{O_2,init}$ (see Equation 8.1).

$$\phi = \frac{X_{O_2,St}}{X_{O_2,init}} \tag{8.1}$$

It changes from one case – fuel and temperature – to another.

Thus, both for coal and lignite modeling at 800°C, $\phi \approx 0.7$. This means that the gas phase reactions occur in fuel lean conditions. In all the other cases (other fuels and other temperatures), $1.4 > \phi > 1.2$; the gas phase reactions occur globally in fuel rich conditions. Nevertheless, for short residence times, the quantity of volatile matters released is small, thus $\phi < 1$. At short residence times, these fuel lean conditions are correlated to the low temperatures (see Figures 8.9 to 8.13). This may explain the conversion of NO into NO_2 at 800°C, and at short residence times for coal at 900°C and for lignite at 1000°C. It should be noted that no NO_2 was measured experimentally whatever the temperature.

The similar behaviors observed for coal at 900°C and for lignite at 1000°C may be also explained by the higher devolatilisation kinetics of lignite than that of coal. Indeed, in the case of lignite, the same quantity of volatiles is released than released by coal for a shorter residence time, when the temperatures are not stabilized. Thus, the NO is converted into NO_2 at $t = 0.09$ s for lignite, and at $t = 0.15$ s in the case of coal. At these times, the gas temperatures are very similar: 870°C in the case of coal and 895°C for lignite. At longer residence, the recycling of NO_2 into NO appears for both fuels between 900 and 950°C.

Concerning the reduction of NO into N_2, in the case of coal that has a high N-content, the reactions in the gas phase are dominated by SNCR mechanisms for gas temperatures below 950°C. Above 1000°C, the reduction mechanism is dominated by the reactions involved in the reburning process. This is always correlated with a high concentration of radicals involved in the hydrocarbon oxidation (HCCO, OH, H, CH_3 and CH_2). One should note that HCN is an intermediate species in the reburning mechanisms, but it is also generated by devolatilisation.

In the case of lignite at 800°C, a lower quantity of N-volatiles species are released (see Table 7.1), thus the reduction process is not dominated by SNCR. At 1000°C, more N-volatiles are released, thus for short dates – $t = 0.09$ – the temperature is 895°C and the reduction of NO into N_2 is governed by SNCR reactions. Note that the NO reduction at this time is very small compared to that observed for higher dates.

Lignite releases high quantities of CO during pyrolysis, its contribution to the reduction

of NO appear only for high CO concentrations – i.e. 3300 ppm in each case. Finally, in the case of lignite, the NO reduction into N_2 follows four main routes involving NH_3, HNO hydrocarbons (reburning) and CO. Their relative influence vary with the temperature.

8.2.5.2 Effect of N-contents

The strong contribution of the N-species released during pyrolysis – i.e. NH_3 and HCN – in the NO reduction is discussed below. Indeed, the efficiency of the SNCR mechanisms is well known, but its contribution to the NO reduction in coal reburning conditions is surprising.

A sensitivity analysis on the total NO mole fraction, X_{NO}, was performed in the case of coal at 1000°C to identify the influence of the parameters governing the N-release on the NO reduction. Variation of the parameters p, listed below, were carried out in the model. The sensitivities expressed as in Equation 8.2 are plotted in Figure 8.28.

$$\text{sensitivity} = S = \frac{X_{\text{NO}} - X_{\text{NO}}^{init}}{X_{\text{NO}}^{init}} \tag{8.2}$$

Where the superscript ^{init} represents the initial modeling, without any change of p.

The influence of the following parameters p was studied :

- N-content: the initial value is 1.71 %, simulations were ran with the N-content artificially set to 0.5 and 3 %, to cover the range of nitrogen contained in solid fuels;
- α_N, the fraction of N released in the volatiles matters: the initial value was 0.37, variations of ±50 % were performed to set α_N to 0.185 and 0.555;
- δ_v and ε_v, fraction of the N present in volatiles, that are released into HCN or NH_3 respectively. The variations of the parameters δ_v and ε_v are coupled: when δ_v increases by 10 %, ε_v decreases by 10 %. The initial values for δ_v and ε_v were 0.541 and 0.087. First, a simulation was run with δ_v and ε_v values inverted. Secondly, the case where no NH_3 is released during pyrolysis – i.e. $\delta_v = 0.628$ and $\varepsilon_v = 0$ – was simulated.

In Figure 8.28, a curve below zero indicates that NO was more reduced than in the reference case. It appears clearly from the plot:

- a higher N-content of the coal, leads to a higher NO reduction: an increase up to 3 % of the coal intial N-content implies a total NO concentration 10 % lower that that of the reference case after a residence time of 2 s (black solid line), whereas the decrease of the N atoms in the fuel up to 0.5 % implies an increase of the modeled NO mole fraction of about 10 % afer 2 s (solid red line).
- the more N is released during the pyrolysis, the more NO is reduced. When α_N is increased by 50 %, the NO concentration is reduced by 10 % after 2 s (dashed black line). The decrease by 50 % of the N-volatiles induces an increase of the total NO concentration of about 8 % (dashed red line).

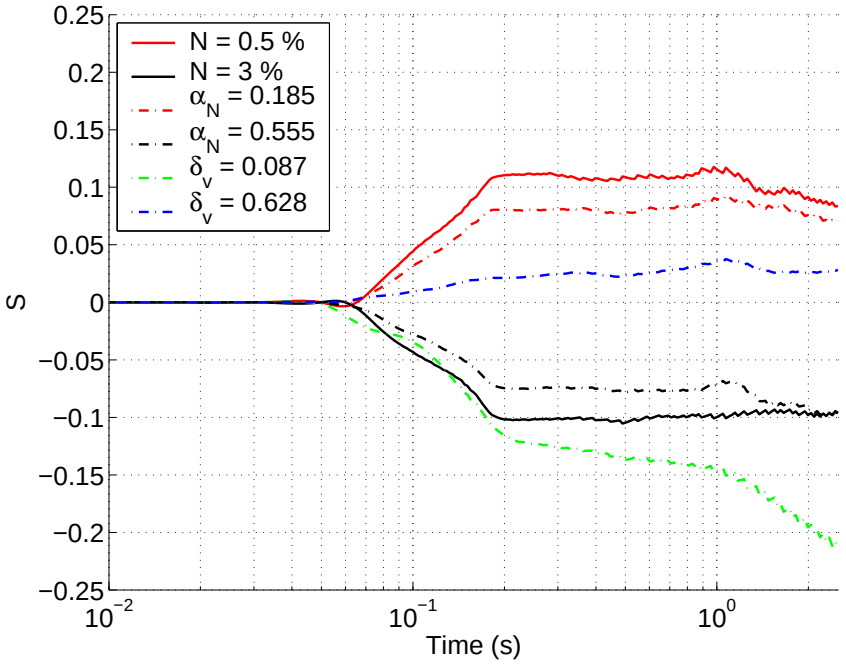

Figure 8.28: The reduced sensitivity for N-content and repartition.

- when no NH_3 is released – $\delta_v = 0.628$ – final NO mole fraction increased by ≈ 3 %. The inversion of δ_v and ε_v implies a significant drop of the predicted NO mole fraction at the residence time of 2 s: - 20 %.

8.2.6 Synthesis

The gas phase NO reduction by volatile matters from the devolatilisation of solid fuels is a very complex process. A lot of competitive reactions occur simultaneously. This implies that the dominant mechanisms change with varying temperature. In the present cases, the NO situation can shift from reduction to production along time, making interpretation difficult:

- the choice of the dates to perform the detailed analysis is not easy.
- the detailed interpretation of the chemical reactions occurring in the gas phase is quite heavy.

However, these analyzes provide some answers to the surprising behaviors observed in the modelings of solid fuels reburning.

- With lignite, that has a higher content of volatile matters than coal, the gas phase reduces less NO than with coal. This may be explained by the lower N-content of lignite than that of coal. Indeed N-species play a major role in the fuel rich reduction. If this N is removed from to reach the lignite value of ≈ 0.5 %, the final NO consumption decrease by 10 %. When N is increased to 3 %, the final NO reduction also increased by 10 %.
- The non monotonic evolution over temperature for the gas phase of coal and lignite is simply explained by the NO conversion into NO_2 at low temperatures. Indeed, the NO

decrease seems very high at 800°C, in both cases of coal and lignite, but the NO is only converted into NO_2. The overall NO_x reduction is in fact low at this temperature.

- The time variations of the NO formation rate observed in the cases of lignite at 1000°C and coal at 900°C is also due to the conversion of NO into NO_2 at low temperatures, corresponding with short residence times.

Some conclusions on the gas phase reduction mechanisms are possible. The reduction through gas phase reactions is highly dependent on the original fuel composition and on the temperature. The main reaction paths change considerably with temperature both for coal and for lignite.

- Coal – that contains 1,72 % of nitrogen – reduces NO through a SNCR scheme with a strong influence of NH_3 when the gas temperature in comprised between 800 and 950°C, corresponding to the optimum temperature for this process.
- Above 1000°C in the gas phase, the reburning reaction path becomes predominant in the case of coal. NH_3, that is both released during devolatilisation and char oxidation, has a strong influence.
- For lignite, the reduction of NO follows four different routes; their relative influence vary with the gas temperature.

The complex behavior of the NO reduction, correlated to the varying gas temperature, oxygen content, CO content will be retrieved in industrial cases. This makes it very difficult to explain or predict the efficiency of NO reduction thanks to reburning with solid fuels.

The significant differences observed between experimental and modeling values for gas concentrations imply careful interpretations of the model and homogeneous reactions analysis results. Moreover, the chemical reactions in the gas phase occur at very short residence times, where no experimental observation is possible. Nevertheless, the modeling approach used for the present work provide very useful information to understand the governing mechanisms in solid fuels reburning.

Conclusions

Conclusion générale

Ce travail permet aujourd'hui de proposer une analyse des mécanismes mis en jeux lors de la réduction du NO par quatre combustibles solides couvrant une large gamme de propriétés. Ces résultats sont originaux.

Cet objectif a été atteint grâce à la mise en oeuvre, en parallèle, d'un dispositif expérimental performant et d'une modélisation numérique détaillée. La démarche originale d'une décomposition du problème en un ensemble de réactions hétérogènes et homogènes a été retenue. Ainsi le reburning a été décrit

- par trois réactions "hétérogènes". Ces réactions, dont les paramètres réactionnels sont spécifiques à chaque combustible, ont été caractérisées de façon intrinsèque, séparément, d'un point de vue cinétique et d'un point de vue bilan des espèces produites. Ce travail représente une grande partie de la thèse.

- par un ensemble de réactions chimiques en phase gazeuse, qui a été décrit au travers d'un schéma cinétique détaillé parmi les plus récents disponibles dans la littérature.

En confrontant le modèle complet à des expériences de reburning conduites à trois températures (800, 900 et 1000°C) et sans calage d'aucun paramètre, on ne parvient pas à retrouver précisément les résultats expérimentaux, mais les tendances sont retrouvées de façon assez satisfaisante pour proposer des analyses détaillées du reburning avec les quatre combustibles solides.

Les grandes difficultés rencontrées – et qui peuvent expliquer les écarts entre expériences et modélisations du reburning – ont été les suivantes :

- La préparation d'un char qui s'apparente à celui effectivement présent lors du reburning est délicate : sans la présence d'O_2, des goudrons se condensent à sa surface et modifient ses propriétés.

- La dévolatilisation des combustible génère une grande fraction de goudrons : la moitié environ de la masse totale des matières volatiles, soit jusqu'à plus de 25 % de la masse initiale de combustible solide. Il est illusoire de chercher à caractériser espèce par espèce ces goudrons pour décrire leur évolution dans la phase gazeuse. De plus, les mécanismes de craquage de ces goudrons et leurs interactions avec le NO ne sont pas connus. La prise en compte des goudrons dans le modèle – ils sont assimilés à du carbone solide et réagissent comme le char – reste une voie d'amélioration de cette approche.

Les principaux résultats de ce travail sont

Durant la dévolatilisation : Les expériences de pyrolyse sous 100 % d'azote ont permis de qualifier et de quantifier les différentes espèces – majeures et mineures – dégagées lors de la dévolatilisation; une cinétique de perte de masse a pu être trouvée pour chacun des combustibles utilisé. La vitesse de pyrolyse semble être inversement corrélée avec le rang des combustibles : le lignite se pyrolyse plus de six fois plus vite que le petcoke et deux fois plus rapidement que l'anthracite et le charbon. Deux combustibles ont un fort taux de matières volatiles – le lignite et le charbon – deux ont une faible teneur en matières volatiles – l'anthracite et le petcoke. Il apparaît que l'hydrogène est l'espèce gazeuse la plus concentrée en volume dans les produits de pyrolyse mesurés. CO et CO_2 sont aussi très concentrés dans les gaz. Parmi les hydrocarbures, CH_4 est l'espèce la plus présente, alors que C_2H_2 et C_2H_4 sont souvent du même ordre de grandeur.

Durant l'oxydation du char : Les expériences et modélisations d'oxydation du char sous 3 % d'O_2 ont permis de déterminer les constantes cinétiques relatives à cette réaction hétérogène. Les chars des deux combustibles de bas rang – lignite et coal – présentent des réactivités supérieures de plusieurs ordres de grandeurs à celles des combustibles à faibles taux de matières volatiles, l'anthracite et le petcoke.

Durant la réduction du NO sur le char : La réduction du NO sur le char est elle aussi caractérisée. Il apparaît que les réactivités des chars des combustibles à forte teneur en matière volatiles (ou de bas rang) – le charbon et le lignite – sont plus élevées que celles des chars des combustibles de bas rangs, anthracite et petcoke. Toutefois, les réactivités des chars étudiés vis à vis du NO sont 10 à 1000 fois plus fortes que la valeur moyenne proposée par Aarna et al. [90].

Une corrélation franche entre les réactivités des chars à O_2 d'une part et à NO d'autre part est mise en évidence: un char qui s'oxyde rapidement est un char qui réduit efficacement le NO.

Durant le reburning du NO : En première approche, les deux combustibles à fort taux de matières volatiles – lignite et charbon – réduisent beaucoup plus le NO que les deux combustibles à faible taux de matières volatiles. Ce potentiel de réduction du NO croît avec la température pour chacun des combustibles.

La modélisation de ce type d'expériences permet de décrire de manière satisfaisante les tendances mises en valeur par les résultats expérimentaux, tout en utilisant les paramètres cinétiques déterminés lors de la caractérisation des réactions hétérogènes élémentaires. Aucun paramètre du modèle n'est calé lors de cette étape. Le modèle permet de proposer une analyse des différentes contributions responsables de la réduction du NO. La dévolatilisation n'a pas d'effet direct sur les quantités de NO formées; l'oxydation du char n'a pas non plus d'impact direct significatif en terme de production de NO du fait des conditions riches étudiées lors de ce travail. Ce sont la réduction du NO sur le char et les réactions homogènes qui représentent les grands termes de formation/réduction du NO; ces deux phénomènes ont des effets du même ordre de grandeur après un temps de séjour d'environ

2 s. Les réactions en phase gazeuse opèrent la réduction du NO aux temps très courts: 0,05–0,3 s. La réduction du NO sur le char démarre plus tard (0,1–0,5 s) et croît sans interruption pour devenir prépondérante aux temps longs (plusieurs secondes). La réduction du NO sur le char augmente sensiblement et de façon monotone avec la température. La très forte différence observée entre les combustibles de bas rangs – lignite et charbon – et ceux à faible teneur en matières volatiles – anthracite et petcoke – s'explique:

- d'une part par la très grande différence de réactivité des chars au NO,
- d'autre part par les plus fortes quantités d'hydrocarbures dégagées lors de la pyrolyse du lignite et du charbon.

Des singularités, décrites ci-dessous, qui sont apparues lors de la première interprétation des résultats ont trouvé une explication lors de l'étude détaillée des réactions en phase gazeuse finalement proposée

- le lignite produit plus de matières volatiles que le charbon, mais réduit moins de NO dans la phase gazeuse,
- l'évolution de la quantité de NO réduit par les réactions homogènes n'est pas toujours monotone en fonction de la température,
- l'évolution temporelle de la concentration de NO varie de manière singulière dans certains cas, passant par des phases successives de réduction puis formation de NO.

L'analyse des voies réactionnelles en phase gazeuse est complexe, car les mécanismes prépondérants changent en fonction de la température. Il apparaît qu'à des températures de gaz inférieures à 1000°C, NO est réduit en N_2 par NH_2. Il s'agit là de la principale réaction mise en oeuvre dans le mécanisme de la SNCR[1]. Au delà de 1000°C, les réactions homogènes sont dominées par les réactions de reburning. Le NO est réduit en HCN puis N_2 par des espèces radicalaires issues de la décomposition des hydrocarbures : CH, CH_2, CH_3 et HCCO. De manière surprenante, la teneur en azote du combustible a un effet positif sur la réduction homogène du NO. Ceci s'explique par la très grande importance de HCN et NH_3 – dégagés lors de la pyrolyse et de l'oxydation du char – dans les voies conduisant de NO à N_2.

[1]SNCR : Selective Non Catalytic Reduction

General conclusions

This work allows today to propose an analysis of the mechanisms playing a role during the reduction of NO by four solid fuels covering a large range of properties. These results are original.

This objective was achieved thanks to the parallel use of a powerful experimental device and of a detailed numerical modeling. The original decomposition process of the problem in heterogeneous and homogeneous reactions was retained. Thus, the reburning was described

- by three heterogeneous reaction. These reactions, whose reactions parameters are specific to each fuel, were separately characterized in an intrinsic way, from a kinetic point of view and from a point of view of the produced species balance. This work represents a large part of the thesis.
- by a large number of gas phase reactions, described by a detailed chemical mechanism from the most recent available in the literature.

While confronting the complete model results with reburning experiments performed at three temperatures (800, 900, and 1000°C), and without adjusting any parameter, one does not manage to find the experimental results precisely, but the tendencies are retrieved satisfactorily enough to propose detailed analyzes of the reburning of the four fuels.

The great encountered difficulties – which can explain the differences between experiments and modelings of the reburning – were as follows:

- The preparation of a char that represent effectively the char present during reburning is difficult: without any O_2, tars condense at the char surface and modify its properties.
- The fuel devolatilisation generates a large fraction of tars: approximately half of the total volatile matters mass, i.e. up to 25 % of the initial mass of fuel. It is illusory to try to characterize species by species the tars to describe their evolution in the gas phase. Moreover, the mechanisms of cracking of tars and their interactions with NO are not known. The taking into account of the tars in the model – they are assimilated to solid carbon and react as the char – remains improvement way of this approach.

The principal results of this work are

During the devolatilisation: The experiments of pyrolysis under 100 % of nitrogen made it possible to qualify and quantify the various species – major and minor – released during the

devolatilisation; mass loss kinetics could be found for each fuel used. The pyrolysis velocity seems to be inversely correlated to the fuels rank: lignite pyrolyzes six times quicker than the petcoke and twice quicker than anthracite and coal. Two fuels have a high amount of volatile matters – lignite and coal – two have a low volatiles content – anthracite and the petcoke. It appears that hydrogen is the gas species most concentrated in volume in the measured products of pyrolysis. CO and CO_2 are also very concentrated in gases. Among hydrocarbons, CH_4 is the most present species, whereas C_2H_2 and C_2H_4 are often of the same order of magnitude.

During char oxidation: The experiments and modelings of char oxidation under 3 % O_2 allowed the kinetic parameters relative to this heterogeneous reaction to be determined. The chars of the two low rank fuels – lignite and coal – have reactivities higher of several orders of magnitude than those of fuels with low volatile matters content, anthracite and petcoke.

During NO reduction by char: The NO reduction by char is also characterized. It appears that char reactivities of high-volatiles fuels (or of low rank) – coal and lignite – are higher than those of the char of low rank fuels, anthracite and petcoke. However, the reactivity to NO of studied chars are 10 to 1000 times larger than the average value suggested by Aarna et al. [90].

A clear correlation between the chars reactivities to O_2 on the one hand and to NO on the other hand is highlighted: a char that oxidizes rapidly is a char that reduces NO effectively.

During the NO reburning: In a first approach, the two high-volatiles fuels – lignite and coal – reduce much more NO than the two low-volatiles fuels. This NO reduction potential grows with the temperature for each fuel.

The modeling of this type of experiments enables to describe satisfactorily the tendencies highlighted by the experimental results, by using the kinetic parameters determined during the characterization of the elementary heterogeneous reactions. At this stage, no more parameters were adjusted. The model enables to propose an analysis of the different contributions responsible for the NO reduction. The devolatilisation does not have a direct effect on the formed quantities of NO because of the fuel-rich conditions studied in the present work; the char oxidation does not have either a significant direct impact in term of NO production. The heterogeneous NO reduction by char and gas phase reactions represent the major terms of NO formation/reduction; these two phenomena have effects of the same order of magnitude after a residence time of approximately 2 s. The gas phase reactions reduce NO at very short times: 0.05–0.3 s. The NO reduction by char starts later (0.1–0.5 s) and grows without interruption to become dominating after long residence times (several seconds). The NO reduction at the char surface increases appreciably and monotonically with temperature. The very large difference observed between low rank fuels – lignite and coal – and those with a low volatile matters content – anthracite and petcoke – is explained:

- on the one hand, by the large reactivity difference of chars to NO,
- and on the other hand, by the larger hydrocarbons quantities released during lignite and coal pyrolysis.

Singularities, described below, which appeared during the first results interpretation found an explanation in the detailed gas phase reactions finally suggested

- lignite releases more volatile matters than coal but reduces less NO in the gas phase,
- the evolution of the NO reduced quantity by the homogeneous reactions is not always monotonic with the temperature.
- the temporal evolution of the NO concentration varies singularly in some cases, with successive phases of reduction then formation of NO.

The analysis the main reaction paths in gas phase is complex, because the dominating mechanisms change with the temperature. It appears that at gas temperatures lower than 1000°C, NO is reduced into N_2 by NH_2. This is the main reaction occurring in the SNCR[2] process. Above 1000°C, the homogeneous reactions are dominated by the reactions of reburning. NO is reduced into HCN and then N_2 by radical species resulting from the decomposition of hydrocarbons: CH, CH_2, CH_3 and HCCO. Surprisingly, the nitrogen content of fuel has a positive effect on the homogeneous NO reduction. This is explained by the very high importance of HCN and NH_3 – released during the pyrolysis and the char oxidation – in the paths leading from NO to N_2.

[2]SNCR : Selective Non Catalytic Reduction

Nomenclature

Nomenclature

Latin Letters

A_{NO}	NO reduction by char pre-exponential factor: expressed in terms of NO consumption	$\mathrm{mol_{NO}.m^{-2}.s^{-1}.atm^{-}}m$
A_p	external area of the particle: $A_p = \pi.d_p^2$	$\mathrm{m^2}$
A_{dev}	devolatilisation pre-exponential factor	$\mathrm{s^{-1}}$
$a_{n,i}$	polynomial coefficients to fit the thermodynamic data	depends on n
A_{OxChar}	char oxidation pre-exponential factor: expressed in terms of char consumption	$\mathrm{kg_{C_s}.m^{-2}.s^{-1}.atm^{-}}n$
Ash	ash content in fuel (standard test value)	$\mathrm{kg_{Ash}.kg_{Fuel}^{-1}}$
$[C_i]$	molar concentration of each reactant and product species i	$\mathrm{mol.m^{-3}}$
Cp	particle specific heat	$\mathrm{J.kg^{-1}.K^{-1}}$
Cp_i	molar specific heats at constant pressure of species i	$\mathrm{J.mol^{-1}.K^{-1}}$
cp_i	mass specific heats at constant pressure of species i	$\mathrm{J.kg^{-1}.K^{-1}}$
C_{fix}	fixed carbon content in fuel (standard test value)	$\mathrm{kg_{C_{fix}}.kg_{Fuel}^{-1}}$
d_p	particle diameter	m
D_{eff}	effective diffusion coefficient	$\mathrm{m^2.s^{-1}}$
D_{Knu}	Knudsen diffusion coefficient	$\mathrm{m^2.s^{-1}}$
D_{mol}	molecular diffusion coefficient	$\mathrm{m^2.s^{-1}}$
d_{pore}	mean pore diameter	m
$E_{a_{\mathrm{NO}}}$	NO reduction by char activation energy	$\mathrm{J.mol^{-1}}$
$E_{a_{dev}}$	devolatilisation activation energy	$\mathrm{J.mol^{-1}}$
$E_{a_{OxChar}}$	char oxidation activation energy	$\mathrm{J.mol^{-1}}$
fr_{CO}	mole fraction of CO released during char oxidation	-
g	gravity acceleration	$\mathrm{m.s^{-2}}$
H_i	molar enthalpy of species i	$\mathrm{J.mol^{-1}}$
h_i	mass enthalpy of the species i	$\mathrm{J.kg^{-1}}$

h_p	convective heat transfer coefficient between the particle and the gas environment	$\mathrm{W.m^{-2}.K^{-1}}$
h_{fe}	convective heat transfer coefficient between furnace wall and gas environment	$\mathrm{W.kg^{-1}.K^{-1}}$
$[i]$	concentration of the species i	$\mathrm{mol.m^{-3}}$
K	constant devolatilisation mass loss rate	$\mathrm{kg_{\mathit{Fuel}}.s^{-1}}$
k_{NO}	NO reduction by char constant rate: expressed in terms of NO consumption	$\mathrm{mol_{NO}.m^{-2}.s^{-1}.atm^{-\mathit{m}}}$
k_m	transfer coefficient through the particle boundary layer	$\mathrm{m.s^{-1}}$
k_r	constant rate for the reaction r	unit vary
K_{c_r}	equilibrium constant for the reaction r	unit vary
k_{dev}	devolatilisation constant rate	$\mathrm{s^{-1}}$
k_{OxChar}	char oxidation constant rate: expressed in terms of char consumption	$\mathrm{kg_{C_\mathit{s}}.m^{-2}.s^{-1}.atm^{-\mathit{n}}}$
K_{p_r}	pressure equilibrium constant for the reaction r	unit vary
$\mathcal{M}_i$	symbol denoting species i	
m	mass	kg
M_i	molecular mass of species i	$\mathrm{kg.mol^{-1}}$
m_i	mass of the species i	kg
m_p	particle mass	kg
$moist.$	moisture content in fuel (standard test value)	$\mathrm{kg_{\mathit{Ash}}.kg^{-1}_{\mathit{Fuel}}}$
N	number of chemical species in the system	-
N_R	number of reactions	-
Nu	Nusselt number	
P	pressure	atm
P_{NO}	NO partial pressure	atm
$P_{\mathrm{O_2}}$	$\mathrm{O_2}$ partial pressure	atm
$\hat{R}_i$	molar production rate of the species i	$\mathrm{mol.m^{-3}.s^{-1}}$
R	ideal gas constant	$= 8.314\ \mathrm{J.mol^{-1}.K^{-1}}$
r_{NO}	NO reduction by char reaction rate	$\mathrm{g_{NO}.s^{-1}}$
Re	Reynolds number	-
$\mathrm{ROC}(i)$	normalized rates of consumption	-
$\mathrm{ROP}(i)$	normalized rates of production	-
S	cross sectional area of the reactor	$\mathrm{m^2}$
S_i	molar entropy of the species i	$\mathrm{J.mol^{-1}.K^{-1}}$
S_{reac}	reactive surface	$\mathrm{m^2}$
S_{Spe}	specific pore surface	$\mathrm{m^2.kg^{-1}}$
Sh	Sherwood number	-
T	temperature	K
t	time	s
T_p	particle temperature	K
$\bar{U}$	mean gas velocity in the reactor	$\mathrm{m.s^{-1}}$

u	gas velocity in the reactor	$\mathrm{m.s^{-1}}$
u^*	dimensionless gas velocity in the reactor	-
U_{max}	maximum gas velocity in the reactor	$\mathrm{m.s^{-1}}$
v_{gas}	gas velocity in the sampled section	$\mathrm{m.s^{-1}}$
v_{part}	particle velocity in the sampled section	$\mathrm{m.s^{-1}}$
v_{slide}	sliding velocity between gas and particles	$\mathrm{m.s^{-1}}$
VM	volatile matters content in fuel (standard test value)	$\mathrm{kg_{VM}.kg_{Fuel}^{-1}}$
X_i	mole fraction of the species i	-
z	sampling distance to particle injection	m

Greek Letters

α_{N}	fraction of N released in volatile matters	-
α_{S}	fraction of S released in volatile matters	-
$\alpha_{\mathrm{H}\rightarrow\mathrm{C}_x\mathrm{H}_y}$	fraction of H released into $\mathrm{C}_x\mathrm{H}_y$ during pyrolysis	-
$\alpha_{\mathrm{O}\rightarrow\mathrm{CO_2}}$	fraction of O released into $\mathrm{CO_2}$ during pyrolysis	-
$\alpha_{\mathrm{O}\rightarrow\mathrm{CO}}$	fraction of O released into CO during pyrolysis	-
α_{dev}	volatile matters mass fraction released during pyrolysis	$\mathrm{kg_{gas}.kg_{Fuel}^{-1}}$
β	stoichiometry ratio in the char oxidation	-
β_c	fraction of char N yielding $\mathrm{N_2O}$ during char oxidation	-
β_r	temperature exponent fro reaction r	-
β_v	fraction of volatile N yielding $\mathrm{N_2O}$ during pyrolysis	-
δ_c	fraction of char N yieding HCN during char oxidation	-
δ_v	fraction of volatile N yielding HCN during pyrolysis	-
ϵ_p	particle emissivity	-
ε	particle porosity	
ε_c	fraction of char N yielding $\mathrm{NH_3}$ during char oxidation	-
ε_v	fraction of volatile N yielding $\mathrm{NH_3}$ during pyrolysis	-
γ_c	fraction of char N yielding $\mathrm{N_2}$ during char oxidation	-
γ_v	fraction of volatile N yielding $\mathrm{N_2}$ during pyrolysis	-
ΔH_r	molar reaction enthalpy of reaction r	$\mathrm{J.mol^{-1}}$
Δh_r	mass reaction enthalpy of the reaction r	$\mathrm{J.kg^{-1}}$
η	Thiele effectiveness factor	-

η_c	fraction of char N yielding NO during char oxidation	-
η_v	fraction of volatile N yielding NO during pyrolysis	-
λ	air excess	-
λ_g	gas conductivity	$\mathrm{W.m^{-1}.K^{-1}}$
μ	dynamic viscosity	$\mathrm{kg.m^{-1}.s^{-1}}$
$\nu''_{i,r}$	stoichiometric coefficient for product i in reaction r	-
$\nu'_{i,r}$	stoichiometric coefficient for reactant i in reaction r	-
ϕ	Thiele modulus	-
ϕ	oxidation equivalence ratio	-
$\phi_{\mathrm{O_2}}$	oxygen consumed by the particle	$\mathrm{mol.s^{-1}}$
ρ_p	particle density	$\mathrm{kg.m^{-3}}$
ΔS_r	molar reaction entropy of reaction r	$\mathrm{J.mol^{-1}.K^{-1}}$
σ_0	Boltzmann constant	$= 5.67 \times 10^{-8}$ $\mathrm{W.m^{-2}.K^{-4}}$
Δt_{gas}	gas residence time in the sampled section	s
Δt_{part}	particle residence time in the sampled section	s
τ	PSR residence time	s

Superscripts

0	standard-state pressure 1 atm	
m	NO reduction by char reaction order	-
n	char oxidation reaction order	-

Subscripts

b	backward reaction
$Char$	Char
$Char, \mathrm{NO}$	char consumption by NO reduction
$Char, Ox$	char consumption by char oxidation
dev	devolatilisation
env	particle surrounding environment
f	forward reaction
f	furnace
$Fuel$	Fuel
gas	gas
$part$	particle
het	heterogeneous reactions
i	species i

p	particle
pore	pore
pycno	skeletal density
r	reaction r
St	Stoichiometry
Vol	Volatile Matters
n	number of nitrogen atoms in a molecule
s	number of sulfur atoms in a molecule
x	number of carbon atoms in a molecule
y	number of hydrogen atoms in a molecule
z	number of oxygen atoms in a molecule

Bibliography references

Bibliography

[1] Ministère de l'économie, des finances et de l'industrie. Énergie et matières premières – statistiques énergétiques de la france. `www.industrie.gouv.fr/energie/statisti/pdf/depliant.pdf`, Mars 2006.

[2] European Commission – Directorate-General for Energy and Transport. Energy & transport in figures 2005. `http://ec.europa.eu/dgs/energy_transport/figures/pocketbook/doc/2005/etif_2005_whole_en.pdf`, consulted the 18.08.2006.

[3] World Energy Council. The world energy book, Autumn 2005.

[4] Energy Information Administration – Official Energy Statitistics from the U.S. Government. NYMEX light sweet crude oil futures prices. `http://www.eia.doe.gov/emeu/international/crude2.html`, consulted the 18.08.2006.

[5] World Coal Institute. Coal: Secure energy, October 2005.

[6] British Petroleum Company. Quantifying energy – bp statistical review of world energy 2006 – coal, consulted the 18.08.2006.

[7] L. S. Jensen. *NO_x from ciment production - Reduction by primary measures.* PhD thesis, Departement of chemical Engineering, Technical University of Denmark, Lyngby, 1999.

[8] Activity report 2004. Technical report, CEMBUREAU, 2004.

[9] ADEME. Guide d'actions de réduction des NO_x de l'industrie française. Technical report, ADEME, 2003.

[10] W. Duda. *Cement data book.* Bauverlag GmbH, Wiesbaden und Berlin, 1976.

[11] Reference document on best available techniques in the cement and lime manufactring industries. Technical report, European commission, 2000.

[12] Seidel, Huckauf, and Stark. *Technologie des ciments, chaux, plâtre.* SEPTIMA – Paris, 1980.

[13] K. L. Smith, L. D. Smoot, and T. H. Fletcher. *Fundamental of coal combustion for clean and efficient use*, chapter 3 - Coal characteristics, structure, and reaction rates, pages 131–298. Elsevier, 1993.

[14] S. Pillet. *Réalisation d'un système expérimental pour caractériser la combustion et les émissions d'oxydes d'azote des combustibles solides : application aux charbons et à la biomasse.* PhD thesis, Université d'Orléans, Décembre 2004.

[15] L. Van de Steene. *Thermochimie de la combustion à basses températures de solides pulvérisés : Application à un charbon.* PhD thesis, Institut National Polytechnique de Toulouse, 1999.

[16] U.S. Department of Energy – Energy Information Administration. *Coal Production Report – Instructions*, March 2005.

[17] AFNOR. *NF M03-002 – Combustibles minéraux solides – Détermination de l'humidité*, Juillet 1995.

[18] AFNOR. *NF M03-004 – Combustibles minéraux solides – Détermination de l'indice de matières volatiles du charbon et du coke*, Février 2003.

[19] AFNOR. *NF M03-003 – Combustibles minéraux solides – Détermination du taux de cendres*, Octobre 1994.

[20] AFNOR. *NF M03-006 – Combustibles minéraux solides – Détermination du taux de carbone fixe*, Octobre 1994.

[21] P. Solomon, D. Hamblen, R. Carangelo, M. Serio, and G. Deshpande. General model of coal devolatilization. *Energy and Fuel*, pages 405–422, 1988.

[22] P. Solomon, A. Serio, and E. Suuberg. Coal pyrolysis: experiments, kinetic rates and mechanisms. *Progress in Energy and Combustion Science*, 18:133–220, 1992.

[23] H. Zhang. *Nitrogen evolution and soot formation during secondary pyrolysis.* PhD thesis, Brigham Young University, 2001.

[24] J.-M. Commandré. *Formation des oxydes d'azote lors de la combustion de cokes de pétrole dans des conditions de précalcinateur de cimenterie.* PhD thesis, Institut National Polytechnique de Toulouse, 2002.

[25] S. Cho, D. Marlow, and S. Niksa. Burning velocities of multicomponent organic fuel mixtures derived from various coals. *Combustion and Flame*, 101:399–410, 1995.

[26] H.-Y. Cai, A. Güell, I. Chatzakis, J.-Y. Lim, D. Dugwell, and R. Kandiyoti. Combustion reactivity and morphological change in coal chars: effect of pyrolysis temperature, heating rate and pressure. *Fuel*, 75:15–24, 1996.

[27] A. Harding, S. Brown, and K. Thomas. Release of NO from the combustion of coal chars. *Combustion and Flame*, 107:336–350, 1996.

[28] S. Pillet, R. Bussac, V. Landrault, T. Douetil, and P. Dagaut. Combustion study of coal and biomass in a drop tube furnace. In *Proceeding of the European Combustion Meeting*, 2003.

[29] C. Schönnenbeck. *Etude cinétique de la formation et réduction du monoxyde d'azote lors de la combustion du charbon à haute température*. PhD thesis, Université de Haute Alsace, 2003.

[30] S. Cho and S. Niksa. Elementary reaction models and correlations for burning velocities of multicomponent organic fuel mixtures. *Combustion and Flame*, 101:411–427, 1995.

[31] M. Serio, D. Hamblen, J. Markham, and P. Solomon. Kinetics of volatile product evolution in coal pyrolysis: Experiment and theory. *Energy and Fuel*, pages 138–152, 1987.

[32] M. Serio, W. Peters, and H. J.B. Kinetics of vapor-phase secondary reactions of prompt coal pyrolysis tars. *Industrial and Engineering Chemistry Research*, 26:1831–1838, 1987.

[33] E. Suuberg, W. Peter, and J. Howard. Product compositions and formation kinetics in rapid pyrolysis of pulverised coal - implications for combustions. In *17th International Symposium on Combustion*, pages 117–130. The Combustion Institute, 1978.

[34] H. Rüdiger, U. Greul, H. Spliethoff, and K. R. Hein. Distribution of fuel nitrogen in pyrolysis products used for reburning. *Fuel*, 76(3):201–205, 1997.

[35] F. Mermoud, S. Salvador, L. Van de Steene, and F. Golfier. Influence of the pyrolysis heating rate on the steam gasification rate of large wood char particles. *Fuel*, 85:1473–1482, 2006.

[36] J. Cances, J. Commandré, and S. Salvador. Interactions between NO and volatile matters released by a coal and a petcoke. In *Eigth International Conference on Energy for a Clean Environment – Clean Air 2005*, June 2005.

[37] J. Cances, J. Commandré, and S. Salvador. Interactions between NO and volatile matters released by a coal and a petcoke. *Clean Air: International Journal on Energy for a Clean Environment*, 2006. In Press.

[38] H. Kobayashi, J. Howard, and A. Sarofim. Coal devolatilisation at high temperatures. In *16th International Symposium on Combustion*, pages 441–495. The Combustion Institute, 1976.

[39] S. Ubhayakar, D. Stickler, C. Von Rosenberg, and R. Gannon. Rapid devolatilization of pulverized coal in hot combustion gases. In *16th International Symposium on Combustion*, pages 427–436. The Combustion Institute, 1976.

[40] S. Niksa. Predicting the devolatilisation behavior of any coal from its ultimate analysis. *Combustion and Flame*, 100:384–394, 1995.

[41] S. T. Perry and T. H. Fletcher. Modeling nitrogen evolution during coal pyrolysis based on a global free-radical mechanism. *Energy and Fuel*, 14:1094–1102, 2000.

[42] P. Dagaut. Formation et réduction des polluants en combustion. École de Combustion 2004, 9-15 mai 2004, Oléron, 2004 CNRS (LCD, UPR 9028) et Groupement Français de Combustion, CNRS, Laboratoire de Combustion et Systèmes réactifs, 1C, avenue de la recherche scientifique, 45071 Orléans cedex 2, mai 2004.

[43] C. Westbrook and F. Dryer. Simplified reaction mechanisms for the oxidation of hydrocarbon fuels in flames. *Combustion Science and Technology*, 27:31–43, 1981.

[44] G. De Soete. *Aspects fondamentaux de la combustion en phase gazeuse.* Editions Technip, 1976.

[45] R. Borghi and M. Destriau. *La combustion et les flammes.* Editions Technip, 1995.

[46] J. Warnatz, U. Maas, and R. Dibble. *Combustion.* Springer Ed., 1999.

[47] R. J. Kee, F. M. Rupley, and J. A. Miller. CHEMKIN II: a fortran chemical kinetics package for the analysis of the gas-phase chemical kinetics. Technical Report SAND89-8009, Sandia National Laboratories, 1989.

[48] R. J. Kee, F. M. Rupley, and J. A. Miller. The CHEMKIN thermodynamic data base. Technical Report SAND87-8215B, Sandia National Laboratories, 1990.

[49] P. Dagaut, F. Lecomte, S. Chevallier, and M. Cathonnet. Experimental and kinetic modeling of nitric oxide reduction by acetylene in an atmospheric pressure jet-stirred reactor. *Fuel*, 78:1245–1252, 1999.

[50] P. Dagaut, F. Lecomte, S. Chevallier, and M. Cathonnet. The reduction of NO by ethylene in a jet-stirred reactor at 1 atm : experimental and kinetic modelling. *Combustion and Flame*, 119:494–504, 1999.

[51] F. Lecomte, P. Dagaut, S. Chevallier, and M. Cathonnet. NO-reduction by ethane in a JSR at atmospheric pressure : experimental and kinetic modeling. *Combustion Science and Technology*, 150:181–203, 2000.

[52] P. Dagaut, J. Luche, and M. Cathonnet. Experimental and kinetic modeling of the reduction of NO by propene at 1 atm. *Combustion and Flame*, 121:651–661, 2000.

[53] P. Dagaut, J. Luche, and M. Cathonnet. Reduction of NO by propane in a JSR at 1 atm : experimental and kinetic modeling. *Fuel*, 80:979–986, 2001.

[54] P. Dagaut and F. Lecomte. Experimental and kinetic modeling study of the reduction of NO by hydrocarbons and interactions with SO_2 at 1 atm. *Fuel*, 82:1033–1040, 2003.

[55] M. U. Alzueta, P. Glarborg, and K. Dam-Johansen. Low temperature interactions between hydrocarbons and nitric oxide : an experimental study. *Combustion and Flame*, 109:25–36, 1997.

[56] J. Arthur. Reactions between carbon and oxygen. *Trans. Faraday Soc.*, 47:164–178, 1951.

[57] B. Peters. *Thermal conversion of solid fuels.* WIT Press, 2003.

[58] I. Iliuta, K. Dam-Johansen, and L. Jensen. Mathematical modeling of an in-line low NO_x calciner. *Chemical Engineering Science*, 57:805–820, 2002.

[59] I. Iliuta, K. Dam-Johansen, A. Jensen, and L. Jensen. Modeling of in-line low-NO_x calciners – a parametric study. *Chemical Engineering Science*, 57:789–803, 2002.

[60] I. W. Smith. The intrinsic reactivity of carbons to oxygen. *Fuel*, 57:409–414, 1978.

[61] I. Smith. The combustion rates of coal chars : a review. In *19th International Symposium on Combustion*, pages 1045–1065. The Combustion Institute, 1982.

[62] L. Tang, R. Gupta, C. Sheng, and T. Wall. The estimation of char reactivity from coal reflectogram. *Fuel*, 84:127–134, 2005.

[63] S. Salvador, J.-M. Commandré, B. Stanmore, and R. Gadiou. The catalytic effect of vanadium on the reactivity of petroleum cokes with NO. *Energy and Fuels*, 18:296–301, 2004.

[64] T. Ganga Devi and M. Kannan. Calcium catalysis in air gasification of cellulosic char. *Fuel*, 77:1825–1830, 98.

[65] B.-G. Ma, X.-G. Li, L. Xu, K. Wang, and X.-G. Wang. Investigation on catalyzed combustion of high ash coal by thermogravimetric analysis. *Thermochemica Acta*, 445:19–22, 2006.

[66] I. Aarna and E. M. Suuberg. Changes in reactive surface area and porosity during char oxidation. In *27th International Symposium on Combustion*, pages 2933–2939. The Combustion Institute, August 1998.

[67] J. Commandré, B. Stanmore, and S. Salvador. The high temperature reaction of carbon with nitric oxide. *Combustion and Flame*, 128:211–216, 2002.

[68] E. Thiele. Relation between catalytic activity and size of particle. *Industrial Engineering Chemistry*, 31:916–920, 1939.

[69] H. S. Fogler. *Element of chemical reaction engineering*, chapter 12 – Diffusion and reaction in porous catalysts, pages 738–808. Prentice Hall International Series in the Physical and Chemical Engineering Sciences, 3rd edition, 1999.

[70] F. Ramade. *Dictionnaire encyclopédique des pollutions*. Ediscience international, 2000.

[71] L. Smoot, S. Hill, and H. Xu. NO_x control through reburning. *Progress in Energy and Combustion Science*, 24:385–408, 1998.

[72] J. A. Miller and C. T. Bowman. Mechanism and modelling of nitrogen chemistry in combustion. *Progress in Energy and Combustion Science*, 15:287–338, 1989.

[73] S. Chaiklangmuang, J. Jones, M. Pourkashanian, and A. Williams. Conversion of volatile-nitrogen and char-nitrogen to NO during combustion. *Fuel*, 81:2363–2369, 2002.

[74] P. Glarborg, A. Jensen, and J. Johnsson. Fuel nitrogen conversion in solid fuel fired systems. *Progress in Energy and Combustion Science*, 29:89–113, 2003.

[75] J. Jones, P. Patterson, M. Pourkashanian, and A. Williams. Approches to modelling heterogeneous char NO formation/destruction during pulverised coal combustion. *Carbon*, 37:1545–1552, 1999.

[76] P. F. Nelson, C.-Z. Li, and E. Ledesma. Formation of HNCO from the rapid pyrolysis of coals. *Energy and Fuel*, 10:264–265, 1996.

[77] S. Hill and L. D. Smoot. Modeling of nitrogen oxides formation and destruction in combustion systems. *Progress in Energy and Combustion Science*, 26:417–458, 2000.

[78] S. Visona and B. R. Stanmore. Modeling NO_x release from a single coal particle – I. formation of NO from volatile nitrogen. *Combustion and Flame*, 105:92–103, 1996.

[79] V. Wargadalam, G. Löffler, F. Winter, and H. Hofbauer. Homogeneous formation of NO and N_2O from the oxidation of HCN and NH_3 at 600-1000°c. *Combustion and Flame*, 120:465–478, 2000.

[80] S. Visona and B. R. Stanmore. Modeling NO_x release from a single coal particle – II. formation of NO from char-nitrogen. *Combustion and Flame*, 106:207–218, 1996.

[81] A. pour la qualité de l'air. Techniques de réduction des emissions d'oxydes d'azote par modification des conditions de combustion. Technical report, Agence pour la qualité de l'air, Mars 1991.

[82] J. Beér. Combustion technology developments in power generation in response to environmental challenges. *Progress in Energy and Combustion Science*, 26:301–327, 2000.

[83] J. Wendt. Mechanisms governing the formation and destruction of NO_x and other nitrogenous species in low NO_x coal combustion systems. *Combustion Science and Technology*, 108:323–344, 1995.

[84] P. Dagaut. The kinetics of hydrocarbons-NO interactions in relation with reburning. *Trends in Physical Chemistry*, 7:25–46, 1999.

[85] F. Cadavid. *Simulation numérique de la réaction des émissions de NO_x dans un four pilote de 4 MW et une chaudière tangentielle de 609 MW à charbon pulvérisé.* PhD thesis, Université de Valencienne et du Hainaut Cambrésis, Décembre 2004.

[86] E. Hampartsoumian, O. Folayan, W. Nimmo, and B. Gibbs. Optimisation of NO_x reduction in advanced coal reburning systems and the effect of coal type. *Fuel*, 82:373–384, 2003.

[87] P. Dagaut, J. Luche, and M. Cathonnet. The kinetics of C_1 to C_4 hydrocarbons/NO interactions in relation with reburning. In *28th International Symposium on Combustion*, pages 2459–2465. The Combustion Institute, 2000.

[88] P. Glarborg, M. U. Alzueta, K. Dam-Johansen, and J. A. Miller. Kinetic modeling of hydrocarbon/nitric oxide interactions in a flow reactor. *Combustion and Flame*, 115:1–27, 1998.

[89] J. A. Miller, J. L. Durant, and P. Glarborg. Some chemical kinetics issues in reburning : the branching fraction of the HCCO + NO reaction. In *27th International Symposium on Combustion*, pages 235–243. The Combustion Institute, August 1998.

[90] I. Aarna and E. M. Suuberg. A review of the kinetics of the nitric oxyde-carbone reaction. *Fuel*, 76(6):475–491, 1997.

[91] E. Garijo, A. Jensen, and P. Glarborg. Reactivity of coal char in reducing NO. *Combustion and Flame*, 136:249–253, 2004.

[92] A. Molina, E. G. Eddings, D. W. Pershing, and A. F. Sarofim. Nitric oxide destruction during coal and char oxidation under pulverized-coal combustion conditions. *Combustion and Flame*, 136:303–312, 2004.

[93] H. Liu, E. Hampartsoumian, and B. M. Gibbs. Evaluation of the optimal fuel characteristics for efficient NO reduction by coal reburning. *Fuel*, 76, 1997.

[94] V. M. Zamansky, M. S. Sheldon, and P. M. Maly. Enhanced NO_x reduction by interaction of nitrogen and sodium compounds in the reburning zone. In *27th International Symposium on Combustion*, pages 3001–3008. The Combustion Institute, August 1998.

[95] Ø. Skreiberg, P. Kilpinen, and P. Glarborg. Ammonia chemistry below 1400 k under fuel-rich conditions in a flow reactor. *Combustion and Flame*, 136:501–518, 2004.

[96] J. Miller and P. Glarborg. Modeling the thermal De-NO_x process: Closing in on a final solution. *International Journal of Chemical Kinetics*, 31:757–765, 1999.

[97] P. Dagaut. On the kinetics of hydrocarbons oxidation from natural gas to kerosene and diesel fuel. *Physical Chemistry Chemical Physics*, 4:2079–2094, 2002.

[98] L. Prada and J. Miller. Reburning using several hydrocarbon fuels: a kinetic modeling study. *Combustion Science and Technology*, 132:225–250, 1998.

[99] M. U. Alzueta, R. Bilbao, and P. Glarborg. Inhibition and sensitization of fuel oxidation by SO_2. *Combustion and Flame*, 127:2234–2251, 2001.

[100] C. Schönnenbeck, R. Gadiou, and D. Schwartz. A kinetic study of the high temperature NO-char reaction. *Fuel*, 83:443–450, 2004.

[101] Y. Li, L. Radovic, G. Lu, and V. Rudolph. A new kinetic model for the NO-carbon reaction. *Chemical Engineering Science*, 54:4125–4136, 1999.

[102] R. Zevenhoven and M. Huppa. The reactivity of chars from coal, peat and wood towards NO, with and without CO. *Fuel*, 77:1169–1176, 1998.

[103] F. Guo and W. C. Hecker. Effects of CaO and burnout on the kinetics of NO reduction by beulah zap char. In *26th International Symposium on Combustion*, pages 2251–2257. The Combustion Institute, 1996.

[104] J.-M. Commandré and S. Salvador. Lack of correlation between the properties of a petroleum coke and its behaviour during combustion. *Fuel Processing Technology*, 86:795–808, 2005.

[105] J.-M. Commandré, S. Salvador, L. Van de Steene, and R. Gadiou. The formation and reduction of NO during the combustion of powdered petroleum coke – the case of cement plant precalciner conditions. *Combustion Science and Technology*, 177(3):579–611, 2005.

[106] A. Williams, M. Pourkashanian, and J. Jones. Combustion of pulverised coal and biomass. *Progress in Energy and Combustion Science*, 27:587–610, 2001.

[107] K. Radhakrishnan and A. C. Hindmarsh. Description and use of LSODE, the livermore solver for ordinary differential equations. Technical report, LLNL report UCRL-ID-113855, 1993.

[108] V. Gururajan, T. Wall, and J. Truelove. The combustion of evolved volatile matter in the vicinity of a coal particle – an evolution of the diffusion limited model. *Combustion and Flame*, 72:1–12, 1988.

[109] C. Dupont, G. Boissonnet, J.-M. Seiler, P. Gauthier, and D. Schweich. Study about the kinetic process of biomass steam gasification. *Fuel*, In press, 2006.

[110] P. Dagaut and A. Nicolle. Experimental and kinetic modeling study of the effect of SO_2 on the reduction of NO by ammonia. *Proc. Combust. Inst.*, 30:1211–1218, 2005.

[111] The university of Warwick. Flame ionisation. `http://www.eng.warwick.ac.uk/oel/courses/engine/ic005.htm`, consulted the 07.07.2006.

[112] G. Toupance, A. Person, Y. Le Moullec, P. Masclet, and P. E. Perros. Pollution atmosphérique gazeuse – mesure des gaz. In *Techniques de l'Ingénieur*.

[113] M. Dalibart and L. Servant. Spectroscopie dans l'infrarouge. In *Techniques de l'Ingénieur*, chapter Analyse et Caractérisation.

Appendix

Appendix A

Temperature measurements and corrections

Temperature measurements

The temperature profiles measurements in the EFR at 900°C were carried out with fine stripped K thermocouples (diameter 0.25 mm). The thermocouples were placed over a reactor diameter, as depicted in the temperature probe representation in Figure A.1.

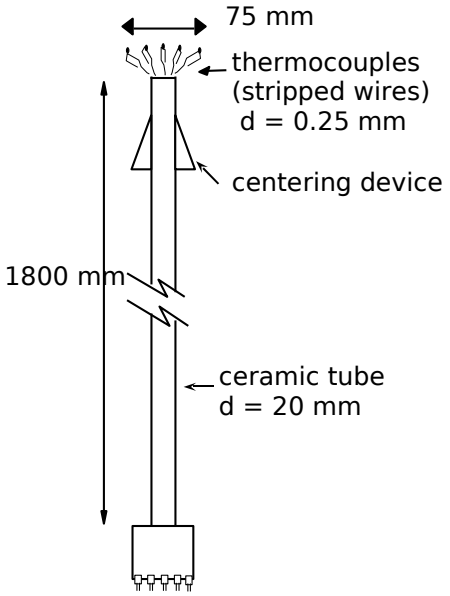

Figure A.1: Temperature probe.

Temperature correction

The experimental temperatures were then corrected to take radiation into account [24].

A thermal balance on the thermocouple allow the following Equation A.1 to be written:

$$F_{TC/ext}.\varepsilon.S_{TC}.\sigma_0.(T_{ext}^4-T_{TC}^4)+F_{TC/wall}.\varepsilon.S_{TC}.\sigma_0.(T_{wall}^4-T_{TC}^4) = h_{cv}.S_{TC}.(T_{TC}-T_{flow}) \quad \text{(A.1)}$$

with

$$F_{TC/ext} + F_{TC/wall} = 1 \quad \text{(A.2)}$$

and

$F_{TC/ext}$	:	Form factor between thermocouple and the exterior of the EFR
$F_{TC/wall}$	:	Form factor between thermocouple and the wall of the EFR
σ_0	:	Stefan-Boltzmann constant $= 5,67.10^{-8}$(W.m^{-2}.K^{-4})
T_{ext}	:	Temperature outside of the EFR (K)
T_{TC}	:	Thermocouple temperature (K)
T_{flow}	:	Flow temperature (K)
ε	:	Emissivity of the thermocouple weld
S_{TC}	:	Surface of the thermocouple weld (m^2)
h_{cv}	:	Convection heat transfer coefficient on the of the thermocouple weld (W.m^{-2}.K^{-1})

The form factor are calculated with the next expressions:

$$F_{TC/ext} \approx \frac{r^2}{z^2+r^2} \approx 0,039 \quad \text{(A.3)}$$

$$F_{TC/wall} \approx \frac{z^2}{z^2+r^2} \approx 0.961 \quad \text{(A.4)}$$

$$F_{TC/ext} \ll F_{TC/wall} \quad \text{(A.5)}$$

where z is the length of the temperature probe inside the reactor and r is the tube furnace radius. The radiation effect of the exterior of the EFR on the thermocouple is then neglected. This allow to write the flow temperature T_{flow} as follows:

$$T_{flow} = T_{TC} - \frac{\varepsilon}{h_{cv}}.\sigma_0.(T_{wall}^4 - T_{TC}^4) \quad \text{(A.6)}$$

Appendix B

Determination of the ratio $\beta = v_{gas}/\bar{U}$

Mean velocity

The parabolic velocity profile over a cross section of a cylinder – or the Entrained Flow Reactor – may be written as in Equation B.1:

$$u(r) = U_{max}.\left[1 - \left(\frac{r}{R}\right)^2\right] \tag{B.1}$$

where R is the internal tube radius, U_{max} the maximal velocity and $u(r)$ the velocity at the radius r.

The definition of the mean velocity yields:

$$\bar{U} = \frac{Q_{tot}}{A_{tube}} = \frac{1}{\pi R^2}.\int_0^R 2\pi r.u(r).dr \tag{B.2}$$

$$= \frac{1}{\pi R^2}.2\pi.U_{max}.\left[\frac{R^2}{2} - \frac{R^4}{4.R^2}\right] \tag{B.3}$$

$$= \frac{U_{max}}{2} \tag{B.4}$$

with $\bar{U}$ the mean velocity, Q_{tot} the total volumic flow and A_{tube} the tube cross-section area.

Sampled section

Sampled flow

The sampled flow, Q_{Samp}, sucked in the sampling probe may be written following different expressions.

It can be defined in relation to the total flow :

$$Q_{Samp} = \alpha Q_{tot} = \alpha.A_{tube}.\bar{U} \tag{B.5}$$

Or in relation to the radius of the sampled section, R_{Samp} :

$$Q_{Samp} = \int_0^{R_{Samp}} 2\pi r.u(r).dr = \pi.R_{Samp}^2.U_{max}.\left[1 - \frac{R_{Samp}^2}{2R^2}\right] \tag{B.6}$$

Mean velocity of the sampled gas

The mean velocity of the sampled flow is written as in Equation B.7:

$$v_{gas} = \overline{U_{Samp}} = \frac{Q_{Samp}}{A_{Samp}} = \frac{1}{\pi R_{Samp}^2}.\int_0^{R_{Samp}} 2\pi r.u(r).dr \tag{B.7}$$

$$= U_{max}.\left[1 - \frac{R_{Samp}^2}{2.R^2}\right] \tag{B.8}$$

Mathematical solution

The purpose is to express clearly the mean velocity of the sampled flow – $U_{Asp_{moy}}$ – in function of the mean velocity of the total flow mean:

$$\overline{U_{Samp}} = \beta.\bar{U} \tag{B.9}$$

Radius of the sampled section: R_{Samp}^2

The Equation B.6 my be re-written. One obtains the next polynome:

$$Q_{Samp} - \pi.U_{max}.R_{Samp}^2 + \frac{\pi.U_{max}}{2R^2}.R_{Samp}^4 = 0 \tag{B.10}$$

If $X = R_{Samp}^2$ and $a = \pi.U_{max}$, the expression above may be simplified in a conventional second order polynome:

$$X^2 - 2R^2.X + \frac{2R^2}{a}.Q_{Samp} = 0 \tag{B.11}$$

One may write $b = \frac{2R^2}{a}.Q_{Samp}$ to simplify the expression once again:

$$X^2 - 2R^2.X + b = 0 \tag{B.12}$$

Here, the determinant $\Delta = 4\left(R^4 - b\right)$ allow to obtain the solutions:

$$X_{1,2} = R_{Samp}^2 = \frac{2R^2 \pm 2\sqrt{R^4 - b}}{2} \tag{B.13}$$

$$= R^2.\left(1 \pm \sqrt{1 - \frac{b}{R^4}}\right) \tag{B.14}$$

The solution $R_{Samp}^2 = R^2.\left(1+\sqrt{1-\frac{b}{R^4}}\right)$ is not valid, because R_{Samp} could not be greater than R.

The Equation B.14 may be simplified as follows:

$$\begin{aligned}
\frac{b}{R^4} &= \frac{2R^2}{\pi.U_{max}}.\frac{Q_{Samp}}{R^4} && \text{(B.15)}\\
&= \frac{2}{U_{max}}.\frac{Q_{Samp}}{\pi.R^2} && \text{(B.16)}\\
&= \frac{1}{\bar{U}}.\frac{Q_{Samp}}{A_{tube}} && \text{(B.17)}\\
&= \frac{Q_{Samp}}{Q_{tot}} && \text{(B.18)}\\
&= \alpha && \text{(B.19)}
\end{aligned}$$

And finally:

$$R_{Samp}^2 = R^2.\left(1-\sqrt{1-\alpha}\right) \qquad \text{(B.20)}$$

Expression of β

The expression of β (cf. Equation B.9) may be written:

$$\begin{aligned}
\beta = \frac{\overline{U_{Samp}}}{\bar{U}} &= \frac{2}{U_{max}}.U_{max}.\left[1-\frac{R_{Samp}^2}{2.R^2}\right] && \text{(B.21)}\\
&= 2\left[1-\frac{R_{Samp}^2}{2.R^2}\right] && \text{(B.22)}\\
&= 2\left[1-\frac{1-\sqrt{1-\alpha}}{2}\right] && \text{(B.23)}\\
&= 2\left[\frac{1}{2}+\frac{1}{2}\sqrt{1-\alpha}\right] && \text{(B.24)}\\
&= 1+\sqrt{1-\alpha} && \text{(B.25)}
\end{aligned}$$

Numerical values

In all the experiments presented in this work, $\alpha = \frac{Q_{Samp}}{Q_{tot}} = \frac{2}{3}$ of the main flow is pumped through the sampling probe:

$$\beta = \frac{v_{gas}}{\bar{U}} = \frac{\overline{U_{Samp}}}{\bar{U}} = 1+\sqrt{1-\frac{2}{3}} = 1,577 \approx 1,6 \qquad \text{(B.26)}$$

Appendix C

The gas analyzers

C.1 The hydrocarbons analyzer

C.1.1 Principle of the measurement

The Flame Ionization Detector is used to measure concentrations of hydrocarbons within a sampled gas. The presence of hydrocarbons is detectable by burning the sampled gas in an air-hydrogen flame. Burning just pure hydrogen with air produces only trace amounts of ions. The presence of hydrocarbons in the sampled gas, when burnt in an air-hydrogen mix causes a level of ionization that is proportional to the number of carbon atoms within the sample.

An electrostatic field is set up around the burner; ions then flow to the collector and electrons flow to the burner. The flow of electrons and ions causes DC current to be produced between the burner jet and the collector, proportional to the ionization. The DC current is measured by an ammeter which is calibrated directly in number of hydrocarbons, the meter can be calibrated using samples of known hydrocarbons [111, 112].

Our FID analyzer allows also the Methane, and by difference the Non-Methane to be measured. Indeed, the COSMA Graphite 655 model has two burners. The first one is used for the THC; the second one is preceded by a catalyst that oxidizes the non CH_4 species into CO and CO_2. Thus only CH_4 remains when the gas reaches the second burner.

C.1.2 Calibration

The FID analyzer was calibrated each morning before starting the experiments. The detection range was set to 0–10000 ppm. The zero is calibrated by injecting pure air. The two burners are further calibrated with a CH_4 calibration gas at 4981 ppm.

The measurement precision is of 2 % of the read value, and the detection limit is evaluated to 10 ppm.

C.2 The O_2, CO, CO_2, SO_2 and NO analyzers

C.2.1 Principle of the measurement

Four cells with Non Dispersive InfraRed analyzers allow the CO, CO_2, SO_2 and NO to be quantified.

Before their injection in the analyzers, the combustion gases flow through a gas conditioner that traps H_2S and can convert NO_2 into NO (this allows to measure either NO or NO+NO_2). In our case we measure only NO. The combustion gases are also dried thanks to a Peltier thermoelement and a permeation membrane.

The gas quantification by InfraRed analyzers is based on the radiation absorption properties of gas. Indeed, in a gas sample with a thickness d, at the concentration C, the absorbance $\mathcal{A}$ follows the Bouguer-Beer-Lambert law :

$$\mathcal{A}(\lambda) = \log\left(\frac{I_0}{I_t}\right) = \epsilon(\lambda).C.d \tag{C.1}$$

where I_0 and I_t are respectively the incident and the transmitted radiation intensity, ε is the molar absorption coefficient (in $m^3.mol^{-1}.m^{-1}$). Thus, if ε and d are known, the absorbance varies proportionally to C.

In the NDIR system an incident IR radiation crosses a well known thickness of gas. A detector measures the radiation intensity at a defined wave length and provides the gas concentration [113].

The mole fraction of O_2 is determined with a paramagnetic detector. Here, the paramagnetic properties of O_2 are used: a magnetic field is modified proportionally to the O_2 concentration. A detector quantifies this concentration.

C.2.2 Calibration

The apparatus was calibrated every morning before starting experiments. The calibration is realized by injection of a calibration mixture of O_2, CO, CO_2 and SO_2. Another calibration gas is used for NO. The zero point is realized with a high purity N_2 calibration gas.

C.3 The quantification of various species with a FTIR

C.3.1 Principle of the measurement

The mole fraction of NO, NO_2, N_2O, NH_3, HCN, CO, CO_2, CH_4, C_2H_2, C_2H_4, C_2H_6, C_3H_8, C_6H_6 and SO_2 are quantified with the FTIR.

The Fourier Transform InfraRed (FTIR) analyzer uses also the gas IR absorption properties. Indeed, the $\varepsilon(\lambda)$ corresponds to vibration modes of the molecule, excited by the IR incident radiation. Thus, each molecule has its own vibration frequencies: this is the absorption spectra.

Here the detector covers the whole IR spectra (from 650 cm^{-1} to 4000 cm^{-1}) with a resolution of 0,5 cm^{-1}, and through a Fourier Transform allows to identify the different absorption wave lengths, and as a consequence, the different species present in the mixture. More detailed descriptions of the FTIR spectrometer principle are available in [14, 24, 113].

C.3.2 Calibration

The quantification of the different species is performed through a quantification method presented here. The different calibration gases are injected in the FTIR cell at known concentration. Each species is identified and quantified by its absorption at well defined wave lengths.

The FTIR spectrometer was calibrated for the present work for the 14 following gaseous species: NO, NO_2, N_2O, NH_3, HCN, CO, CO_2, CH_4, C_2H_2, C_2H_4, C_2H_6, C_3H_8, C_6H_6 and SO_2.

The software QUANTPAD from the OMNIC package allows the simultaneous quantification of the concentrations of a large number of species present in the mixture. Thus, we need the following data:

- the species to analyze (listed above),
- the spectral domain were species are quantified,
- the calibration spectra at different concentrations of each gas.

The quantification method uses a spectral analysis over regions divided into spectral windows and proceeds following two steps:

- the first qualitative step allows to detect the presence of the species by comparing with the calibration spectra,
- and the quantitative one enables to calculate the concentration present in the analyzed sample through the determination of the multiplication factor related to the concentration of the corresponding calibration gas.

Ideally, the spectral regions should be chosen were only one gas absorbs the IR radiations. It is generally possible to find such zones, but in case of hydrocarbons mainly, it is sometimes difficult to determine a spectral zone for only one gas.

The Table C.1 indicate the spectral zones where the each gas is determined and quantified. Note that methane is quantified in two different regions. This is a mean to verify the quality of the method.

Regions	Components in Regions														
Start – End	NO	NO_2	N_2O	NH_3	HCN	CO	CO_2	CH_4	CH_4-2	C_2H_2	C_2H_4	C_2H_6	C_3H_8	C_6H_6	SO_2
650 – 665	I	-	-	I	-	I	-	-	-	I	-	-	-	S	-
901 – 944	-	-	I	-	-	-	-	-	-	-	S	-	-	-	-
911 – 964.5	-	-	S	-	-	-	-	-	-	-	I	-	-	-	-
1145 – 1181	I	I	I	I	-	-	I	I	I	-	-	-	-	-	S
1585 – 1611.5	-	S	I	-	-	-	-	-	-	-	-	I	I	-	-
1893 – 1910	S	-	-	-	-	I	-	-	-	-	I	-	-	-	I
2080.5 – 2126	-	-	-	-	S	I	-	-	-	-	I	-	-	-	-
2177.5 – 2202.5	-	-	-	-	I	-	-	-	-	-	-	-	-	-	-
2840 – 2880	-	-	-	-	-	-	S	I	I	-	-	I	S	I	-
2888 – 2900	-	-	-	-	-	-	I	I	I	-	-	S	I	I	-
3027.5 – 3060	-	-	-	-	-	-	I	S	-	-	I	I	I	I	-
3083 – 3125	-	-	-	-	-	-	I	-	S	-	I	I	I	I	-
3230 – 3307	-	-	-	S	-	-	-	-	-	I	-	-	-	-	-
3260 – 3320	-	-	-	I	-	-	-	-	-	S	-	-	-	-	-
3621.5 – 3673.5	I	-	-	I	-	S	-	-	-	-	-	-	-	-	-

Table C.1: Quantification regions (Start and End in cm^{-1}; –: non used region for this gas, I: interaction region, without quantification and S: quantification region

The Bouguer-Beer-Lambert law (Equation C.1) indicates that absorbance $\mathcal{A}$ varies linearly with the gas concentration. This is not true when a large concentration domain is considered. Thus, calibration polynomials have to be determined for gases at different concentrations.

Four mass-flow meters allow to dilute the calibration gases with high purity N_2. The calibration gases were provided by Air Liquide, with precisions from 1 to 5 % of the indicated concentration.

Then, the creation of a quantification method begins with the collection of a large number of spectra of calibration gases at different concentrations.

The calibration curves for the 14 species are plotted in the next figures of this document. Note that the quantification of CO_2 was divided into two concentration domains in order to get the best fit for the calibration curves.

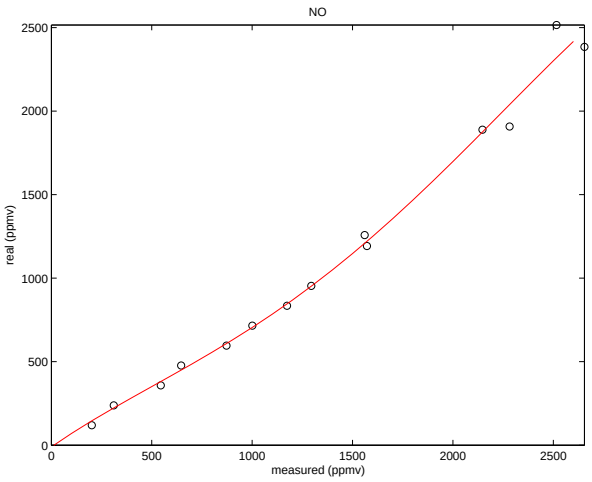

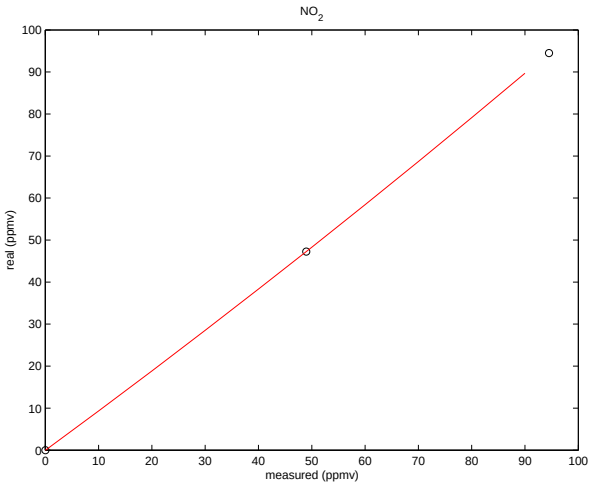

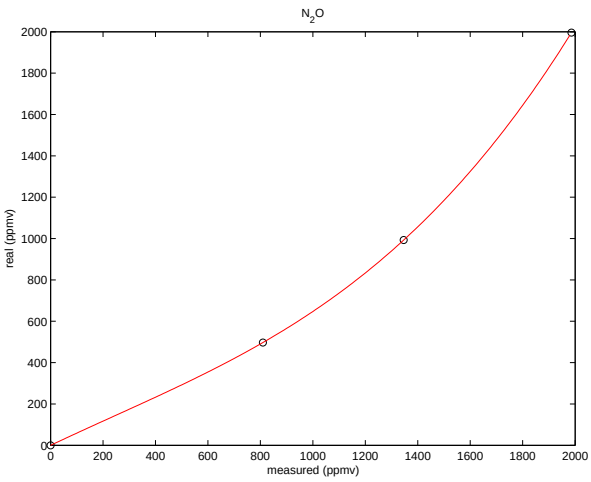

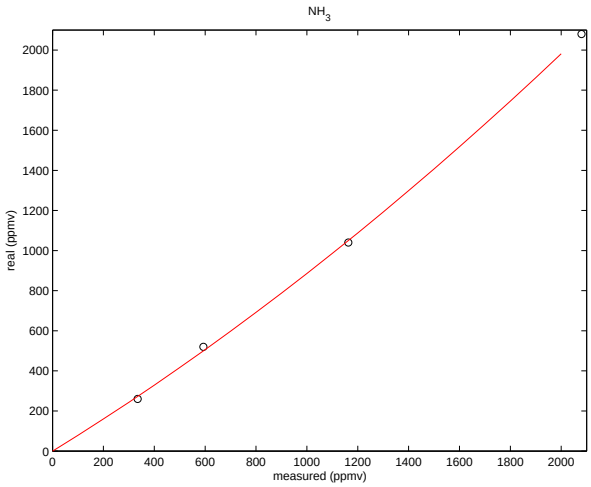

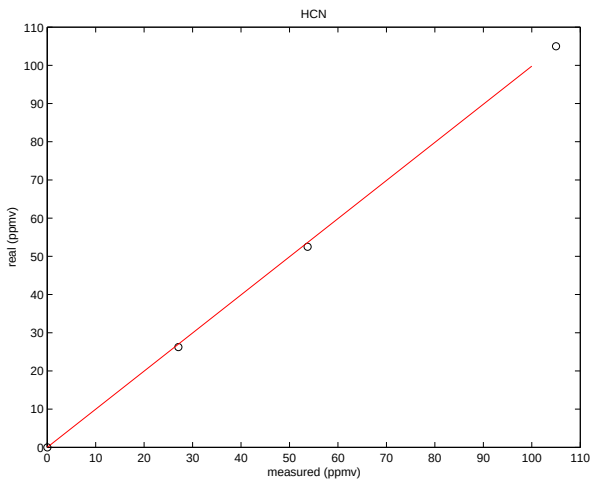
HCN
real (ppmv)
measured (ppmv)

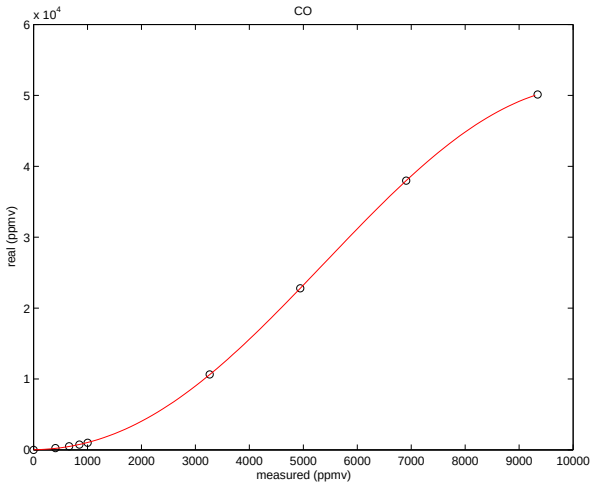
CO
x 10^4
real (ppmv)
measured (ppmv)

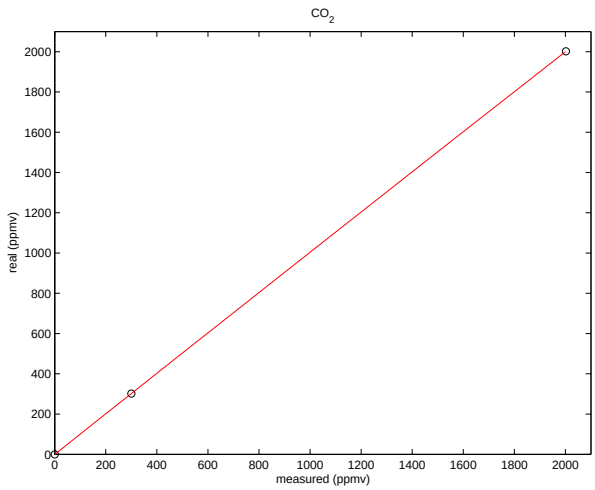
CO2
real (ppmv)
measured (ppmv)

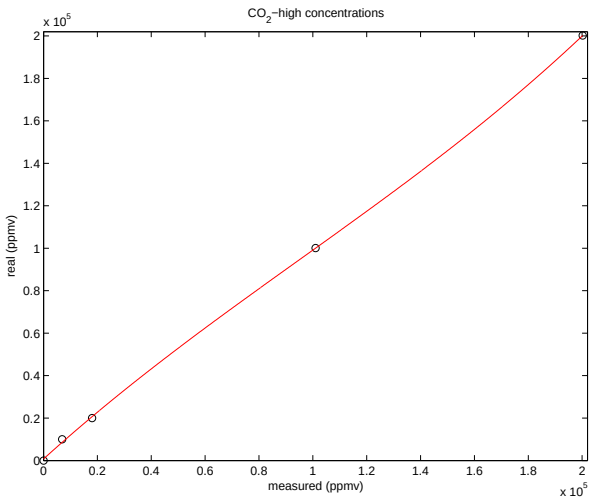
CO2−high concentrations
x 10^5
real (ppmv)
measured (ppmv)
x 10^5

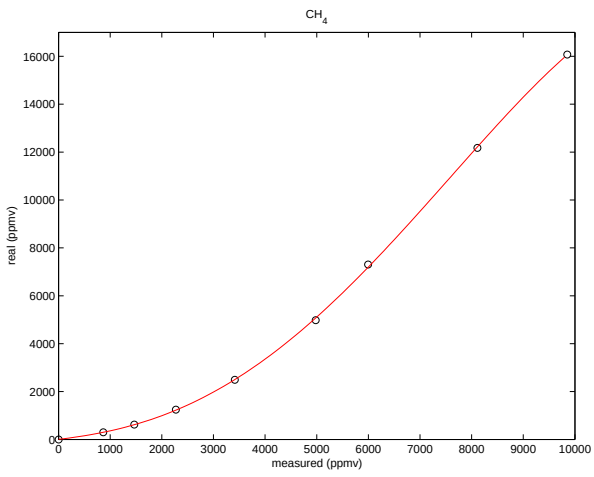
CH4
real (ppmv)
measured (ppmv)

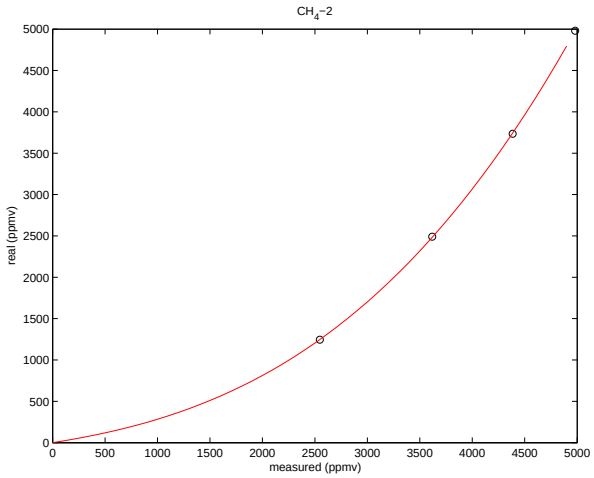
CH4−2
real (ppmv)
measured (ppmv)

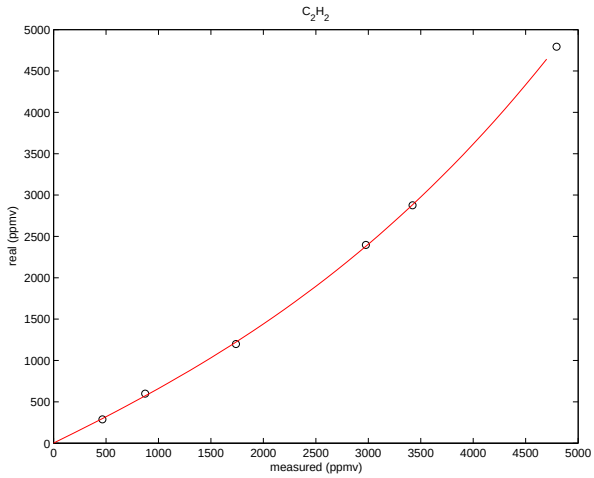
C_2H_2
real (ppmv)
measured (ppmv)
0
500
1000
1500
2000
2500
3000
3500
4000
4500
5000

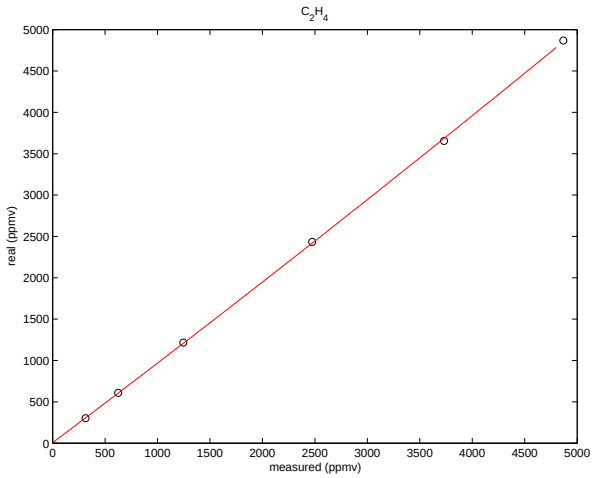
C_2H_4
real (ppmv)
measured (ppmv)
0
500
1000
1500
2000
2500
3000
3500
4000
4500
5000

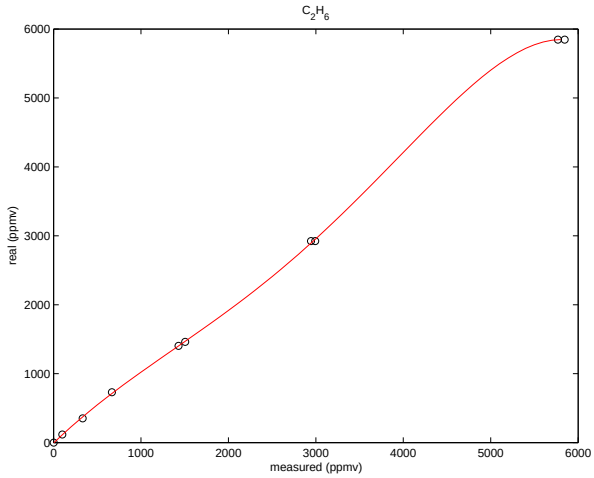
C_2H_6
real (ppmv)
measured (ppmv)
0
1000
2000
3000
4000
5000
6000

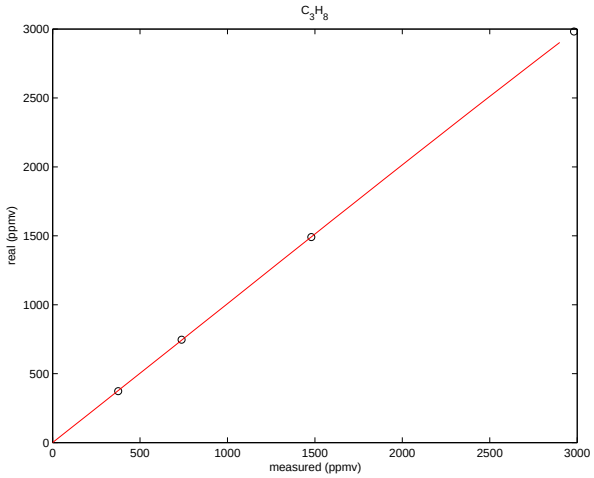
C_3H_8
real (ppmv)
measured (ppmv)
0
500
1000
1500
2000
2500
3000

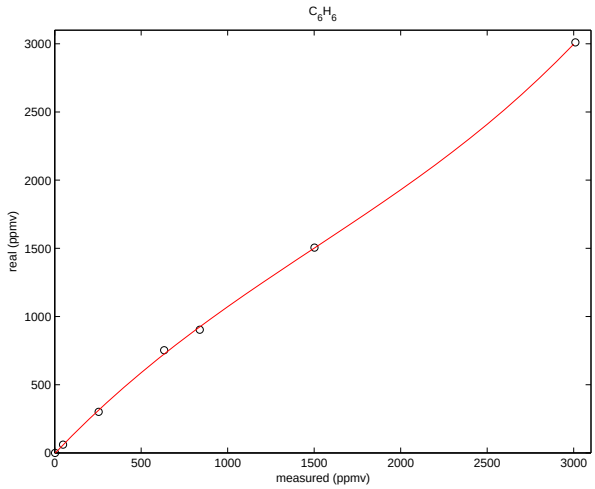
C_6H_6
real (ppmv)
measured (ppmv)
0
500
1000
1500
2000
2500
3000

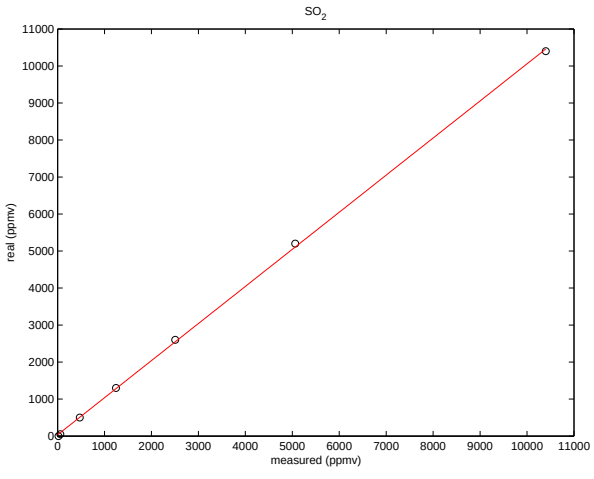
SO_2
real (ppmv)
measured (ppmv)
0
1000
2000
3000
4000
5000
6000
7000
8000
9000
10000
11000

C.4 The H_2 analyzer

C.4.1 Principle of the measurement

The H_2 measurement used a Thermal Conductivity Detector (TCD) – or katharometer. Indeed, the thermal conductivity of gas is inversely related to its molecular weight. For example, the hydrogen conductivity is approximately six times higher than that of nitrogen.

In the measuring cell, a metallic wire is heated by electric current. The surrounding gas cools the wire and after short time a temperature equilibrium is reached. The temperature of the metallic wire – which is measured by a Wheatstone measurement bridge – enables the determination of the gas conductivity.

C.4.2 Calibration

The calibration of the H_2 analyzer was performed every week. The zero point was set with a high purity nitrogen calibration gas, whereas the set value was calibrated with a 4 % of H_2 in N_2 calibration gas.

Appendix D

Detailed chemical mechanism

Detailed mechanism proposed by Dagaut et al [54].

Elements considered

Element Symbol	Molar mass [g/mol]
C	12.0112
H	1.00797
O	15.9994
N	14.0067
S	32.0640

Species considered

1. H
2. O
3. OH
4. O2
5. H2
6. H2O
7. HO2
8. H2O2
9. CO
10. CO2
11. HCO
12. CH2O
13. HCN
14. NO
15. HNCO
16. N2O
17. NH3
18. NO2
19. HNO
20. HONO
21. H2NO
22. N
23. H2CN
24. NNH
25. NH2
26. NH
27. N2H2
28. CN
29. NCO
30. C2N2
31. HOCN
32. HCNO
33. NCN
34. N2
35. SO2
36. SO3
37. SO
38. HSO
39. HOS
40. HOSO
41. HSO2
42. HOSO2
43. HOSOH
44. HOSHO
45. H2SO
46. HSOH
47. S
48. SH
49. H2S
50. S2
51. NH2SO2
52. NHSO2
53. CNSO2
54. CH4
55. C2H6
56. C2H4
57. C2H2
58. C3H3
59. C2H5
60. CH3O
61. CH3OH
62. CH2OH
63. C3H6
64. CH2CO
65. C2H3
66. CH3HCO
67. C2H4O2H
68. CH2HCO
69. C2H
70. CHOCHO
71. AC3H4
72. C2H3O
73. CH3CO
74. C4H4
75. C4H6
76. HCCOH
77. C2H2OH
78. AC3H5
79. SC3H5
80. IC4H3
81. C4H2
82. CHOCO
83. C2H4O
84. HCCO
85. CH2
86. CH3
87. SCH2
88. CH
89. PC3H4
90. C
91. C3H8
92. NC3H7
93. IC3H7
94. TC3H5
95. C3H6O
96. C3H5O
97. ACROL
98. C3H4O2H
99. C3H4O
100. C3H3O
101. C3H4OH
102. C3H2
103. NC4H3
104. NC4H5
105. IC4H5
106. H2C4O
107. C2H3CO
108. MEALL
109. C6H615
110. BUTYNE
111. C4H8
112. C2C4H8
113. T2C4H8
114. C6H6
115. NC4H10
116. PC4H9
117. SC4H9
118. CPD
119. HEX1245
120. CC6H6
121. FULVENE
122. C6H10
123. C6H7C
124. C6H9
125. C6H5
126. C6H5O
127. C5H5
128. C6H5OH
129. C5H5O13
130. C5H4OH
131. C5H4O
132. C4H
133. CH3O2
134. CH3O2H
135. CH3NO
136. CH3NO2
137. CH3ONO2
138. H2CNO2
139. CH3ONO
140. C2H5O2
141. C2H5O2H
142. C2H5O
143. NO3
144. O3
145. HONO2

Reactions considered

with $k = A.T^b.\exp\left(\frac{-E}{RT}\right)$

Units:

A in mole-cm-sec-K,

E in cal/mole.

#	Reaction	A	b	E
1.	S+H2=SH+H	1.40E+14	0.0	19300
2.	SH+O2=HSO+O	1.90E+13	0.0	17925
3.	S+O2=SO+O	5.20E+06	1.8	-1200
4.	SO3+O=SO2+O2	2.00E+12	0.0	20000
5.	SO3+SO=SO2+SO2	1.00E+12	0.0	10000
6.	SO+O(+M)=SO2(+M)	3.20E+13	0.0	0
	Low pressure limit:	1.20E+21	-1.5	0
	TROE centering:	5.50E-01	0.0	1.00E+30
	N2	Enh. by		1.50E+00
	SO2	Enh. by		1.00E+01
	H2O	Enh. by		1.00E+01
7.	SO2+O(+M)=SO3(+M)	9.20E+10	0.0	2384
	Low pressure limit:	4.00E+28	-4.0	5.25E+03
	N2	Enh. by		1.30E+00
	SO2	Enh. by		1.00E+01
	H2O	Enh. by		1.00E+01
8.	SO2+OH(+M)=HOSO2(+M)	7.20E+12	0.0	715
	Low pressure limit:	4.50E+25	-3.3	7.15E+02
	TROE centering:	7.00E-01	0.0	1.00E+30
	N2	Enh. by		1.50E+00
	SO2	Enh. by		1.00E+01
	H2O	Enh. by		1.00E+01
9.	SO+OH(+M)=HOSO(+M)	1.60E+12	0.5	-400
	Low pressure limit:	9.50E+27	-3.5	9.70E+02
	N2	Enh. by		1.50E+00
	SO2	Enh. by		1.00E+01
	H2O	Enh. by		1.00E+01
10.	SO+OH=SO2+H	1.10E+17	-1.4	0
11.	SO+O2=SO2+O	7.60E+03	2.4	2970
12.	HSO+H=SO+H2	1.00E+13	0.0	0
13.	HOSO(+M)=HSO2(+M)	1.00E+09	1.0	50000
	Low pressure limit:	1.70E+35	-5.6	5.54E+04
	TROE centering:	4.00E-01	0.0	1.00E+30
	N2	Enh. by		1.00E+00
	SO2	Enh. by		1.00E+01
	H2O	Enh. by		1.00E+01
14.	HOSO+H=SO2+H2	3.00E+13	0.0	0
15.	HSO2+H=SO2+H2	3.00E+13	0.0	0
16.	HSO2+OH=SO2+H2O	1.00E+13	0.0	0
17.	HSO2+O2=HO2+SO2	1.00E+13	0.0	0
18.	HSO2(+M)=H+SO2(+M)	2.00E+11	0.9	18360
	Low pressure limit:	3.50E+25	-3.3	1.91E+04
	N2	Enh. by		1.00E+00
	SO2	Enh. by		1.00E+01
	H2O	Enh. by		1.00E+01
19.	H2S+M=S+H2+M	2.00E+14	0.0	66000
20.	H2S+H=SH+H2	1.20E+07	2.1	700
21.	H2S+O=SH+OH	6.40E+07	1.8	2840
22.	H2S+OH=SH+H2O	2.70E+12	0.0	0
23.	H2S+S=SH+SH	4.00E+14	0.0	15100
24.	SH+O=H+SO	1.00E+14	0.0	0
25.	SH+OH=S+H2O	1.00E+13	0.0	0
26.	SH+HO2=HSO+OH	1.00E+12	0.0	0
27.	SH+S=S2+H	3.00E+12	0.0	0
28.	S+OH=H+SO	4.00E+13	0.0	0
29.	SO3+H=HOSO+O	2.50E+05	2.9	50278
				...

...

#	Reaction	A	b	E
30.	SO2+OH=HOSO+O	3.90E+08	1.9	75987
31.	SO2+OH=SO3+H	4.90E+02	2.7	23840
32.	SO2+CO=SO+CO2	2.70E+12	0.0	48300
33.	SO+M=S+O+M	4.00E+14	0.0	107000
34.	SO+H+M=HSO+M	5.00E+15	0.0	0
35.	SO+SO=SO2+S	2.00E+12	0.0	4000
36.	HSO+H=HSOH	2.50E+20	-3.1	919
37.	HSO+H=SH+OH	4.90E+19	-1.9	1560
38.	HSO+H=S+H2O	1.60E+09	1.4	-343
39.	HSO+H=H2SO	1.80E+17	-2.5	51
40.	HSO+H=H2S+O	1.10E+06	1.0	10358
41.	HSO+O+M=HSO2+M	1.13E+19	-1.7	-50
42.	HSO+O=H+SO2	4.52E+14	-0.4	0
43.	HSO+O+M=HOSO+M	6.93E+19	-1.6	1590
44.	HSO+O=O+HOS	4.78E+08	1.0	5340
45.	HSO+O=OH+SO	1.35E+13	0.1	300
46.	HSO+OH=HOSHO	5.20E+28	-5.4	3168
47.	HSO+OH=HOSO+H	5.30E+07	1.6	3750
48.	HSO+OH=SO+H2O	1.70E+09	1.0	474
49.	HSO+O2=SO2+OH	1.00E+12	0.0	10000
50.	HSOH=SH+OH	2.80E+39	-8.8	75248
51.	HSOH=S+H2O	5.80E+29	-5.6	54505
52.	HSOH=H2S+O	9.80E+16	-3.4	86502
53.	H2SO=H2S+O	4.90E+28	-6.7	71655
54.	HOSO+M=O+HOS+M	2.47E+30	-4.8	118560
55.	HOSO+H=SO+H2O	6.30E-10	6.3	-1884
56.	HOSO+OH=SO2+H2O	1.00E+12	0.0	0
57.	HOSO+O2=HO2+SO2	1.00E+12	0.0	1000
58.	H+SO2+M=HOSO+M	2.10E+31	-4.4	10810
	N2	Enh. by		1.00E+00
	SO2	Enh. by		1.00E+01
	H2O	Enh. by		1.00E+01
59.	HOSO2=HOSO+O	5.40E+18	-2.3	106345
60.	HOSO2=SO3+H	1.40E+18	-2.9	54919
61.	HOSO2+H=SO2+H2O	1.00E+12	0.0	0
62.	HOSO2+O=SO3+OH	5.00E+12	0.0	0
63.	HOSO2+OH=SO3+H2O	1.00E+12	0.0	0
64.	HOSO2+O2=HO2+SO3	7.80E+11	0.0	656
65.	HOSHO=HOSO+H	6.40E+30	-5.9	73806
66.	HOSHO=SO+H2O	1.20E+24	-3.6	59512
67.	HOSHO+H=HOSO+H2	1.00E+12	0.0	0
68.	HOSHO+O=HOSO+OH	5.00E+12	0.0	0
69.	HOSHO+OH=HOSO+H2O	1.00E+12	0.0	0
70.	SO+NO2=SO2+NO	8.40E+12	0.0	0
71.	SO2+NO2=NO+SO3	6.30E+12	0.0	27000
72.	HSO+NO2=HOSO+NO	5.80E+12	0.0	0
73.	SO2+NH2=>NH2SO2	1.50E+14	-1.3	0
74.	SO2+NH=>NHSO2	1.50E+14	-1.3	0
75.	CN+SO2=>CNSO2	2.65E+12	0.0	0
76.	N2+M=N+N+M	1.89E+18	-0.8	224950
	H2O	Enh. by		1.63E+01
	CO	Enh. by		1.88E+00
	CO2	Enh. by		3.75E+00
	CH4	Enh. by		1.63E+01
	C2H6	Enh. by		1.63E+01
77.	N+O+M=NO+M	7.60E+14	-0.1	-1770
	H2O	Enh. by		1.63E+01
	CO	Enh. by		1.88E+00
	CO2	Enh. by		3.75E+00
	CH4	Enh. by		1.63E+01
	C2H6	Enh. by		1.63E+01
78.	N2+O=N+NO	1.00E+14	0.0	75490
79.	N+NO2=N2O+O	1.80E+12	0.0	0
80.	N+O2=NO+O	6.40E+09	1.0	6280
				...

#	Reaction	A	b	E
81.	N+OH=NO+H	3.80E+13	0.0	0
82.	NH+O2=HNO+O	4.60E+05	2.0	6500
83.	NH+O2=NO+OH	1.30E+06	1.5	100
84.	NH+OH=HNO+H	2.00E+13	0.0	0
85.	NH+OH=N+H2O	5.00E+11	0.5	2000
86.	NH+OH=NO+H2	2.00E+13	0.0	0
87.	NH+H=N+H2	3.00E+13	0.0	0
88.	NH+O=NO+H	9.20E+13	0.0	0
89.	NH+N=N2+H	3.00E+13	0.0	0
90.	NH+NH=N2+H+H	2.54E+13	0.0	0
91.	NH+NO=N2O+H	4.30E+14	-0.5	0
92.	NH+NO=N2+OH	2.20E+13	-0.2	0
93.	NH+NO2=N2O+OH	1.00E+13	0.0	0
94.	NH2+O2=HNO+OH	4.50E+12	0.0	25000
95.	NH2+O=NH+OH	6.80E+12	0.0	0
96.	NH2+O=H2+NO	1.30E+08	1.0	-627
97.	NH2+O=HNO+H	6.60E+14	-0.5	0
98.	NH2+OH=NH+H2O	4.00E+06	2.0	1000
99.	NH2+H=NH+H2	4.00E+13	0.0	3650
100.	NH2+NO=NNH+OH	2.80E+13	-0.6	0
101.	NH2+NO=N2+H2O	5.00E+12	0.0	0
102.	NH2+NO=N2O+H2	3.90E+13	0.0	20160
103.	NH2+N=N2+H+H	7.20E+13	0.0	0
104.	NH2+NH=N2H2+H	5.00E+13	0.0	0
105.	NH2+NH2=N2H2+H2	8.50E+11	0.0	0
106.	NH2+NH2=NH3+NH	4.00E+13	0.0	10000
107.	NH2+HO2=H2NO+OH	5.00E+13	0.0	0
108.	NH2+HO2=NH3+O2	1.00E+13	0.0	0
109.	NH2+NO2=N2O+H2O	3.20E+18	-2.2	0
110.	NH3+M=NH+H2+M	6.31E+14	0.0	93400
	H2O	Enh. by		1.63E+01
	CO	Enh. by		1.88E+00
	CO2	Enh. by		3.75E+00
	CH4	Enh. by		1.63E+01
	C2H6	Enh. by		1.63E+01
111.	NH3+M=NH2+H+M	2.51E+16	0.0	93800
	H2O	Enh. by		1.63E+01
	CO	Enh. by		1.88E+00
	CO2	Enh. by		3.75E+00
	CH4	Enh. by		1.63E+01
	C2H6	Enh. by		1.63E+01
112.	NH3+OH=NH2+H2O	2.04E+06	2.0	566
113.	NH3+H=NH2+H2	6.36E+05	2.4	10171
114.	NH3+O=NH2+OH	9.40E+06	1.9	6460
115.	NH3+HO2=NH2+H2O2	3.00E+11	0.0	22000
116.	NNH+M=N2+H+M	2.00E+14	0.0	20000
	H2O	Enh. by		1.63E+01
	CO	Enh. by		1.88E+00
	CO2	Enh. by		3.75E+00
	CH4	Enh. by		1.63E+01
	C2H6	Enh. by		1.63E+01
117.	NNH+NO=N2+HNO	5.00E+13	0.0	0
118.	NNH+H=N2+H2	1.00E+14	0.0	0
119.	NNH+OH=N2+H2O	5.00E+13	0.0	0
120.	NNH+NH2=N2+NH3	5.00E+13	0.0	0
121.	NNH+NH=N2+NH2	5.00E+13	0.0	0
122.	NNH+O=N2O+H	1.00E+14	0.0	0
123.	HNO+O=NO+OH	1.00E+13	0.0	0
124.	HNO+OH=NO+H2O	3.60E+13	0.0	0
125.	HNO+H=NO+H2	4.40E+11	0.7	650
126.	HNO+NH2=NO+NH3	2.00E+13	0.0	1000
127.	HNO+N=NO+NH	1.00E+13	0.0	1990
128.	HNO+NO2=NO+HONO	6.00E+11	0.0	2000
129.	HNO+O2=NO+HO2	1.00E+13	0.0	25000
130.	HNO+HNO=N2O+H2O	3.95E+12	0.0	5000
131.	HNO+NO=N2O+OH	2.00E+12	0.0	26000
132.	N2H2+M=NNH+H+M	1.00E+17	0.0	50000
	H2O	Enh. by		1.63E+01
	CO	Enh. by		1.88E+00
	CO2	Enh. by		3.75E+00
	CH4	Enh. by		1.63E+01
	C2H6	Enh. by		1.63E+01
133.	N2H2+H=NNH+H2	5.00E+13	0.0	1000
134.	N2H2+O=NH2+NO	1.00E+13	0.0	1000
135.	N2H2+O=NNH+OH	2.00E+13	0.0	1000
136.	N2H2+OH=NNH+H2O	1.00E+13	0.0	1000
137.	N2H2+NO=N2O+NH2	3.00E+12	0.0	0
138.	N2H2+NH=NNH+NH2	1.00E+13	0.0	1000
139.	N2H2+NH2=NH3+NNH	1.00E+13	0.0	1000
140.	NO+HO2=NO2+OH	2.10E+12	0.0	-480
141.	NO+OH+M=HONO+M	5.10E+23	-2.5	-68
	H2O	Enh. by		5.00E+00
142.	NO+H+M=HNO+M	2.34E+18	-0.9	0
	H2O	Enh. by		1.63E+01
	CO	Enh. by		1.88E+00
	CO2	Enh. by		3.75E+00
	CH4	Enh. by		1.63E+01
	C2H6	Enh. by		1.63E+01
143.	NO+HCO=HNO+CO	7.20E+12	0.0	0
144.	NO2+H2=HONO+H	2.40E+13	0.0	29000
145.	NO2+H=NO+OH	1.00E+14	0.0	362
146.	NO2+O=NO+O2	1.00E+13	0.0	600
147.	NO2+M=NO+O+M	1.10E+16	0.0	66000
	H2O	Enh. by		1.63E+01
	CO	Enh. by		1.88E+00
	CO2	Enh. by		3.75E+00
	CH4	Enh. by		1.63E+01
	C2H6	Enh. by		1.63E+01
148.	NO2+NO2=NO+NO+O2	2.00E+12	0.0	26825
149.	NO2+HO2=HONO+O2	4.64E+11	0.0	-480
150.	NO2+HCO=CO+NO+OH	9.45E+12	0.0	-430
151.	NO2+HCO=H+CO2+NO	5.55E+12	0.0	-430
152.	NO2+CO=NO+CO2	2.19E+13	0.0	29200
153.	NO2+NO=N2O+O2	1.00E+12	0.0	60000
154.	N2O+OH=N2+HO2	2.00E+12	0.0	40000
155.	N2O+H=N2+OH	2.08E-06	5.6	1820
156.	N2O+M=N2+O+M	3.00E+14	0.0	55500
	H2O	Enh. by		1.63E+01
	CO	Enh. by		1.88E+00
	CO2	Enh. by		3.75E+00
	CH4	Enh. by		1.63E+01
	C2H6	Enh. by		1.63E+01
157.	N2O+O=N2+O2	1.40E+12	0.0	10800
158.	N2O+O=NO+NO	2.90E+13	0.0	23150
159.	N2O+N=N2+NO	1.00E+13	0.0	19870
160.	N2O+CO=N2+CO2	2.70E+11	0.0	20237
161.	C+NO=CN+O	6.60E+13	0.0	0
162.	CH+NO=HCN+O	1.10E+14	0.0	0
163.	SCH2+NO=HCN+OH	2.00E+13	0.0	0
164.	CH2+NO=HCNO+H	1.30E+12	0.0	-378
165.	CH2+NO=HCN+OH	2.20E+12	0.0	-378
166.	CH3+NO=HCN+H2O	1.50E-01	3.5	3950
167.	CH3+NO=H2CN+OH	1.50E-01	3.5	3950
168.	HCCO+NO=HCNO+CO	4.89E+12	0.1	-584
169.	HCCO+NO=HCN+CO2	1.64E+13	-0.3	-707
170.	HCNO+H=HCN+OH	5.70E+12	0.0	0
171.	HCNO+O=NO+HCO	7.00E+13	0.0	0
172.	HCNO+OH=NO+CH2O	2.00E+13	0.0	0

#	Reaction	A	b	E
173.	HOCN+OH=NCO+H2O	6.40E+05	2.0	2560
174.	HOCN+O=NCO+OH	1.50E+04	2.6	4000
175.	HOCN+H=HNCO+H	2.00E+07	2.0	2000
176.	HNCO+M=NH+CO+M	1.10E+16	0.0	86000
177.	HNCO+HO2=NCO+H2O2	3.00E+11	0.0	29000
178.	HNCO+O2=HNO+CO2	1.00E+12	0.0	35000
179.	HNCO+NH2=NH3+NCO	5.00E+12	0.0	6200
180.	HNCO+NH=NH2+NCO	3.00E+13	0.0	23700
181.	HNCO+H=NH2+CO	2.20E+07	1.7	3800
182.	HNCO+CN=NCO+HCN	2.50E+12	0.0	0
183.	HNCO+O=NCO+OH	2.20E+06	2.1	11430
184.	HNCO+O=CO2+NH	9.65E+07	1.4	8520
185.	HNCO+O=HNO+CO	1.50E+08	1.6	44012
186.	HNCO+OH=NCO+H2O	4.20E+05	2.0	2560
187.	HCN+OH=CN+H2O	3.20E+06	1.8	10300
188.	HCN+OH=HOCN+H	5.85E+04	2.4	12500
189.	HCN+OH=HNCO+H	4.00E-03	4.0	1000
190.	HCN+OH=NH2+CO	7.83E-04	4.0	4000
191.	HCN+O=NCO+H	1.38E+04	2.6	4980
192.	HCN+O=NH+CO	3.45E+03	2.6	4980
193.	HCN+O=CN+OH	2.70E+09	1.6	29200
194.	CN+OH=NH+CO	6.00E+12	0.0	0
195.	CN+OH=HNCO	6.00E+12	0.0	0
196.	CN+OH=NCO+H	6.00E+13	0.0	0
197.	CN+NO=NCO+N	9.64E+13	0.0	42100
198.	CN+NO=CO+N2	9.64E+13	0.0	42100
199.	CN+HNO=HCN+NO	1.80E+13	0.0	0
200.	CN+HONO=HCN+NO2	1.20E+13	0.0	0
201.	CN+H2=HCN+H	3.00E+05	2.5	2237
202.	CN+O=CO+N	7.70E+13	0.0	0
203.	CN+O2=NCO+O	7.50E+12	0.0	-389
204.	CN+N=C+N2	1.04E+15	-0.5	0
205.	CN+HCN=C2N2+H	1.50E+07	1.7	1530
206.	CN+NO2=NCO+NO	2.40E+13	0.0	-370
207.	CN+N2O=NCO+N2	1.00E+13	0.0	0
208.	CN+N2O=NCN+NO	3.80E+03	2.6	3700
209.	CN+CO2=NCO+CO	3.70E+06	2.2	26900
210.	CN+CH2O=HCN+HCO	4.22E+13	0.0	0
211.	C2N2+O=NCO+CN	4.57E+12	0.0	8880
212.	C2N2+OH=HOCN+CN	1.86E+11	0.0	2900
213.	NCO+H=NH+CO	5.00E+13	0.0	0
214.	NCO+CH2O=HNCO+HCO	6.02E+12	0.0	0
215.	NCO+HCO=HNCO+CO	3.62E+13	0.0	0
216.	NCO+NO=N2O+CO	5.23E+17	-1.7	763
217.	NCO+NO=CO2+N2	4.11E+17	-1.7	763
218.	NCO+NO2=CO+NO+NO	1.39E+13	0.0	0
219.	NCO+NO2=CO2+N2O	5.40E+12	0.0	0
220.	NCO+HNO=HNCO+NO	1.80E+13	0.0	0
221.	NCO+HONO=HNCO+NO2	3.60E+12	0.0	0
222.	NCO+N2O=N2+NO+CO	9.00E+13	0.0	27800
223.	NCO+NCO=N2+CO+CO	1.80E+13	0.0	0
224.	NCO+O=NO+CO	2.00E+13	0.0	0
225.	NCO+N=N2+CO	2.00E+13	0.0	0
226.	NCO+OH=HCO+NO	5.00E+12	0.0	15000
227.	NCO+M=N+CO+M	3.10E+16	-0.5	48000
	H2O	Enh. by		1.63E+01
	CO	Enh. by		1.88E+00
	CO2	Enh. by		3.75E+00
	CH4	Enh. by		1.63E+01
	C2H6	Enh. by		1.63E+01
228.	NCO+H2=HNCO+H	7.60E+02	3.0	4000
229.	NCO+O2=NO+CO2	2.00E+12	0.0	20000
230.	NCO+CN=NCN+CO	1.80E+13	0.0	0
231.	NCN+H=HCN+N	1.00E+14	0.0	0
232.	NCN+O=CN+NO	1.00E+14	0.0	0
233.	NCN+OH=HCN+NO	5.00E+13	0.0	0
234.	NCN+O2=NO+NCO	1.00E+13	0.0	0
235.	H2NO+O=NH2+O2	4.00E+13	0.0	0
236.	H2NO+M=HNO+H+M	2.50E+15	0.0	50000
	H2O	Enh. by		5.00E+00
	N2	Enh. by		2.00E+00
237.	H2NO+H=HNO+H2	3.00E+07	2.0	2000
238.	H2NO+H=NH2+OH	5.00E+13	0.0	0
239.	H2NO+O=HNO+OH	3.00E+07	2.0	2000
240.	H2NO+OH=HNO+H2O	2.00E+07	2.0	1000
241.	H2NO+NO=HNO+HNO	2.00E+07	2.0	13000
242.	H2NO+NH2=HNO+NH3	3.00E+12	0.0	1000
243.	HONO+O=NO2+OH	1.20E+13	0.0	6000
244.	HONO+OH=NO2+H2O	1.30E+10	1.0	135
245.	CH2+N2=HCN+NH	1.00E+13	0.0	74000
246.	CH+N2=HCN+N	3.00E+11	0.0	13600
247.	CH2+N=HCN+H	5.00E+13	0.0	0
248.	CH+N=CN+H	1.30E+13	0.0	0
249.	CO2+N=CO+NO	1.90E+11	0.0	3400
250.	CH3+N=H2CN+H	3.00E+13	0.0	0
251.	C2H3+N=HCN+CH2	2.00E+13	0.0	0
252.	C3H3+N=HCN+C2H2	1.00E+13	0.0	0
253.	H2CN+N=N2+CH2	2.00E+13	0.0	0
254.	H2CN+M=HCN+H+M	3.00E+14	0.0	22000
	H2O	Enh. by		1.63E+01
	CO	Enh. by		1.88E+00
	CO2	Enh. by		3.75E+00
	CH4	Enh. by		1.63E+01
	C2H6	Enh. by		1.63E+01
255.	CH2O+NO2=HCO+HONO	8.00E+02	2.8	13730
256.	HCO+HNO=CH2O+NO	6.00E+11	0.0	2000
257.	HONO+HONO=H2O+NO+NO2	3.49E-01	3.6	12140
258.	NCO+CH4=HNCO+CH3	1.00E+13	0.0	8126
259.	NCO+C2H6=HNCO+C2H5	1.45E-09	6.9	2916
260.	CH3O+HNO=CH3OH+NO	3.16E+13	0.0	0
261.	CH2HCO+NO2=CH2O+HCO+NO	8.90E+12	0.0	-159
262.	H+H+M=H2+M	7.31E+17	-1.0	0
	H2O	Enh. by		1.63E+01
	CO	Enh. by		1.88E+00
	CO2	Enh. by		3.75E+00
	CH4	Enh. by		1.63E+01
	C2H6	Enh. by		1.63E+01
263.	O+O+M=O2+M	1.14E+17	-1.0	0
	H2O	Enh. by		1.63E+01
	CO	Enh. by		1.88E+00
	CO2	Enh. by		3.75E+00
	CH4	Enh. by		1.63E+01
	C2H6	Enh. by		1.63E+01
264.	O+H+M=OH+M	6.20E+16	-0.6	0
	H2O	Enh. by		1.63E+01
	CO	Enh. by		1.88E+00
	CO2	Enh. by		3.75E+00
	CH4	Enh. by		1.63E+01
	C2H6	Enh. by		1.63E+01
265.	H2+O2=OH+OH	1.70E+13	0.0	47780
266.	O+H2=OH+H	1.10E+04	2.8	5922
267.	H+O2=OH+O	1.90E+14	0.0	16812
268.	H+O2+M=HO2+M	8.00E+17	-0.8	0
	H2O	Enh. by		1.63E+01
	CO	Enh. by		1.88E+00
	CO2	Enh. by		3.75E+00
	CH4	Enh. by		1.63E+01
	C2H6	Enh. by		1.63E+01

#	Reaction	A	b	E
269.	H+OH+M=H2O+M	8.62E+21	-2.0	0
	H2O	Enh. by		1.63E+01
	CO	Enh. by		1.88E+00
	CO2	Enh. by		3.75E+00
	CH4	Enh. by		1.63E+01
	C2H6	Enh. by		1.63E+01
270.	H2+OH=H2O+H	2.16E+08	1.5	3430
271.	H2O+O=OH+OH	1.50E+10	1.1	17260
272.	HO2+OH=H2O+O2	2.89E+13	0.0	-497
273.	HO2+O=OH+O2	1.81E+13	0.0	-400
274.	H+HO2=H2+O2	4.28E+13	0.0	1411
275.	H+HO2=OH+OH	1.69E+14	0.0	874
276.	H+HO2=H2O+O	3.01E+13	0.0	1721
277.	HO2+HO2=H2O2+O2	4.08E+02	3.3	1979
278.	OH+OH=H2O2	1.33E+16	-1.5	61
279.	H2O2+OH=HO2+H2O	5.80E+14	0.0	9557
280.	H2O2+H=HO2+H2	1.70E+12	0.0	3750
281.	H2O2+H=H2O+OH	1.00E+13	0.0	3590
282.	H2O2+O=HO2+OH	2.80E+13	0.0	6400
283.	CO+HO2=CO2+OH	1.50E+14	0.0	23650
284.	CO+OH=CO2+H	4.40E+06	1.5	-740
285.	CO+O+M=CO2+M	2.83E+13	0.0	-4540
	H2O	Enh. by		1.63E+01
	CO	Enh. by		1.88E+00
	CO2	Enh. by		3.75E+00
	CH4	Enh. by		1.63E+01
	C2H6	Enh. by		1.63E+01
286.	CO+O2=CO2+O	2.53E+12	0.0	47700
287.	HCO+M=H+CO+M	1.85E+17	-1.0	17000
	H2O	Enh. by		1.63E+01
	CO	Enh. by		1.88E+00
	CO2	Enh. by		3.75E+00
	CH4	Enh. by		1.63E+01
	C2H6	Enh. by		1.63E+01
288.	HCO+OH=CO+H2O	1.00E+14	0.0	0
289.	HCO+O=CO+OH	3.00E+13	0.0	0
290.	HCO+O=CO2+H	3.00E+13	0.0	0
291.	HCO+H=CO+H2	7.22E+13	0.0	0
292.	HCO+O2=CO+HO2	4.72E+12	0.0	250
293.	HCO+CH3=CO+CH4	1.20E+14	0.0	0
294.	HCO+HO2=CO2+OH+H	3.00E+13	0.0	0
295.	HCO+C2H6=CH2O+C2H5	4.70E+04	2.7	18235
296.	HCO+HCO=CH2O+CO	1.80E+13	0.0	0
297.	HCO+HCO=H2+CO+CO	3.00E+12	0.0	0
298.	CH4=CH3+H	2.13E+31	-5.3	104906
299.	CH4+HO2=CH3+H2O2	1.12E+13	0.0	24641
300.	CH4+OH=CH3+H2O	1.60E+06	2.1	2462
301.	CH4+O=CH3+OH	1.62E+06	2.3	7094
302.	CH4+H=CH3+H2	2.25E+04	3.0	8756.6
303.	CH4+CH2=CH3+CH3	4.30E+12	0.0	10038
304.	CH4+O2=CH3+HO2	4.04E+13	0.0	56913
305.	CH3+M=CH2+H+M	1.90E+16	0.0	91600
	H2O	Enh. by		1.63E+01
	CO	Enh. by		1.88E+00
	CO2	Enh. by		3.75E+00
	CH4	Enh. by		1.63E+01
	C2H6	Enh. by		1.63E+01
306.	CH3+M=CH+H2+M	6.90E+14	0.0	82460
	H2O	Enh. by		1.63E+01
	CO	Enh. by		1.88E+00
	CO2	Enh. by		3.75E+00
	CH4	Enh. by		1.63E+01
	C2H6	Enh. by		1.63E+01
307.	CH3+HO2=CH3O+OH	5.00E+12	0.0	0
308.	CH3OH=CH3+OH	1.56E+46	-9.3	103522
309.	CH3+OH=CH2O+H2	3.19E+12	-0.5	10810
310.	CH3+OH=CH2OH+H	2.64E+19	-1.8	8068
311.	CH3+OH=CH3O+H	5.74E+12	-0.2	13931
312.	CH3+OH=SCH2+H2O	8.90E+18	-1.8	8067
313.	CH3+O=CH2O+H	8.43E+13	0.0	0
314.	CH3+H=CH2+H2	7.00E+13	0.0	15100
315.	CH3+O2=CH3O+O	1.32E+14	0.0	31398
316.	CH3+O2=CH2O+OH	4.38E+11	0.0	14656
317.	CH3+CH3=C2H5+H	3.01E+13	0.0	13513
318.	CH3+CH3=C2H6	2.39E+38	-7.6	11359
319.	CH3+CH3O=CH4+CH2O	2.41E+13	0.0	0
320.	CH3+CH2OH=CH4+CH2O	2.41E+12	0.0	0
321.	CH2+OH=CH+H2O	1.13E+07	2.0	3000
322.	CH2+OH=CH2O+H	2.50E+13	0.0	0
323.	CH2+O=CO+H+H	5.00E+13	0.0	0
324.	CH2+O=CO+H2	6.00E+13	0.0	0
325.	CH2+H=CH+H2	1.00E+18	-1.6	0
326.	CH2+O2=HCO+OH	4.30E+10	0.0	-500
327.	CH2+O2=CO2+H2	3.45E+11	0.0	1000
328.	CH2+O2=CO2+H+H	1.60E+12	0.0	1000
329.	CH2+O2=CO+H2O	1.87E+10	0.0	-1000
330.	CH2+O2=CO+OH+H	8.64E+10	0.0	-500
331.	CH2+O2=CH2O+O	5.00E+13	0.0	9000
332.	CH2+CO2=CH2O+CO	1.10E+11	0.0	1000
333.	CH2+CH2=C2H2+H2	3.20E+13	0.0	0
334.	CH2+CH2=C2H2+H+H	4.00E+13	0.0	0
335.	CH2+CH3=C2H4+H	4.00E+13	0.0	0
336.	CH2+CH=C2H2+H	4.00E+13	0.0	0
337.	CH2+C2H2=H+C3H3	1.20E+13	0.0	6620
338.	CH2+C2H4=C3H6	4.30E+12	0.0	10038
339.	CH2+C2H6=CH3+C2H5	6.50E+12	0.0	7911
340.	SCH2+M=CH2+M	1.00E+13	0.0	0
	H2O	Enh. by		1.63E+01
	CO	Enh. by		1.88E+00
	CO2	Enh. by		3.75E+00
	CH4	Enh. by		1.63E+01
	C2H6	Enh. by		1.63E+01
341.	SCH2+O2=CO+OH+H	3.00E+13	0.0	0
342.	SCH2+H2=CH3+H	7.00E+13	0.0	0
343.	SCH2+H=CH2+H	2.00E+14	0.0	0
344.	SCH2+H=CH+H2	3.00E+13	0.0	0
345.	SCH2+O=CO+H+H	1.50E+13	0.0	0
346.	SCH2+O=CO+H2	1.50E+13	0.0	0
347.	SCH2+OH=CH2O+H	3.00E+13	0.0	0
348.	SCH2+HO2=CH2O+OH	3.00E+13	0.0	0
349.	SCH2+H2O2=CH3O+OH	3.00E+13	0.0	0
350.	SCH2+H2O=CH3OH	1.80E+13	0.0	0
351.	SCH2+CH2O=CH3+HCO	1.20E+12	0.0	0
352.	SCH2+HCO=CH3+CO	1.80E+13	0.0	0
353.	SCH2+CH3=C2H4+H	1.80E+13	0.0	0
354.	SCH2+CH4=CH3+CH3	4.00E+13	0.0	0
355.	SCH2+C2H6=CH3+C2H5	1.20E+14	0.0	0
356.	SCH2+C2H4=AC3H5+H	1.30E+14	0.0	0
357.	SCH2+C2H2=C3H3+H	1.80E+14	0.0	0
358.	SCH2+H2O=CH2+H2O	3.00E+13	0.0	0
359.	SCH2+CO2=CH2O+CO	3.00E+12	0.0	0
360.	SCH2+CH2CO=C2H4+CO	1.60E+14	0.0	0
361.	CH+OH=HCO+H	3.00E+13	0.0	0
362.	CH+O=CO+H	1.00E+14	0.0	0
363.	CH+O2=HCO+O	3.30E+13	0.0	0
364.	CH+O2=CO+OH	2.00E+13	0.0	0
365.	CH+CO2=HCO+CO	3.40E+12	0.0	690
366.	CH+CH4=C2H4+H	6.00E+13	0.0	0

#	Reaction	A	b	E
367.	CH+CH3=C2H3+H	3.00E+13	0.0	0
368.	CH3O+M=CH2O+H+M	4.88E+15	0.0	22773
	H2O	Enh. by		1.63E+01
	CO	Enh. by		1.88E+00
	CO2	Enh. by		3.75E+00
	CH4	Enh. by		1.63E+01
	C2H6	Enh. by		1.63E+01
369.	CH3O+HO2=CH2O+H2O2	3.00E+11	0.0	0
370.	CH3O+OH=CH2O+H2O	1.00E+13	0.0	0
371.	CH3O+O=CH2O+OH	1.30E+13	0.0	0
372.	CH3O+H=CH2O+H2	2.00E+13	0.0	0
373.	CH3O+O2=CH2O+HO2	2.35E+10	0.0	1788
374.	CH3O+CH2O=CH3OH+HCO	1.15E+11	0.0	1280
375.	CH3O+CO=CH3+CO2	1.57E+13	0.0	11804
376.	CH3O+HCO=CH3OH+CO	9.00E+13	0.0	0
377.	CH3O+C2H5=CH2O+C2H6	2.41E+13	0.0	0
378.	CH3O+C2H3=CH2O+C2H4	2.41E+13	0.0	0
379.	CH3O+C2H4=CH2O+C2H5	1.20E+11	0.0	7000
380.	CH2O+M=HCO+H+M	1.26E+16	0.0	77898
	H2O	Enh. by		1.63E+01
	CO	Enh. by		1.88E+00
	CO2	Enh. by		3.75E+00
	CH4	Enh. by		1.63E+01
	C2H6	Enh. by		1.63E+01
381.	CH2O+HO2=HCO+H2O2	4.00E+12	0.0	11665
382.	CH2O+OH=HCO+H2O	1.72E+09	1.2	-447
383.	CH2O+O=HCO+OH	1.81E+13	0.0	3088
384.	CH2O+H=HCO+H2	1.26E+08	1.6	2170
385.	CH2O+O2=HCO+HO2	2.04E+13	0.0	39000
386.	CH2O+CH3=HCO+CH4	4.09E+12	0.0	8843
387.	C2H6=C2H5+H	2.08E+38	-7.1	106507
388.	C2H6+HO2=C2H5+H2O2	1.21E+12	0.0	17600
389.	C2H6+OH=C2H5+H2O	5.11E+06	2.1	854
390.	C2H6+O=C2H5+OH	9.99E+08	1.5	5803
391.	C2H6+H=C2H5+H2	5.25E+14	0.0	12800
392.	C2H6+O2=C2H5+HO2	1.00E+13	0.0	51000
393.	C2H6+CH3O=C2H5+CH3OH	3.02E+11	0.0	7000
394.	C2H6+CH3=C2H5+CH4	7.54E+00	3.7	9883
395.	C2H5+HO2=C2H4+H2O2	3.00E+11	0.0	0
396.	C2H5+OH=C2H4+H2O	2.41E+13	0.0	0
397.	C2H5+OH=>CH3+CH2O+H	2.41E+13	0.0	0
398.	C2H5+O=CH2O+CH3	4.24E+13	0.0	0
399.	C2H5+O=CH3HCO+H	5.30E+13	0.0	0
400.	C2H5+O=C2H4+OH	3.05E+13	0.0	0
401.	C2H5=C2H4+H	4.59E+25	-4.2	40479
402.	C2H5+H=C2H4+H2	1.25E+14	0.0	8000
403.	C2H5+O2=C2H4+HO2	3.00E+20	-2.9	6761
404.	C2H5+O2=C2H4O2H	1.25E+40	-9.4	11030
405.	C2H5+O2=CH3HCO+OH	1.58E+14	-1.2	10390
406.	C2H5+CH3=C2H4+CH4	1.14E+12	0.0	0
407.	C2H5+C2H5=C2H4+C2H6	1.40E+12	0.0	0
408.	C2H4+M=C2H2+H2+M	3.00E+17	0.0	79350
	H2O	Enh. by		1.63E+01
	CO	Enh. by		1.88E+00
	CO2	Enh. by		3.75E+00
	CH4	Enh. by		1.63E+01
	C2H6	Enh. by		1.63E+01
409.	C2H4+M=C2H3+H+M	2.97E+17	0.0	96560
	H2O	Enh. by		1.63E+01
	CO	Enh. by		1.88E+00
	CO2	Enh. by		3.75E+00
	CH4	Enh. by		1.63E+01
	C2H6	Enh. by		1.63E+01
410.	C2H4+HO2=C2H4O2H	2.00E+11	0.0	8000
411.	C2H4+OH=C2H3+H2O	2.02E+13	0.0	5936
412.	C2H4+O=CH3+HCO	1.20E+08	1.4	530
413.	C2H4+O=CH2HCO+H	2.00E+08	1.4	530
414.	C2H4+H=C2H3+H2	3.36E-07	6.0	1692
415.	C2H4+O2=C2H3+HO2	4.00E+13	0.0	61500
416.	C2H4+C2H4=C2H5+C2H3	5.00E+14	0.0	64700
417.	C2H4+CH3=C2H3+CH4	4.15E+12	0.0	11128
418.	C2H3+HO2=>CH3+CO+OH	3.00E+13	0.0	0
419.	C2H3+OH=C2H2+H2O	3.00E+13	0.0	0
420.	C2H3+H=C2H2+H2	3.00E+13	0.0	0
421.	C2H3+O=CH3+CO	1.50E+13	0.0	0
422.	C2H3+O=CH2CO+H	1.50E+13	0.0	0
423.	C2H3+O2=CH2HCO+O	1.45E+15	-0.8	3135
424.	C2H3+O2=CH2O+HCO	1.85E+23	-3.3	3892
425.	C2H3+O2=CHOCHO+H	1.91E+18	-2.2	2398
426.	C2H3+O2=C2H2+HO2	5.20E+15	-1.3	3310
427.	C2H3+CH=CH2+C2H2	5.00E+13	0.0	0
428.	C2H3+CH2=AC3H4+H	3.00E+13	0.0	0
429.	C2H3+CH3=C2H2+CH4	3.91E+11	0.0	0
430.	C2H3+C2H6=C2H4+C2H5	1.50E+13	0.0	10000
431.	C2H3+C2H=C2H2+C2H2	9.64E+11	0.0	0
432.	C2H3+C2H2=C4H4+H	2.00E+12	0.0	5000
433.	C2H3+HCO=C2H4+CO	9.03E+13	0.0	0
434.	C2H3+CH2O=C2H4+HCO	5.42E+03	2.8	5862
435.	C2H3+C2H3=C2H2+C2H4	1.08E+13	0.0	0
436.	C2H3+C2H3=C4H6	5.00E+13	0.0	0
437.	C2H3+C2H4=C4H6+H	1.27E+12	0.0	7305
438.	C2H2+H(+M)=C2H3(+M)	2.34E+15	-0.9	3064
	Low pressure limit:	2.25E+40	-7.3	6.58E+03
	TROE centering:	5.00E-01	675.0	6.75E+02
	H2O	Enh. by		5.00E+00
	CO	Enh. by		2.00E+00
	CO2	Enh. by		3.00E+00
	H2	Enh. by		2.00E+00
439.	C2H2=C2H+H	2.37E+32	-5.3	130688
440.	C2H2+O2=HCCO+OH	2.00E+08	1.5	30100
441.	C2H2+O2=C2H+HO2	1.21E+13	0.0	74520
442.	C2H2+HO2=CH2CO+OH	6.09E+09	0.0	7948
443.	C2H2+OH=C2H+H2O	3.40E+07	2.0	14000
444.	C2H2+OH=CH3+CO	4.84E-04	4.0	-2000
445.	C2H2+OH=CH2CO+H	2.19E-04	4.5	-1000
446.	C2H2+OH=HCCOH+H	5.06E+05	2.3	13500
447.	C2H2+OH=C2H2OH	1.92E+22	-3.4	6596
448.	C2H2+O=CH2+CO	1.98E+04	2.6	656
449.	C2H2+O=HCCO+H	4.62E+04	2.6	656
450.	C2H2+CH3=C2H+CH4	1.80E+11	0.0	17290
451.	C2H2+CH3=PC3H4+H	4.78E+03	2.4	12893
452.	C2H2+CH3=AC3H5	1.40E+04	2.2	16502
453.	C2H2+CH3=SC3H5	3.85E+56	-13.7	27892
454.	C2H2+C2H2=IC4H3+H	6.31E+13	0.0	41600
455.	C2H2+C2H=C4H2+H	1.82E+14	0.0	467
456.	C2H+H2=C2H2+H	1.51E+13	0.0	3100
457.	C2H+OH=HCCO+H	2.00E+13	0.0	0
458.	C2H+O=CO+CH	1.00E+13	0.0	0
459.	C2H+O2=CO+HCO	2.41E+12	0.0	0
460.	CH2HCO=CH3+CO	1.17E+43	-9.8	43756
461.	CH2HCO=CH2CO+H	1.81E+43	-9.6	45868
462.	CH2HCO+O2=CH2CO+HO2	1.58E+10	0.0	0
463.	CH2HCO+O2=CH2O+CO+OH	2.51E+10	0.0	0
464.	CH2HCO+O2=OH+CHOCHO	2.76E+12	0.0	3000
465.	CH2HCO+O=CH2O+HCO	3.98E+13	0.0	0
466.	CH2HCO+OH=CH2CO+H2O	2.00E+13	0.0	0
467.	CH2HCO+HO2=CH2O+HCO+OH	1.10E+13	0.0	0
468.	CHOCHO=CH2O+CO	1.18E+16	-1.3	50937

#	Reaction	A	b	E
469.	CHOCHO=CO+CO+H2	6.52E+39	-7.7	67469
470.	CHOCHO+OH=CHOCO+H2O	1.00E+13	0.0	0
471.	CHOCHO+O=CHOCO+OH	7.24E+12	0.0	1970
472.	CHOCHO+H=CH2O+HCO	1.00E+12	0.0	0
473.	CHOCHO+HO2=CHOCO+H2O2	1.70E+12	0.0	10700
474.	CHOCHO+CH3=CHOCO+CH4	1.74E+12	0.0	8440
475.	CHOCHO+O2=HCO+CO+HO2	6.30E+13	0.0	30000
476.	CHOCO=HCO+CO	2.00E+07	0.0	0
477.	CHOCO+O2=CO+CO+HO2	6.30E+13	0.0	30000
478.	C2H4O2H=C2H4O+OH	3.16E+11	0.0	19500
479.	C2H4O=CH4+CO	1.21E+13	0.0	57200
480.	C2H4O=CH3HCO	6.00E+13	0.0	57200
481.	C2H4O=CH3+HCO	4.90E+13	0.0	57200
482.	C2H4O+O2=C2H3O+HO2	4.00E+13	0.0	61500
483.	C2H4O+H=C2H3O+H2	2.00E+13	0.0	8300
484.	C2H4O+H=C2H3+H2O	5.00E+09	0.0	5000
485.	C2H4O+H=C2H4+OH	9.51E+10	0.0	5000
486.	C2H4O+O=C2H3O+OH	1.91E+12	0.0	5250
487.	C2H4O+OH=C2H3O+H2O	4.79E+13	0.0	5955
488.	C2H4O+HO2=C2H3O+H2O2	4.00E+12	0.0	17000
489.	C2H4O+CH3=CH4+C2H3O	1.07E+12	0.0	11830
490.	C2H3O=CH2CO+H	1.60E+13	0.0	35000
491.	C2H3O=CH3CO	8.51E+14	0.0	14000
492.	C2H2OH=CH2CO+H	5.00E+15	0.0	28000
493.	C2H2OH+H=CH2CO+H2	2.00E+13	0.0	4000
494.	C2H2OH+O=CH2CO+OH	2.00E+13	0.0	4000
495.	C2H2OH+OH=CH2CO+H2O	1.00E+13	0.0	2000
496.	C2H2OH+O2=>HCO+CO2+H2	4.00E+12	0.0	-250
497.	HCCOH+H=CH2CO+H	1.00E+13	0.0	0
498.	CH2CO+M=CH2+CO+M	3.60E+15	0.0	59270
	H2O	Enh. by		1.63E+01
	CO	Enh. by		1.88E+00
	CO2	Enh. by		3.75E+00
	CH4	Enh. by		1.63E+01
	C2H6	Enh. by		1.63E+01
499.	CH2CO+O2=CH2O+CO2	2.00E+13	0.0	61500
500.	CH2CO+HO2=>CH2O+CO+OH	6.00E+11	0.0	12738
501.	CH2CO+O=CH2+CO2	1.76E+12	0.0	1349
502.	CH2CO+O=HCCO+OH	1.00E+13	0.0	8000
503.	CH2CO+OH=CH2OH+CO	6.93E+12	0.0	0
504.	CH2CO+OH=HCO+CH2O	2.04E+11	0.0	0
505.	CH2CO+OH=HCCO+H2O	1.02E+11	0.0	0
506.	CH2CO+OH=CH3+CO2	3.10E+12	0.0	0
507.	CH2CO+H=CH3+CO	1.50E+04	2.8	673
508.	CH2CO+H=HCCO+H2	1.80E+14	0.0	8600
509.	CH2CO+CH3=C2H5+CO	6.00E+10	0.0	0
510.	CH2CO+CH3=HCCO+CH4	7.50E+12	0.0	13000
511.	CH2CO+CH2=HCCO+CH3	1.00E+12	0.0	0
512.	CH2CO+CH2=C2H4+CO	3.60E+13	0.0	11000
513.	HCCO+M=CH+CO+M	6.00E+15	0.0	58821
	H2O	Enh. by		1.63E+01
	CO	Enh. by		1.88E+00
	CO2	Enh. by		3.75E+00
	CH4	Enh. by		1.63E+01
	C2H6	Enh. by		1.63E+01
514.	HCCO+OH=HCO+CO+H	1.00E+13	0.0	0
515.	HCCO+O=CO+CO+H	1.93E+14	0.0	590
516.	HCCO+H=SCH2+CO	1.50E+14	0.0	0
517.	HCCO+O2=CO+CO+OH	1.40E+09	1.0	0
518.	HCCO+CH2=C2H+CH2O	1.00E+13	0.0	2000
519.	HCCO+CH2=C2H3+CO	3.00E+13	0.0	0
520.	HCCO+C2H2=C3H3+CO	1.00E+11	0.0	3000
521.	HCCO+CH=C2H2+CO	5.00E+13	0.0	0
522.	HCCO+HCCO=C2H2+CO+CO	1.00E+13	0.0	0
523.	CH3OH+HO2=CH2OH+H2O2	6.30E+12	0.0	19360
524.	CH3OH+OH=CH2OH+H2O	4.53E+11	0.3	1160
525.	CH3OH+OH=CH3O+H2O	3.63E+11	0.7	5868
526.	CH3OH+O=CH2OH+OH	1.63E+13	0.0	5030
527.	CH3OH+H=CH2OH+H2	4.00E+13	0.0	6100
528.	CH3OH+CH2O=CH3O+CH3O	1.55E+12	0.0	79570
529.	CH3OH+CH3=CH2OH+CH4	3.57E+11	0.0	8663
530.	CH3OH+CH3=CH3O+CH4	4.68E+05	2.3	12764
531.	CH2OH+M=CH2O+H+M	1.00E+14	0.0	25100
	H2O	Enh. by		1.63E+01
	CO	Enh. by		1.88E+00
	CO2	Enh. by		3.75E+00
	CH4	Enh. by		1.63E+01
	C2H6	Enh. by		1.63E+01
532.	CH2OH+H=CH2O+H2	3.00E+13	0.0	0
533.	CH2OH+O2=CH2O+HO2	2.17E+14	0.0	4690
534.	CH3HCO=CH3+HCO	2.45E+16	0.0	84128
535.	CH3HCO+HO2=CH3CO+H2O2	1.70E+12	0.0	10700
536.	CH3HCO+OH=CH3CO+H2O	2.35E+10	0.7	-1113
537.	CH3HCO+O=CH3CO+OH	5.85E+12	0.0	1808
538.	CH3HCO+H=CH3CO+H2	4.10E+09	1.2	2405
539.	CH3HCO+O2=CH3CO+HO2	2.00E+13	0.5	42200
540.	CH3HCO+CH3=CH3CO+CH4	1.70E+12	0.0	8440
541.	CH3HCO+HCO=CH3CO+CH2O	7.80E+13	0.0	8440
542.	CH3CO+M=CH3+CO+M	8.64E+15	0.0	14400
	H2O	Enh. by		1.63E+01
	CO	Enh. by		1.88E+00
	CO2	Enh. by		3.75E+00
	CH4	Enh. by		1.63E+01
	C2H6	Enh. by		1.63E+01
543.	NC3H7=C3H6+H	3.00E+29	-5.2	39758
544.	NC3H7=C2H4+CH3	3.74E+29	-5.3	35022
545.	NC3H7+O2=C3H6+HO2	1.00E+12	0.0	5020
546.	IC3H7=C2H4+CH3	2.50E+13	0.0	41000
547.	IC3H7+O2=C3H6+HO2	2.75E+10	0.0	-2151
548.	IC3H7+C2H2=C4H6+CH3	2.77E+10	0.0	6504
549.	IC3H7+H=C2H5+CH3	5.00E+13	0.0	0
550.	NC3H7+H=C2H5+CH3	1.00E+14	0.0	0
551.	C3H6=AC3H5+H	1.06E+47	-9.3	104551
552.	C3H6=SC3H5+H	7.59E+14	0.0	101300
553.	C3H6=TC3H5+H	1.45E+15	0.0	98060
554.	C3H6=C2H3+CH3	1.10E+21	-1.2	97720
555.	C3H6+O2=AC3H5+HO2	1.95E+12	0.0	39000
556.	C3H6+O2=SC3H5+HO2	1.40E+13	0.0	60200
557.	C3H6+O2=TC3H5+HO2	7.00E+12	0.0	60200
558.	C3H6+HO2=C3H6O+OH	1.02E+12	0.0	14964
559.	C3H6+HO2=AC3H5+H2O2	1.50E+11	0.0	14190
560.	C3H6+HO2=SC3H5+H2O2	7.50E+09	0.0	12570
561.	C3H6+HO2=TC3H5+H2O2	3.00E+09	0.0	9930
562.	C3H6+OH=AC3H5+H2O	7.70E+05	2.2	622
563.	C3H6+OH=SC3H5+H2O	1.01E+13	0.0	5960
564.	C3H6+OH=TC3H5+H2O	1.11E+06	2.0	1450
565.	C3H6+O=C2H4+CH2O	7.02E+07	1.6	-628
566.	C3H6+O=CH3+CH2HCO	3.90E+07	1.6	-628
567.	C3H6+O=C2H5+HCO	4.69E+07	1.6	-628
568.	C3H6+O=AC3H5+OH	1.75E+11	0.7	5884
569.	C3H6+O=SC3H5+OH	1.20E+11	0.7	8960
570.	C3H6+O=TC3H5+OH	6.00E+10	0.7	7633
571.	C3H6+H=IC3H7	5.70E+09	1.2	874
572.	C3H6+H=C2H4+CH3	7.23E+12	0.0	1302
573.	C3H6+H=AC3H5+H2	1.73E+05	2.5	2492
574.	C3H6+H=SC3H5+H2	3.46E+14	0.0	17422
575.	C3H6+H=TC3H5+H2	1.67E+14	0.0	14818
576.	C3H6+CH3=AC3H5+CH4	1.60E+11	0.0	8800

#	Reaction	A	b	E
577.	C3H6+CH3=SC3H5+CH4	3.30E+11	0.0	10110
578.	C3H6+CH3=TC3H5+CH4	5.00E+10	0.0	8030
579.	C3H6+C2H5=AC3H5+C2H6	1.00E+11	0.0	9800
580.	C3H6+C2H3=C4H6+CH3	7.20E+11	0.0	5008
581.	C3H6+C2H3=AC3H5+C2H4	2.21E+00	3.5	4682
582.	C3H6+C2H3=SC3H5+C2H4	2.21E+00	3.5	4682
583.	C3H6+C2H3=TC3H5+C2H4	2.21E+00	3.5	4682
584.	C3H6O=>C2H5+HCO	1.26E+14	0.0	58000
585.	AC3H5+O2=ACROL+OH	1.82E+13	-0.4	22859
586.	AC3H5+O2=AC3H4+HO2	5.00E+15	-1.4	22428
587.	AC3H5+O2=CH2HCO+CH2O	1.06E+10	0.3	12838
588.	AC3H5+O2=C2H2+CH2O+OH	2.78E+25	-4.8	15468
589.	AC3H5+HO2=C3H5O+OH	7.50E+11	0.0	0
590.	C3H5O=ACROL+H	1.00E+14	0.0	19000
591.	AC3H5+H=AC3H4+H2	6.03E+12	0.0	0
592.	AC3H5+O=ACROL+H	6.03E+13	0.0	0
593.	AC3H5+CH3=AC3H4+CH4	1.00E+11	0.0	0
594.	AC3H5+HCO=C3H6+CO	6.00E+13	0.0	0
595.	AC3H5+CH2=C4H6+H	3.00E+13	0.0	0
596.	AC3H5+C2H5=AC3H4+C2H6	4.00E+11	0.0	0
597.	AC3H5+C2H3=AC3H4+C2H4	1.00E+12	0.0	0
598.	SC3H5=PC3H4+H	5.62E+12	0.0	43500
599.	SC3H5+O2=CH3HCO+HCO	4.34E+12	0.0	0
600.	SC3H5+HO2=>			
	CH2CO+CH3+OH	4.50E+12	0.0	0
601.	SC3H5+H=AC3H4+H2	3.33E+12	0.0	0
602.	SC3H5+H=PC3H4+H2	4.00E+13	0.0	0
603.	SC3H5+OH=PC3H4+H2O	2.00E+13	0.0	0
604.	SC3H5+O=CH2CO+CH3	1.81E+14	0.0	0
605.	SC3H5+CH3=AC3H4+CH4	1.00E+11	0.0	0
606.	SC3H5+C2H5=AC3H4+C2H6	1.00E+11	0.0	0
607.	SC3H5+C2H3=AC3H4+C2H4	1.00E+11	0.0	0
608.	TC3H5=AC3H5	2.00E+13	0.0	47000
609.	TC3H5+O2=CH3CO+CH2O	5.01E+12	0.0	19000
610.	TC3H5+O=>CH2CO+CH3	1.81E+14	0.0	0
611.	TC3H5+H=PC3H4+H2	1.00E+13	0.0	0
612.	TC3H5+CH3=PC3H4+CH4	1.00E+11	0.0	0
613.	TC3H5+C2H5=PC3H4+C2H6	1.00E+11	0.0	0
614.	TC3H5+C2H3=PC3H4+C2H4	1.00E+11	0.0	0
615.	TC3H5+HO2=>			
	CH2CO+CH3+OH	4.50E+12	0.0	0
616.	TC3H5+CH2=C4H6+H	3.00E+13	0.0	0
617.	AC3H4+M=C3H3+H+M	2.00E+18	0.0	80000
	H2O	Enh. by		1.63E+01
	CO	Enh. by		1.88E+00
	CO2	Enh. by		3.75E+00
	CH4	Enh. by		1.63E+01
	C2H6	Enh. by		1.63E+01
618.	AC3H4=PC3H4	1.20E+15	0.0	92400
	Declared duplicate reaction...			
619.	AC3H4=PC3H4	6.53E+68	-16.3	94518
	Declared duplicate reaction			
620.	AC3H4+O2=C3H3+HO2	4.00E+13	0.0	61500
621.	AC3H4+OH=C3H3+H2O	3.62E+12	0.0	4170
622.	AC3H4+OH=CH2CO+CH3	8.44E+11	0.0	-393
623.	AC3H4+OH=HCO+C2H4	1.25E+11	0.0	-393
624.	AC3H4+OH=C2H5+CO	1.88E+11	0.0	-393
625.	AC3H4+OH=ACROL+H	5.62E+11	0.0	-393
626.	AC3H4+HO2=>C3H4O2H	3.00E+11	0.0	8000
627.	C3H4O2H=>AC3H4+HO2	3.16E+11	0.0	19500
628.	C3H4O2H=>C3H4O+OH	3.16E+11	0.0	19500
629.	C3H4O=>ACROL	2.45E+14	0.0	58485
630.	C3H4O+O2=>C3H3O+HO2	4.00E+13	0.0	61500
631.	C3H4O+HO2=>			
	CH2CO+CH2O+OH	1.00E+12	0.0	14340
632.	C3H4O+HO2=>C3H3O+H2O2	4.00E+12	0.0	17000
633.	C3H4O+OH=>C3H3O+H2O	4.79E+13	0.0	5955
634.	C3H3O=>C2H3CO	8.51E+14	0.0	14000
635.	C3H3O+O2=>HCCO+HCO+OH	5.01E+12	0.0	19192
636.	AC3H4+HO2=C3H3+H2O2	1.80E+13	0.0	19000
637.	AC3H4+HO2=>			
	CH2CO+CH2+OH	5.00E+11	0.0	19000
638.	AC3H4+HO2=>ACROL+OH	5.00E+11	0.0	19000
639.	AC3H4+HO2=>			
	C2H2+CH2O+OH	5.00E+11	0.0	19000
640.	AC3H4+O=C2H4+CO	1.12E-02	4.6	-4243
641.	AC3H4+O=C2H3+HCO	5.00E-04	4.6	-4243
642.	AC3H4+O=CH2CO+CH2	1.00E-03	4.6	-4243
643.	AC3H4+O=C2H2+CH2O	2.50E-03	4.6	-4243
644.	AC3H4+H=AC3H5	1.20E+12	0.0	2700
645.	AC3H4+H=SC3H5	8.00E+11	0.0	2000
646.	AC3H4+H=C3H3+H2	1.00E+14	0.0	15009
647.	AC3H4+CH3=C3H3+CH4	2.00E+12	0.0	7700
648.	AC3H4+AC3H5=C3H3+C3H6	2.00E+12	0.0	7700
649.	PC3H4+M=C3H3+H+M	3.39E+22	-2.0	92370
	H2O	Enh. by		1.63E+01
	CO	Enh. by		1.88E+00
	CO2	Enh. by		3.75E+00
	CH4	Enh. by		1.63E+01
	C2H6	Enh. by		1.63E+01
650.	PC3H4+O2=C3H3+HO2	2.50E+12	0.0	51000
651.	PC3H4+HO2=CH3CO+CH2O	3.00E+12	0.0	16000
652.	PC3H4+HO2=CH3HCO+HCO	4.50E+12	0.0	16000
653.	PC3H4+HO2=C3H3+H2O2	5.00E+11	0.0	19000
654.	PC3H4+OH=C3H3+H2O	6.50E+02	3.0	200
655.	PC3H4+OH=>C3H4OH	1.92E+22	-3.4	6596
656.	C3H4OH=>CH2CO+CH3	3.00E+15	0.0	28000
657.	C3H4OH=>HCO+C2H4	5.00E+14	0.0	28000
658.	C3H4OH=>CH2O+C2H3	1.00E+15	0.0	28000
659.	C3H4OH=>ACROL+H	5.00E+14	0.0	28000
660.	PC3H4+OH=CH2CO+CH3	2.00E-04	4.5	-1000
661.	PC3H4+OH=HCO+C2H4	1.00E-04	4.5	-1000
662.	PC3H4+OH=CH2O+C2H3	1.00E-04	4.5	-1000
663.	PC3H4+OH=ACROL+H	1.00E-04	4.5	-1000
664.	PC3H4+O=CH2CO+CH2	6.40E+12	0.0	2100
665.	PC3H4+O=C2H3+HCO	3.20E+12	0.0	2100
666.	PC3H4+O=HCCO+CH3	9.18E+12	0.0	2100
667.	PC3H4+O=CH2O+C2H2	3.20E+11	0.0	2100
668.	PC3H4+H=C3H3+H2	1.00E+12	0.0	1500
669.	PC3H4+CH3=C3H3+CH4	4.00E+11	0.0	7700
670.	PC3H4+C2H3=C3H3+C2H4	1.00E+11	0.0	7700
671.	PC3H4+C2H=C3H3+C2H2	4.20E+16	0.0	100000
672.	C3H3+O2=CH2CO+HCO	3.01E+10	0.0	2870
673.	C3H3+HO2=C3H2+H2O2	2.00E+12	0.0	0
674.	C3H3+OH=C3H2+H2O	5.00E+12	0.0	0
675.	C3H3+OH=HCCO+CH3	5.00E+12	0.0	0
676.	C3H3+O=C2H3+CO	4.62E+13	0.0	0
677.	C3H3+O=C2H+CH2O	4.62E+13	0.0	0
678.	C3H3+O=>C2H2+CO+H	4.62E+13	0.0	0
679.	C3H3+H=C3H2+H2	5.00E+13	0.0	3000
680.	C3H3+CH=IC4H3+H	7.00E+13	0.0	0
681.	C3H3+CH=NC4H3+H	7.00E+13	0.0	0
682.	C3H3+CH2=C4H4+H	4.00E+13	0.0	0
683.	C3H3+HCCO=C4H4+CO	2.50E+13	0.0	0
684.	C3H3+CH3=C4H6	3.33E+12	0.0	0
685.	CH+C2H2=C3H2+H	1.00E+14	0.0	0
686.	C3H2+O2=HCCO+HCO	3.00E+10	0.0	2870
687.	C3H2+OH=C2H2+HCO	5.00E+13	0.0	0

#	Reaction	A	b	E
688.	C3H2+CH2=IC4H3+H	3.00E+13	0.0	0
689.	ACROL=C2H3+HCO	2.45E+16	0.0	84128
690.	ACROL+O=C2H3CO+OH	5.01E+12	0.0	1790
691.	ACROL+H=C2H3CO+H2	3.98E+13	0.0	4200
692.	ACROL+OH=C2H3CO+H2O	1.00E+12	0.0	0
693.	ACROL+HO2=C2H3CO+H2O2	3.40E+11	0.0	10700
694.	ACROL+CH3=C2H3CO+CH4	1.74E+12	0.0	8440
695.	ACROL+C2H3=C2H3CO+C2H4	1.74E+12	0.0	8440
696.	ACROL+AC3H5= C2H3CO+C3H6	1.00E+12	0.0	8000
697.	ACROL+C2H5=C2H3CO+C2H6	1.74E+12	0.0	8440
698.	C2H3CO+M=C2H3+CO+M	8.60E+15	0.0	23000
	H2O	Enh. by		1.63E+01
	CO	Enh. by		1.88E+00
	CO2	Enh. by		3.75E+00
	CH4	Enh. by		1.63E+01
	C2H6	Enh. by		1.63E+01
699.	MEALL=C4H6+H	2.33E+13	0.0	60220
700.	MEALL=C2H4+C2H3	1.00E+11	0.0	37000
701.	MEALL+O2=C4H6+HO2	1.00E+11	0.0	0
702.	MEALL+HO2=C4H6+H2O2	1.80E+12	0.0	0
703.	MEALL+OH=C4H6+H2O	1.80E+13	0.0	0
704.	MEALL+O=C4H6+OH	1.80E+13	0.0	0
705.	MEALL+H=C4H6+H2	3.16E+13	0.0	0
706.	MEALL+CH3=C4H6+CH4	7.94E+12	0.0	0
707.	MEALL+C2H3=C4H6+C2H4	4.00E+12	0.0	0
708.	MEALL+C2H5=C4H6+C2H6	4.00E+12	0.0	0
709.	MEALL+C3H3=C4H6+PC3H4	4.00E+12	0.0	0
710.	MEALL+C3H3=C4H6+AC3H4	4.00E+12	0.0	0
711.	MEALL+AC3H5=C4H6+C3H6	6.30E+12	0.0	0
712.	C4H6=NC4H5+H	1.58E+16	0.0	110000
713.	C4H6+O2=NC4H5+HO2	4.00E+13	0.0	57895
714.	C4H6+HO2=NC4H5+H2O2	1.50E+10	0.0	12570
715.	C4H6+HO2=IC4H5+H2O2	6.00E+09	0.0	9930
716.	C4H6+HO2=> HCO+AC3H5+OH	2.00E+12	0.0	14340
717.	C4H6+OH=CH3HCO+C2H3	3.00E+12	0.0	-393
718.	C4H6+OH=NC4H5+H2O	2.00E+07	2.0	5000
719.	C4H6+OH=IC4H5+H2O	1.00E+07	2.0	2000
720.	C4H6+O=C2H4+CH2CO	4.50E+08	1.4	-858
721.	C4H6+O=AC3H5+HCO	4.50E+08	1.4	-858
722.	C4H6+H=NC4H5+H2	3.00E+07	2.0	13000
723.	C4H6+H=IC4H5+H2	6.30E+10	0.7	5999
724.	C4H6+C2H3=NC4H5+C2H4	6.31E+13	0.0	14517
725.	IC4H5+M=C4H4+H+M	4.00E+15	0.0	45000
	H2O	Enh. by		1.63E+01
	CO	Enh. by		1.88E+00
	CO2	Enh. by		3.75E+00
	CH4	Enh. by		1.63E+01
	C2H6	Enh. by		1.63E+01
726.	IC4H5=NC4H5	1.50E+13	0.0	67765
727.	IC4H5+OH=C4H4+H2O	2.00E+07	2.0	1000
728.	IC4H5+H=C4H4+H2	1.00E+14	1.0	0
729.	NC4H5=C2H3+C2H2	2.00E+12	0.0	46043
730.	NC4H5+M=C4H4+H+M	1.50E+14	0.0	30000
	H2O	Enh. by		1.63E+01
	CO	Enh. by		1.88E+00
	CO2	Enh. by		3.75E+00
	CH4	Enh. by		1.63E+01
	C2H6	Enh. by		1.63E+01
731.	NC4H5+OH=C4H4+H2O	2.00E+07	2.0	1000
732.	NC4H5+H=C4H4+H2	3.00E+07	2.0	1000
733.	NC4H5+H=IC4H5+H	1.00E+14	0.0	0
734.	C4H4=C2H2+C2H2	3.20E+13	0.0	77100
735.	C4H4+M=IC4H3+H+M	1.00E+20	0.0	99300
	H2O	Enh. by		1.63E+01
	CO	Enh. by		1.88E+00
	CO2	Enh. by		3.75E+00
	CH4	Enh. by		1.63E+01
	C2H6	Enh. by		1.63E+01
736.	C4H4=C4H2+H2	1.26E+15	0.0	94700
737.	C4H4+OH=IC4H3+H2O	2.00E+07	2.0	2000
738.	C4H4+OH=NC4H3+H2O	7.50E+06	2.0	5000
739.	C4H4+H=NC4H3+H2	2.00E+07	2.0	15000
740.	C4H4+H=IC4H3+H2	1.00E+14	0.0	0
741.	C4H4+O=AC3H4+CO	3.00E+13	0.0	1811
742.	C4H4+C2H=IC4H3+C2H2	3.98E+13	0.0	0
743.	IC4H3+M=C4H2+H+M	4.46E+15	0.0	46516
	H2O	Enh. by		1.63E+01
	CO	Enh. by		1.88E+00
	CO2	Enh. by		3.75E+00
	CH4	Enh. by		1.63E+01
	C2H6	Enh. by		1.63E+01
744.	IC4H3=NC4H3	1.50E+13	0.0	67765
745.	IC4H3+O2=CH2CO+HCCO	1.00E+12	0.0	0
746.	IC4H3+OH=C4H2+H2O	3.00E+13	0.0	0
747.	IC4H3+O=CH2CO+C2H	2.00E+13	0.0	0
748.	IC4H3+O=H2C4O+H	2.00E+13	0.0	0
749.	IC4H3+H=C4H2+H2	5.00E+13	0.0	0
750.	IC4H3+CH2=AC3H4+C2H	2.00E+13	0.0	0
751.	NC4H3+M=C4H2+H+M	1.00E+16	0.0	59700
	H2O	Enh. by		1.63E+01
	CO	Enh. by		1.88E+00
	CO2	Enh. by		3.75E+00
	CH4	Enh. by		1.63E+01
	C2H6	Enh. by		1.63E+01
752.	NC4H3+OH=C4H2+H2O	3.00E+13	0.0	0
753.	NC4H3+H=C4H2+H2	5.00E+13	0.0	0
754.	NC4H3+H=IC4H3+H	1.00E+14	0.0	0
755.	H2C4O+OH=CH2CO+HCCO	1.00E+07	2.0	2000
756.	H2C4O+H=C2H2+HCCO	5.00E+13	0.0	3000
757.	C4H2+OH=H2C4O+H	6.66E+12	0.0	-410
758.	C4H2+O=C3H2+CO	1.20E+12	0.0	0
759.	C4H2+M=C4H+H+M	3.50E+17	0.0	80065
760.	C4H+O2=C2H+CO+CO	1.00E+14	0.0	0
761.	NC4H5+C2H2=C6H6+H	2.80E+03	2.9	1400
762.	C3H3+C3H3=C6H615	4.00E+12	0.0	0
763.	C6H615=HEX1245	1.80E+11	0.0	35804
764.	HEX1245=CC6H6	5.00E+11	0.0	22081
765.	CC6H6=FULVENE	4.26E+13	0.0	49282
766.	CC6H6=C6H6	3.79E+13	0.0	22000
767.	FULVENE=C6H6	7.58E+13	0.0	73923
768.	C3H6+C2H=BUTYNE+CH	1.20E+13	0.0	0
769.	C3H3+CH3=BUTYNE	2.50E+12	0.0	0
770.	MEALL+MEALL= C4H6+C4H8	3.16E+12	0.0	0
771.	MEALL+C2H5=C4H8+C2H4	5.00E+11	0.0	0
772.	MEALL+C2H5=T2C4H8+C2H4	5.00E+11	0.0	0
773.	MEALL+C2H5=C2C4H8+C2H4	5.00E+11	0.0	0
774.	C4H8=MEALL+H	4.08E+18	-1.0	97350
775.	C4H8=C2C4H8	4.00E+11	0.0	60000
776.	C4H8=T2C4H8	4.00E+11	0.0	60000
777.	C4H8=AC3H5+CH3	1.50E+19	-1.0	73400
778.	C4H8=C2H3+C2H5	1.00E+19	-1.0	96770
779.	C4H8+O2=MEALL+HO2	1.30E+12	0.0	39000
780.	C4H8+HO2=MEALL+H2O2	1.00E+11	0.0	17060
781.	C4H8+HO2=>CH2O+C3H6+OH	2.50E+12	0.0	14340
782.	C4H8+OH=MEALL+H2O	4.19E+06	2.0	-543

#	Reaction	A	b	E
783.	C4H8+OH=CH2O+NC3H7	2.00E+12	0.0	-928
784.	C4H8+OH=CH3HCO+C2H5	6.90E+11	0.0	-928
785.	C4H8+O=C3H6+CH2O	7.23E+05	2.3	-1050
786.	C4H8+O=CH3HCO+C2H4	1.30E+13	0.0	850
787.	C4H8+O=C2H5+CH3CO	1.62E+13	0.0	850
788.	C4H8+O=MEALL+OH	2.60E+12	0.0	4500
789.	C4H8+H=MEALL+H2	1.95E+13	0.0	4445
790.	C4H8+CH3=MEALL+CH4	1.00E+11	0.0	7300
791.	C4H8+C2H5=MEALL+C2H6	1.00E+11	0.0	8300
792.	C4H8+AC3H5=MEALL+C3H6	8.00E+10	0.0	12400
793.	C4H8+SC3H5=MEALL+C3H6	8.00E+10	0.0	12400
794.	C4H8+TC3H5=MEALL+C3H6	8.00E+10	0.0	12400
795.	C2C4H8=T2C4H8	8.14E+13	0.0	62850
796.	C2C4H8=C4H6+H2	1.00E+13	0.0	65500
797.	C2C4H8=MEALL+H	4.07E+18	-1.0	97350
798.	C2C4H8=SC3H5+CH3	2.00E+16	0.0	71300
799.	C2C4H8+OH=MEALL+H2O	9.00E+06	2.0	-60
800.	C2C4H8+O=IC3H7+HCO	6.03E+12	0.0	0
801.	C2C4H8+O=CH3HCO+C2H4	1.00E+12	0.0	0
802.	C2C4H8+H=MEALL+H2	1.00E+13	0.0	3500
803.	C2C4H8+CH3=MEALL+CH4	1.00E+11	0.0	8200
804.	T2C4H8=MEALL+H	4.07E+18	-1.0	97350
805.	T2C4H8=SC3H5+CH3	2.00E+16	0.0	71300
806.	T2C4H8+OH=MEALL+H2O	9.00E+06	2.0	-60
807.	T2C4H8+O=IC3H7+HCO	6.03E+12	0.0	0
808.	T2C4H8+O=CH3HCO+C2H4	1.00E+12	0.0	0
809.	T2C4H8+H=MEALL+H2	5.00E+12	0.0	3500
810.	T2C4H8+CH3=MEALL+CH4	1.00E+11	0.0	8200
811.	BUTYNE+HO2=NC4H5+H2O2	5.00E+11	0.0	17000
812.	BUTYNE+HO2=IC4H5+H2O2	5.00E+11	0.0	17000
813.	BUTYNE+OH=NC4H5+H2O	2.60E+02	3.0	200
814.	BUTYNE+OH=IC4H5+H2O	2.60E+02	3.0	200
815.	BUTYNE+OH=CH2CO+C2H5	4.00E-04	4.5	-1000
816.	BUTYNE+O=C3H6+CO	2.00E+13	0.0	1660
817.	BUTYNE+H=AC3H4+CH3	1.30E+05	2.5	1000
818.	BUTYNE+H=C2H5+C2H2	6.50E+04	2.5	1000
819.	BUTYNE+H=IC4H5+H2	6.50E+13	0.0	9400
820.	BUTYNE+H=NC4H5+H2	6.50E+13	0.0	9400
821.	BUTYNE+CH3=IC4H5+CH4	1.00E+14	0.0	19500
822.	BUTYNE+CH3=NC4H5+CH4	1.00E+14	0.0	19500
823.	AC3H5+AC3H5=C6H10	1.02E+13	0.0	-263
824.	C2H2+NC4H5=C6H7C	2.78E+11	0.0	3509
825.	C6H7C+O2=C6H6+HO2	1.00E+12	0.0	0
826.	C6H7C+HO2=C6H6+H2O2	1.00E+12	0.0	0
827.	C6H7C+HO2=>CPD+HCO+OH	4.50E+12	0.0	0
828.	C6H7C+OH=C6H6+H2O	6.02E+12	0.0	0
829.	C6H7C+O=C6H6+OH	1.80E+13	0.0	0
830.	C6H7C+O=CPD+HCO	8.26E+13	0.0	0
831.	C6H7C+H=C6H6+H2	3.16E+12	0.0	0
832.	C6H7C+CH3=C6H6+CH4	1.00E+13	0.0	0
833.	C6H7C+C2H3=C6H6+C2H4	4.00E+12	0.0	0
834.	C6H7C+C2H5=C6H6+C2H6	4.00E+12	0.0	0
835.	C6H7C+AC3H5=C6H6+C3H6	4.00E+12	0.0	0
836.	C6H7C+SC3H5=C6H6+C3H6	4.00E+12	0.0	0
837.	C6H7C+TC3H5=C6H6+C3H6	4.00E+12	0.0	0
838.	C6H7C+HCO=C6H6+CH2O	4.00E+12	0.0	0
839.	C6H10+O2=C6H9+HO2	1.00E+11	0.0	25050
840.	C6H10+HO2=C6H9+H2O2	1.64E+11	0.0	12583
841.	C6H10+OH=C6H9+H2O	5.60E+12	0.0	861
842.	C6H10+H=C6H9+H2	1.00E+14	0.0	3900
843.	C6H10+CH3=C6H9+CH4	2.50E+11	0.0	8300
844.	C6H10+C2H5=C6H9+C2H6	1.00E+11	0.0	8300
845.	C6H10+C2H3=C6H9+C2H4	6.30E+12	0.0	13000
846.	C6H10+AC3H5=C6H9+C3H6	1.00E+12	0.0	10500
847.	C6H5+H=C6H6	2.20E+14	0.0	0
848.	C6H6=C4H4+C2H2	9.00E+15	0.0	107430
849.	C6H6+O2=C6H5+HO2	6.30E+13	0.0	60000
850.	C6H6+HO2=C6H5+H2O2	1.52E+11	0.0	17000
851.	C6H6+HO2=>C6H5O+OH+H	2.52E+12	0.0	14340
852.	C6H6+OH=C6H5+H2O	2.11E+13	0.0	4570
853.	C6H6+O=C6H5O+H	2.78E+13	0.0	4970
854.	C6H6+H=C6H5+H2	2.50E+14	0.0	16000
855.	C6H6+H=C6H7C	4.04E+13	0.0	4312
856.	C6H6+C2H5=C6H5+C2H6	6.31E+11	0.0	14866
857.	C6H6+C5H5=C6H5+CPD	6.31E+11	0.0	14866
858.	C6H6+C6H5O=C6H5+C6H5OH	6.31E+11	0.0	14866
859.	C6H5+O2=C6H5O+O	6.27E+12	0.0	7470
860.	C6H5O=>C5H5+CO	7.53E+11	0.0	43900
861.	C6H5O+H=C6H5OH	8.36E+13	0.0	0
862.	C6H5OH+OH=C6H5O+H2O	6.00E+12	0.0	0
863.	C6H5OH+H=C6H6+OH	2.21E+13	0.0	7910
864.	C6H5OH+H=C6H5O+H2	1.15E+14	0.0	12400
865.	C6H5OH+O=C6H5O+OH	2.81E+13	0.0	7352
866.	C6H5OH+C2H3=C6H5O+C2H4	6.00E+12	0.0	0
867.	C6H5OH+NC4H5=C6H5O+C4H6	6.00E+12	0.0	0
868.	C5H5+H=CPD	3.33E+13	0.0	0
869.	C5H5+O=NC4H5+CO	1.00E+14	0.0	0
870.	C5H5+HO2=C5H5O13+OH	1.80E+14	0.0	0
871.	C5H5+OH=C5H4OH+H	3.00E+13	0.0	0
872.	C5H5O13=NC4H5+CO	2.51E+11	0.0	43900
873.	C5H4OH=C5H4O+H	2.51E+11	0.0	48000
874.	C5H4O=>CO+C2H2+C2H2	2.51E+11	0.0	48000
875.	AC3H5+C2H2=CPD+H	1.00E+14	0.0	24892
876.	CPD+O2=C5H5+HO2	2.00E+13	0.0	25000
877.	CPD+HO2=C5H5+H2O2	2.00E+12	0.0	11660
878.	CPD+OH=C5H5+H2O	3.43E+09	1.2	-447
879.	CPD+H=C5H5+H2	2.19E+08	1.8	3000
880.	CPD+O=C5H5+OH	1.81E+13	0.0	3080
881.	CPD+C2H3=C5H5+C2H4	6.00E+12	0.0	0
882.	CPD+NC4H5=C5H5+C4H6	6.00E+12	0.0	0
883.	CPD+C6H5O=C5H5+C6H5OH	3.16E+11	0.0	8000
884.	NC4H10=C2H5+C2H5	2.00E+16	0.0	81300
885.	NC4H10=NC3H7+CH3	1.00E+17	0.0	85400
886.	NC4H10=PC4H9+H	1.58E+16	0.0	98000
887.	NC4H10=SC4H9+H	1.00E+16	0.0	95000
888.	NC4H10+O2=PC4H9+HO2	2.51E+13	0.0	49000
889.	NC4H10+O2=SC4H9+HO2	3.98E+13	0.0	47600
890.	NC4H10+H=PC4H9+H2	5.63E+07	2.0	7700
891.	NC4H10+H=SC4H9+H2	4.78E+06	2.5	7369
892.	NC4H10+O=PC4H9+OH	4.89E+06	2.4	5505
893.	NC4H10+O=SC4H9+OH	4.28E+05	2.6	2583
894.	NC4H10+OH=PC4H9+H2O	4.14E+07	1.7	753
895.	NC4H10+OH=SC4H9+H2O	7.23E+07	1.6	-246
896.	NC4H10+HO2=PC4H9+H2O2	1.70E+13	0.0	20460
897.	NC4H10+HO2=SC4H9+H2O2	4.00E+12	0.0	18150
898.	NC4H10+CH3=PC4H9+CH4	2.19E+11	0.0	11400
899.	NC4H10+CH3=SC4H9+CH4	2.19E+11	0.0	9600
900.	NC4H10+C2H3=PC4H9+C2H4	1.00E+12	0.0	18000
901.	NC4H10+C2H3=SC4H9+C2H4	7.94E+11	0.0	16800
902.	NC4H10+C2H5=PC4H9+C2H6	1.00E+11	0.0	13400
903.	NC4H10+C2H5=SC4H9+C2H6	1.00E+11	0.0	10400
904.	NC4H10+AC3H5=PC4H9+C3H6	7.94E+11	0.0	20500
905.	NC4H10+AC3H5=SC4H9+C3H6	3.16E+11	0.0	16400
906.	NC4H10+CH3O=PC4H9+CH3OH	3.00E+11	0.0	7000
907.	NC4H10+CH3O=SC4H9+CH3OH	6.00E+11	0.0	7000
908.	PC4H9=C2H5+C2H4	2.50E+13	0.0	28800
909.	PC4H9=C4H8+H	1.26E+13	0.0	38600
910.	PC4H9=SC4H9	1.32E+12	0.0	32770

#	Reaction	A	b	E
911.	PC4H9+O2=C4H8+HO2	3.80E+10	0.0	-2000
912.	PC4H9+HO2=C4H8+H2O2	1.00E+12	0.0	2000
913.	SC4H9=C4H8+H	1.29E+13	0.0	36366
914.	SC4H9=T2C4H8+H	4.57E+12	0.0	34000
915.	SC4H9=C2C4H8+H	4.17E+12	0.0	34780
916.	SC4H9=C3H6+CH3	9.33E+12	0.0	29210
917.	SC4H9+O2=C4H8+HO2	7.59E+09	0.0	-2000
918.	SC4H9+O2=T2C4H8+HO2	9.00E+09	0.0	-2000
919.	SC4H9+O2=C2C4H8+HO2	9.00E+09	0.0	-2000
920.	SC4H9+HO2=T2C4H8+H2O2	1.00E+12	0.0	0
921.	SC4H9+HO2=C2C4H8+H2O2	1.00E+12	0.0	0
922.	CH3+O2(+M)=CH3O2(+M)	7.83E+08	1.2	0
	Low pressure limit:	5.80E+25	-3.3	0
	TROE centering:	6.64E-01	10E5	10
923.	CH3O2H=CH3O+OH	6.30E+14	0.0	42300
924.	CH3O2+CH2O=CH3O2H+HCO	2.00E+12	0.0	11700
925.	CH3O2+CH4=CH3O2H+CH3	1.80E+11	0.0	18500
926.	CH3O2+CH3OH=			
	CH3O2H+CH2OH	1.80E+12	0.0	13712
927.	CH3O2+HO2=CH3O2H+O2	1.81E+11	0.0	-1431
928.	CH3O2+HO2=CH2O+H2O+O2	1.80E+10	0.0	-1431
929.	CH3O2+CH3O2=			
	CH2O+CH3OH+O2	1.05E+09	0.0	-3589
930.	CH3O2+CH3O2=			
	O2+CH3O+CH3O	7.74E+10	0.0	-61
931.	CH3O2+C2H6=CH3O2H+C2H5	2.95E+11	0.0	15000
932.	CH3O2+CH3=CH3O+CH3O	8.17E+12	0.0	-906
933.	CH3O2+OH=CH3OH+O2	6.00E+13	0.0	0
934.	CH3O2+H=CH3O+OH	9.60E+13	0.0	0
935.	CH3O2+H2O2=CH3O2H+HO2	2.41E+12	0.0	9936
936.	CH3O2+C2H5O2=			
	O2+CH3O+C2H5O	7.74E+10	0.0	-61
937.	CH3O2+C2H5=CH3O+C2H5O	8.17E+12	0.0	-906
938.	C2H5+O2=C2H5O2	5.17E+35	-7.6	6033
939.	C2H5+O2=C2H5O+O	1.10E+13	-0.2	27937
940.	C2H5O2H=C2H5O+OH	6.30E+14	0.0	42300
941.	C2H5O2+CH4=C2H5O2H+CH3	1.80E+11	0.0	18500
942.	C2H5O2+C2H6=C2H5O2H+C2H5	2.95E+11	0.0	15000
943.	C2H5O2+CH3=C2H5O+CH3O	8.17E+12	0.0	-906
944.	C2H5O+H=CH3+CH2OH	1.00E+13	0.0	0
945.	C2H5O+H=CH3HCO+H2	1.00E+13	0.0	0
946.	C2H5O+OH=CH3HCO+H2O	4.82E+14	0.0	5017
947.	C2H5O2+CH2O=C2H5O2H+HCO	2.00E+12	0.0	11700
948.	C2H5O2+HO2=C2H5O2H+O2	3.37E+11	0.0	-1292
949.	C2H5O2+C2H5O2=			
	O2+C2H5O+C2H5O	1.26E+11	0.0	497
950.	C2H5O=CH3HCO+H	2.50E+14	0.0	23400
951.	C2H5O=CH3+CH2O	5.00E+13	0.0	21600
952.	C2H5O+HO2=CH3HCO+H2O2	3.00E+11	0.0	0
953.	C2H5O+O2=CH3HCO+HO2	3.60E+10	0.0	1093
954.	CH3+NO(+M)=CH3NO(+M)	2.20E+11	0.6	0
	Low pressure limit:	2.06E+27	-3.5	0
955.	CH3NO2(+M)=CH3+NO2(+M)	1.78E+16	0.0	59000
	Low pressure limit:	1.26E+17	0.0	4.2E+4
956.	CH3+NO2=CH3O+NO	1.51E+13	0.0	0
957.	CH3O+NO2=CH2O+HONO	6.02E+12	0.0	2285
958.	CH3O+NO2(+M)=			
	CH3ONO2(+M)	1.20E+13	0.0	0
	Low pressure limit:	1.40E+30	-4.5	0
959.	CH3O+NO=CH2O+HNO	1.30E+14	-0.7	0
960.	CH3O2+NO=CH3O+NO2	2.53E+12	0.0	-358
961.	CH3NO2+O=H2CNO2+OH	1.51E+13	0.0	5350
962.	CH3NO2+OH=H2CNO2+H2O	1.49E+13	0.0	5740
963.	CH3NO2+H=H2CNO2+H2	7.50E+12	0.0	10000
964.	CH3NO2+H=HONO+CH3	3.27E+12	0.0	3730
965.	CH3NO2+H=CH3NO+OH	1.40E+12	0.0	3730
966.	CH3NO2+CH3=H2CNO2+CH4	7.08E+11	0.0	11140
967.	CH3NO2+CH3O=			
	H2CNO2+CH3OH	3.00E+11	0.0	7000
968.	CH3NO2+C2H5=H2CNO2+C2H6	3.00E+11	0.0	11700
969.	CH3NO2+HO2=H2CNO2+H2O2	1.50E+11	0.0	15000
970.	H2CNO2=CH2O+NO	1.00E+13	0.0	36000
971.	H2CNO2+HONO=CH3NO2+NO2	1.00E+12	0.0	0
972.	CH3O+NO(+M)=CH3ONO(+M)	1.21E+13	0.0	-332
	Low pressure limit:	2.70E+27	-3.5	0
973.	CH3NO2=CH3ONO	2.90E+14	0.0	67000
974.	C2H5+NO2=C2H5O+NO	1.00E+13	0.0	0
975.	C2H5O+NO2=CH3HCO+HONO	4.00E+11	0.0	0
976.	C2H5O+NO=CH3HCO+HNO	1.30E+14	-0.7	0
977.	C2H5O2+NO=C2H5O+NO2	3.00E+12	0.0	-358
978.	HO2+NO+M=HONO2+M	2.23E-12	-3.5	2200
979.	NO2+OH(+M)=HONO2(+M)	3.61E+13	0.0	0
	Low pressure limit:	1.44E+25	-2.9	0
980.	HONO2+OH=H2O+NO3	1.03E+10	0.0	-1240
981.	NO3+OH=HO2+NO2	1.38E+13	0.0	0
982.	NO3+O=O2+NO2	1.02E+13	0.0	0
983.	NO3+H=NO2+OH	6.00E+13	0.0	0
984.	NO3+HO2=O2+HONO2	5.60E+11	0.0	0
985.	NO3+HO2=O2+OH+NO2	2.00E+12	0.0	0
986.	NO3+NO3=O2+NO2+NO2	5.12E+11	0.0	4840
987.	NO3+M=O2+NO+M	2.05E+08	1.0	12122
988.	NO3+NO2=NO2+NO+O2	2.35E+10	0.0	2960
989.	NO3+NO=NO2+NO2	1.08E+13	0.0	-219
990.	NO2+O(+M)=NO3(+M)	1.20E+13	0.0	0
	Low pressure limit:	2.94E+21	-2.0	0
991.	NO2+O3=NO3+O2	7.23E+10	0.0	4870
992.	O+O2+M=O3+M	1.88E+21	-2.8	0
993.	O+O3=O2+O2	4.80E+12	0.0	4090
994.	H+O3=OH+O2	8.43E+13	0.0	950
995.	OH+O3=HO2+O2	1.14E+12	0.0	2000
996.	NO+O3=NO2+O2	1.08E+12	0.0	2720
997.	HO2+O3=OH+O2+O2	8.43E+09	0.0	1200
998.	CH3+O3=CH3O+O2	1.57E+12	0.0	0
999.	CH3+HONO=CH4+NO2	8.10E+05	1.9	5504
1000.	C2H5+HONO=C2H6+NO2	8.10E+05	1.9	5504
1001.	C2H3+HONO=C2H4+NO2	8.10E+05	1.9	5504
1002.	CH3O+HONO=CH3OH+NO2	8.10E+05	1.9	5504
1003.	CH3O2H+H=CH3O2+H2	8.80E+10	0.0	1860
1004.	CH3O2H+H=CH3O+H2O	8.20E+10	0.0	1860
1005.	CH3O2H+O=CH3O2+OH	1.00E+12	0.0	3000
1006.	CH3O2H+OH=CH3O2+H2O	1.80E+12	0.0	-378

Formation et réduction de NO_x par un charbon, un lignite, un anthracite et un coke de pétrole dans les conditions d'un précalcinateur de cimenterie

Résumé :

L'industrie cimentière est extrêmement consommatrice d'énergie. Cette énergie est principalement fournie par la combustion de solides carbonés pulvérisés. Jusqu'à 60 % de cet apport en combustible peut être injecté dans le précalcinateur. La combustion de solides carbonés produit des polluants, au premier rang desquels on trouve les NO_x. Plusieurs techniques de réduction de NO_x existent à l'heure actuelle. L'une des plus prometteuses en terme d'efficacité, conjuguée à son coût, est le "reburning" qui consiste en une injection secondaire de combustible, créant ainsi une zone riche et favorable à la réduction des NO_x. L'injection de combustibles solides dans les précalcinateurs de cimenteries s'apparente à cette technique. Ces solides interagissent avec les NO_x par différents mécanismes :

- par l'intermédiaire de réactions dans la phase gaz avec les matières volatiles dégagées lors de la pyrolyse;
- par l'intermédiaire de réactions hétérogènes entre le résidu solide et son environnement gazeux : l'oxydation du char qui produit des espèces azotées et la réduction du NO sur le char.

Une démarche couplée d'expérimentations et de modélisation a été développée pour déterminer l'influence relative de ces différents phénomènes. Les combustibles utilisés sont de quatre types distincts et sont communément utilisés dans les cimenteries : lignite, charbon, anthracite et petcoke. Ainsi, les réactions hétérogènes élémentaires – dévolatilisation, oxydation du char et réduction du NO sur le char – ont-elles été caractérisées individuellement par des expériences et des modélisations spécifiques. On observe une forte disparité entre les quatre combustibles, autant sur les paramètres cinétiques des réactions hétérogènes que sur la quantités de matières volatiles dégagées.

Enfin, les expériences et modélisations représentatives de l'ensemble des réactions qui se déroulent simultanément lors du reburning dans les conditions précalcinateur de cimenteries ont été conduites. Il apparaît que l'effet de la réduction du NO dans la phase gaz est du même ordre de grandeur que l'effet de la réduction sur le char après un temps de séjour des particules de 2 s. La réduction du NO sur le char croît continuellement avec la température alors que la réduction dans la phase gaz présente des singularités en fonction de la température pour les combustibles : la réduction du NO est plus faible à 900°C dans le cas du lignite et du charbon qu'à 800 et 1000°C. L'étude détaillée de ces singularités a été menée et a permis de déterminer les chemins réactionnels intervenant dans la formation et réduction de NO_x dans la phase gazeuse.

Mots clefs : Combustion, oxydes d'azote, précalcinateur, reburning, expériences, modélisations

NO_x formation and reduction by a coal, a lignite, an anthracite and a petroleum coke in conditions of cement plant calciner

Abstract :

The cement industry is a high energy consumer. This energy is mostly provided by the combustion of pulverized carbonaceous solid fuels. Up to 60 % of this fuel income may be injected into the calciner. However, the combustion of solid fuels produces pollutants, particularly NO_x. Several reduction technology were developed. The most promising one, in term of cost and efficiency, is the reburning. It consists in a secondary fuel injection, creating a fuel rich zone favorable to NO_x reduction. The fuel injection in cement plant calciners may be compared to this technique. The solids interact with NO_x at different levels:

- through gas phase reactions with volatile matters released during the pyrolysis,
- and through solid-gas heterogeneous reactions: i.e. char oxidation that produces N-species and NO reduction at the char surface.

A coupled experimental and modeling protocol was developed to determine the relative contribution of these different phenomena. The used fuels are of four distinct types, commonly used in cement plants: a lignite, a coal, an anthracite and a petcoke. Thus, the elementary heterogeneous reactions – devolatilisation, char oxidation and NO reduction by char – were characterized by specific experiments and modelings. One observes a large disparity between the four fuels in terms of kinetic parameters and quantity of volatile matters released.

Finally, the experiments and modelings representative of the reactions occurring simultaneously during reburning in calciner conditions were performed. It appears that the effect of NO reduction in the gas phase is of the same order of magnitude that the effect of reduction by char after a particle residence time of 2 s. The NO reduction by char increases continuously with the temperature, whereas the gas phase reduction presents singularities in function of the temperature for the high volatile fuels: The NO reduction is lower at 900°C than at 800 and 1000°C, in case of lignite and coal. A detailed chemical analysis of these singularities was carried out and enabled to determine the main reaction paths occurring during NO_x formation and reduction in the gas phase.

Keywords : Combustion, nitric oxide, calciner, reburning, experiments, modelings